SOME STUDIES ON THE OCEAN CIRCULATION

A THESIS

by

David M. Garner

A dissertation in the Department of Meteorology and Oceanography submitted to the faculty of the Graduate School of Arts and Science in partial fulfillment of the requirements for the degree of Doctor of Philosophy at New York University.

New York

~~September~~ Oct. 1962

Approved

Willard J. Pierson

Research adviser

Table of Contents

Table of Contents (cont.)

List of Figures

List of Figures (cont.)

List of Figures (cont.)

List of Figures (cont.)

List of Figures (cont.)

List of Tables

Acknowledgments

The writer wishes to record his gratitude for financial support from the New Zealand Government, through the Oceanographic Institute of the Department of Scientific and Industrial Research, and from New York University through appointment as Assistant Research Scientist under a contract with the Office of Naval Research (Nonr 285-03) and with the U. S. Navy Hydrographic Office under contract N-62306-794.

Particular acknowledgment is made of the friendly counsel, patience, and generous Assistantship administration of the Directors of research under these contracts, Professor Willard J. Pierson, Professor Gerhard Neumann, and Dr. El Sayed Mohamed Hassan.

The facilities of the AEC-NYU Computing Center of the Courant Institute of Mathematical Sciences were used for the numerical aspects of the following study, and those of the Photographic Section, Research Division, College of Engineering for the final preparation of figures.

It has been a pleasure to have the assistance of Mrs. Sadelle Wladaver, Mrs. Lillian Bloom, and Mrs. Jutta Neumann in the preparation of the manuscript.

Abstract

The following study is based on papers by H. U. Sverdrup, H. Stommel, and G. Neumann which have examined analytically the properties of the vertically integrated wind-driven circulation in ocean models based on the linearized, steady-state hydrodynamic equations of motion.

A critical review is offered of the fundamental principles on which these models were based, the progressive development of the vorticity balance theme which links these contributions being stressed, and several aspects of the material reviewed are chosen for further analysis.

The model of Sverdrup describes the vertically integrated circulation in an ocean bounded only on its eastern side by a meridionally oriented coast. Dynamically, the model portrays a state of balance between the curl of the driving wind stress field (the "anemographic vorticity") and the interaction between the responding circulation and the earth's rotation (the "planetary vorticity"). The geometry of the stream and integrated pressure functions which characterize the Sverdrup model for selected particular driving wind stress patterns is described, and a table is presented from which this geometry may be estimated in terms of a Fourier series approximation to a general driving wind stress. Sverdrup's rectangular Cartesian analysis is repeated in spherical coordinates to show the influence on the model of the convergence of meridians on a spherical earth.

Expansion of the vorticity balance concept to include the effects of friction in the ocean circulation (the "frictional vorticity") is discussed. This development increases the order of the differential vorticity equation permitting examination of a completely bounded ocean. The model of Stommel treated a rectangular ocean driven by a zonally-directed wind stress with sinusoidal variation in the meridional direction. The analytical procedure involved in solution of the boundary value problem associated with the Stommel model is analyzed in detail. An assessment is made of the relative importance of the various terms in Stommel's equations of motion, and of the dependence of the total quantity of circulating water on the model's dimensions. The method of treating a non-sinusoidal zonal wind stress in the Stommel model by Fourier series analysis is described, and the consequences of a spherical coordinate analysis of the Stommel model are discussed.

The model of Neumann is discussed as an extension of the earlier work to include the dynamical effects of a variable depth lower boundary of the wind driven circulation (the "topographic vorticity"). Neumann indicated how topographic effects might modify the planetary effects which dominate the Stommel model and suggested that these two vorticities tended to balance each other over much of the world ocean, if the level of no motion derived by Defant were taken as the lower boundary. An analytic solution, analogous to that of Stommel, has been found to an idealization of the Neumann model. This solution contains a parameter which expresses the degree of compensation of the planetary vorticity

by the topographic vorticity, and streamlines of the vertically integrated mass transport in a rectangular Neumann ocean are exhibited for values of this parameter ranging from zero to complete compensation. Numerical solutions have been found for the full Neumann vorticity equation applied to several realizations of the dynamical structure of the Atlantic Ocean to illustrate the effect of the topographic term.

Some objections are raised to certain aspects of Neumann's interpretation of the topographic vorticity in a baroclinic ocean, and it is suggested that the use of a variational technique may provide a means for resolving this difficulty, in particular, and for determining in general the unique reaction of an ocean, which has several degrees of freedom, to a given set of dynamical constraints.

A discussion of the significance to the circulation problem of natural radiocarbon measurements in the ocean, based on a balance between diffusion, advection, and radioactive decay, concludes the study.

1. Introduction

Dynamical oceanography treats the circulation of the oceans according to the behavior of a mechanical system subject to the classical Newtonian laws of motion. In particular, Newton's Second Law is applied. This states that in an inertial frame of reference, the total time derivative of the momentum of a particle equals the vector sum of the forces applied to it. Since mass is conserved for oceanic flow (regarding as entirely negligible the loss of mass through such processes as evaporation and radioactive decay) the acceleration, $\dot{\vec{V}}$, of each fluid element (which contains always the same set of fluid particles) may be described in terms of the sum of the various forces acting on that element. This concept may be expressed in equation (1.1).

$$\dot{\vec{V}}_a = \sum_{i=1}^{n} \frac{\vec{F}_i}{m} \tag{1.1}$$

where $\vec{V}_a$ is the velocity vector of a fluid element of mass m, relative to an inertial frame, and $\vec{F}_i$ is the i^{th} member of a set of n forces applied to the fluid element. The superscripted dot denotes total time differentiation.

Classical hydrodynamics studies a fluid as a continuum. The fluid "elements" or "particles" referred to above are thus symbolic conceptions. For meaning to be assigned to definitions of such properties as temperature or density at a point or of a particle in such a fluid, it is simply necessary for all macroscopic dimensions of the system to be very much larger than the mean free path of the fluid molecules, and for the macroscopic gradients of these properties

to be sufficiently small for changes within the distance of a molecular mean free path to be entirely negligible. The "velocity" at some point in this continuous fluid is to be interpreted as a stream velocity which, in the molecular domain, is the mass average molecular velocity evaluated at that point.

The absolute acceleration on the left hand side of equation (1.1) is most usefully expressed in terms of the corresponding acceleration relative to the earth's surface. The transformation described in any treatise on geophysical hydrodynamics (for example, see Haltiner and Martin, 1957, p. 159; Goldstein, 1959, p. 135) introduces the effect of the rotating coordinate system in the form of the well-known Coriolis and centripetal accelerations. The full expansion of the left hand side of equation (1.1) after transformation to a uniformly rotating frame of reference, appears in equation (1.2).

$$\frac{\partial \vec{V}}{\partial t} + \vec{V} \cdot \nabla \vec{V} + 2(\vec{\Omega}, \vec{V}) + (\vec{\Omega}, (\vec{\Omega}, \vec{R})) = -\frac{1}{\rho}\nabla p - \nabla \Phi + \vec{F} \qquad (1.2)$$

In the left hand side of equation (1.2), $\vec{V}$ is the velocity vector measured relative to the earth's surface. The notation $\nabla \vec{V}$ is to be interpreted as the vector sum of the gradients of the scalar components of the vector $\vec{V}$. The first two terms represent the local and advective components of the total time (t) rate change of this velocity vector, that is to say, the total acceleration of the fluid element relative to the earth's surface. The Coriolis and centripetal accelerations complete the left hand side, $\vec{\Omega}$ is the angular velocity of rotation, and R is the radius of the earth. The notation (,) represents the outer ("cross") product of two vectors. The right hand side contains a list

of the important real forces (per unit mass) that are expected to act on the fluid element. The first term represents the force due to the gradient of pressure, p, in the fluid, and ρ is the density of the fluid element. The central term describes an external conservative force field whose potential is Φ. The last term accounts for the non-conservative forces acting in the system, usually frictional in character. In the present state of knowledge, such forces are not amenable to general mathematical expression. Attempts to create such expressions are responsible for much of the mathematical complexity of the problem of the oceanic circulation. The essence of the application of equation (1.2) to this problem lies in a process of approximation to a state of mathematical tractability without too great a departure from adequate representation of the physics of the real ocean.

As unknowns to be evaluated, the usual geohydrodynamic problem lists four quantities comprising the pressure, p, with the three scalar components of the vector velocity, $\vec{V}$. Equation (1.2) yields three component scalar equations. For a set of equations sufficient to solve the above problem, at least in principle, a further relation, independent of (1.2), is required. This additional information is customarily taken from a budget of the mass flux passing through an elemental volume in the fluid, keeping in mind the requirements of mass conservation. This relation is usually called the "equation of continuity." If the flux of mass out of the volume derived from diffusive processes, the nature of which need not be specified at the moment, be represented by $\mathcal{D}$, the equation of continuity may

be written

$$\dot{\rho} + \rho \nabla \cdot \vec{V} + \mathcal{D} = 0 \qquad (1.3)$$

In this equation the quantity V strictly represents the sum of the fluid stream velocity and the diffusion velocities of the various properties defining the field of oceanic density.

In the simultaneous solution of equations (1.2) and (1.3) prime interest lies normally within the velocity field. The first step in the analysis is thus usually to eliminate the pressure gradient term from the equation of motion (1.2). This may conveniently be accomplished by taking the curl of each term in this equation since the curl of the gradient of any scalar field vanishes identically. The resulting equation describes the curl of the velocity field and is called the "vorticity" equation for the problem.

The discussion following will be centered about a critical review of contributions by H. U. Sverdrup, by H. Stommel, and by G. Neumann. These studies develop a theory of vertically integrated mass transports in the wind-driven ocean circulation, using a progressive evolution of the linearized vorticity equation.

As far as possible, a consistent symbolism is employed in the mathematical expression of this study. A symbol will be described in full following the equation in which it is first introduced, and will thereafter be used without further explanation. A summary of this symbolism appears for reference in Appendix I.

The symbols x, y, and z used throughout this work will refer to a right handed set of orthogonal coordinates in which:

(a) the x-axis is positively directed towards the east,

(b) the y-axis is positively directed towards the north,

(c) the z-axis is positively directed upwards.

The horizontal coordinates x and y will at times refer to a rectilinear Cartesian system and at other times to a curvilinear spherical system.

2. Balance between anemographic and planetary vorticities

2.1. The Sverdrup model

Sverdrup (1947) studied wind-driven currents in a baroclinic ocean with application to the equatorial currents of the eastern Pacific. The following simplifications of equation (1.2) were made:

(a) Stationary conditions were assumed so that

$$\frac{\partial \vec{V}}{\partial t} \equiv 0 \qquad (2.1)$$

(b) Flow was considered to be completely unaccelerated with respect to the earth, so that

$$\vec{V} \cdot \nabla \vec{V} \equiv 0 \qquad (2.2)$$

Care must thus be taken to apply the results of this analysis neither to non-steady state conditions nor to any situation in which the velocity and velocity gradient vectors would have significant parallel components. It should not be overlooked that use of such an unaccelerated equation of motion does not guarantee a solution in which the scalar products represented by (2.2) are negligible. This point is examined in more detail in section 3.

(c) The Coriolis term in equation (1.2) may be expanded as shown in equation (2.3).

$$2(\vec{\Omega}, \vec{V}) = \vec{i}\,[\underline{2v\Omega \sin\phi} - 2w\Omega\cos\phi] + \vec{j}(\underline{2u\Omega\sin\phi}) + \vec{k}(2u\Omega\cos\phi) \quad (2.3)$$

In this equation $(\vec{i}, \vec{j}, \vec{k})$ are, respectively, the unit vectors in the (x, y, z) directions. (u, v, w) are the components of the velocity vector, $\vec{V}$, in those directions, and ϕ is the geographic latitude. In his analysis, Sverdrup used only the terms underlined in (2.3). This requires that the component $(w\cos\phi)$ be very small compared with $(v\sin\phi)$, and that the term $(2\Omega u\cos\phi)$ be negligible compared with the gravitational acceleration. These requirements are adequately met in many oceanic situations.

(d) The externally applied forces are assumed to be solely gravitational. The potential gradient is thus vertically directed and, in the relatively thin layer of the earth's crust occupied by the oceans, may be regarded as constant. Since the value of this constant depends only on position, it is customary to include the centripetal term in its expression and to write

$$\nabla\Phi + (\vec{\Omega}, (\vec{\Omega}, \vec{R})) = -\vec{g} \quad (2.4)$$

(e) The frictional term is expressed as the vertical shear of the horizontal eddy stress vector

$$\vec{F} = \frac{1}{\rho}\frac{\partial \vec{\tau}}{\partial z} \quad (2.5)$$

where $\vec{\tau}$ is the eddy stress exerted on horizontal surfaces because of turbulent exchange, in the vertical, of horizontal momentum. There must thus be no significant momentum exchange horizontally so far as the present analysis is concerned. It should be noted that Sverdrup, in his treatment, introduced a more complex expression

for the frictional force which involved setting the stress vector proportional to the vertical shear of the velocity vector. However, this resolution of the stress was later lost in the manipulation and the equivalent expression (2.5) seems preferable in the interests of simplicity.

The equations of horizontal motion, thus modified, may be expressed in Cartesian component form as equations (2.6) and (2.7).

$$-fv = -\frac{1}{\rho}\frac{\partial p}{\partial x} + \frac{1}{\rho}\frac{\partial \tau_x}{\partial z} \tag{2.6}$$

$$+fu = -\frac{1}{\rho}\frac{\partial p}{\partial y} + \frac{1}{\rho}\frac{\partial \tau_y}{\partial z} \tag{2.7}$$

Apart from the form of the Coriolis parameter, $f \equiv 2\Omega \sin\phi$, the spherical shape of the earth was neglected in Sverdrup's analysis; the effects of sphericity are examined in a later section here.

It may be shown that the horizontally directed pressure gradient force is constant with depth in a homogeneous (ρ = constant) ocean. In the real ocean, however, baroclinic conditions prevail and the pressure gradient force becomes a function of depth. Except, perhaps, at high latitudes, the pressure gradient force very likely vanishes at some distance above the physical ocean bottom, due to geostrophic control on the mass distribution. With due regard to the nature of frictional forces in this region (see section 4) this process may define a level of no motion for steady state flow corresponding to a pressure gradient set up variations of surface sea level (for example, see Neumann, 1955, p. 18). To include these baroclinic effects in some measure, the equations of motion (2.6), (2.7) were integrated vertically between

the surface at $z = \zeta(x, y)$ and some level surface, $z = d$ which is everywhere deeper than the depth of no motion. The equations, thus integrated, become equations (2.8) and (2.9).

$$- fV = - \frac{\partial P}{\partial x} + (\tau_x)_\zeta - (\tau_x)_d \tag{2.8}$$

$$+ fU = - \frac{\partial P}{\partial y} + (\tau_y)_\zeta - (\tau_y)_d \tag{2.9}$$

where

$$\begin{Bmatrix} U \\ V \end{Bmatrix} \equiv \int_d^\zeta \rho \begin{Bmatrix} u \\ v \end{Bmatrix} dz \tag{2.10}$$

represents the x and y components of the integrated mass transport, $\vec{T}$, of currents, and

$$\frac{\partial P}{\partial \xi} \equiv \int_d^\zeta \frac{\partial p}{\partial \xi} dz \ , \ \xi \equiv x \text{ or } y \tag{2.11}$$

$$= \frac{\partial}{\partial \xi} \int_d^\zeta p \, dz - \cancelto{0}{p_\zeta} \frac{\partial \zeta}{\partial \xi} + \cancelto{0}{p_d \frac{\partial d}{\partial \xi}} \tag{2.12}$$

or

$$P = \int_d^\zeta p \, dz + (\text{an arbitrary function of } z) \tag{2.13}$$

the indicated factors in (2.12) vanishing by hypothesis. Sverdrup then identified the stress components evaluated at $z = \zeta$ with the components of the stress of the wind acting on the sea surface (which shall henceforth be written simply as (τ_x, τ_y) and assumed that the stress components vanished at $z = d$. The equations of horizontal motion are thus reduced to (2.14) and (2.15).

$$\frac{\partial P}{\partial x} = fV + \tau_x \tag{2.14}$$

$$\frac{\partial P}{\partial y} = -fU + \tau_y \tag{2.15}$$

These equations relate the mass transport to the mass distribution. In homogeneous water, and with no pressure terms, they describe the pure (Ekman) integrated wind drift transport.

For stationary $\left(\frac{\partial \rho}{\partial t} = 0\right)$ and non-diffusive ($\mathcal{D} = 0$) conditions, the continuity equation (1.3) may be written

$$\nabla \cdot (\rho \vec{V}) = 0 \tag{2.16}$$

This equation must be integrated vertically.

$$\int_d^\zeta \nabla \cdot (\rho \vec{V})\, dz = \frac{\partial U}{\partial x} - (\rho u)_\zeta \frac{\partial \zeta}{\partial x} + \frac{\partial V}{\partial y} - (\rho v)_\zeta \frac{\partial \zeta}{\partial y} + (\rho w)_\zeta = 0 \tag{2.17}$$

since $\zeta = \zeta(x, y)$; see equation (4.2).

If the sea surface is in a stationary condition, so that

$$\rho_\zeta \frac{\partial \zeta}{\partial t} = 0 = (\rho w)_\zeta - (\rho u)_\zeta \frac{\partial \zeta}{\partial x} - (\rho v)_\zeta \frac{\partial \zeta}{\partial y}$$

then the integrated continuity equation becomes

$$\frac{\partial U}{\partial x} + \frac{\partial V}{\partial y} = 0 \tag{2.18}$$

This treatment (used, for example, by Neumann, 1955, p. 12) renders unnecessary Sverdrup's serious restriction of zero vertical velocity at the sea surface.

Formation of the vorticity equation is accomplished by differentiation, first of equation (2.14) partially with respect to y, then of (2.15) with respect to x, subtraction of the resulting equations, and

finally, elimination of appropriate terms with equation (2.18). The result is expressed in equation (2.19).

$$V \frac{\partial f}{\partial y} = \frac{\partial \tau_y}{\partial x} - \frac{\partial \tau_x}{\partial y} = \text{curl}_z \vec{\tau} \tag{2.19}$$

This equation expresses a state of balance between two vorticities. The term on the left hand side comes from the rotational properties of the earth, and has been called the "planetary vorticity." On the right hand side appears the curl of the wind stress field; this has been called the "anemographic vorticity." These terms are due to V. W. Ekman (1923).

The vorticity equation (2.19) determines the meridionally directed transport without further calculation:

$$V = \frac{R}{2\Omega \cos\phi}\left(\frac{\partial \tau_y}{\partial x} - \frac{\partial \tau_x}{\partial y}\right) \tag{2.20}$$

The omission of a negative sign in the central term of Sverdrup's equation 14 should be noted at this point.

The physical significance of the vorticity equation (2.19) has been demonstrated by Stommel (1960, pp.155, 156) in an interesting fashion. The equations of motion (2.14) and (2.15) may be written:

$$V = -\frac{\tau_x}{f} + \frac{1}{f}\frac{\partial P}{\partial x} = E_y + G_y \tag{2.21}$$

$$U = +\frac{\tau_y}{f} - \frac{1}{f}\frac{\partial P}{\partial y} = E_x + G_x \tag{2.22}$$

Thus the vertically integrated mass transport vector, $\vec{T}$, may be thought of in terms of the sum of two vector components, $\vec{E}$ and $\vec{G}$, where

$$\vec{E} = + \frac{1}{f} \vec{\tau} \times \vec{k} \tag{2.23}$$

and

$$\vec{G} = - \frac{1}{f} \nabla_H P \times \vec{k} \tag{2.24}$$

where the differential operator ∇_H contains only horizontal derivatives.

Formation of vorticity equations from (2.23) and (2.24) yields equations (2.25) and (2.26).

$$\nabla \cdot \vec{E} = \frac{1}{f} \text{curl } \vec{\tau} - E_y \frac{\partial f}{\partial y} \tag{2.25}$$

$$\nabla \cdot \vec{G} = - G_y \frac{\partial f}{\partial y} \tag{2.26}$$

The sum of the right hand sides of these equations becomes an expression of Sverdrup's vorticity equation if the sum of the divergences on the left hand sides vanishes, to satisfy the integrated continuity equation (2.18). Stommel noted that equations (2.23) and (2.24) were, respectively, identical with expressions for the integrated transports of the simple Ekman (spiral) wind drift (Ekman, 1905, p. 9) and for the vertical integrated geostrophic transport. It was thus suggested that the Sverdrup model described that particular transport pattern whose geostrophic divergence (2.26) compensated exactly for the integrated divergence induced in the Ekman frictional boundary layer (2.25) by the rotational wind field. This interpretation may require modification when boundary conditions are considered later (see the Introduction to Section 3).

Sverdrup continued his analysis by substitution of the meridional transport equation (2.20) into the continuity equation (2.18) to obtain an expression describing the zonal transport component (2.27).

$$\frac{\partial V}{\partial y} = -\frac{\partial U}{\partial x} = \frac{1}{2\Omega\cos\phi}\left[\left(\frac{\partial \tau_y}{\partial x} - \frac{\partial \tau_x}{\partial y}\right)\tan\phi + R\left(\frac{\partial^2 \tau_y}{\partial x \partial y} - \frac{\partial^2 \tau_x}{\partial y^2}\right)\right] \qquad (2.27)$$

If the zonal variation of the wind stress is specified, equation (2.27) may be integrated to define the zonal transport. Sverdrup chose to consider a zonally directed wind stress field, which was invariant in the x-direction, claiming this to represent a good approximation to conditions obtaining in the eastern equatorial Pacific Ocean, where application of the theoretical analysis was made. In this case integration of equation (2.27) yields:

$$U = \frac{x}{2\Omega\cos\phi}\left(\frac{\partial \tau_x}{\partial y}\tan\phi + \frac{\partial^2 \tau_x}{\partial y^2} R\right) \qquad (2.28)$$

where it has been assumed that $U = 0$ at $x = 0$. This boundary condition would permit either placing a rigid vertical wall (coast) at $x = 0$, or having flow and counterflow in such proportion at $x = 0$ that no net transport results through any given vertical column (Arthur, 1960, p. 294). Note the misprint in the last line of p. 322 of Sverdrup's paper: for M_o read M_x, corresponding to U in the present treatment. Equation (2.28) contains no provision for adjustment of the solution to give no net zonal transport across a western boundary wall, say, $U_L = 0$ at $x = L$. This is because neglect of both lateral stress and inertial terms has derived a first order differential equation of motion which admits the application of only one boundary condition. The model can thus not be applied to an ocean bounded by two meridional coasts. It is customary in studies of the dynamics of vertically integrated circulation models, first to identify the stress at the ocean surface with the stress exerted by the wind on that surface, and then to

proceed with the integration of the equations of motion, attending to the appropriate boundary value problem, independently of this stress specification, as was done in the Sverdrup analysis, above. However, E. S. M. Hassan (pers. comm.) has pointed out a danger of over-specification of the problem in this process. Setting the value of the stress acting in any surface is equivalent to a condition imposed on the vertical velocity gradient evaluated at that surface, or on the momentum exchange coefficient, A, or on both, through the relation

$$\vec{\tau} = A \frac{\partial \vec{V}}{\partial z} \tag{2.29}$$

Care must be taken, then, to avoid inconsistency in boundary conditions at lateral boundaries. In the Sverdrup analysis, above, for instance, setting $U = 0$ at a rigid meridional boundary implies the stronger condition $u = 0$ for all z in the unintegrated situation, and hence, that $\partial u/\partial z$ should also vanish for all z. This requirement is incompatible, in terms of equation (2.29) with the adoption of an arbitrary value of the wind stress component, τ_x, at the boundary.

The property of non-divergence imposed on the integrated transport field by equation (2.18) permits a succinct description of Sverdrup's solution in terms of a stream function, Ψ, defined by equations (2.30) and (2.31).

$$U \equiv \frac{\partial \Psi}{\partial y} \tag{2.30}$$

$$V \equiv - \frac{\partial \Psi}{\partial x} \tag{2.31}$$

$$\Psi = - \frac{Rx}{2\Omega \cos\phi} \mathrm{curl}_z \vec{\tau} \tag{2.32}$$

Equation (2.32) is the general expression for the stream function corresponding to a Sverdrup ocean bounded by an eastern meridional coastal wall. With the simplification of the wind stress field adopted for the derivation of equation (2.28), this expression reduces to

$$\Psi = \frac{Rx}{2\Omega\cos\phi} \frac{\partial \tau_x}{\partial y} \tag{2.33}$$

From equations (2.14), (2.15), and (2.33), the corresponding integrated pressure function, **P**, is determined to be

$$\mathbf{P} = x\left(\tau_x - R \tan\phi \frac{\partial \tau_x}{\partial y}\right) \tag{2.34}$$

where both stream and pressure functions have been chosen to vanish at $x = 0$, without loss of generality.

2.2. Properties of the Sverdrup solution

It will be noted that the Sverdrup solution will not permit consideration of circulation in a uniformly rotating ocean (including the non-rotating case) over which the Coriolis parameter, f, is constant. Essentially, this restriction stems from the simplified expression for friction used in the original equations of motion. For uniform rotation, equation (2.26) shows that there will be no geostrophic divergence, and hence, to satisfy continuity, only an irrotational field of applied wind stress, leading to no net circulation of water through any vertical volumn (not necessarily no flow through all points in that column) will enable Sverdrup's vorticity equation (2.19) to be satisfied.

The nature of the solution depends on the properties of the curl of the wind stress, and not on the magnitude and direction of the stress

vector itself. Westwards from the eastern boundary of an ocean, the planetary vorticity will always have the same sign as the local anemographic vorticity, and a state of vorticity balance as defined by equation (2.19) is thus possible. To the east of a western ocean boundary, however, these curl fields will always be of mutually opposite sign, and no basis exists for expressing vorticity balance. A Sverdrup solution must therefore always be built up westwards from a coast bounding an ocean in the east, if a meridional boundary is to be introduced.

There exists a particular pattern of applied wind stress which, although rotational, results in zero zonal transport everywhere. This pattern is derived from setting to zero the term in parentheses in equation (2.28)

$$R\tau_x'' + \tan\phi\ \tau_x' = 0 \qquad (2.35)$$

the general solution of which is

$$\tau_x = K_1 \sin\phi + K_2 \qquad (2.36)$$

where K_1, K_2 are constants of integration. The corresponding meridional transport is constant,

$$V = - K_1/2\Omega \qquad (2.37)$$

north-going if $K_1 < 0$, south-going if $K_1 > 0$.

The meridional transport will follow the direction of increasing wind stress, while the behavior of the zonal component depends on the relative magnitudes and signs of both gradient and curvature in the field of applied stress.

The properties of the Sverdrup solution with respect to one

form of variation in the applied wind stress curl are illustrated in figure 2.1. Streamlines of the vertically integrated mass transport are shown, generated by a zonal wind stress described by equation (2.38):

$$\tau_x = F\phi^{\eta} \tag{2.38}$$

where F and η are constants, and ϕ is the latitude expressed in radians. With this wind stress pattern, equation (2.33) for the stream function is transformed to equation (2.39).

$$\Psi = \frac{\eta x F \phi^{\eta-1}}{2\Omega \cos\phi} \tag{2.39}$$

The stream function plotted in figure 2.1 is the convenient non-dimensional quantity, $(2\Omega\Psi/FR)$. Ordinates represent degrees of latitude, and abscissae are values of the ratio (x/R). Variation of the parameter η in equation (2.38) successively over the values 1, 1/2, and 1/4 yielded the components (a), (b), and (c), respectively, of figure 2.1. In figure 2.1(a), the zonally directed stress is proportional to the latitude so that the stress curl is everywhere constant. In this case, the streamlines become concave toward the coast, with the zonally-directed transport component vanishing at the equator. This behavior is due, essentially, to the presence of the cosine term in equation (2.39), that is, to the variability of the Coriolis parameter along the meridian. The application of an anemographic curl everywhere just sufficient to counteract this planetary influence (equation (2.36)), will straighten these streamlines to lie parallel with the coastline (see figure 2.2). An increase in the magnitude of the anemographic influence beyond this point results in a change of curvature of the

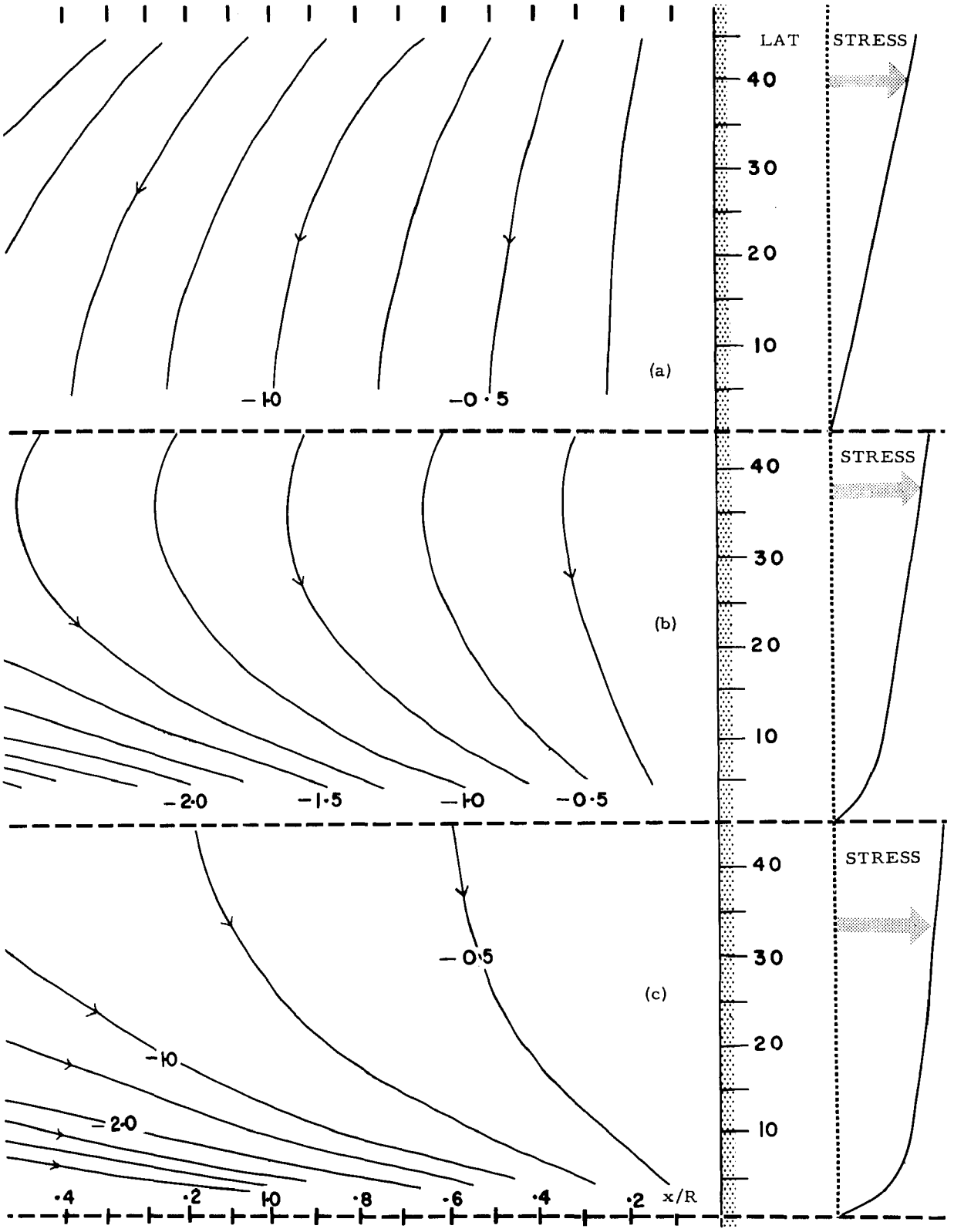

Figure 2.1 Streamlines of the vertically integrated mass transport in a Sverdrup ocean subject to zonally-directed wind stress proportional (a) to the latitude (b) to the square root of the latitude (c) to the fourth root of the latitude. Ordinates are in degrees of latitude, abscissae represent longitudes westwards from a meridionally oriented coast and streamlines map the non-dimensional function $2\Omega\Psi/FR$ as defined in equation (2.39).

transport streamlines. This progressive domination of the wind stress curl over the planetary vorticity may be seen in lower latitudes of figures 2.1(b) and (c) as the increasing anemographic vorticity in equatorial regions "pulls" streamlines in towards the coast.

Examples of circulation patterns in a Sverdrup ocean, resulting from the application of zonal wind stress patterns which vary sinusoidally in the meridional direction, appear in the literature. Reid (1948, figures 13 and 14) has approximated the circulation of the northeastern equatorial Pacific region, while Stommel (1957, figure 5) and Defant (1962, figure 265) have sketched the transport streamlines in an idealized Sverdrup ocean responding to such a stress distribution. Inasmuch as almost any zonally-directed wind stress pattern may be represented by a Fourier sine expansion, it is of interest to examine the nature of the response of the Sverdrup model to a generalized driving stress having the form of equation (2.40).

$$\tau_x = F \sin(n\phi + \phi_o) \qquad (2.40)$$

where F is again a constant, here representing the maximum value of the stress, ϕ_o is another constant, setting the phase of the sinusoidal variation with respect to the equator, and n is an integer which specifies the number of cycles of this driving function occurring in any given range of latitude. For such a stress distribution, the transport stream function and associated integrated pressure function are described, respectively, by equations (2.41) and (2.42).

$$\Psi = F \frac{nx \cos(n\phi + \phi_o)}{2\Omega \cos\phi} \tag{2.41}$$

$$P = Fx[\sin(n\phi + \phi_o) - n \tan\phi \cos(n\phi + \phi_o)] \tag{2.42}$$

For $\phi_o = 0$, values of the quantities $(2\Omega\Psi/nFR)$ and (P/FR) are tabulated in Appendix II over a range of latitude, ϕ, from 0° through 85° at intervals of 5°; over a range of "longitude", (x/R), from 0 through 1 at intervals of 0.05; and for values of the parameter (n) from 1 through 10. These tables will facilitate the construction of a Sverdrup solution for a general stress function which has been resolved into its Fourier sine components. To illustrate the present discussion, the transport and pressure function patterns for values of n = 1 and 6 have been plotted in detail in figures 2.2 and 2.3. For n = 1, the situation described by equation (2.36) is reproduced. In this situation the Coriolis term in the vertically integrated equation of motion exactly balances the applied wind stress, and the integrated pressure function is thus everywhere constant (zero, in terms of the formulation of equation (2.42)).

For positive integral values of $n > 1$, the characteristics of equations (2.41) and (2.42) are typified in figure 2.3 with n = 6. The circulation pattern is broken up into gyres bounded by those latitudes where the wind stress curl, and therefore by equation (2.20), the meridional transport component, vanishes. Except in the vicinity of the equator, these circulation cells are associated with rather similarly shaped "highs" and "lows" in the vertically integrated pressure distribution, as may be seen in figure 2.4. The sense of the circulation around these pressure features is essentially that expected from the

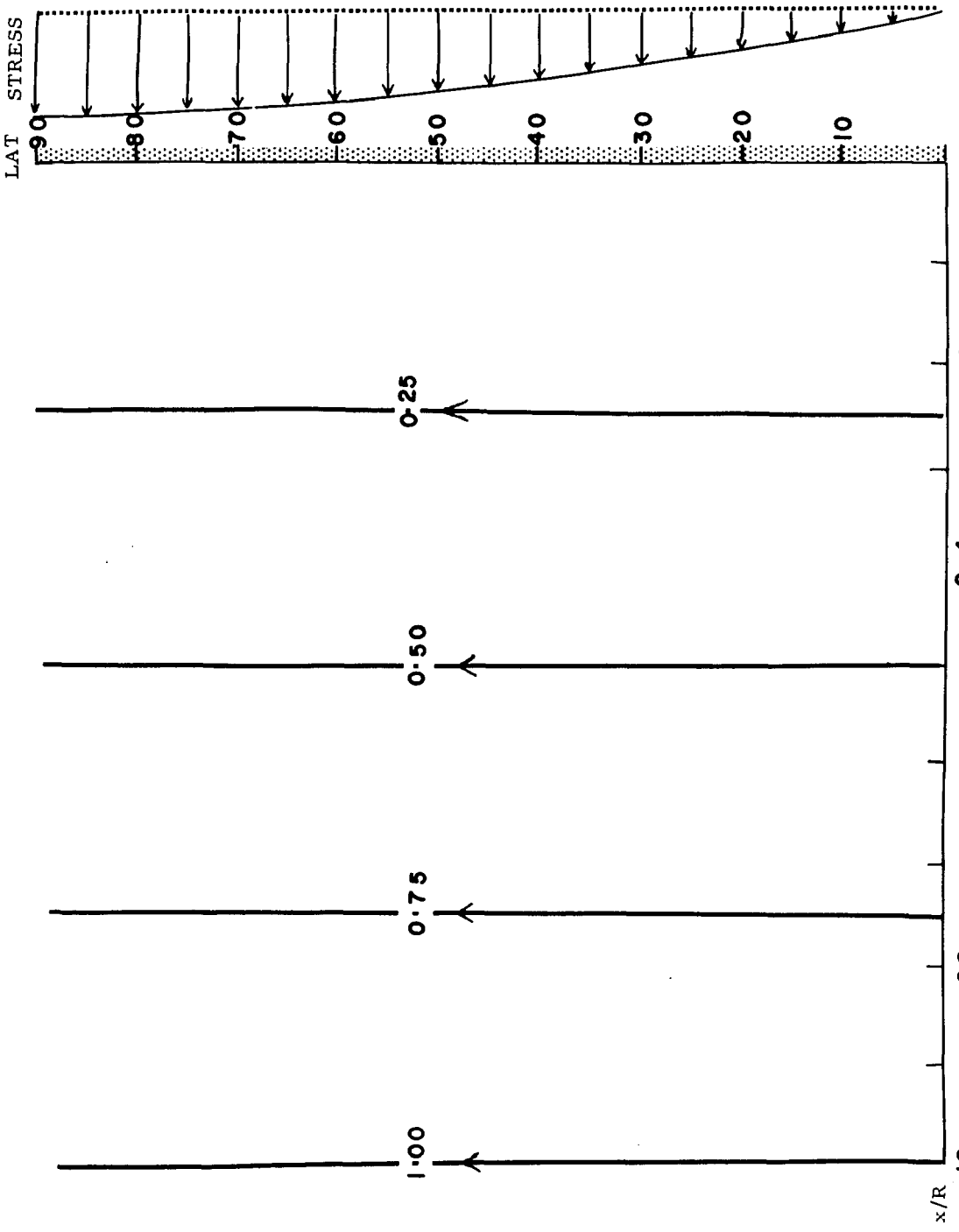

Figure 2.2 Streamlines of the vertically integrated mass transport in a Sverdrup ocean driven by a zonally-directed wind stress proportional to the sine of the latitude. Streamlines map the non-dimensional function $2\Omega\Psi/FR$ as defined in equation (2.41) for $n = 1$, $\phi_o = 0$.

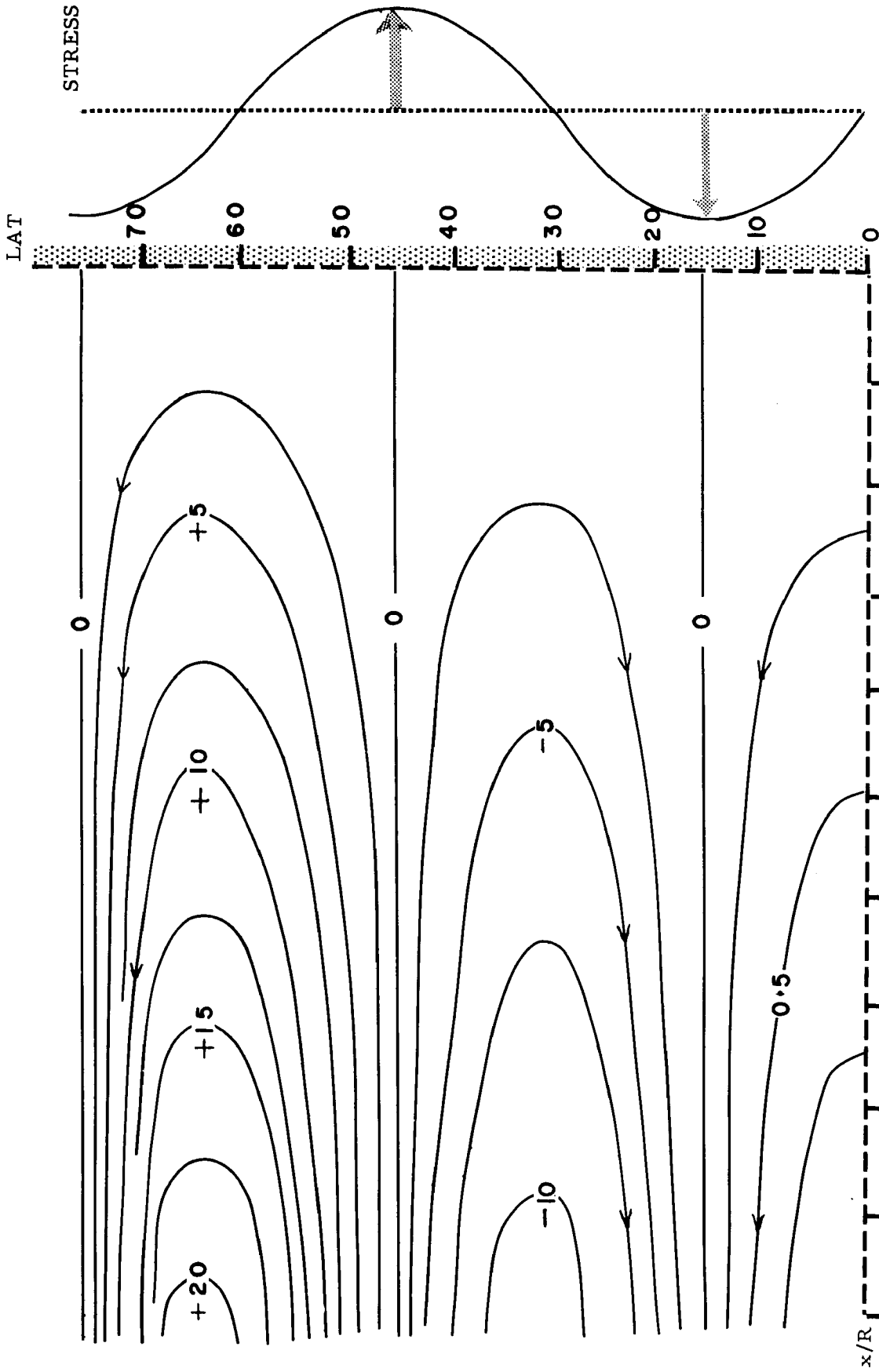

Figure 2.3 Behavior of the non-dimensional stream function, $2\Omega\Psi/FR$, for a Sverdrup ocean driven by a zonally-directed wind stress proportional to the sine of six times the latitude, according to equation (2.41) with $n = 6$, $\phi_o = 0$.

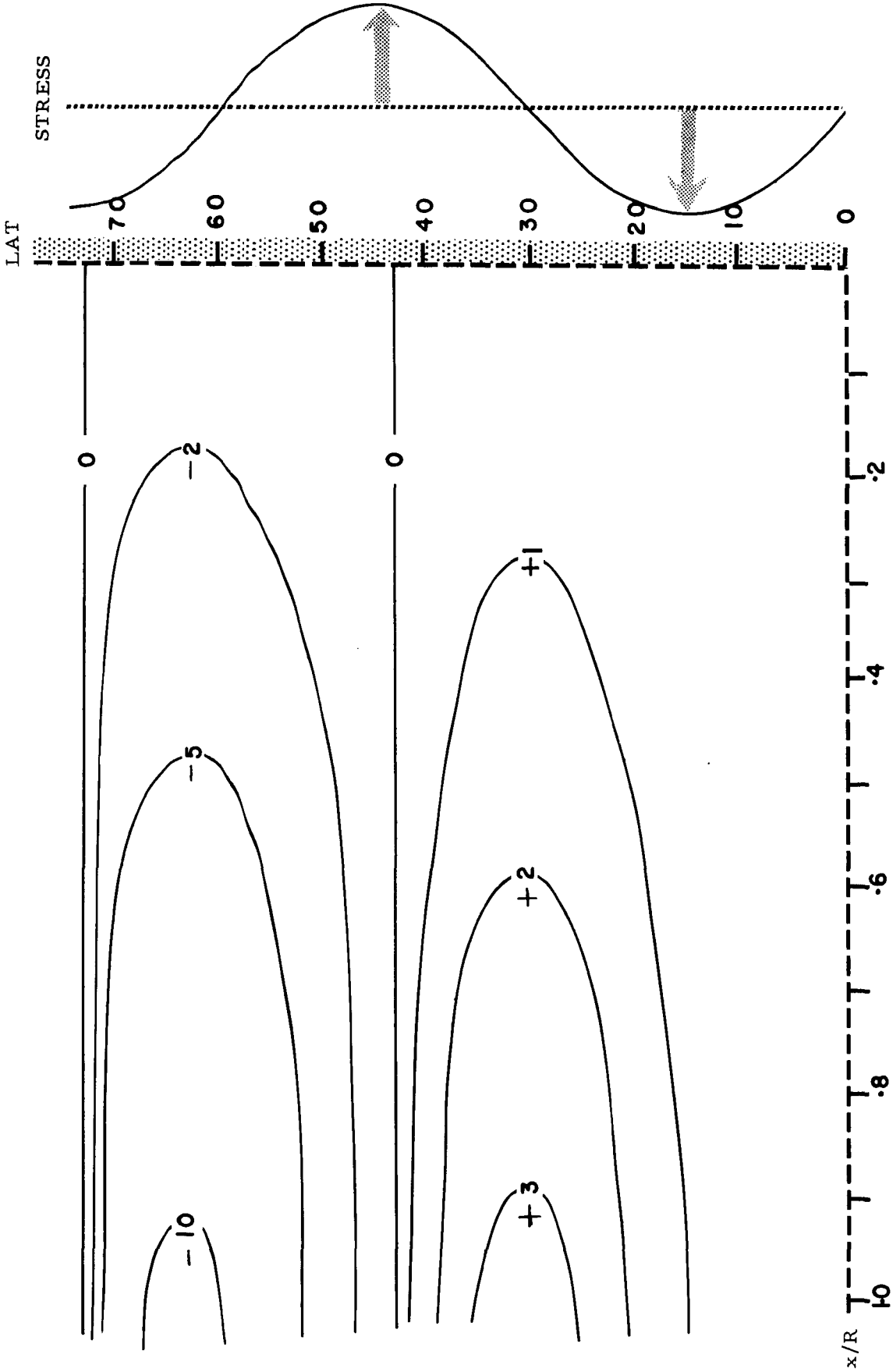

Figure 2.4 Behavior of the integrated pressure function, P/FR, in the Sverdrup ocean of Figure 2.3 according to equation (2.42) with n = 6, $\phi_o = 0$.

geostrophic relationship, --i. e., cyclonic flow around the "low" and anticyclonic flow around the "high". Except in the vicinity of the equator and near the meridional coastal boundary, the integrated pressure distribution is qualitatively that which would be expected from consideration of the divergence associated with the Ekman transports (equation (2.25)). For example, in figures 2.3 and 2.4, convergence of the integrated Ekman transport is expected in the vicinity of 30°N with an associated "high" in the pressure function, the reverse situation occurring around 60°N. It should be remembered, however, that the Sverdrup model differs fundamentally from the Ekman model in that no provision exists in the Sverdrup equations of motion (2.14, 2.15) for consideration of bottom stresses, or rather, the particular specification of vanishing bottom stress has been chosen, and divergence in the surface frictional boundary layer is balanced by a geostrophic divergence (equation (2.26)) rather than by divergence in the bottom frictional boundary layer of Ekman. This is why only a trivial solution of the Sverdrup problem is possible for a uniformly rotating ocean (compare the remarks on this point made earlier, following equation (2.34)). Because geostrophic divergence must always be present in the Sverdrup model, transport will never become purely zonally directed (except at latitudes of vanishing anemographic vorticity) and thus the effect of the meridional boundary extends westwards without limit. Flow is strictly geostrophic, with streamlines lying parallel to isobars of the $\mathbf{P}$-function, only where the applied wind stress vector is parallel to the gradient of the stream function. This condition will hold only at turning points of Ψ and $\mathbf{P}$. The latitudes of these turning points coincide and by differentiation

of equations (2.41) and (2.42) partially with respect to y, are seen to be specified by equation (2.43).

$$\tan\phi = n \tan n\phi \tag{2.43}$$

For the case $n = 6$, the roots of this equation lie at $\phi = 0$, and, approximately, 31° and 63°. The zeros of the **P**-function are characterized by equation (2.44)

$$n \tan\phi = \tan n\phi \tag{2.44}$$

i.e., $\phi = 0$, and approximately, 43° and 75° for $n = 6$. The stream function vanishes at the zeros of $\cos n\phi$, i.e., at $\phi = 15°$, 45°, and 75°, for $n = 6$.

2.3 The Sverdrup analysis in spherical coordinates

As was mentioned following equation (2.7), the full effects of the sphericity of the earth remain to be evaluated. To this end, it is instructive to perform the Sverdrup analysis in spherical horizontal coordinates, but neglecting convergence of the verticals in the relatively thin oceanic crust. If ϕ is again the geographic latitude and λ the longitude counted positive towards the east from a zero meridian at the coastal boundary, the vertically integrated equations of motion corresponding to equations (2.14) and (2.15) are

$$-fV = -\frac{1}{R\cos\phi}\frac{\partial P}{\partial \lambda} + \tau_\lambda \tag{2.45}$$

$$+fU = -\frac{1}{R}\frac{\partial P}{\partial \phi} + \tau_\phi \tag{2.46}$$

Perform the differentiation $\frac{1}{R\cos\phi}\frac{\partial}{\partial\lambda}$ on equation (2.46) and the differentiation $\frac{1}{R}\frac{\partial}{\partial\phi}$ on (2.45) and subtract the resulting equations. This gives the vorticity equation (2.47).

$$\frac{f}{R}\left(\frac{1}{\cos\phi}\frac{\partial U}{\partial \lambda}+\frac{\partial V}{\partial \phi}\right)+V\frac{\partial f}{\partial y}=\frac{1}{R}\left(\frac{1}{\cos\phi}\frac{\partial \tau_\phi}{\partial \lambda}-\frac{\partial \tau_x}{\partial \phi}\right)+\frac{\sin\phi}{R^2\cos^2\phi}\frac{\partial P}{\partial \lambda} \quad (2.47)$$

In spherical coordinates, the continuity equation $\nabla \cdot \vec{V} = 0$ may be written as equation (2.48).

$$\frac{1}{\cos\phi}\frac{\partial U}{\partial \lambda}+\frac{\partial V}{\partial \phi}=V\tan\phi \quad (2.48)$$

This equation introduces the effect of the convergence of the meridians on a spherical earth. Neglect of this effect in the previous rectangular coordinate analysis results in difficulties of application and interpretation at the higher latitudes. Use of equations (2.48) and (2.45) simplifies equation (2.47) to give equation (2.49), the vorticity equation corresponding to equation (2.19).

$$V\frac{\partial f}{\partial y}=\text{curl}_z\vec{\tau}+\frac{\tau_\lambda}{R}\tan\phi \quad (2.49)$$

From this equation, the meridional transport component is now determined to be

$$V=\frac{R\ \text{curl}_z\vec{\tau}+\tau_\lambda\tan\phi}{2\Omega\cos\phi} \quad (2.50)$$

If, following Sverdrup, the anemographic vorticity is simplified as

$$\text{curl}_z\vec{\tau}=\frac{1}{R}\frac{\partial \tau_\lambda}{\partial \phi} \quad (2.51)$$

the meridional transport becomes

$$V=\left(\tau_\lambda\tan\phi-\frac{\partial \tau_\lambda}{\partial \phi}\right)\frac{1}{2\Omega\cos\phi} \quad (2.52)$$

Differentiation of equation (2.52) partially with respect to ϕ, substitution for $(\partial U/\partial\phi)$ from equation (2.48) and for V from (2.52)

derives equation (2.53).

$$\frac{\partial U}{\partial \lambda} = \frac{1}{2\Omega}\left(\tau_\lambda \sec^2\phi + \tan\phi \frac{\partial \tau_\lambda}{\partial \phi} - \frac{\partial^2 \tau_\lambda}{\partial \phi^2}\right) \tag{2.53}$$

Integration of (2.53) with respect to λ, with $U = 0$ when $\lambda = 0$ gives the zonally directed component of the wind-driven transport as equation (2.54).

$$U = \frac{\lambda}{2\Omega}\left(\frac{\partial^2 \tau_\lambda}{\partial \phi^2} - \tan\phi \frac{\partial \tau_\lambda}{\partial \phi} - \tau_\lambda \sec^2\phi\right) \tag{2.54}$$

Because of equation (2.48), a stream function, Ψ, which contains the transport components U and V may be defined:

$$U = \frac{1}{R}\frac{\partial \Psi}{\partial \phi} \tag{2.55}$$

$$V = -\frac{1}{R\cos\phi}\frac{\partial \Psi}{\partial \lambda} \tag{2.56}$$

and it may be evaluated from the relation preceeding as

$$\Psi = \frac{R\lambda}{2\Omega}\left(\frac{\partial \tau_\lambda}{\partial \phi} - \tau_\lambda \tan\phi\right) \tag{2.57}$$

The associated pressure function is

$$P = R\lambda\cos\phi\left(\tau_\lambda \sec^2\phi - \tan\phi \frac{\partial \tau_\lambda}{\partial \phi}\right) \tag{2.58}$$

For $\tau_\lambda = F \sin n\phi$, these functions may be written

$$\Psi = \frac{FR\lambda}{2\Omega\cos\phi}(n \cos n\phi \cos\phi - \sin n\phi \sin\phi) \tag{2.59}$$

$$P = FR\lambda\left(\frac{\sin n\phi}{\cos\phi} - n\sin\phi \cos n\phi\right) \tag{2.60}$$

In spherical coordinates, it is physically appropriate that $\tau_\lambda = 0$ at $\phi = \pi/2$ for all n, and thus odd values of n must be excluded from consideration in the formulae above. Both the stream and pressure

functions (2.59) and (2.60) remain defined over the whole interval $0 \leq \phi \leq \pi/2$, for factorization of $\sin n\phi$ (e.g., Durell, 1946, p. 224) reduces the ratio $(\sin n\phi / \cos\phi)$ for n <u>even</u>, to

$$\frac{\sin n\phi}{\cos\phi} = n \sin\phi \prod_{r=1}^{\frac{1}{2}(n-1)} \cdot \left[1 - \frac{\sin^2\phi}{\sin^2 (\frac{r\pi}{n})} \right] \qquad (2.61)$$

which is bounded at $\phi = \pi/2$ in spite of the presence of the cosine term in the denominator. In contrast, although the expression would not find application at high latitudes, it may be noticed that the Cartesian form of the stream function, equation (2.41) with $\phi_o = 0$, remains regular at $\phi = 90°$ for n <u>odd</u>, for

$$\lim_{\phi \to \frac{\pi}{2}} \left(\frac{\cos n\phi}{\cos\phi} \right) = \lim_{\phi \to 0} \left[\frac{\cos n \left(\frac{\pi}{2} - \phi \right)}{\cos \left(\frac{\pi}{2} - \phi \right)} \right] = n(-1)^{\frac{1}{2}(n-1)} \qquad (2.62)$$

Values of the stream and pressure functions tabulated for the Cartesian analysis in Appendix II , and described following equation (2.42), are accompanied by the corresponding values derived from the spherical analysis, values of λ for the latter ranging from 0° through 85° in steps of 5°. Graphical comparison of the two sets of results is made in figures 2.5 and 2.6, where the meridional variation of Ψ, P, and τ_x is plotted for $x = R$, $\lambda = 85°$. If the spherical coordinate analysis is compared with the rectangular analysis, it may be seen that (a) the discrepancy between adjacent extreme values of the stream and pressure function appearing in the rectangular analysis is considerably reduced in the spherical, and (b) a shift towards lower latitudes of both the zeros and turning points of Ψ and P results in a greater degree of meridional symmetry in

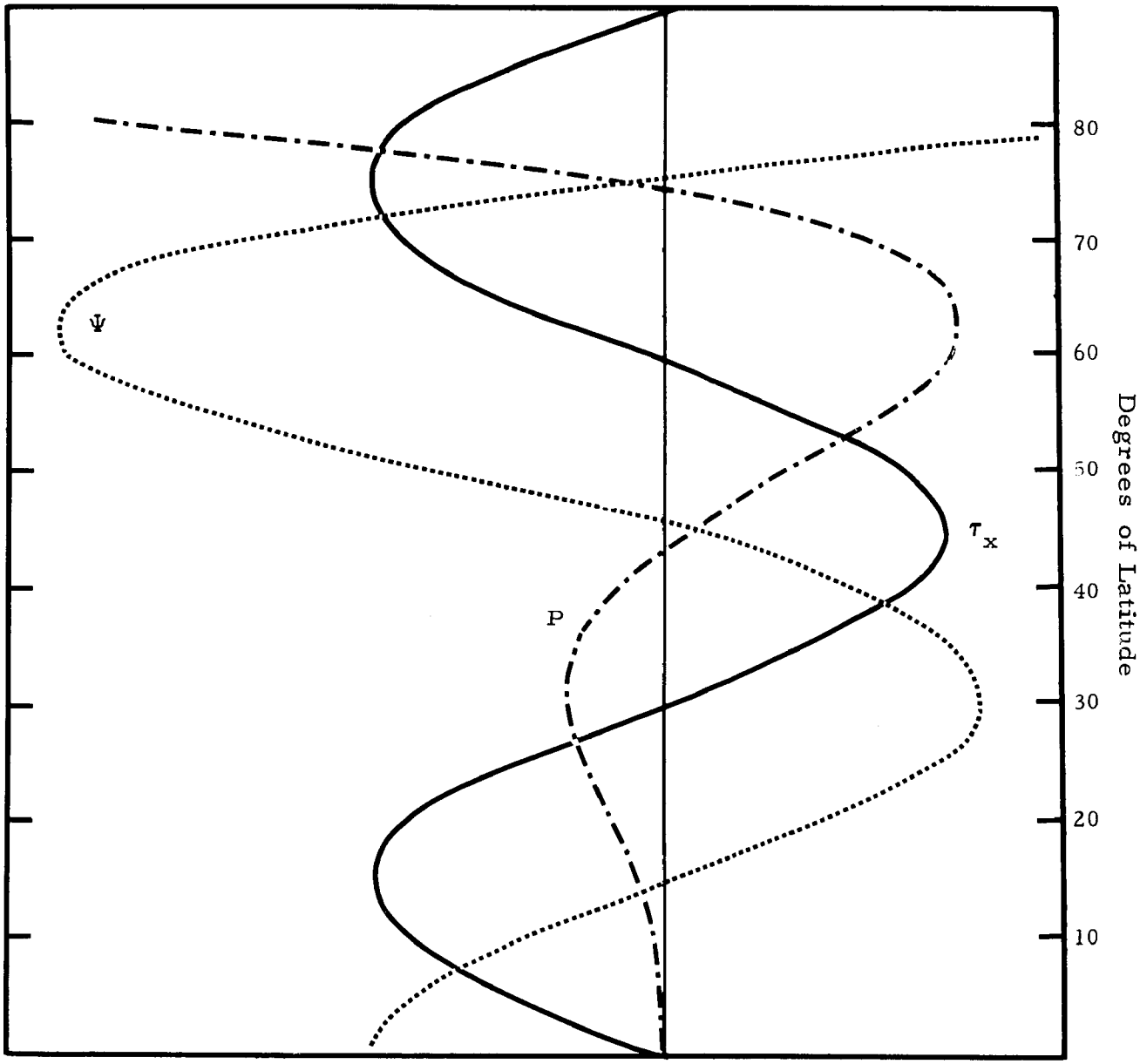

Figure 2.5 Plot of the relative meridional variation of the wind stress, τ, stream function Ψ, and pressure function P, in arbitrary units, for the rectangular Cartesian Sverdrup ocean represented by Figures 2.3 and 2.4.

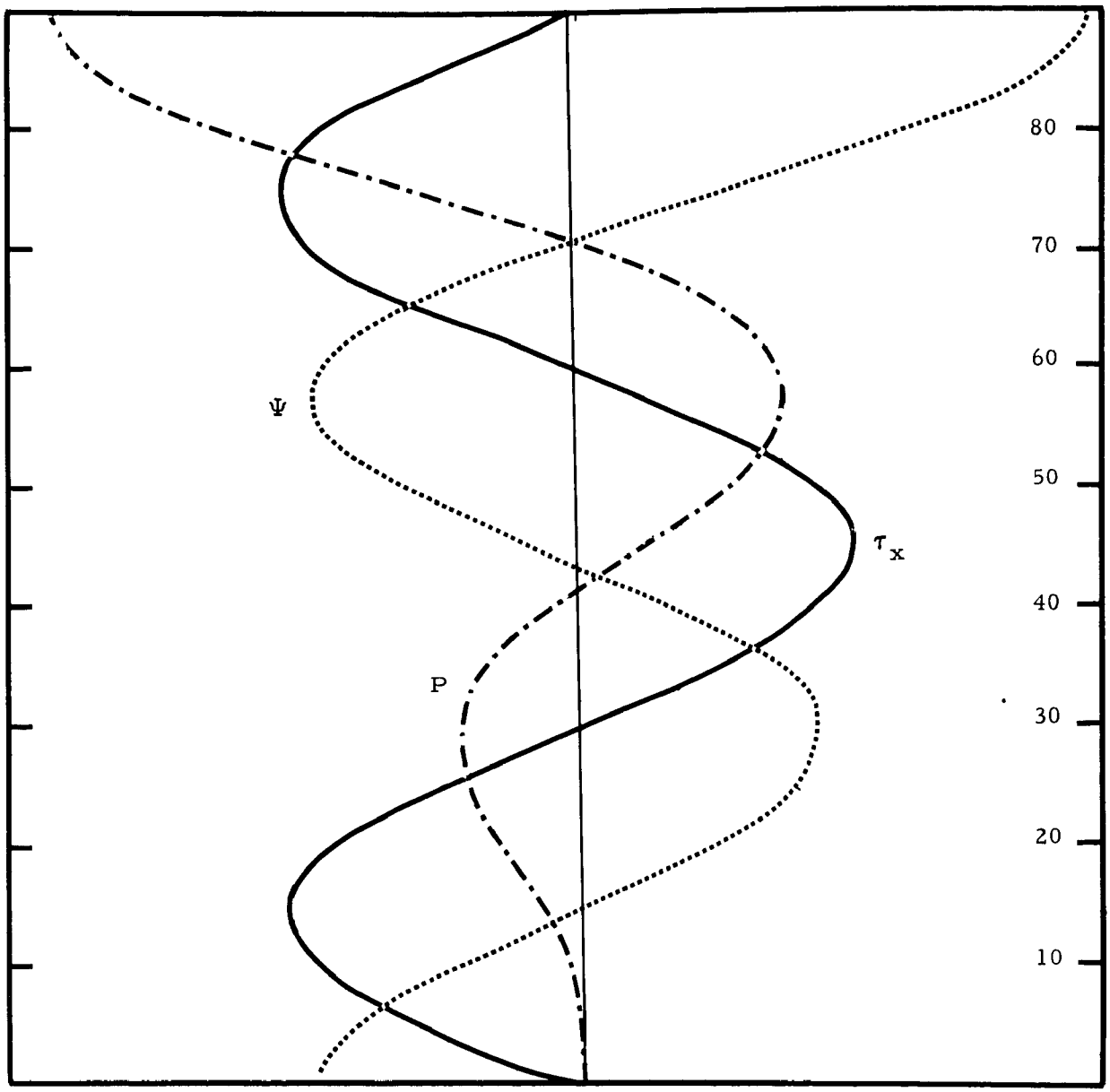

Figure 2.6 Plot of the relative meridional variation of the wind stress τ_x, stream function Ψ, and pressure function P, in arbitrary units, for the spherical coordinate Sverdrup ocean represented by equations (2.59) and (2.60), with n = 6.

gyre structure for the spherical analysis as compared with the rectangular analysis.

2.4 Response of a Sverdrup ocean to a meridionally-directed wind stress

A brief examination of the response of the Sverdrup model to a meridionally directed wind stress with sinusoidal zonal variation will complete the present section.

Consider a wind stress field specified by equation (2.63).

$$\tau_x = 0 \; ; \quad \tau_y = -G \sin\left(n\pi \frac{x}{R}\right) \tag{2.63}$$

From equation (2.32) the streamlines of the vertically integrated transport are described in the plane coordinate system by equation (2.64)

$$\Psi = \frac{n\pi RG}{2\Omega \cos\phi} \cdot \frac{x}{R} \cdot \cos\left(n\pi \frac{x}{R}\right) \tag{2.64}$$

from whence the zonally-directed transport component is given as equation (2.65),

$$U = \frac{n\pi G}{2\Omega \cos\phi} \cdot \frac{x}{R} \cdot \tan\phi \cos\left(n\pi \frac{x}{R}\right) \tag{2.65}$$

and the meridionally-directed component as equation (2.66)

$$V = \frac{n\pi G}{2\Omega \cos\phi} \left[n\pi \frac{x}{R} \sin\left(n\pi \frac{x}{R}\right) - \cos\left(n\pi \frac{x}{R}\right) \right] \tag{2.66}$$

The geometry of this response is illustrated in figure 2.7 for $n = 2$ by a plot of the function $(2\Omega\Psi/\pi RG)$ in a portion of the $(\phi, x/R)$ plane. The integrated transport is entirely in the zonal direction at those values of (x/R) for which

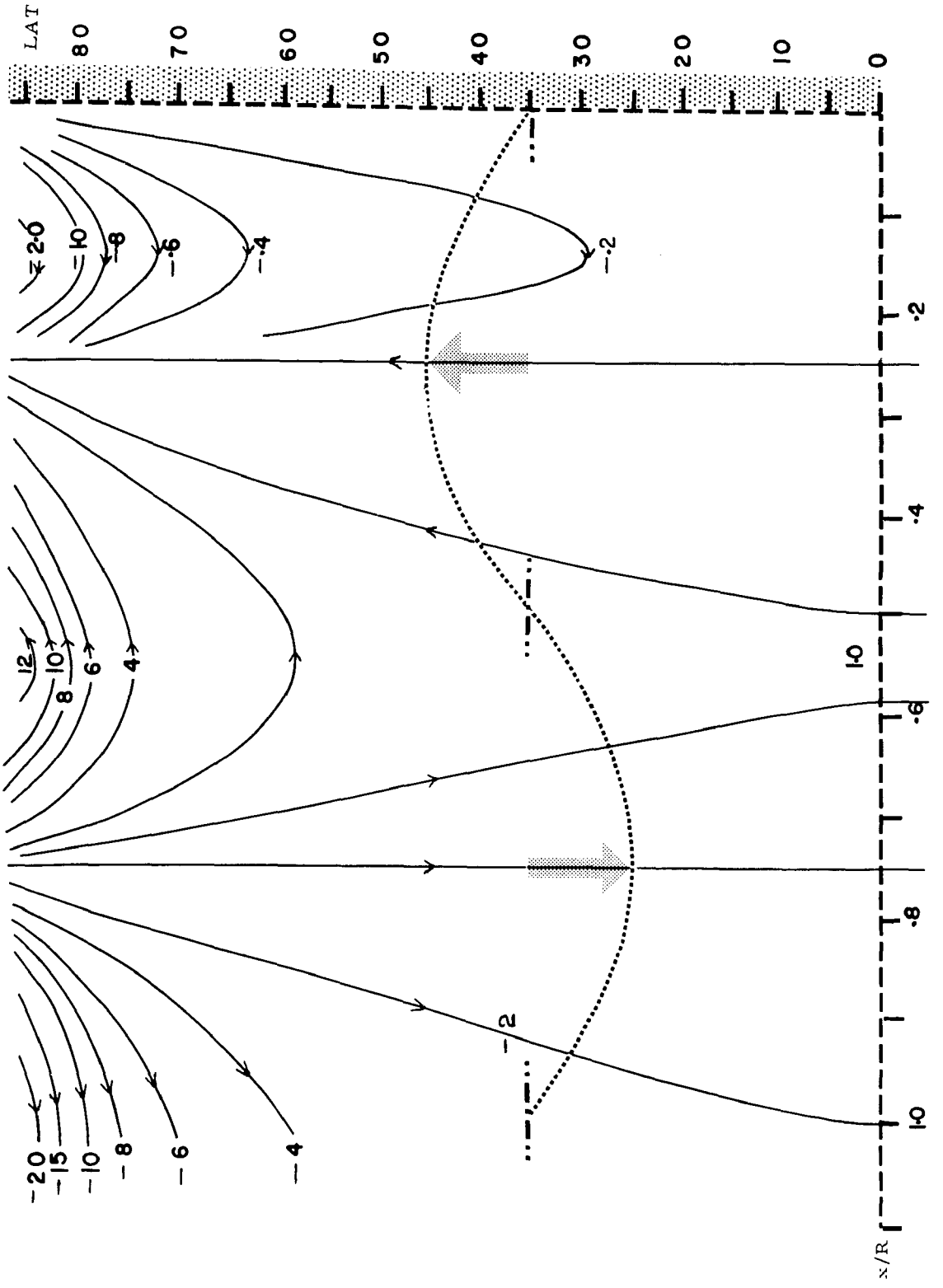

Figure 2.7 Behavior of the non-dimensional stream function $2\Omega\Psi/\pi RG$ (equation (2.64), $n = 2$) in a Sverdrup ocean driven by a meridionally directed wind stress varying sinusoidally in the zonal direction as shown by the broken curve superimposed on the full streamlines.

$$\cot\left(n\pi \frac{x}{R}\right) = \left(n\pi \frac{x}{R}\right) \tag{2.67}$$

that is, at the turning points of the stream function, Ψ, where $V = 0$. The first three roots of equation (2.67) are, approximately, for $n = 2$, $\frac{x}{R} = 0.14$, 0.54, and 1.02 radians. Transport becomes wholly directed in the meridian where $U = 0$, that is, at the zeros of the wind stress curl, or at $\frac{x}{R} = 0$, 0.25, 0.75, $\cdots$. The effect of the planetary vorticity, from which is derived the members $\tan\phi$ and $\cos\phi$ of the above expressions, shows in figure 2.7 as a progressive poleward increase in the zonal stream function gradient in the neighborhood of the meridians of vanishing anemographic vorticity. This effect would be removed if the magnitude of the meridional wind stress decreased according to the cosine of the latitude, for, consider the effect of a stress described by equation (2.68).

$$\tau_y = - G \sin\left(n\pi \frac{x}{R}\right) \cos(\phi + \phi_o) \tag{2.68}$$

In this case the stream function is described by equation (2.69).

$$\Psi = \frac{n\pi RG}{2\Omega}\left(\frac{x}{R}\right) \cos\left(n\pi \frac{x}{R}\right)(\cos\phi_o - \tan\phi \sin\phi_o) \tag{2.69}$$

This equation represents purely meridional transport if $\phi_o = 0$. For $|\phi_o| > 0$, the cosine term in the wind stress curl decreases polewards either faster or slower than the matching term in the planetary vorticity, depending on the sign of ϕ_o, and corresponding changes in the zonal transport component will appear. The nature of these changes is illustrated by figures 2.8 and 2.9 which plot $2\Omega\Psi/\pi RG$ derived from equation (2.69) for $n = 2$. In

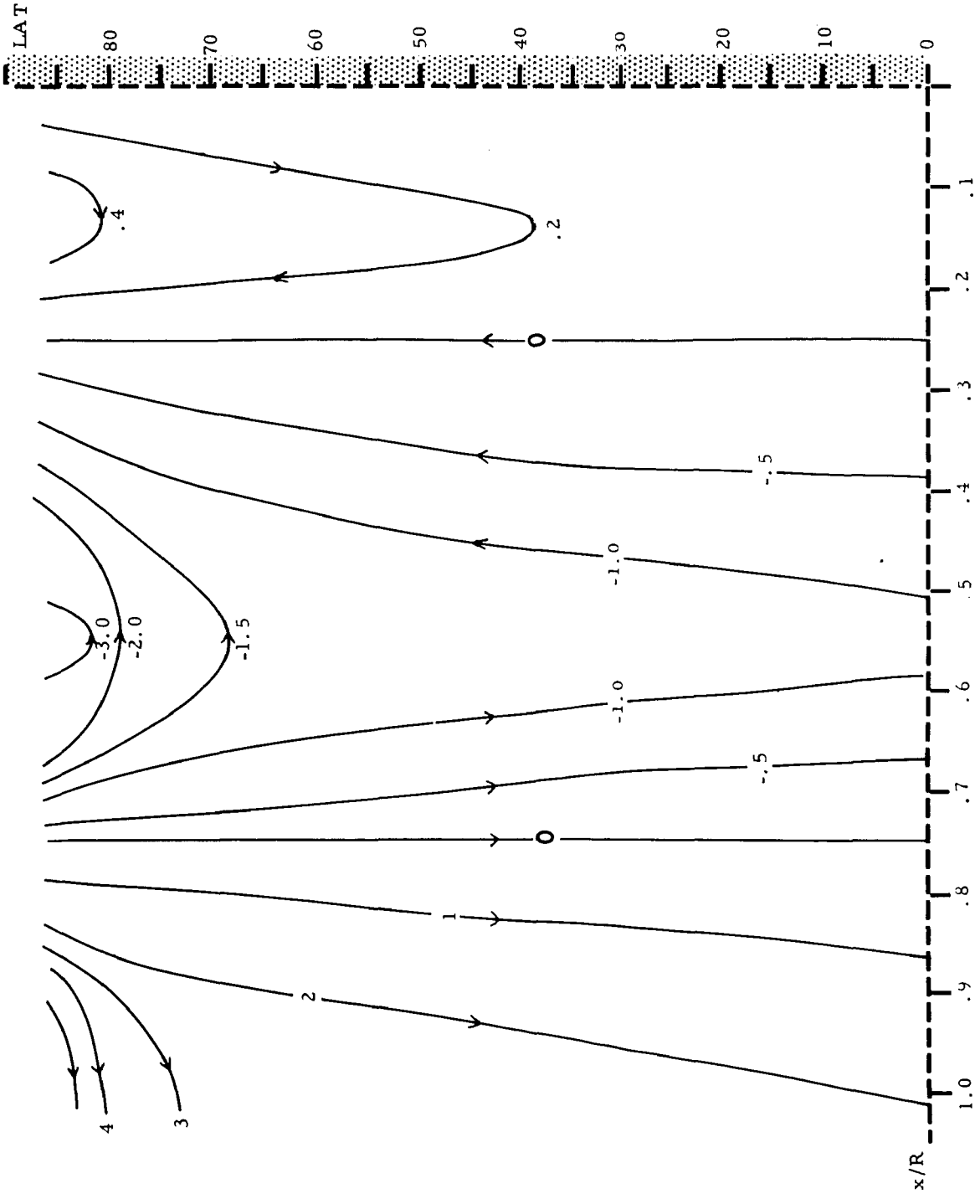

Figure 2.8 Behavior of the non-dimensional stream function $2\Omega\Psi/\pi RG$ for a Sverdrup ocean driven by a meridionally directed wind stress which varies sinusoidally in both zonal and meridional directions according to equation (2.68) with $\phi_o = 10°$.

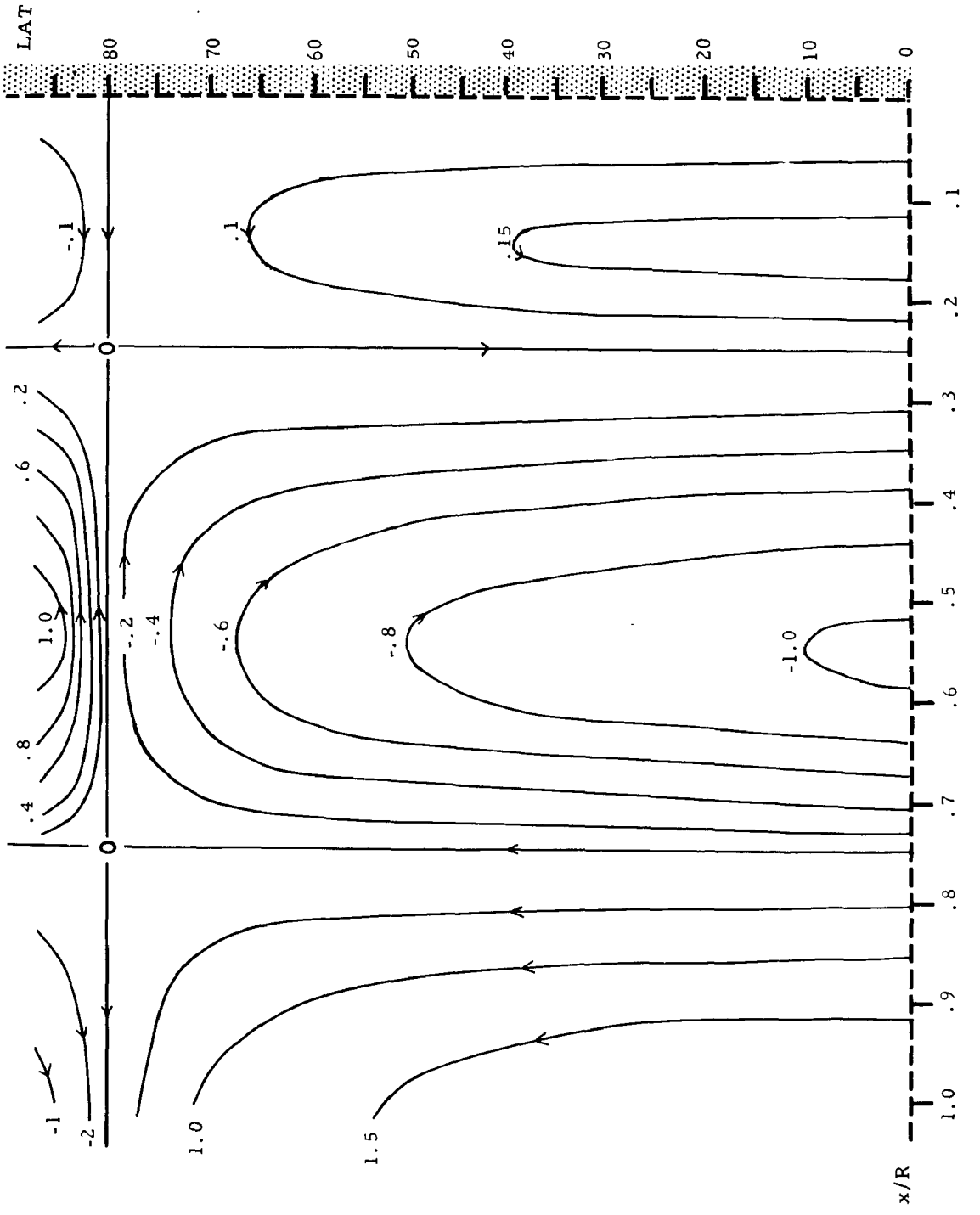

Figure 2.9 Behavior of the non-dimensional stream function $2\Omega\Psi/\pi RG$ for a Sverdrup ocean driven by a meridionally directed wind stress which varies sinusoidally in both zonal and meridional directions according to equation (2.68) with $\phi_o = +10°$.

figure 2.8, $\phi_o = -10°$, while for figure 2.9, $\phi_o = +10°$. If the convergence of the meridians on a spherical earth is included in the vorticity relationships, the situation is rather different. For a meridional stress pattern without meridional variation,

$$\tau_\phi = -G \sin n\lambda \tag{2.70}$$

equation (2.57) shows that streamlines will lie on meridians. Introduction of meridional variation, however, is accompanied by the formation of characteristic zonal transport patterns of the kind described above.

3. Introduction of the frictional vorticity

3.1 The rôle of friction in vorticity balance

Referring to the ocean circulation problem, Defant (1962, p. 580) stated: "Sverdrup (1947) has shown that a steady state solution can be found ··· even when frictional effects are neglected." Now the driving of the ocean circulation by the wind is primarily due to frictional coupling between air and ocean at their interface. This coupling is then transferred through successively deeper layers in the ocean by the vertical exchange of horizontal momentum because of turbulence in the water. This process is responsible for much of the frictional dissipation of the work done by the wind stress on the sea surface. Perhaps, then, a more revealing statement would be that of Stommel (1960, p. 156) who pointed out that "the rôle assigned to friction (in the Sverdrup analysis) is comparatively insignificant (compared to later models) ··· dynamically important only in the Ekman wind-drift layer" (parentheses added). In Stommel's inter-

pretation, then, the Sverdrup analysis is essentially a study of the geostrophic circulation in a frictionless water mass, on the upper surface of which lies a frictionless boundary layer. Anisobaric components appearing in the vertically integrated transport would be derived from phenomena occurring in this boundary layer. If the meridional boundary introduced into the Sverdrup model is to be interpreted as an impermeable wall (coast), however, then equation (2.23) may not necessarily properly be identified with a thin surface boundary layer. Derivation of the latter assumes an unbounded ocean. Indeed, Hassan (1962) has presented evidence to suggest that the Ekman "depth of frictional influence" may extend its spiral characteristics throughout the whole column of circulating water in an ocean closed by coastal boundaries. Both the Ekman and Hassan analyses would be more versatile in application if means could be found for admitting the free development of a vertical velocity field. This would permit closer study of the influence of coastal boundaries on the properties of the "surface frictional boundary layer".

Association of frictional processes with regions of the ocean other than a surface boundary layer, results in greater mathematical complexity than was evident in Section 2, but at the same time gives greater freedom in interpretation and application of the solutions derived. Within the class of linear, vertically integrated circulations discussed in the present work, two examples of this enlargement on the dynamical role of friction are mentioned, and one of these is chosen for detailed study in the section following.

(a) Munk (1950) retained the concept of baroclinic stratification and consequent formation of a motionless layer in which

the horizontal stress disappears, leaving only the stress at the sea surface in the vertically integrated equations of motion. In addition, however, he introduced further stresses throughout the water mass caused by the turbulent exchange of horizontal momentum across horizontal velocity gradients.

(b) Providing both comparison and contrast with this technique, Stommel (1948) retained the relatively simple equations of motion used by Sverdrup but considered a homogeneous (ρ = constant) ocean rather than one stratified baroclinically. In such a condition, currents responding to pressure gradients induced by the wind at the surface extend without vertical shear to the physical ocean bottom, irrespective of the depth. In this case, it becomes physically appropriate to introduce a lower frictional boundary layer in which the velocity may vanish at the sea bottom. Such a concept requires retention in the dynamical argument of the bottom stress terms which previously have been neglected in the derivation of equations (2.14) and (2.15) from (2.8) and (2.9).

Stommel's modelling of this bottom stress, and Munk's expression for lateral friction each serve to introduce velocity-dependent dissipative terms into the equations of motion. The vorticity equation formed from equations thus augmented, contains a term additional to the planetary and anemographic terms already defined. This new term will be called the <u>frictional vorticity</u>. The greater sophistication of the new vorticity equation derives, in each of the cases mentioned above, from an increase in the order of the differential equation introduced by the frictional vorticity. This

gives greater freedom in boundary value specification than was permitted by the Sverdrup model.

3.2 The Stommel model

The details of Stommel's analysis will now be pursued in some detail. The presentation in its original published form commences with the set of vertically integrated equations of motion reproduced here as equation (3.8) and (3.9). In the interests of continuity in the present work, a derivation of these equations from the fundamental considerations of the previous section will be offered.

In this model the sea bottom is a level surface and the z-axis is positively directed vertically upwards with its origin in this surface. The ocean is assumed to be in hydrostatic equilibrium, that is to say

$$\frac{\partial p}{\partial z} = \rho g \qquad (3.1)$$

This assumption may be used in place of a third Cartesian component of the vector equation of motion, (1.2) for an unaccelerated model provided $2\rho\Omega u \cos\phi$ is very much smaller than either of the terms in equation (3.1), as may be seen from equation (2.3). The use of this assumption is almost always thoroughly justified in dynamical meteorology and oceanography. The pressure at any given level $z = z_o$ may thus be determined by integration of the hydrostatic equation (3.1) between that level and the sea surface at $z = D + \zeta$

$$p(z_o) = \rho g (D - z_o + \zeta) \qquad (3.2)$$

where D is the (constant) depth of the motionless ocean. From equation (3.2), horizontal pressure gradients may thus be expressed in terms of the slope of the sea surface, for such a homogeneous ocean, permitting the equations of horizontal motion (2.6) and (2.7) to be rewritten.

$$- fv = - g \frac{\partial \zeta}{\partial x} + \frac{1}{\rho} \frac{\partial \tau_x}{\partial z} \tag{3.3}$$

$$+ fu = - g \frac{\partial \zeta}{\partial y} + \frac{1}{\rho} \frac{\partial \tau_y}{\partial z} \tag{3.4}$$

These equations may now be integrated with respect to z between the bottom at $z = 0$ to the free surface at $z = D + \zeta$ to give equations (3.5) and (3.6).

$$0 = - g \frac{\partial \zeta}{\partial x} (D + \zeta) + f \bar{v}(D + \zeta) + \frac{1}{\rho} [(\tau_x)_{D+\zeta} - (\tau_x)_o] \tag{3.5}$$

$$0 = - g \frac{\partial \zeta}{\partial x} (D + \zeta) - f \bar{u}(D + \zeta) + \frac{1}{\rho} [(\tau_y)_{D+\zeta} - (\tau_y)_o] \tag{3.6}$$

$\bar{u}$ and $\bar{v}$ represent integral mean values over depth of the horizontal velocity components. This provision, which does not appear in Stommel's development, has been inserted because vertical velocity gradients will be found in the surface and bottom frictional ("spiral") boundary layers, even though the homogeneous water assumption will ensure the flow of gradient currents whose velocity is invariant with depth. Such a provision would make unnecessary Stommel's (1960, p. 88) assumption that the wind acts on the water "essentially as a body force, and not as a surface stress."

As in the Sverdrup analysis, Stommel identified the quantity

$(\vec{\tau})_{D+\zeta}$ with the wind stress on the sea surface, the components of which will be noted hereafter simply as τ_x and τ_y. For simplicity, the bars over the quantities u and v will also be omitted in the discussion following. Stommel expressed the components of the horizontal stress acting on the sea bottom as in equations (3.7).

$$(\tau_x)_o = Ku \; ; \qquad (\tau_y)_o = Kv \tag{3.7}$$

where K is a constant. This formulation has been chosen more with an eye to the subsequent mathematical development than out of any regard for the physics of the lower boundary layer. Some notes on this form of friction appear in a later section. With these substitutions, the vertically integrated equations of motion are now expressed as equations (3.8) and (3.9).

$$0 = -\rho g \frac{\partial \zeta}{\partial x}(D + \zeta) + f\rho v(D + \zeta) - Ku + \tau_x \tag{3.8}$$

$$0 = -\rho g \frac{\partial \zeta}{\partial y}(D + \zeta) - f\rho u(D + \zeta) - Kv + \tau_y \tag{3.9}$$

These equations are now identical with Stommel's (1948) introductory equations [1] and [2] except for the appearance of the factor ρ, omission of which from the original equations was noted by Montgomery (1959). Alternatively, Stommel could have regarded the constants F and R in his equations as containing the density, implicitly, since this is constant. The integrated continuity equation, developed previously as equation (2.18), would appear in the present notation as equation (3.10).

$$\frac{\partial}{\partial x}[u(D + \zeta)] + \frac{\partial}{\partial y}[v(D + \zeta)] = 0 \tag{3.10}$$

Formation of the vorticity equation by cross-differentiation and subtraction in equations (3.8), (3.9), together with the use of equation (3.10), yields equation (3.11).

$$K\left(\frac{\partial v}{\partial x} - \frac{\partial u}{\partial y}\right) + \rho(D + \zeta)\frac{\partial f}{\partial y} v = \text{curl}_z \vec{\tau} \qquad (3.11)$$

This equation expresses a state of balance between frictional, planetary, and anemographic vorticities, respectively, reading the terms from left to right. A stream function, Ψ, may be defined from equation (3.10) as follows:

$$\frac{\partial \Psi}{\partial y} = u(D + \zeta) \qquad (3.12)$$

$$\frac{\partial \Psi}{\partial x} = -v(D+\zeta) \qquad (3.13)$$

Introduction of this function gives the vorticity equation (3.11) in the form (3.14).

$$\nabla^2\Psi - \frac{1}{D}(\nabla\Psi \cdot \nabla\zeta) + \rho \frac{D}{K}\frac{\partial f}{\partial y}\frac{\partial \Psi}{\partial x} = -\frac{D}{K}\text{curl}_z \vec{\tau} \qquad (3.14)$$

where the del operator contains derivatives with respect to x and y, only, and the small displacement ζ is neglected where it appears in sum with the depth D. This treatment has reproduced the vorticity equation derived by Stommel (1948, equation [9]] with the addition, here, of the scalar product on the left hand side of equation (3.14). This term arises through an important difference between this treatment and the original. Stommel assumed that the assumption $\zeta << D$ permits reduction of the integrated continuity equation to the form

$$\frac{\partial u}{\partial x} + \frac{\partial v}{\partial y} = 0 \qquad (3.15)$$

to the same degree of approximation as was employed in simplifying the vorticity equation, in spite of the appearance of the term $(D + \zeta)$ under a differential operator in equation (3.10). From equation (3.15) a stream function

$$u = \frac{\partial \Psi}{\partial y} \tag{3.16}$$

$$v = -\frac{\partial \Psi}{\partial x} \tag{3.17}$$

was introduced into equation (3.11) to give the vorticity equation in the form

$$\nabla^2 \Psi + \left(\rho \frac{D}{K} \frac{\partial f}{\partial y}\right) \frac{\partial \Psi}{\partial x} = -\frac{1}{K} \operatorname{curl}_z \vec{\tau} \tag{3.18}$$

It thus appears that Stommel's treatment involves the unstated assumption that the streamlines of mean flow are everywhere parallel to the contours of the sea surface topography, so that the identity of equations (3.14) and (3.18) may be assured. This assumption is unduly restrictive, and is not compatible with the properties of particular solutions of (3.18) discussed later. A derivation of equation (3.18) which is not subject to this restriction may be offered if some modification of the bottom stress formulation (3.7) is permitted. Since this formulation is quite arbitrary, little objection can be raised to a modification in terms of equation (3.19).

$$(\tau_x)_o = Ku(D + \zeta) \; ; \qquad (\tau_y)_o = Kv(D + \zeta) \tag{3.19}$$

Use of equations (3.8), (3.9), (3.10), and (3.19) now permits the derivation of equation (3.18) without restriction on $\nabla\zeta$.

Equation (3.18) is linear in the independent variable Ψ and thus its complete solution may be expressed as the sum of a particular

integral and a complementary function, the latter being the general solution of the equation homogeneous in Ψ,

$$\nabla^2\Psi + a \frac{\partial \Psi}{\partial x} = 0 \tag{3.20}$$

where $a \equiv \rho \frac{D}{K} \frac{\partial f}{\partial y}$. If a is constant and the Rossby parameter is assumed to be invariant in the meridian, the complementary function is readily found, for the coordinates are separable. Assumption of a solution of equation (3.20) having the form $X(x) \cdot Y(y)$ yields the ordinary differential equations (3.21).

$$\frac{1}{X} \frac{d^2X}{dx^2} + \frac{a}{X} \frac{dX}{dx} = - \frac{1}{Y} \frac{d^2Y}{dy^2} = k \tag{3.21}$$

where k is the separation constant, which in general may be any complex number, including zero. Stommel considered that solution generated by a real positive separation constant, $k = n^2$. This reduces (3.21) to equations (3.22) and (3.23).

$$\frac{d^2X}{dx^2} + a \frac{dX}{dx} - n^2X = 0 \tag{3.22}$$

$$\frac{d^2Y}{dy^2} + n^2Y = 0 \tag{3.23}$$

The general solutions of these equations have the form

$$X = pe^{Ax} + qe^{Bx} \tag{3.24}$$

$$Y = c \sin ny + h \cos ny \tag{3.25}$$

where p, q, c, and h are constants of integration and A, B are the roots of the characteristic equation of (3.22), that is

$$A = -\frac{a}{2} + \left[\left(\frac{a}{2}\right)^2 + n^2\right]^{1/2} \tag{3.26}$$

$$B = -\frac{a}{2} - \left[\left(\frac{a}{2}\right)^2 + n^2\right]^{1/2} \tag{3.27}$$

The general form of the solution of equation (3.20) is thus

$$\Psi_h = \int_0^\infty \left[p(n)e^{A(n)x} + q(n)e^{B(n)x}\right] [c(n) \sin ny + h(n) \cos ny]\, d(n^2) \tag{3.28}$$

where the integral over n is necessary because no restriction has yet been placed on this parameter. The various constants appearing in equation (3.28) may be defined by specification of appropriate boundary conditions. Stommel considered a rectangular ocean of zonal width (a) and of meridional width (b), and allowed no transport through the boundaries. This condition was applied in the specific form

$$\Psi(x, 0) = \Psi(x, b) = \Psi(0, y) = \Psi(a, y) \tag{3.29}$$

where Ψ is the complete solution of (3.18). To make this vorticity equation more specific, Stommel chose an applied wind stress of the form

$$\tau_x = -F \cos \frac{\pi y}{b}; \quad \tau_y = 0 \tag{3.30}$$

where F is a positive constant. As will be seen shortly, this choice was probably motivated by the form of the solution to the y-dependent separated equation (3.25) of the homogeneous equation. The convenience of this functional interdependence will be further emphasized in Section 5. Stommel remarks, however, that the expression (3.30)

models a zonally-directed wind system over the ocean with westerlies prevailing over the northern half and easterlies over the southern portion, a situation suggestive of the climatological mean wind pattern over actual ocean areas. With the wind stress field thus defined, the vorticity equation (3.18) becomes

$$\nabla^2\Psi + a\frac{\partial\Psi}{\partial x} = \frac{F\pi}{Kb}\sin\frac{\pi y}{b} \tag{3.31}$$

a particular integral of which is

$$\Psi_p = -\frac{Fb}{K\pi}\sin\frac{\pi y}{b} \tag{3.32}$$

The complete solution of the vorticity equation (3.18) is thus the sum of this particular integral (3.22) and the complementary function (3.28).

$$\Psi = \int_0^\infty \left\{\left(pe^{Ax} + qe^{Bx}\right)(c\sin ny + h\cos ny)\right\} dn^2 - \frac{Fb}{K\pi}\sin\frac{\pi y}{b} \tag{3.33}$$

This expression may now be made more specific by application of the boundary conditions (3.29).

If $\Psi(x, 0) = 0$,

$$\int_0^\infty h\left(pe^{Ax} + qe^{Bx}\right)dn^2 = 0 \tag{3.34}$$

This integral may vanish for all x only if the integrand likewise vanishes. Hence $h(n) = 0$ for all n.

If $\Psi(x, b) = 0$,

$$\int_0^\infty c\sin nb\left(pe^{Ax} + qe^{Bx}\right)dn^2 = 0 \tag{3.35}$$

for all n. Except for the trivial situation $c = 0$, equation (3.35) leads

to the condition $\sin(nb) = 0$ which limits n to a discrete-infinite set of eigenvalues

$$n_j = \frac{\pi}{b} j \,, \quad j = 1, 2, 3, \cdots, \infty \tag{3.36}$$

$j = 0$ is excluded as leading to a trivial solution. The complete solution for Stommel's problem has thus been reduced from the infinite integral form (3.33) to the infinite sum (3.37).

$$\Psi = \sum_{j=1}^{\infty} c_j \sin(n_j y)\left(p_j e^{A_j x} + q_j e^{B_j x}\right) - \frac{Fb}{\pi K} \sin\left(\frac{\pi y}{b}\right) \tag{3.37}$$

where

$$A_j = -\frac{a}{2} + \left[\left(\frac{a}{2}\right)^2 + \left(j\frac{\pi}{b}\right)^2\right]^{1/2} \tag{3.38}$$

$$B_j = -\frac{a}{2} - \left[\left(\frac{a}{2}\right)^2 + \left(j\frac{\pi}{b}\right)^2\right]^{1/2} \tag{3.39}$$

If $\Psi(0, y) = 0$,

$$\frac{Fb}{K\pi} \sin\left(\frac{\pi}{b} y\right) = \sum_{j=1}^{\infty} c_j [p_j + q_j] \sin(n_j y)$$

from which $[p_j + q_j]$ are identified as the set of Euler coefficients of the halfrange Fourier sine expansion of the particular integral, with $c_j = Fb/K\pi$ for all j; i.e.,

$$p_j + q_j = \frac{1}{\pi} \int_0^{2\pi} \sin\left(\frac{\pi}{b} y\right) \sin(n_j y)\, dy \tag{3.40}$$

The orthogonal properties of the circular functions, and in particular, the relation

$$\int_0^{2\pi} \sin(\ell y)\, \sin(ny)\, dy = \begin{cases} \pi, & n = \ell \\ 0, & n \neq \ell \end{cases} \tag{3.41}$$

shows that the sum of the coefficients $(p_j + q_j)$ vanishes for all j except j = 1 for which $n = \pi/b$, and

$$p_1 + q_1 = 1 \tag{3.42}$$

The solution reduces to

$$\Psi = \frac{Fb}{K\pi} \sin\left(\frac{\pi}{b} y\right)\left(p_1 e^{A_1 x} + q_1 e^{B_1 x} - 1\right) \tag{3.43}$$

This is the form given by Stommel, but so far only the sum $(p_1 + q_1)$ has been defined in terms of known parameters.

If $\Psi(a, y) = 0$,

$$0 = \frac{Fb}{K\pi} \sin\left(\frac{\pi}{b} y\right)\left[p_1 e^{A_1 a} + q_1 e^{B_1 a} - 1\right] \tag{3.44}$$

Thus, in terms of the Euler constant definition as before,

$$p_1 e^{A_1 a} + q_1 e^{B_1 a} = p_1 + q_1 = 1$$

and the constants p_1 and q_1 are thus determined as

$$p_1 = \frac{1 - e^{Ba}}{e^{aA} - e^{aB}}, \quad q_1 = 1 - p_1 \tag{3.45}$$

It would seem to be important to the derivation of the solution in the form (3.43), specifically to identify the constant c with the factor $(Fb/K\pi)$ rather than to absorb it in the constants p and q as did Stommel. This does not alter the nature of the solution, of course.

Equation (3.43) together with the definition of constants by equations (3.38), (3.39), and (3.45) thus describes the streamlines

of the vertically integrated transport under the conditions modelled. The components of mean velocity may be obtained by partial differentiation, according to equations (3.12) and (3.13).

$$\bar{u} = \frac{1}{D} \cdot \frac{F}{K} \cos\left(\frac{\pi}{b} y\right) \cdot \left(pe^{Ax} + qe^{Bx} - 1\right) \tag{3.46}$$

[Note the power of two appearing in error in Stommel's equation (21), page 204.]

$$\bar{v} = -\frac{1}{D} \cdot \frac{Fb}{K\pi} \sin\left(\frac{\pi}{b} y\right) \cdot \left[pA\, e^{Ax} + qB\, e^{Bx}\right] \tag{3.47}$$

The topography of the sea surface was obtained by Stommel who integrated the equations of motion (3.8) and (3.9) after substituting these velocity components.

From equation (3.8), regarding y as zero, and integrating with respect to x, we have (assuming $\zeta << D$),

$$\rho g D[\zeta(x,o) - \zeta(0,0)] = \int_o^x (-Ku + \tau_x) d\xi - \frac{F}{D} \int_o^x \left\{\left(pe^{A\xi} + qe^{B\xi} - 1\right) + D\right\} d\xi$$

$$= -F\left[\frac{p}{A} e^{Ax} + \frac{q}{B} e^{Bx} - x - 1\right] - Fx \tag{3.48}$$

From equation (3.9), x is taken as constant and integration performed with respect to y:

$$\rho g D[\zeta(x,y) - \zeta(x,o)] = \int_o^y \left\{ - \frac{\beta \xi \rho F}{K} \cos\left(\frac{\pi\xi}{b}\right) \cdot (pe^{Ax} + qe^{Bx} - 1) \right.$$

$$\left. + \frac{Fb}{\pi} \sin\left(\frac{\pi\xi}{b}\right) \cdot (pA\, e^{Ax} + qB\, e^{Bx}) \right\} d\xi$$

$$= - \frac{\beta\rho F}{K} (pe^{Ax} + qe^{Bx} - 1) \cdot \left[y\left(\frac{b}{\pi}\right) \sin\left(\frac{\pi y}{b}\right) + \left(\frac{b}{\pi}\right)^2 \left[\cos\left(\frac{\pi y}{b}\right) - 1 \right] \right]$$

$$- F\left(\frac{b}{\pi}\right)^2 \left[\cos\left(\frac{\pi y}{b}\right) - 1 \right] \cdot (pA\, e^{Ax} + qB\, e^{Bx}) \qquad (3.49)$$

where $\beta = \partial f / \partial y$. The elevation ζ, of the sea surface at any point (x, y) relative to that at the origin, $(0, 0)$, is given by the sum of the right hand sides of equations (3.48) and (3.49).

$$\rho g D \zeta = - \left[pe^{Ax} + qe^{Bx} - 1 \right] \left[\frac{\beta\rho F}{K} \left\{ y\left(\frac{b}{\pi}\right) \sin\left(\frac{\pi y}{b}\right) + \left(\frac{b}{\pi}\right)^2 \left[\cos\left(\frac{\pi y}{b}\right) - 1 \right] \right\} \right]$$

$$- \left(\frac{p}{A} e^{Ax} + \frac{q}{B} e^{Bx} \right) \frac{F}{D} - (pA\, e^{Ax} + qe^{Bx}) \frac{F}{D} \left(\frac{b}{\pi}\right)^2 \left[\cos\left(\frac{\pi y}{b}\right) - 1 \right] + F \qquad (3.50)$$

$$\zeta(x,y) = - \frac{\beta F b}{gDK\pi} (pe^{Ax} + qe^{Bx} - 1) \left\{ y \sin\left(\frac{\pi y}{b}\right) + \left(\frac{b}{\pi}\right) \left(\cos \frac{\pi y}{b} - 1 \right) \right\}$$

$$- \frac{F}{\rho g D^2} \left(\frac{p}{A} e^{Ax} + \frac{q}{B} e^{Bx} \right) - \frac{F}{\rho g D^2} \left(\frac{b}{\pi}\right)^2 (pA\, e^{Ax} + qe^{Bx}) \left(\cos \frac{\pi y}{b} - 1 \right) + \frac{F}{\rho g D} \qquad (3.51)$$

This duplicates Stommel's equation (23) if:

(i) the bottom stress in equations (16) is modified according to equations (3.19),

(ii) a change in sign before the factor containing $(\partial f / \partial y)$ is admitted,

(iii) the constant term $(F/\rho g D)$ is included.

If the interpretation of u and v as mean values, as suggested

in the remarks following equation (3.6) is necessary, then the full significance of a "surface topography" derived in the equations above in terms of this mean flow remains to be clarified. Perhaps the retention of the integrated pressure function, P, would be more appropriate for this purpose.

Stommel presented streamline and "surface topography" patterns calculated from the above formulae for three different oceans. Constants were chosen as follows:

$a = 10^9$ cm

$b = 2\pi \times 10^8$ cm (note that this quantity was equated to 6249 km by Stommel)

$\beta = 10^{-13}$ cm^{-1} sec^{-1}

$D = 2 \times 10^4$ cm

$F = 1.0$ dyne cm^{-2}

$K = 0.02$, a value chosen so that "velocities in the resulting systems approach those observed in nature" (Stommel).

For an ocean which is either non-rotating, or rotating uniformly, the vorticity equation is identical, equating the Laplacian of the stream function to the wind stress curl. This results in a simple symmetrical circulation gyral. [It should be noted that the sign of the stream function in Stommel's figures should be reversed to be consistent with his definition of this function.]

For a non-rotating ocean the effect of bottom friction is to maintain elevations of the sea surface off downwind portions of the meridional coastal boundaries and depressions off the upwind portions. With the uniformly rotating ocean, however, a central elevation of the sea surface is produced giving rise to pressure gradient forces which,

with the frictional forces, balance the Coriolis forces on the circulating water. Because the frictional forces are relatively small, streamlines are nearly parallel to the topographic contours (they would be accurately parallel in geostrophic flow). An analysis of the balance of forces is given in Tables 3.1 and 3.2. Because of the sphericity of the earth's surface, the Coriolis forces due to the earth's rotation are not uniform, but decrease from a maximum at the equator to zero at the poles, following the cosine of the latitude. For the foregoing analysis a linear variation of the Coriolis parameter with latitude is essential to keep the parameter α constant in equation (3.31). Stommel uses the formula

$$f = y \times 10^{-13} \tag{3.52}$$

as an approximation characteristic of lower geographic latitudes. With this variation, a strongly pronounced asymmetry of the circulation gyral was developed (figure 3.1). This phenomenon was likened to the behavior of the north Atlantic and Pacific Oceans, where strong westward intensification of currents is observed in the Gulf Stream and Kuroshio, respectively.

Stommel notes that the patterns shown should be able to be extended across the equator simply by reflection in the x-axis. A discontinuity in pressure gradient appears at the equator in such a reflection.

3.3 Properties of the Stommel solution

The geometry of Stommel's solution for the stream function, Ψ, and the surface elevation, ζ, has been recomputed, and the results

are sketched in figures 3.1 and 3.2. These figures reproduce the character of Stommel's (1948, figures 5 and 6; 1960, figures 58 and 59) plots, but certain differences are evident. Isopleth values do not compare, although the originally published diagrams do not indicate the results of the quantities shown. The center of the circulation gyre is closer to the western boundary than the original diagram indicates, and the entrance-exit regions of the Gulf Stream show a sharper streamline curvature, thus increasing the "westward intensification" effect. Other minor differences in geometry may be noted.

For comparison of the Stommel analysis with other similar computations, it is of interest to establish the effect of the maximum value of the stream function, which represents the total wind-driven transport, with variation of ocean dimensions. From the symmetry of the solution (3.43) it is apparent that the maximum value of the stream function will always lie on $y = b/2$. Use of this value in (3.43) and setting $\partial\Psi/\partial x = 0$ indicates that the abscissa, x_m, of the maximum value of Ψ is given by equation (3.53).

$$x_m = \frac{1}{A - B} \ln\left(-\frac{qB}{pA}\right) \tag{3.53}$$

Substitution of the value for x back into the solution yields the maximum value of the stream function. Analytically, the resulting expression is too complex for its properties to be readily apparent, but the variation of this maximum value has been computed for various combinations of the model dimensions (a) and (b), and the results are plotted in figure 3.3. In this figure, the full curves represent the maximum value of the stream function as a function of the ratio of

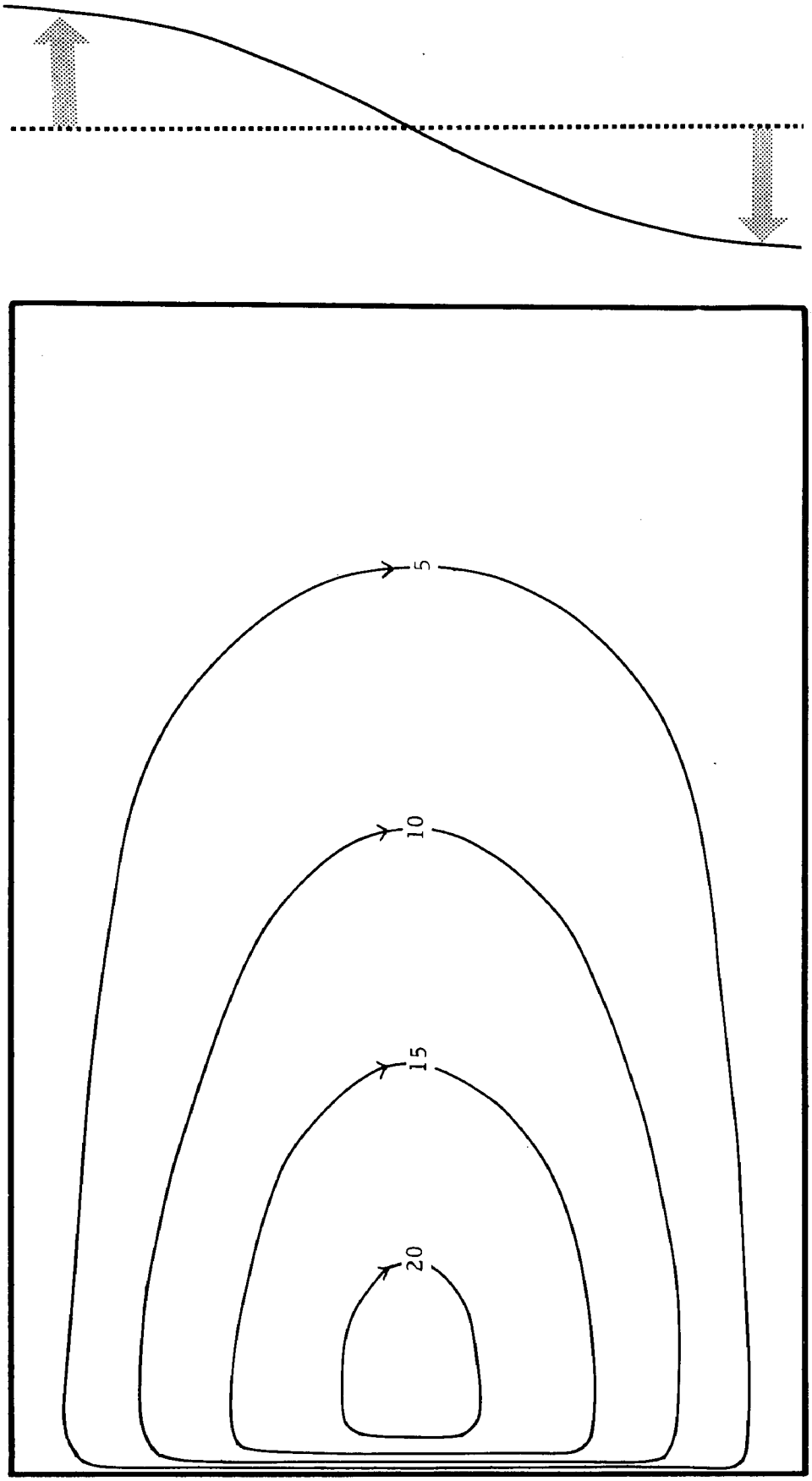

Figure 3.1 Streamlines of the vertically integrated mass transport (gm cm $sec^{-1} \times 10^{-6}$) in a Stommel ocean of zonal width $a = 10^{3}$ cm, meridional width $b = 2\pi \times 10^{8}$ cm, depth $D = 200$ m, coefficient of friction $K = 0.02$ sec^{-1}, and driven by a zonally directed wind stress which has a sinusoidal variation in the meridional direction as shown to the right of the ocean model, according to equation (3.43). The maximum value of the wind stress is $F = 1$ dyne cm^{-2}.

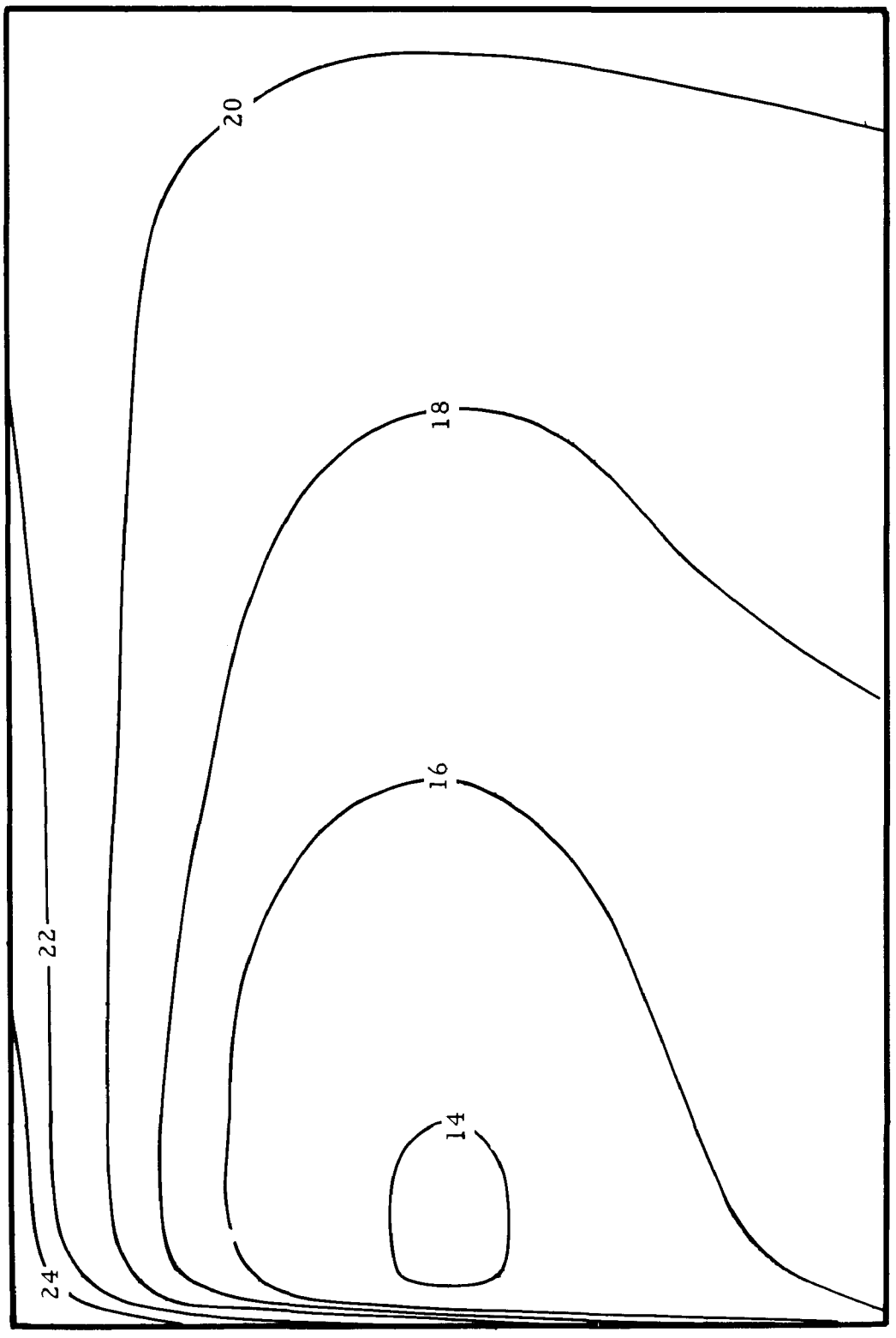

Figure 3.2 Topography, according to equation (3.51), of the surface of the Stommel ocean described in Figure 3.1. Contours represent heights in cm relative to a zero in the southwest (lower left) corner.

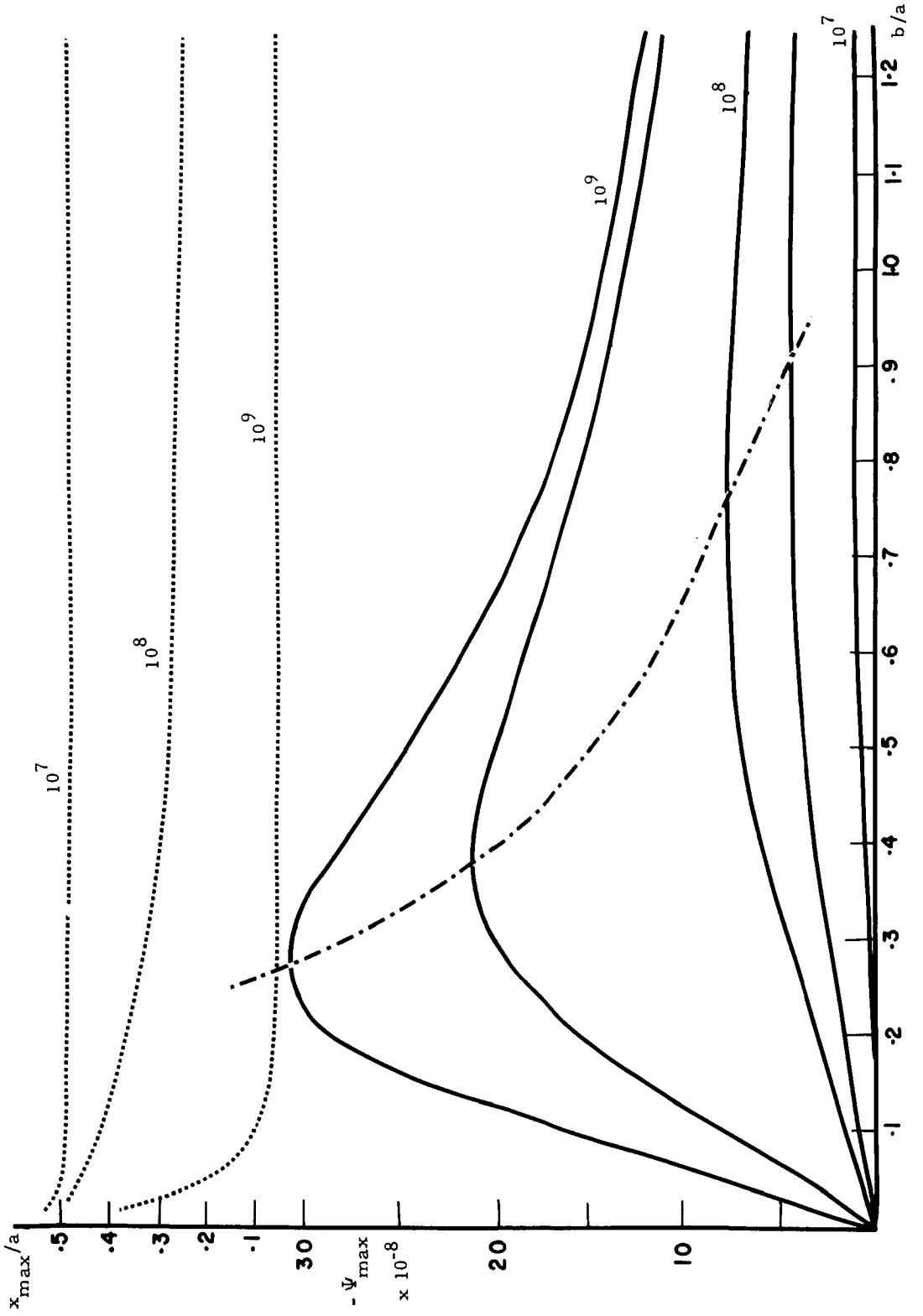

Figure 3.3 Variation with the ratio of meridional ocean width (b) to the zonal width (a) in a Stommel ocean, of the maximum value of the stream function Ψ_{max} (c.g.s. units; full curves) and the abscissa x_{max} (dotted curves) for values of (a) ranging from 10^7 to 10^9 cm. The dash-dot curve follows the locus of the peak in the Ψ_{max} variation.

meridional to zonal dimensions, (b/a), for values of (a) between 10^7 and 10^9 cm. As the ocean is "squeezed" meridionally (the "wavelength" of the applied wind stress distribution shrinking correspondingly), this maximum value increases until a peak is reached occurring at $(b/a) \approx 0.27$ for $(a) = 10^9$ cm. With increasing values of (a) this peak shifts towards lower values of (b/a), and its amplitude increases. The locus of this peak is marked in figure 3.3 by the heavy broken curve. The corresponding shift of the abscissa of this maximum value is shown by the lighter broken curves in figures 3.3. These indicate the effect of varying ocean dimensions on the degree of "westward intensification".

In the next section, occasion will arise to examine the properties of Stommel's maximum stream function with respect to variations in the value of the parameter, α, also in conjunction with variation of ocean dimensions.

It is of interest to examine the relative importance of the various terms making up the balance of forces in the Stommel model expressed in equations (3.8) and (3.9). Values of each of the terms appearing in these equations are listed in Tables 3.1 and 3.2 for a zonal section across Stommel's ocean at a "latitude" of $y = 0.7b$. Table 3.1 provides a detailed analysis of the dynamical balance in the "Gulf Stream" exit region, between $x = 0$ and $x = 0.1a$, while Table 3.2 provides a broad analysis across the whole ocean model. Also included are the inertial terms inherent in the solution. These terms are not members of the equations of motion used in Stommel's analysis, but as remarked following equation (2.2), the unimportance of these terms does not necessarily accompany such neglect. Inspection

Table 3.1. An analysis of the vertically integrated dynamical balance in the "Gulf Stream" exit region of Stommel's model at y = 0.7b, c. g. s. units.

fDv	0.156×10^{3}	0.564×10^{2}	0.198×10^{2}	0.639×10^{1}	0.146×10^{1}	-0.353×10^{0}	-0.102×10^{1}	-0.127×10^{1}	-0.136×10^{1}	-0.140×10^{1}	-0.141×10^{1}	rotation
$\cos \frac{\pi y}{b}$	-0.588×10^{1}											wind stress
Ku	zero	0.810×10^{-1}	0.110×10^{0}	0.120×10^{0}	0.123×10^{0}	0.123×10^{0}	0.123×10^{0}	0.122×10^{0}	0.120×10^{0}	0.119×10^{0}	0.118×10^{0}	friction
$gD \frac{\partial \zeta}{\partial x}$	0.157×10^{3}	0.569×10^{2}	0.203×10^{1}	0.686×10^{1}	0.192×10^{1}	0.112×10^{0}	-0.554×10^{0}	-0.800×10^{0}	-0.892×10^{0}	-0.927×10^{0}	-0.941×10^{0}	pressure
$Du \frac{\partial u}{\partial x}$	zero	0.189×10^{-1}	0.900×10^{-2}	0.316×10^{-2}	0.740×10^{-3}	0.179×10^{-3}	0.516×10^{-3}	0.636×10^{-3}	0.676×10^{-3}	0.688×10^{-3}	0.688×10^{-3}	inertia
$Dv \frac{\partial u}{\partial y}$	zero	0.357×10^{-1}	0.170×10^{-1}	0.599×10^{-2}	0.140×10^{-2}	-0.340×10^{-3}	-0.977×10^{-3}	-0.120×10^{-2}	-0.128×10^{-2}	-0.130×10^{-2}	-0.130×10^{-2}	
x/a	0.00	0.01	0.02	0.03	0.04	0.05	0.06	0.07	0.08	0.09	0.10	
fDu	zero	0.356×10^{1}	0.484×10^{1}	0.572×10^{1}	0.540×10^{1}	0.542×10^{1}	0.539×10^{1}	0.535×10^{1}	0.530×10^{1}	0.525×10^{1}	0.520×10^{1}	rotation
$gD \frac{\partial \zeta}{\partial y}$	-0.355×10^{1}	-0.484×10^{1}	-0.529×10^{1}	-0.542×10^{1}	-0.543×10^{1}	-0.541×10^{1}	-0.537×10^{1}	-0.532×10^{1}	-0.527×10^{1}	-0.522×10^{1}	-0.516×10^{1}	pressure
$Du \frac{\partial v}{\partial x}$	zero	-0.533×10^{0}	-0.266×10^{0}	-0.106×10^{0}	-0.400×10^{-1}	-0.148×10^{-1}	-0.542×10^{-2}	-0.200×10^{-2}	-0.759×10^{-3}	-0.306×10^{-3}	-0.141×10^{-3}	inertia
$Dv \frac{\partial v}{\partial y}$	-0.229×10^{1}	-0.299×10^{0}	-0.369×10^{-1}	-0.383×10^{-2}	-0.200×10^{-3}	-0.117×10^{-4}	-0.976×10^{-4}	-0.151×10^{-3}	-0.173×10^{-3}	-0.183×10^{-3}	-0.187×10^{-3}	
Kv	0.355×10^{1}	0.128×10^{1}	0.451×10^{0}	0.145×10^{0}	0.332×10^{-1}	-0.801×10^{-2}	-0.232×10^{-1}	-0.288×10^{-1}	-0.309×10^{-1}	-0.317×10^{-1}	-0.321×10^{-1}	friction

Table 3.2. An analysis of the vertically integrated dynamical balance along a zonal section across Stommel's model at y = 0.7b, c.g.s. units.

fDv	0.156×10^{3}	-0.141×10^{1}	-0.145×10^{1}	-0.149×10^{1}	-0.153×10^{1}	-0.157×10^{1}	-0.161×10^{1}	-0.165×10^{1}	-0.169×10^{1}	-0.173×10^{1}	-0.177×10^{1}	rotation
$\cos \frac{\pi y}{b}$	-0.588×10^{0}											wind stress
Ku	zero	0.118×10^{0}	0.106×10^{0}	0.941×10^{-1}	0.817×10^{-1}	0.689×10^{-1}	0.558×10^{-1}	0.424×10^{-1}	0.286×10^{-1}	0.145×10^{-1}	zero	friction
$gD\frac{\partial \zeta}{\partial x}$	0.157×10^{3}	-0.941×10^{0}	-0.972×10^{0}	-0.997×10^{0}	-0.102×10^{1}	-0.105×10^{1}	-0.107×10^{1}	-0.110×10^{1}	-0.113×10^{1}	-0.116×10^{1}	-0.119×10^{1}	pressure
$Du\frac{\partial u}{\partial x}$	zero	-0.689×10^{-3}	-0.638×10^{-3}	-0.580×10^{-3}	-0.515×10^{-3}	-0.446×10^{-3}	-0.370×10^{-3}	-0.288×10^{-3}	-0.199×10^{-3}	-0.103×10^{-3}	zero	inertia
$Dv\frac{\partial u}{\partial y}$	zero	-0.130×10^{-2}	-0.121×10^{-2}	-0.110×10^{-2}	-0.976×10^{-3}	-0.844×10^{-3}	-0.702×10^{-3}	-0.546×10^{-3}	-0.378×10^{-3}	-0.196×10^{-3}	zero	
x/a	0.0	0.1	0.2	0.3	0.4	0.5	0.6	0.7	0.8	0.9	1.0	
fDu	zero	0.520×10^{1}	0.468×10^{1}	0.414×10^{1}	0.359×10^{1}	0.303×10^{1}	0.245×10^{1}	0.186×10^{1}	0.126×10^{1}	0.637×10^{1}	zero	rotation
$gD\frac{\partial \zeta}{\partial y}$	-0.355×10^{1}	-0.516×10^{1}	-0.464×10^{1}	-0.411×10^{1}	-0.356×10^{1}	-0.299×10^{1}	-0.242×10^{1}	-0.183×10^{1}	-0.122×10^{1}	-0.597×10^{0}	0.403×10^{-1}	pressure
$Du\frac{\partial v}{\partial x}$	zero	-0.141×10^{-3}	-0.438×10^{-4}	-0.398×10^{-4}	-0.354×10^{-4}	-0.306×10^{-4}	-0.254×10^{-4}	-0.198×10^{-4}	-0.137×10^{-4}	-0.710×10^{-5}	zero	
$Dv\frac{\partial v}{\partial y}$	-0.229×10^{1}	-0.187×10^{-3}	-0.198×10^{-3}	-0.209×10^{-3}	-0.219×10^{-3}	-0.230×10^{-3}	-0.242×10^{-3}	-0.255×10^{-3}	-0.268×10^{-3}	-0.281×10^{-3}	-0.296×10^{-3}	inertia
Kv	0.355×10^{1}	-0.321×10^{-1}	-0.331×10^{-1}	-0.339×10^{-1}	-0.347×10^{-1}	-0.356×10^{-1}	-0.365×10^{-1}	-0.374×10^{-1}	-0.384×10^{-1}	-0.394×10^{-1}	-0.404×10^{-1}	friction

of the tables reveals that these terms are wholly negligible over most of the model, however, being three to four orders of magnitude smaller than terms retained in the equations of motion. The inertial terms rise to significance, compared with other terms, in the region of the intense western boundary current and should thus properly appear in the equations of motion. Observation of this fact has led to several fruitful analyses of the dynamics of such boundary currents with the field accelerations playing a dominant role in the balance of forces; for example, Munk et al., (1950); Stommel, (1953); Charney (1955), Morgan (1956); and Carrier and Robinson (1962). Of course, the values listed in the tables are not necessarily those which would be derived from a solution of the equations of motion which include the inertial terms; such a solution may differ markedly from that of the unaccelerated equations, especially in the region of the western boundary current. It will be beyond the defined scope of the present study to examine the details of these nonlinear theories.

3.4. The Stommel analysis in spherical coordinates

As with the Sverdrup analysis, it will be useful to have the Stommel model formulated in spherical coordinates. In such a coordinate system, the integrated equations of motion (3.8) and (3.9) may be written

$$-\frac{g\rho}{R\cos\phi}\frac{\partial\zeta}{\partial\lambda}(D+\zeta)+2\Omega\sin\phi\,\rho v(D+\zeta)-K\rho u(D+\zeta)+\tau_\lambda=0 \qquad (3.54)$$

$$-\frac{g\rho}{R}\frac{\partial\zeta}{\partial\phi}(D+\zeta)-2\Omega\sin\phi\,\rho u(D+\zeta)-K\rho v(D+\zeta)+\tau_\phi=0 \qquad (3.55)$$

These equations may be regarded as a more highly developed form of equations (2.45) and (2.46). The continuity equation may be

written as

$$\frac{1}{\cos\phi}\frac{\partial}{\partial\lambda}[\rho u(D+\zeta)] + \frac{\partial}{\partial\phi}[\rho v(D+\zeta)] = v\tan\phi \tag{3.56}$$

from which a mass transport stream function emerges as

$$\rho u(D+\zeta) = \frac{1}{R}\frac{\partial\psi}{\partial\phi} \tag{3.57}$$

$$-\rho v(D+\zeta) = \frac{1}{R\cos\phi}\frac{\partial\psi}{\partial\lambda} \tag{3.58}$$

Formation of the vorticity equation from (3.54) and (3.55) followed by substitution from equations (3.56), (3.54), (3.57), and (3.58) yields the spherical coordinate equivalent of Stommel's equation (3.18) in the form (3.59).

$$K\nabla^2\psi + \beta\frac{\partial\psi}{\partial x} - \frac{K}{R}\tan\phi\frac{\partial\psi}{\partial y} = -\frac{1}{R}\,\mathrm{curl}_z\vec{\tau} - \frac{x}{R}\tan\phi \tag{3.59}$$

where $\partial x = R\partial\phi$; $\partial y = R\cos\phi\,\partial\lambda$. For β constant, equation (3.59) is separable as was its counterpart in plane Cartesian coordinates, (3.18). The x-dependent separated equation remains unchanged from equation (3.22), when the same separation procedure is employed. The associated y-dependent equation, however, contains the effect of the convergence of meridians on a spherical earth.

$$\frac{d^2Y}{dy^2} - \frac{\tan\phi}{R}\frac{dY}{dy} + n^2Y = 0 \tag{3.60}.$$

This may be recognized as a form of Legendre's equation, of order

$$s = -\frac{1}{2}[1+\sqrt{1+4n^2R}\,],$$

the canonical form of which (e.g., Wylie, 1960, p. 451) is

$$(1 - z^2)\frac{d^2Y}{dy^2} + 2z\frac{dY}{dz} + s(s + 1)Y = 0 \qquad (3.61)$$

Equations (3.60) and (3.61) are related by the transformation $z = \cos(\frac{\pi}{2} - \phi)$. Solution of equation (3.59) over a field bounded by two parallels and two meridians may thus be built up following the general principles of the foregoing Stommel analysis, with zonal harmonics appearing in place of the trigonometric functions which were previously derived from the y-dependent separated equation (3.25).

In the spherical coordinate formulation, however, chief interest attaches to the vorticity equation (3.59) with the more natural formulation for β as $2\Omega\cos\phi/R$. The result of substituting a separated solution having the form $X(x)\,Y(y)$ into the homogeneous equation formed from (3.59) is equation (3.62).

$$\frac{X''}{X} + \frac{Y''}{Y} + \frac{2\Omega}{KR}\cos\phi \cdot \frac{X'}{X}\frac{\tan\phi}{R}\frac{Y'}{Y} = 0 \qquad (3.62)$$

This clearly is not separable, because of the product $\cos\phi(X'/X)$ appearing in the third term on the left hand side. One is tempted to follow the technique of Munk (1950, eq. [13]) who, when faced with a similar situation in the "lateral frictional circulation model" mentioned briefly in the introductory paragraphs to this section, apparently forced a condition of separability on his mathematical system. The appropriate device for this purpose in the case of equation (3.62) is to set (X'/X) constant, say,

$$X' = -s^2 X \qquad (3.63)$$

whence

$$X = Ae^{-s^2 x} \qquad (3.64)$$

and

$$\frac{X''}{X} = s^2 \tag{3.65}$$

where A and s are constants.

Equation (3.62) now becomes separable, and the y-dependent equation complementing (3.64) is (3.66).

$$\frac{d^2Y}{dy^2} - \frac{\tan\phi}{R}\frac{dY}{dy} + \left[s^4 - \frac{\Omega s^2}{K}\cos\phi\right]Y = 0 \tag{3.66}$$

If $\phi \equiv 2\theta$, this equation may be written

$$\frac{d^2Y}{d\theta^2} - 2\tan 2\theta \frac{dY}{d\theta} + R^2s^2\left[s^2 - \frac{\Omega}{K}\cos 2\theta\right]Y = 0 \tag{3.67}$$

If $Y \equiv Z/2\cos 2\theta$, where Z is some twice differentiable function of ϕ, the latitude-dependent equation reduces to equation (3.68).

$$\frac{d^2Z}{d\theta^2} + R^2s^2\left[(s^2+1) - \frac{\Omega}{K}\cos 2\theta\right]Z = 0 \tag{3.68}$$

provided $\phi \neq \pi/2$. Equation (3.68) is recognized as a form of Mathieu's equation, the canonical form of which, following the notation of McLachlan (1947), is

$$\frac{d^2Y}{dz^2} + [\bar{a} + 2q\cos 2z]Y = 0 \tag{3.69}$$

The $(\bar{a}, q)$ plane is divided into regions of stability and instability with respect to the solutions of equation (3.69). On the characteristic curves which separate these regions, solutions are stable and periodic. For any given value of the constant q, these characteristics define an infinite number of discrete values of $\bar{a}$, in the form of polynomials in q, for which a periodic solution exists. In the present application to equation (3.68), this offers, in principle, a means of selecting a set of eigen-values of the separation constant, s^2. However,

comparison of equations (3.68) and (3.69) shows that this constant appears in both the parameters $\overline{a}$ and q and this situation requires special treatment.

Hassan (unpublished personal communication) has solved the Stommel problem, i.e., equation (3.18) with boundary conditions (3.29), for values of β both constant and proportional to the sine of the latitude, using an iterative process on a finite difference approximation to the vorticity equation. For the variable-β situation, the chief difference from the streamline pattern of figure 3.1 found was a polewards shift of the center of the circulation gyre accompanied by an increase in the total rate of circulation. In the Stommel analysis, the boundary value problem led to a contribution to the final solution from the y-dependent separated equation in the form of a sine function. It is conjectured that the periodic solution of the Mathieu equation which most clearly resembles this contribution is the sine-elliptic Mathieu function of even order which, as the value of the parameter q is moved away from zero, finds its maximum value displaced from sinusoidal symmetry towards higher values of the argument (for example, see Jahnke and Emde, 1945, fig. 177). The nature of the restrictions imposed on the mathematical system consequent on the arbitrary choice of the x-dependent member of the separated solution in the form of equation (3.64) also remains to be clarified. It may well be that an arbitrary choice of this nature denies access to solutions of the original partial differential equation which will satisfy certain classes of boundary conditions, and methods of solution other than the separation of variables must be sought. In this connection, it is

noted that an attempt to find a solution by operating on the partial differential equation with the Laplace transform also led to a form of the Mathieu equation for the transform of the stream function, but it again became uncertain how to proceed usefully because of problems with the boundary conditions. It is hoped to complete this analysis later.

In passing, it might be noted that the quantity (Ω/K), which appears in equation (3.68) for instance, is related to the "Coriolis-friction wave number" introduced by Munk (1950, p. 81) as an important characteristic parameter in his higher order linear circulation model.

3.5 Extension of the Stommel analysis for an arbitrary wind field

In the Stommel analysis of section (3.2) a relatively simple closed form for the stream function solution was due essentially to the particular expression chosen to represent the applied wind stress. Since the models adopted are linear in the stream function, however, an infinite series solution may generally be found for any applied wind stress distribution by expanding this distribution in a series of cosines.

Both to illustrate this procedure, and to emphasize the importance of the role played by the space derivatives of the applied wind stress function in the Stommel-type model, the response of equation (3.18) to a driving stress function which varies linearly in the y-direction will now be studied. The stress function represented by equation (3.70) was chosen.

$$\tau_x = \frac{2}{b} y + 1 \; ; \qquad 0 \leq y \leq b \tag{3.70}$$

If the even extension of this function in the range $-b \leq y \leq 0$ be considered, τ_x may be represented by the Fourier cosine series (3.71).

$$\tau_x = -\frac{8}{\pi^2} \sum_{n=1,3,5,\cdots}^{\infty} \frac{1}{n^2} \cos\left(n\pi \frac{y}{b}\right) \tag{3.71}$$

This stress function has been designed to be similar in functional form to Stommel's driving function (3.30). The Stommel problem may now be reworked for each term of (3.71) in succession, the various terms yielding a sequence of solutions to the vorticity equation (3.18) each of which has the form (3.72).

$$\Psi_n = \frac{8b}{K(n\pi)^3} \sin\left(n\pi \frac{y}{b}\right)\left(p_n e^{A_n x} + q_n e^{B_n x} - 1\right) \tag{3.72}$$

The sum of the expressions (3.72), as n ranges over all the positive odd integers, will define the circulation field responding to the linear driving stress (3.70). Some idea of the rate of convergence of the series (3.71) and that obtained from (3.72) may be gained from figure 3.4 wherein is plotted the partial sums

$$\sum_{n=1}^{N} (\tau_m)_n \quad ; \quad \sum_{n=1}^{N} (\psi_m)_n \tag{3.73}$$

as functions of N, where τ_m represents the maximum value of the applied wind stress (at y = 0 or b) and ψ_m represents the maximum value obtained by the stream function for each partial sum, N. The evolution of the circulation pattern as a whole may be traced through 3.5 to 3.10 in which are drawn the streamline patterns derived from the partial sums for which N = 1, 2, 3, 4, 10, and 20, respectively. Superimposed

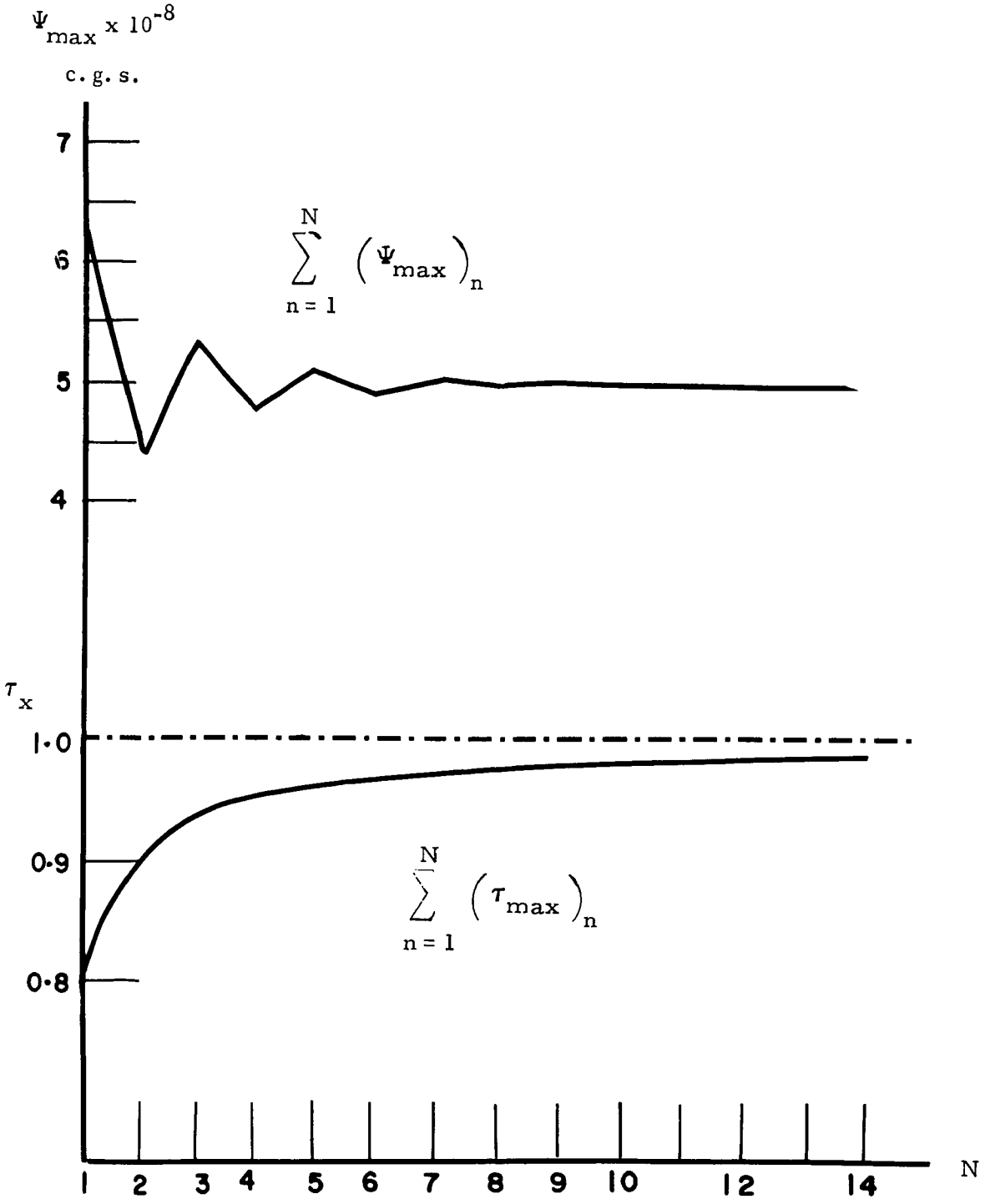

Figure 3.4 Convergence of the Fourier series development for the response of the Stommel ocean described in Figure 3.1 to a zonally-directed wind stress which has a linear meridional variation. Shown are the N^{th} partial sums for the maximum value of the stream function (upper) and the maximum value of the wind stress (lower, dynes cm^{-2}).

on each of these maps is a representation of the corresponding partial sum of the wind stress function. Except for the value of the maximum stream function, the "first harmonic" (figure 3.5) duplicates the geometry of Stommel's original solution. The superposition on this pattern of successively higher order harmonics, each of which contains a greater number of gyres of diminishing amplitude, carries the streamlines of figure 3.5 through a series of sinuous perturbations characteristic of partially converged Fourier approximations (figures 3.6 to 3.9). By the time the 15th partial sum has been formed, the convergence is virtually complete, leading to the circulation pattern of figure 3.10.

Computations up to N = 30 yielded no significant change in this situation, which is thus representative of the response of a Stommel ocean to a zonal wind stress which varies linearly with latitude; that is, to an applied wind stress curl which is everywhere constant. In relation to the constant value for $\beta \equiv \partial f/\partial y$ characteristic of the Stommel model, this situation is analogous to that of the Sverdrup model driven by a zonal wind stress everywhere equal to the sine of the latitude, also matching the behavior of the meridional variation of the Coriolis parameter (equations (2.36), et seq., figure 2.2). In each case, the dominant characteristic of the integrated circulation patterns was the meridional streamline trend. Either an extremum of the wind stress curl or its functional identity with the planetary vorticity, results in the disappearance of the zonal transport, U, with consequent definition of the latitude of the center of a circulation gyre. With the progressive "spreading out"

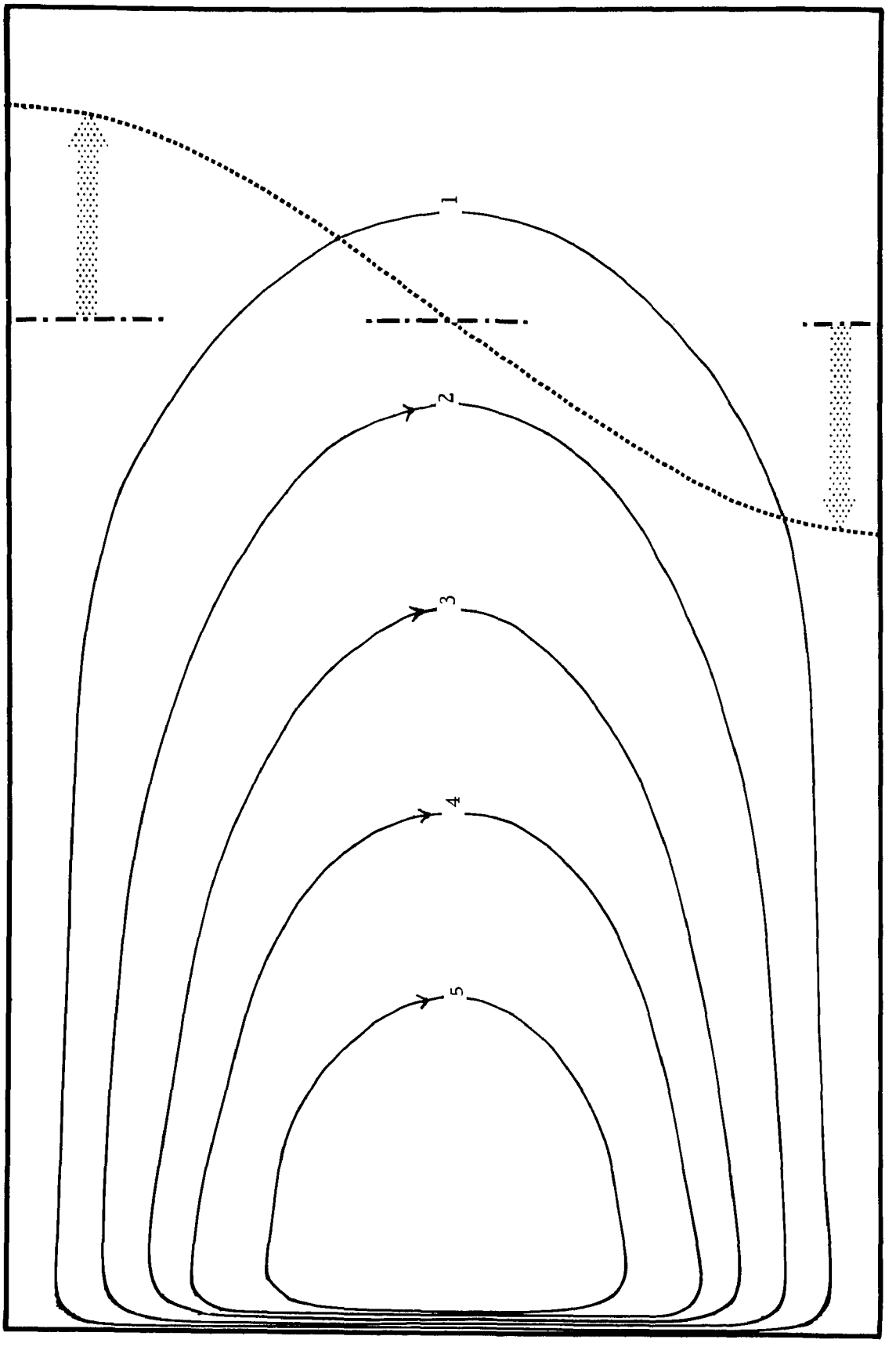

Figure 3.5 Mass transport streamlines (c.g.s. $\times 10^{-6}$) representing the first term of the Fourier series development described in Figure 3.4. The meridional variation of the applied wind stress is superimposed on the right.

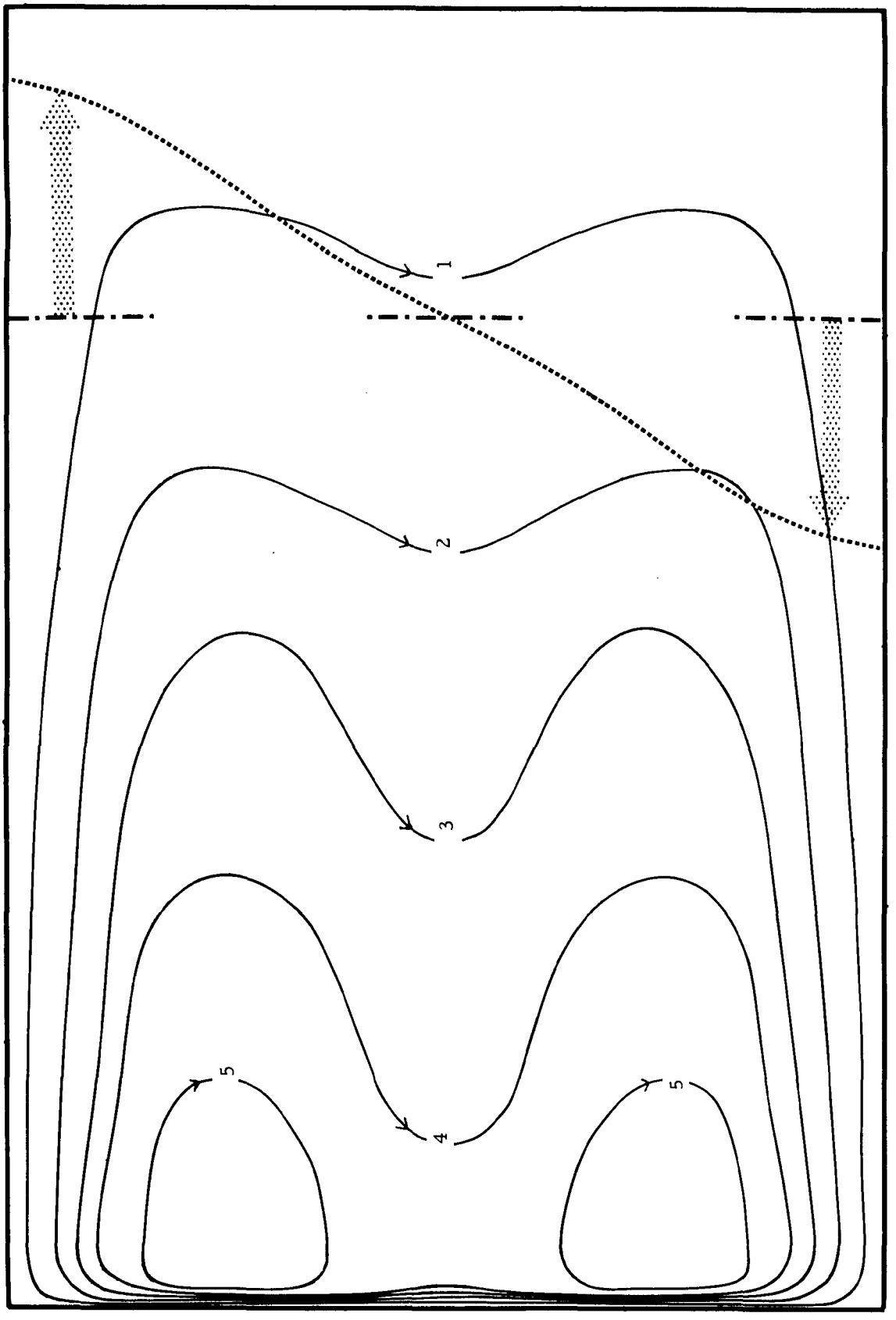

Figure 3.6 Mass transport streamlines (c. g. s. $\times 10^{-6}$) representing the sum of the first two terms in the Fourier series development described in Figure 3.4. The meridional variation of the applied wind stress is superimposed on the right.

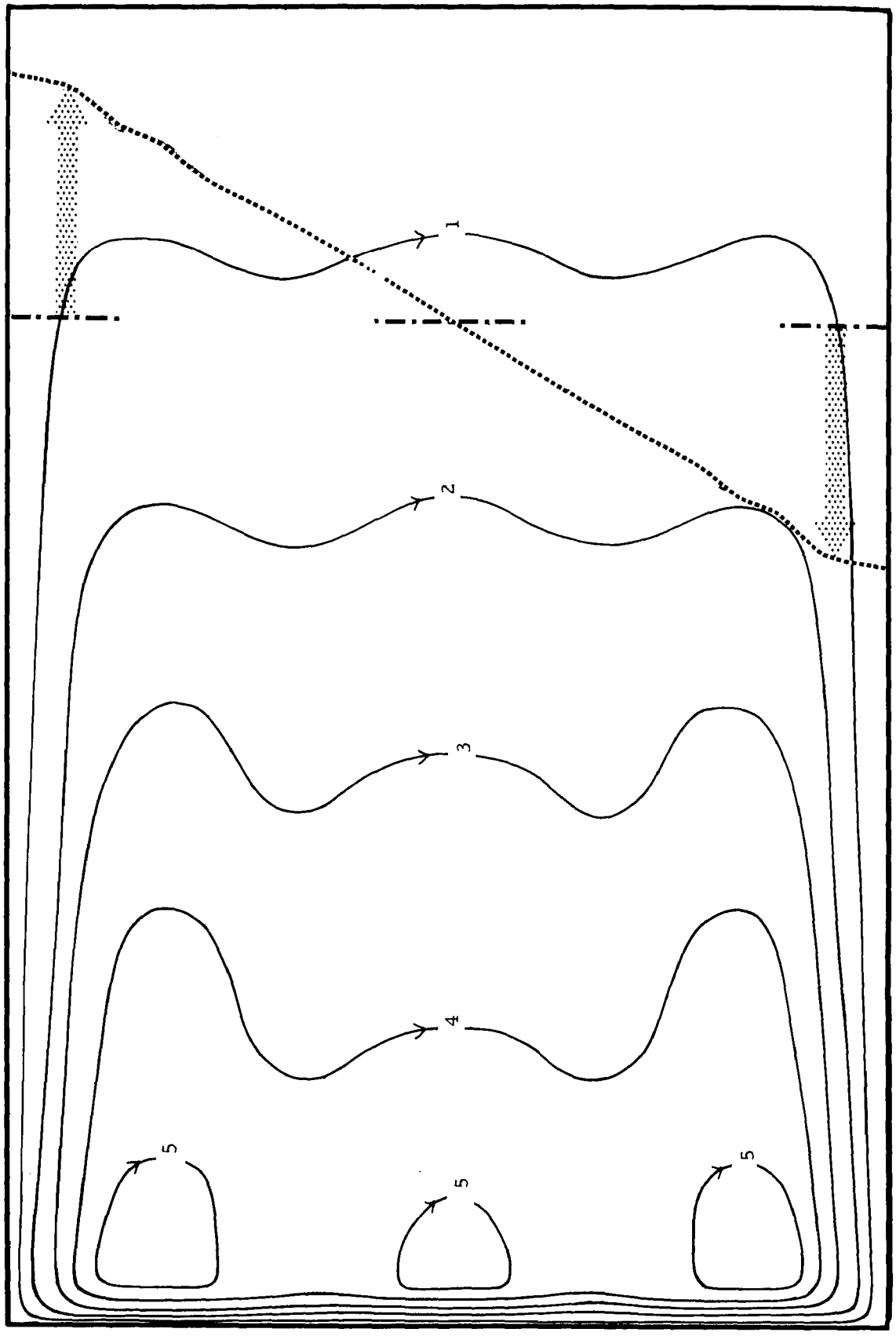

Figure 3.7. Mass transport streamlines (c.g.s. $\times 10^{-5}$) representing the sum of the first three terms in the Fourier series development described in Figure 3.5. The meridional variation of the applied wind stress is superimposed on the right.

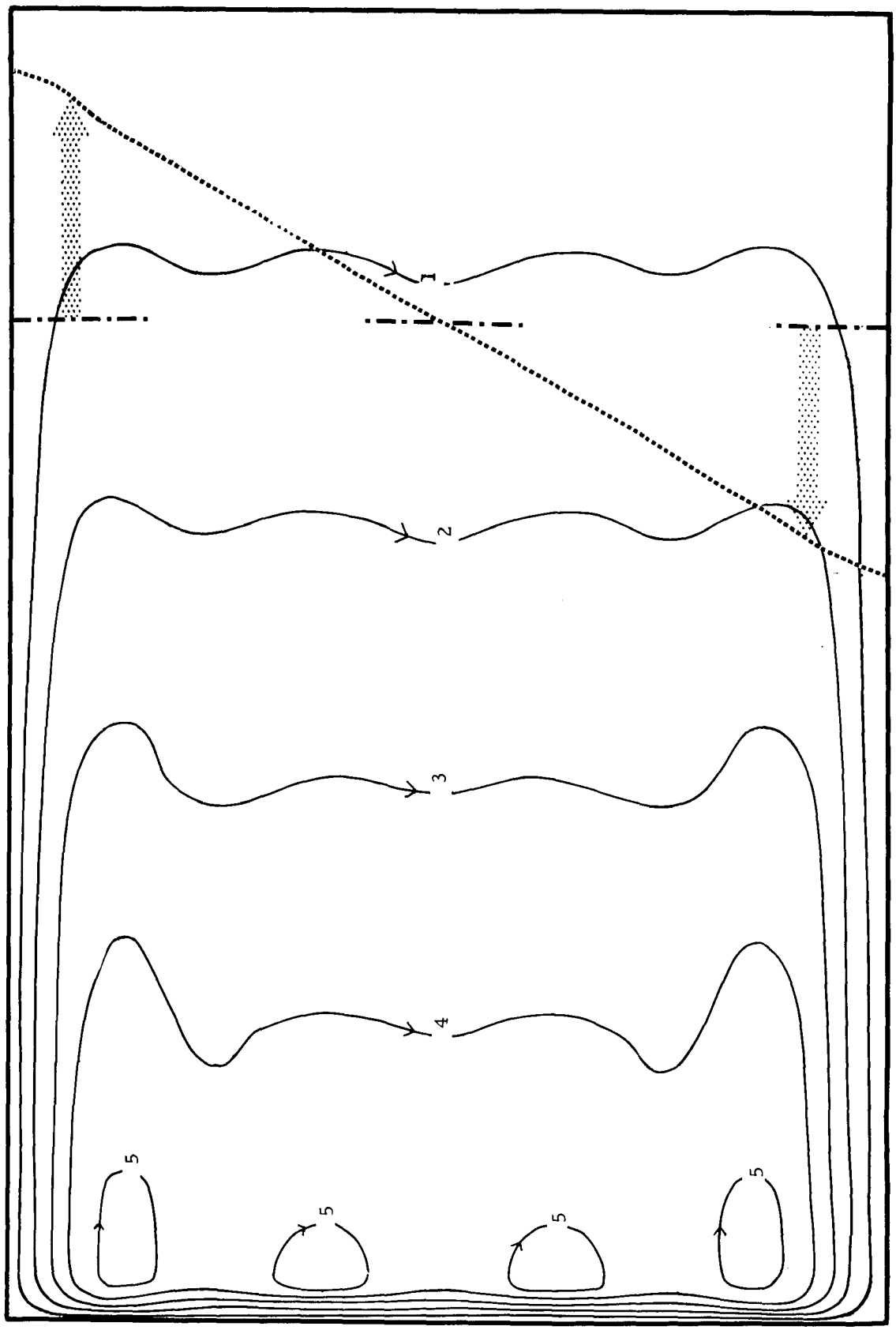

Figure 3.8 Mass transport streamlines (c.g.s. $\times 10^{-5}$) representing the sum of the first four terms in the Fourier series development described in Figure 3.5. The meridional variation of the applied wind stress is superimposed on the right.

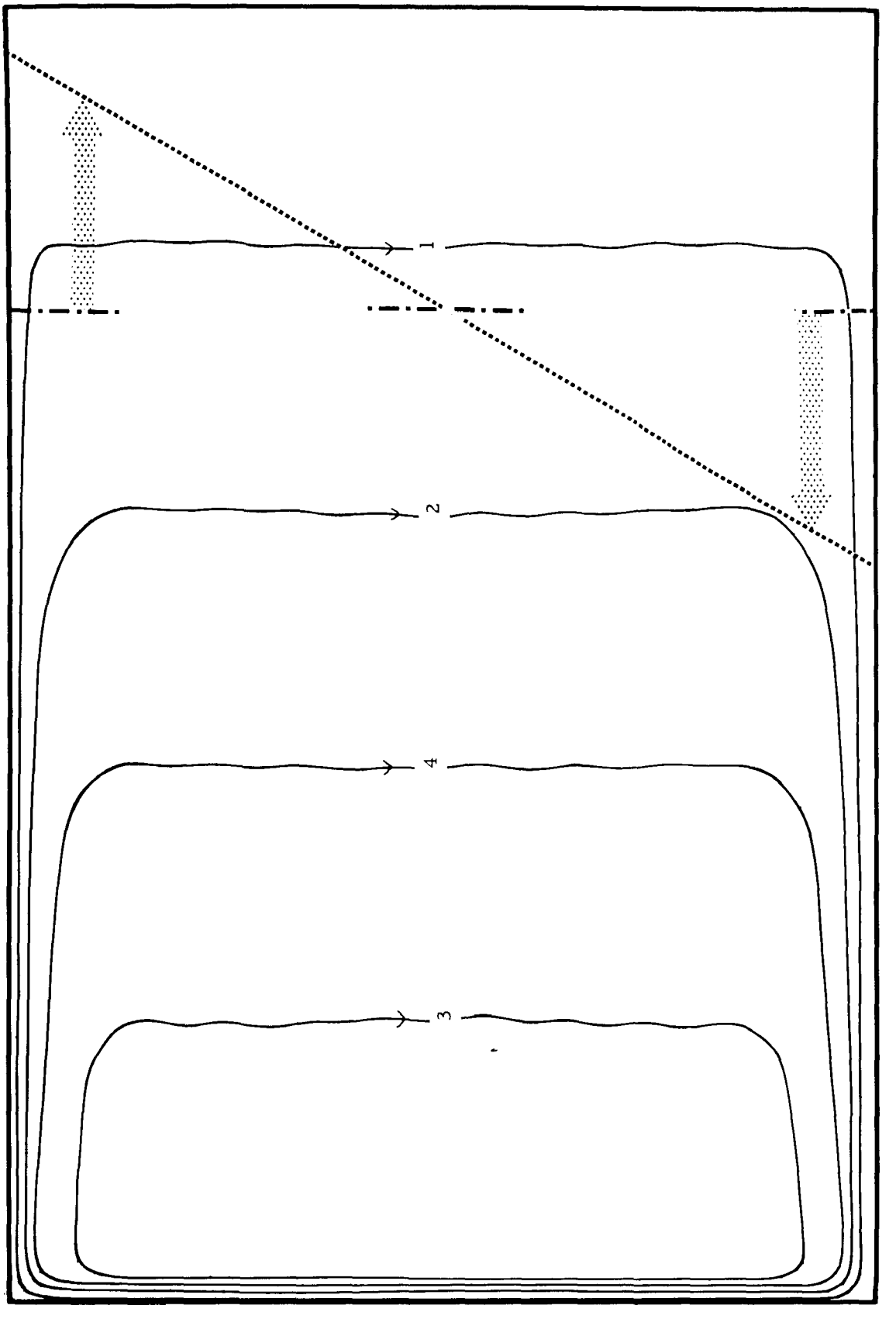

Figure 3.9 Mass transport streamlines (c.g.s. · 10^{-7}) representing the sum of the first ten terms in the Fourier series development described in Figure 3.4. The meridional variation of the applied wind stress is superimposed on the right.

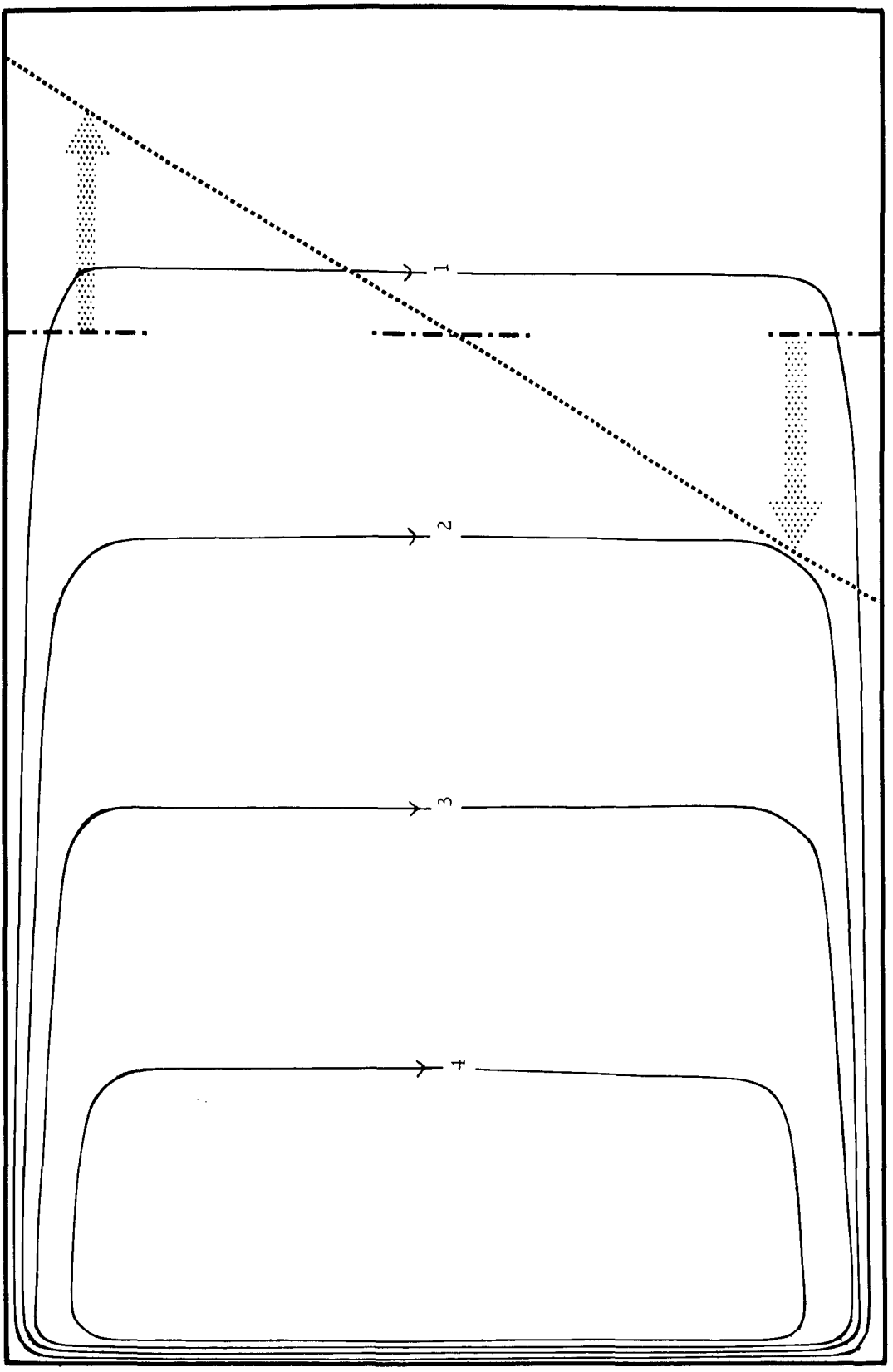

Figure 3.10 Mass transport streamlines (c.g.s. $\times 10^{-6}$) representing the sum of the first twenty terms in the Fourier series development described in Figure 3.4. The meridional variation of the applied wind stress is superimposed on the right.

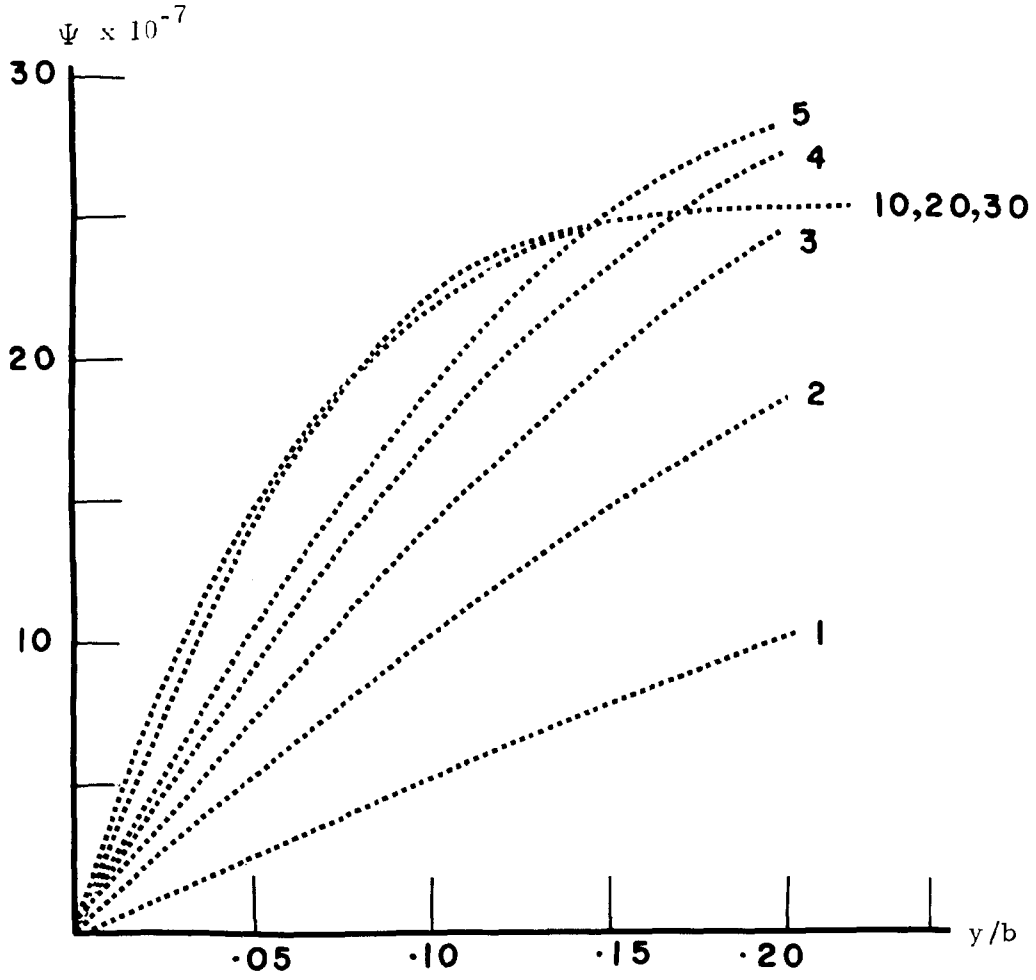

Figure 3.11 Variation of the mass transport stream function (c. g. s. units) in meridional section across the zonal boundary layer region between "latitudes" 0 and 0.2b at "longitude" 0.3a in the Fourier series development described by Figures 3.5 through 3.10. Individual curves are derived from partial sums of the order indicated.

in the meridional direction of the maximum curl, from the central latitude for the first partial sum in (5.41), to cover the whole ocean for the infinite sum, it is thus reasonable to expect a comparable meridional spreading of the region in which U = 0. Because of the zonal boundaries in the Stommel ocean, however, it is perhaps surprising to discover that the relation U = 0 is satisfied over virtually the whole ocean area, the requirements of continuity being met by relatively intense zonal transport in narrow and well-defined zonaly "boundary layers". The development of the limiting value of the meridional variation of the stream function across the lower of these boundary layers is shown in figure 3.11. It is probable that inertial effects in such a layer will no longer be negligible as was noted earlier for the western boundary region.

4. Introduction of the topographic vorticity

4.1 The Neumann model

A further development in the study of the properties of the linearized vertically integrated hydrodynamic equations having simple, first order expression for the friction was offered by Neumann (1955), who examined the effect of variations in total vertical extent of the wind-driven circulation. Responsible for new terms appearing in the vertically integrated vorticity equation is the following theorem governing differentiation of a definite integral whose limits are functions of the variable of differentiation. If $f(\xi, \eta)$ is a continuously differentiable function in some region, and $\ell_1(\xi)$, $\ell_2(\xi)$ have continuous derivatives over the range of ξ for which f is defined in this region, and if

$$F(\xi) = \int_{\ell_1(\xi)}^{\ell_2(\xi)} f(\xi, \eta)\, d\eta \tag{4.1}$$

then

$$F'(\xi) = \int_{\ell_1}^{\ell_2} \frac{\partial f}{\partial \xi}\, d\eta - \ell_1' f[\xi, \ell_1] + \ell_2' f[\xi, \ell_2] \tag{4.2}$$

where primes refer to total differentiation with respect to ξ. Proof of this theorem rests on the chain rule and fundamental theorem of the integral calculus (e. g., Courant, 1937, p. 220). Also called in the analysis following will be a relationship between the space gradient of the pressure, the pressure being evaluated on some surface $S(x, y)$, i. e., $\partial p_s / \partial \xi$, where $\xi = x$ or y, and the space gradient, evaluated on S, of the pressure, i. e., $(\partial p / \partial \xi)_s$. This relationship is approached through the hydrostatic equation (3.1) from which the pressure at some point with coordinate z may be written

$$p_z = g \int_z^{\zeta} \rho(z)\, dz \tag{4.3}$$

whence

$$\left(\frac{\partial p}{\partial \xi}\right)_z = g \int_z^{\zeta} \frac{\partial \rho}{\partial \xi}\, dz + g \rho_{\zeta} \frac{\partial \zeta}{\partial \xi} \tag{4.4}$$

On $z = S(x, y)$, however, using (4.2)

$$\frac{\partial p_S}{\partial \xi} = g \int_S^{\zeta} \frac{\partial \rho}{\partial \xi}\, dz + g \rho_{\zeta} \frac{\partial \zeta}{\partial \xi} - g \rho_S \frac{\partial S}{\partial \xi} \tag{4.5}$$

The required relation is thus obtained from (4.4) and (4.5) as (4.6).

$$\frac{\partial p_S}{\partial \xi} = \left(\frac{\partial p}{\partial \xi}\right)_S + g \rho_S \frac{\partial S}{\partial \xi} \tag{4.6}$$

Neumann considered the primary equations of motion in the form (4.7) and (4.8).

$$-fv = -\frac{1}{\rho}\frac{\partial p}{\partial x} + \frac{1}{\rho}\frac{\partial \tau_x}{\partial z} - K'u \tag{4.7}$$

$$+fu = -\frac{1}{\rho}\frac{\partial p}{\partial y} + \frac{1}{\rho}\frac{\partial \tau_y}{\partial z} - K'v \tag{4.8}$$

Comparison with (2.6), (2.7), or with (3.3), (3.4) shows that equations (4.7), (4.8) are those used by Sverdrup or by Stommel, augmented by a frictional retarding force proportional to the velocity. The procedure outlined in previous sections gives the integrated transport equations (4.9) and (4.10).

$$-fV = -\int_D^\zeta \frac{\partial p}{\partial x}\,dz + (\tau_x)_\zeta - (\tau_x)_D - K'U \tag{4.9}$$

$$+fU = -\int_D^\zeta \frac{\partial p}{\partial y}\,dz + (\tau_y)_\zeta - (\tau_y)_D - K'V \tag{4.10}$$

The now familiar process of cross-differentiation and subtraction in these equations, with the added contribution of equation (4.2) regarding $\ell_1 = D(x, y)$ and $\ell_2 = \zeta(x, y)$, gives a vorticity equation of the form (4.11).

$$f\left(\frac{\partial U}{\partial x} + \frac{\partial V}{\partial y}\right) + K'\left(\frac{\partial V}{\partial x} - \frac{\partial U}{\partial y}\right) + V\frac{\partial f}{\partial y} - \mathrm{curl}_z(\vec{\tau})_\zeta + \mathrm{curl}_z(\vec{\tau})_D$$

$$-\left[\frac{\tan\phi}{R}\int_D^\zeta \frac{\partial p}{\partial x}dz\right] - \left(\frac{\partial p_D}{\partial y}\frac{\partial D}{\partial x} - \frac{\partial p_D}{\partial x}\frac{\partial D}{\partial y}\right) + \left(\frac{\partial p_\zeta}{\partial y}\frac{\partial \zeta}{\partial x} - \frac{\partial p_\zeta}{\partial x}\frac{\partial \zeta}{\partial y}\right) = 0 \tag{4.11}$$

Morgan (1954) has demonstrated that it is immaterial to the final result whether the curl of the equation of motion is taken first to be followed by integration over depth, or whether the reverse order of operations is used, as above. He warns (p. 2) however, that the

latter procedure "is especially apt to introduce extraneous terms".

The expression in square brackets both in the above and in following equations will be retained if the analysis is performed in spherical coordinates so that

$$\partial x = R\cos\phi\,\partial\lambda \quad \text{and} \quad \partial y = R\,\partial\phi \tag{4.12}$$

and will disappear if x and y represent plane Cartesian coordinates. The following simplifying operations were then performed.

(a) The transport divergence in the first term of equation (4.11) was referred to the appropriate continuity equation (2.18) or (2.48), depending on the reference frame.

(b) The integrated equation of motion (4.9) was used to eliminate the pressure dependent term within square brackets in equation (4.11).

(c) An assumption that the sea surface, ζ, is isobaric, permits those terms in (4.11) which contain pressure gradients at the surface to be dropped.

With these operations, equation (4.11) may be reduced to (4.13).

$$\underset{[1]}{K'\left(\frac{\partial V}{\partial x}-\frac{\partial U}{\partial y}\right)}+\underset{[2]}{V\frac{\partial f}{\partial y}}-\underset{[6]}{\mathrm{curl}_z(\vec{\tau})_\zeta}+\mathrm{curl}_z(\vec{\tau})_D$$

$$-\left[\frac{\tan\phi}{R}\left\{\underset{[7]}{(\tau_x)_\zeta}-\underset{[5]}{(\tau_x)_D-K'U}\right\}\right]-\left(\underset{[3]}{\frac{\partial p_D}{\partial y}}\underset{[4]}{\frac{\partial D}{\partial x}}-\frac{\partial p_D}{\partial x}\frac{\partial D}{\partial y}\right)=0 \tag{4.13}$$

The numerals in square brackets are identification indices explained later.

Equation (4.13) corresponds to equation [8] of Neumann (1955, p. 12), except for a term (4.14).

$$\frac{\partial \tau_x}{\partial z}\frac{\partial D}{\partial y} - \frac{\partial \tau_y}{\partial z}\frac{\partial D}{\partial x} \tag{4.14}$$

for which the present analysis has failed to account.

The custom of identifying the vector $(\vec{\tau})_\zeta$ with the stress of the wind acting on the sea surface was continued in this analysis. Treatment of the vector $(\vec{\tau})_D$ depends on the physical nature assigned to the surface D. If D is a solid surface with a frictional boundary layer, the bottom stress may be modelled as a quantity proportional to the total overlying transport as did Stommel in equation (3.7), here written as equation (4.15).

$$(\tau_x)_D = K''U \quad ; \quad (\tau_y)_D = K''V \tag{4.15}$$

where K'' is a constant frictional coefficient. This permits the following adjustments to be made to certain terms in equation (4.13):

$$(\tau_x)_\zeta - (\tau_x)_D - K'U = (\tau_x)_\zeta - KU \tag{4.16}$$

$$K'\left(\frac{\partial V}{\partial x} - \frac{\partial U}{\partial y}\right) + \mathrm{curl}_z(\vec{\tau})_D = K\left(\frac{\partial V}{\partial x} - \frac{\partial U}{\partial y}\right) \tag{4.17}$$

where
$$K \equiv K' + K'' \tag{4.18}$$

Neumann was chiefly concerned, however, with an interpretation of D as a surface of no motion derived naturally from an interaction between the earth's rotation and baroclinicity in the field of flow due to density stratification. This surface was considered to lie everywhere above the solid ocean bottom. In particular, Neumann identified D with the "depth of no motion" postulated by Defant (1941) as an interpretation of a reference level for "dynamical computations" based on the observed oceanic mass distribution. In these computations,

the (geostrophic) velocity typically approaches the assumed zero level asymptotically with increasing depth, so that the vertical velocity shear, and hence the horizontal stress tends to zero as z tends to D. Such considerations prompted Neumann (1955, pp. 9, 16) to regard the surface D as equivalent to "a rigid frictionless boundary" at which "the stress · · · must vanish". If $(\vec{\tau})_D = 0$, substantially the same modifications to equation (4.13) may be made as are indicated by equations (4.15) to (4.17), but with different values of the coefficient of friction. Motivated by a feeling that friction within the body of the ocean should have some dynamical interaction with the sloping lower boundary through the effect of vertical stretching on the vorticity balance, Neumann has retained D-dependent terms in the component (4.19) of (4.13):

$$\overset{[3]}{\frac{\partial p_D}{\partial y}\frac{\partial D}{\partial x}} - \overset{[4]}{\frac{\partial p_D}{\partial x}\frac{\partial D}{\partial y}} \qquad (4.19)$$

which will be called the "topographic vorticity".

This retention has been accomplished through an argument which will not be reviewed in detail here. Essentially it considers the hydrodynamical equations (4.20) and (4.21) for some particular level within the circulating water followed by certain assumptions, the introduction of a particular mathematical form for the vertical velocity profile, and passage through a limiting process designed to render the analysis independent of this particular form. The transformations employed to derive the variable depth vorticity equation in Neumann's final form (4.27) from equation (4.13) may be followed by the identifying numbers appearing in square brackets under terms in (4.13) and succeeding equations.

The equations (4.20), (4.21) mentioned above were written by Neumann (1955, eqn. 27) for $z = h$ as:

$$\underset{[4]}{\frac{\partial p_h}{\partial x}} = \underset{[4a]}{-f\bar{\rho}\, v_h} + \underset{[4b]}{\left.\frac{\partial \tau_x}{\partial z}\right|_h} \underset{[4c]}{- K' u_h} + \left\{ g\, \rho_h \frac{\partial h}{\partial x} \right\} \tag{4.20}$$

$$\underset{[3]}{\frac{\partial p_h}{\partial y}} = \underset{[3a]}{f\bar{\rho}\, u_h} + \underset{[3b]}{\left.\frac{\partial \tau_y}{\partial z}\right|_h} \underset{[3c]}{- K' v_h} + \left\{ g\, \rho_h \frac{\partial h}{\partial y} \right\} \tag{4.21}$$

Neumann's equations[27] omit the last terms (in curly brackets) which are required by equation (4.6). These terms are lost in subsequent manipulation, however. The appearance of the average density, $\bar{\rho}$, in the equations above, rather than the density at the depth h, ρ_h, merits comment. This question is allied to the approximation (4.22)

$$\left\{ \begin{matrix} U \\ V \end{matrix} \right\} = \int_D^{\zeta} \rho \left\{ \begin{matrix} u \\ v \end{matrix} \right\} dz \rightarrow \bar{\rho} \int_D^{\zeta} \left\{ \begin{matrix} u \\ v \end{matrix} \right\} dz \tag{4.22}$$

implied by the relations following equations [2b] and [21a] in the original publication. This latter approximation will presumably be tolerable so long as $\Delta\rho/\rho << \Delta u/u$ or $\Delta v/v$.

The depth $z = h$ was chosen so that

$$\left\{ \begin{matrix} U \\ V \end{matrix} \right\} = \bar{\rho} \left\{ \begin{matrix} u_h \\ v_h \end{matrix} \right\} D \tag{4.23}$$

This equation implies that the velocity vector at $z = h$ is parallel in direction to the integrated transport vector and $(1/\bar{\rho}D)$ times its magnitude.

It might be argued that such a depth does not necessarily

exist in the general case, nor that it is necessarily consistent with the particular velocity profile chosen, i. e., Neumann's equation [22], reproduced here as equation (4.24):

$$c = c_o\left(1 + \frac{z}{D}\right)^{1/n} \tag{4.24}$$

where c is the magnitude of the velocity vector, c_o is a constant, and n is a positive integer.

Use of equation (4.23) in equations (4.20) and (4.21) and the assumption $[\partial\tau/\partial z]_h = \tau_\zeta / D$, yields equations (4.25) and (4.26).

$$\underset{[4]}{\frac{\partial p_h}{\partial x}} = \underset{[4a]}{-\frac{f}{D} V} + \underset{[4b]}{\frac{(\tau_x)_\zeta}{D}} \underset{[4c]}{- \frac{K_1}{D} U} + \left\{ g \rho_h \frac{\partial h}{\partial x} \right\} \tag{4.25}$$

$$\underset{[3]}{\frac{\partial p_h}{\partial y}} = \underset{[3a]}{\frac{f}{D} U} + \underset{[3b]}{\frac{(\tau_y)_\zeta}{D}} \underset{[3c]}{- \frac{K_1}{D} V} + \left\{ g \rho_h \frac{\partial h}{\partial y} \right\} \tag{4.26}$$

Substitution of these equations into the term (4.19) of equation (4.13) and passage through a limiting process, corresponding to $n \to \infty$ in equation (4.24) and adoption of the transport stream function (2.55), (2.56), finally derived the variable depth vorticity equation (4.27) which formed the basis of Neumann's subsequent discussion.

$$\underset{[1]}{K\nabla^2\Psi} + \underset{[2]\ [3a]\ [4c]}{\left(\frac{\partial f}{\partial y} - \frac{f}{D}\frac{\partial D}{\partial y} - \frac{K}{D}\frac{\partial D}{\partial x}\right)\frac{\partial \Psi}{\partial x}} + \underset{[4a]\ [5]\ [3c]}{\left(\frac{f}{D}\frac{\partial D}{\partial x} - \left[\frac{K}{R}\tan\phi\right] - \frac{K}{D}\frac{\partial D}{\partial y}\right)\frac{\partial \Psi}{\partial y}}$$

$$= \underset{[6]}{-\ \mathrm{curl}_z \vec{\tau}} + \underset{[4b]}{\frac{\tau_y}{D}\frac{\partial D}{\partial x}} \underset{[3b]}{- \frac{\tau_x}{D}\frac{\partial D}{\partial y}} - \underset{[7]}{\left[\frac{\tau_x}{R}\tan\phi\right]} \tag{4.27}$$

Stress terms in (4.27) are understood to be referred to the free surface, ζ.

Comparison of equations (4.13) and (4.27) shows that the latter stages of Neumann's derivation are equivalent to the following substitution:

$$\frac{\partial p_D}{\partial x}\frac{\partial D}{\partial y} - \frac{\partial p_D}{\partial y}\frac{\partial D}{\partial x} = \frac{1}{D}\frac{\partial D}{\partial x}(fU + KV - \tau_y) + \frac{1}{D}\frac{\partial D}{\partial y}(fV - KU + \tau_x)$$

$$= -\frac{1}{D}\left[\frac{\partial D}{\partial x}\int_D^\zeta \frac{\partial p}{\partial y}\,dz - \frac{\partial D}{\partial y}\int_\zeta \frac{\partial p}{\partial x}\,dz\right]$$

where use has been made of equations (4.9) and (4.10). If $p_\zeta = 0$ and theorem (4.2) is introduced, this substitution for the topographic vorticity term becomes

$$\frac{\partial p_D}{\partial x}\frac{\partial D}{\partial y} - \frac{\partial p_D}{\partial y}\frac{\partial D}{\partial x} \rightarrow \frac{1}{D}\left[\frac{\partial P}{\partial x}\frac{\partial D}{\partial y} - \frac{\partial P}{\partial y}\frac{\partial D}{\partial x}\right] \tag{4.28}$$

where $$P \equiv \int_D^\zeta p\,dz$$

and physical justification of the substitution (4.28) would provide a derivation of equation (4.27) more acceptable to the present study.

The nature of the limiting process employed is, as Neumann remarks (1955, footnote 2, p. 17) such that "with this approach in a very thin layer above the depth D a strong vertical velocity gradient must result, whereas immediately at the layer D the velocities vanish." This imposition of a strong vertical shear of horizontal velocity in the neighborhood of D does not seem to be compatible with previous assumptions that the stress at D must vanish, and further, appears to reduce the problem to that of a homogeneous ocean with a frictional boundary layer overlying a rigid bottom. In such a case the topographic

term, (4.19), will exert its full influence in the vorticity equation, since the pressure gradient at the lower boundary will be wholly balanced by the frictional forces to give a condition of no motion. In the case of relatively weak density stratification, so that pressure gradients induced by the wind at the sea surface still reach to the physical bottom, then the topographic contribution to the vorticity balance will be "diluted" according to the degree of baroclinicity. With baroclinic conditions sufficiently well developed for the formation of a "natural" depth of no motion, free from the constraint of the physical bottom and without stress, or vertical gradient of stress in the neighborhood of this depth, as modelled by Neumann (1955), then the horizontal pressure gradient at the depth of no motion must vanish. In this case, substitution of equation (4.6) into (4.19) shows that the topographic vorticity term vanishes exactly.

The case of balance between friction forces at the "natural" depth of no motion might be considered. In such a case, at lease one of the equations of motion (4.7), (4.8) will be of the form

$$\pm \frac{\partial p}{\partial x} + A \frac{\partial^2 u}{\partial z^2} = 0 \quad \text{at} \quad z = D \tag{4.29}$$

where $\partial^2 u/\partial z^2 \neq 0$, by hypothesis. But since $u = 0$ at $z = D$, by definition, either (a) $|u| > 0$ for $z \gtrless D$, in contradiction to the definition of D as the lower boundary of the wind-driven circulation. No provision is made in the model for the consideration of other driving mechanisms, such as thermohaline forces; or (b) $\partial p/\partial z$ exhibits discontinuity in z-dependence at D with

$$\left.\frac{\partial p}{\partial z}\right\} \begin{matrix} \neq 0 \text{ for } z > D \\ = 0 \text{ for } z < D \end{matrix} \tag{4.30}$$

While there is no fundamental physical objection to the acceptance of a first order discontinuity in the oceanic pressure field, it does represent rather a special dynamical situation, and the motion is not suggestive of the situation commonly described by applying Defant's method for the identification of the depth of no motion from "dynamical computations" which, as noted above, derive horizontal velocity components approaching the "Defant level" asymptotically with $\partial^2 u/\partial z^2 \rightarrow 0$ as $z \rightarrow D$. In such cases, the dynamical situation tends to that described above for the frictionless depth of no motion in which the topographic vorticity term disappears exactly. It should be noted that the procedure adopted by Sverdrup (1947) and by Munk (1950) of vertical integration of the equations of motion between the surface and some constant level which everywhere lies below the natural depth of no motion must assume that this topographic term is unimportant.

The general philosophy of appeal to the hydrodynamic equations written for a particular depth, and to particular velocity-depth relationships, as a means for manipulation of the vertically integrated vorticity equation is undesirable. As Neumann notes (1955, p. 16) "... with the vertically integrated equations of motion, the vertical profile is meaningless." however, exception is taken to the next sentence which is offered as a corollary of the above principle, viz. "It seems possible to introduce any artificially defined velocity profile that gives the same total mass transport in the whole layer as the vertically integrated mass

transport of the true velocity profile." Again (p. 17) it is claimed: "It follows that the vertically integrated mass transport can be thought to be produced by any equivalent velocity profile in a non-homogeneous ocean with a layer of no motion as the lower boundary of the circulation." The present writer feels that it is possible to prove that a unique steady state velocity field is defined by a given set of equations of motion and continuity, driving wind stress pattern, side boundary conditions, and initial mass distribution. If this is true, then for each point (x, y) there exists a uniquely defined velocity-depth profile with, under appropriate circumstances, its particular depth D.

This question is discussed further in a later section; for present purposes it is sufficient to suggest that rather than being "meaningless", the form of the velocity depth profile is better described as "lost" during the process of vertical integration but still uniquely implied in the dynamical system. From this point of view, then, the adoption of any arbitrary velocity profile will represent an artificial dynamical constraint on the system with consequent artificial distortion of the solution. It is thus suggested that the dangers inherent in the use of any non-integral properties after the primary set of dynamical equations has been integrated vertically, should best be avoided. Presumably, however, the three models chosen for analysis in the present study have resorted to vertical integration of the equations of motion at an early stage of proceedings because of the mathematical difficulties consequent on the omission of this step, rather than because of any primary interest in the behavior of the vertically integrated horizontal transport. Special solutions, such

as this latter quantity or even steady state conditions, should if possible always be obtained by the appropriate equation on a solution of the hydrodynamic problem which yields the three velocity components each as functions of the three space variables and of time. Some progress in this field, using numerical methods, is reported by Hassan (1961).

4.2 Summary

Before proceeding with an examination of some of the properties of Neumann's vorticity equation, a brief summary of the theme of the literature reviewed in the foregoing study will be helpful.

1. Sverdrup considered transport equations which comprised pressure gradient, Coriolis and wind stress terms. The vorticity equation derived from these equations expresses balance between planetary and anemographic terms. A steady state solution for the vertically integrated wind-driven circulation was constructed extending westwards from a meridian at which this transport may be arbitrarily specified.

2. Stommel included a frictional term proportional to the transport in his equations and derived an expression for vorticity balance among planetary, anemographic, and frictional terms. This additional term enabled a circulation pattern to be constructed within a closed boundary. Specifically, the wind-driven transport was defined for a rectangular ocean of constant depth, and a strong zonal asymmetry in the circulation gyre leading to a crowding of streamlines along the western boundary ("westward intensification") was found to be due to the variation with latitude of the Coriolis parameter.

3. Brief mention was made of the work of Munk who also considered a vorticity equation composed of planetary, anemographic, and frictional elements. Consideration of a more sophisticated expression for integrated lateral frictional forces proportional to the second derivative of the transport permitted more physical realism to be incorporated into the boundary conditions, and yielded a complex western boundary transport structure which contained an offshore stream moving counter to the main boundary flow.

4. Neumann has retained the simpler expression for friction introduced by Stommel, although with different interpretation, but added a fourth member to the family of vorticity elements derived from variations in the depth of circulating water. The present study suggests that some restrictions may be necessary on the original interpretation of this topographic effect.

In a nutshell:

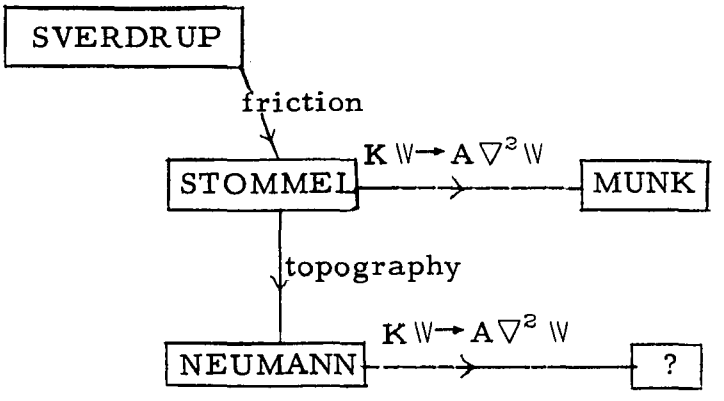

5. The obvious extension suggests itself of applying Munk's enrichment of Stommel's model to Neumann's analysis, i.e., by replacing the question mark in the lower right hand box of the above diagram by a model including planetary and anemographic vorticities together with Neumann topographic and Munk frictional terms.

5. Variations in the oceanic vorticity balance

Stommel (1948) has shown how the rate of change of the Coriolis parameter with latitude, will produce a westward intensification, or zonal asymmetry, in the vertically integrated circulation pattern induced in a rectangular ocean of constant depth by a pattern of applied wind stress symmetrically related to the ocean's boundaries (section 3 of the present study).

Neumann (1955) has considered the consequences of a variable depth ocean on the vorticity balance, and has postulated that this balance may be modified by terms involving the space gradients of the effective depth of the ocean (section 4 of the present study). The primary influence of the planetary vorticity may thus be either enhanced, partially or completely balanced, or even over-compensated for, depending on the effective oceanic bottom topography in terms of these ideas. Neumann further suggested that, in a stratified ocean, if the depth of the physical bottom is sufficiently great in relation to the vertical density gradients, this "effective depth" characterizing the "topographic vorticity" would be the lower boundary of the wind induced circulation. Evidence was presented to suggest that this lower boundary undergoes a natural adjustment over much of the world ocean which largely balances the planetary vorticity.

The full variable depth vorticity equation (4.27) is too general for analytic solution as it stands. The following section will study certain analytical properties of a vorticity equation derived from (4.27), introducing variously defined topographic effects.

Firstly, examination may be made of the rates at which westward intensification of flow and the total circulation change in a meridionally bounded ocean as the magnitude of the coefficient of $\partial\Psi/\partial x$, which contains the planetary vorticity term, is varied. An elementary starting point for such an analysis is the model of Stommel (1948), analyzed in section 3 of the present study. A vorticity equation was derived which described the stream function, Ψ, of the vertically integrated volume transport in the form:

$$\nabla^2\Psi + \frac{\partial f}{\partial y} \cdot \frac{D}{K^*} \frac{\partial\Psi}{\partial x} = -\frac{1}{K} \operatorname{curl}_z \vec{\tau} \tag{5.1}$$

For comparison, Neumann's equation (4.27), reduced to a flat ocean of constant depth, becomes:

$$\nabla^2\Psi + \frac{1}{K} \frac{\partial f}{\partial y} \frac{\partial\Psi}{\partial x} = -\frac{1}{K} \operatorname{curl}_z \vec{\tau} \tag{5.2}$$

The relation (5.3) between the coefficients of friction K and K^* in the above equations should be noted, since the absolute value of the depth, D, apparently occurs in that of Stommel (5.1).

$$K = \frac{K^*}{\zeta - D} \simeq \frac{K^*}{D} \tag{5.3}$$

i.e, Stommel's coefficient of friction, K^*, is proportional to the total depth of the circulating water. Numerically, however, the coefficients of the term $\left(\frac{\partial f}{\partial y} \frac{\partial\Psi}{\partial x}\right)$ in equations (5.1) and (5.2) were equal constants ($= 10^{-6}$ sec^{-1}) in the examples discussed by both authors.

Stommel's solution of equation (5.1), the boundaries of which form a streamline with $\Psi = 0$, is written from (3.43) for a square ocean, with a = b, to simplify notation without loss of generality for the present purpose.

$$\Psi = \frac{Fa}{\pi K^*} \sin\left(\frac{\pi}{a} y\right)[pe^{Ax} + qe^{Bx} - 1] \qquad (5.4)$$

where p, q, A, and B were defined in section 3.

The behavior of the maximum value of the stream function, Ψ, as the magnitude of a, the coefficient of $\partial\Psi/\partial x$ in equation (5.2) is reduced, and will now be investigated. This will give a first approximation to the balancing of the planetary vorticity by the progressive development of a topographic term in the vorticity equation.

Use of equation (3.53) which locates the abscissa of the maximum of the Stommel function in equation (5.4) permits calculation of the variation of this maximum value as a function of the value of the parameter a. The results of such computations for square oceans of various dimensions are plotted in figure 5.1. Figure 5.2 describes the associated variation with a of the abscissa of the stream function maximum. The influence of rectangular boundaries other than square may be estimated from the curves in figure 3.3.

For a large ocean basin, it may be seen that, as the magnitude of the coefficient a is decreased from geographically "natural" maximum of 10^{-7} c. g. s. units to zero, the maximum value of the stream function shifts to the center of the basin from a distance of about 0.1 of the total basin width from the western boundary. At the same time, the maximum value of the stream function is increased nearly three-fold. These effects diminish with decrease in ocean dimensions as the rotational effects become less important.

To discuss the balancing process between the planetary and topographic terms in more detail, the properties of a simple model

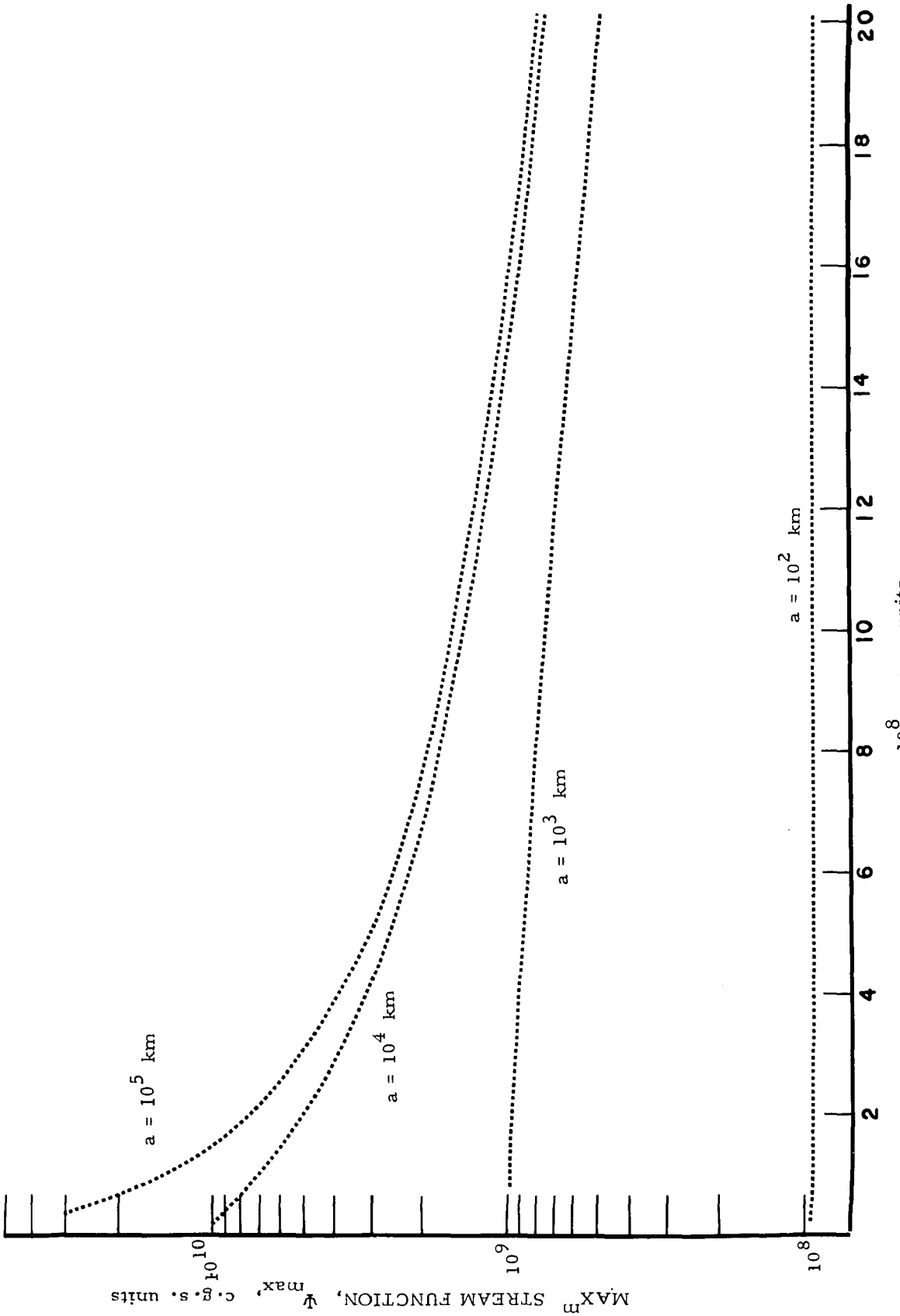

Figure 5.1 Variation of the maximum stream function in square Stommel oceans of various sizes as a function of α, the coefficient of $\partial\Psi/\partial x$ in equation (3.31).

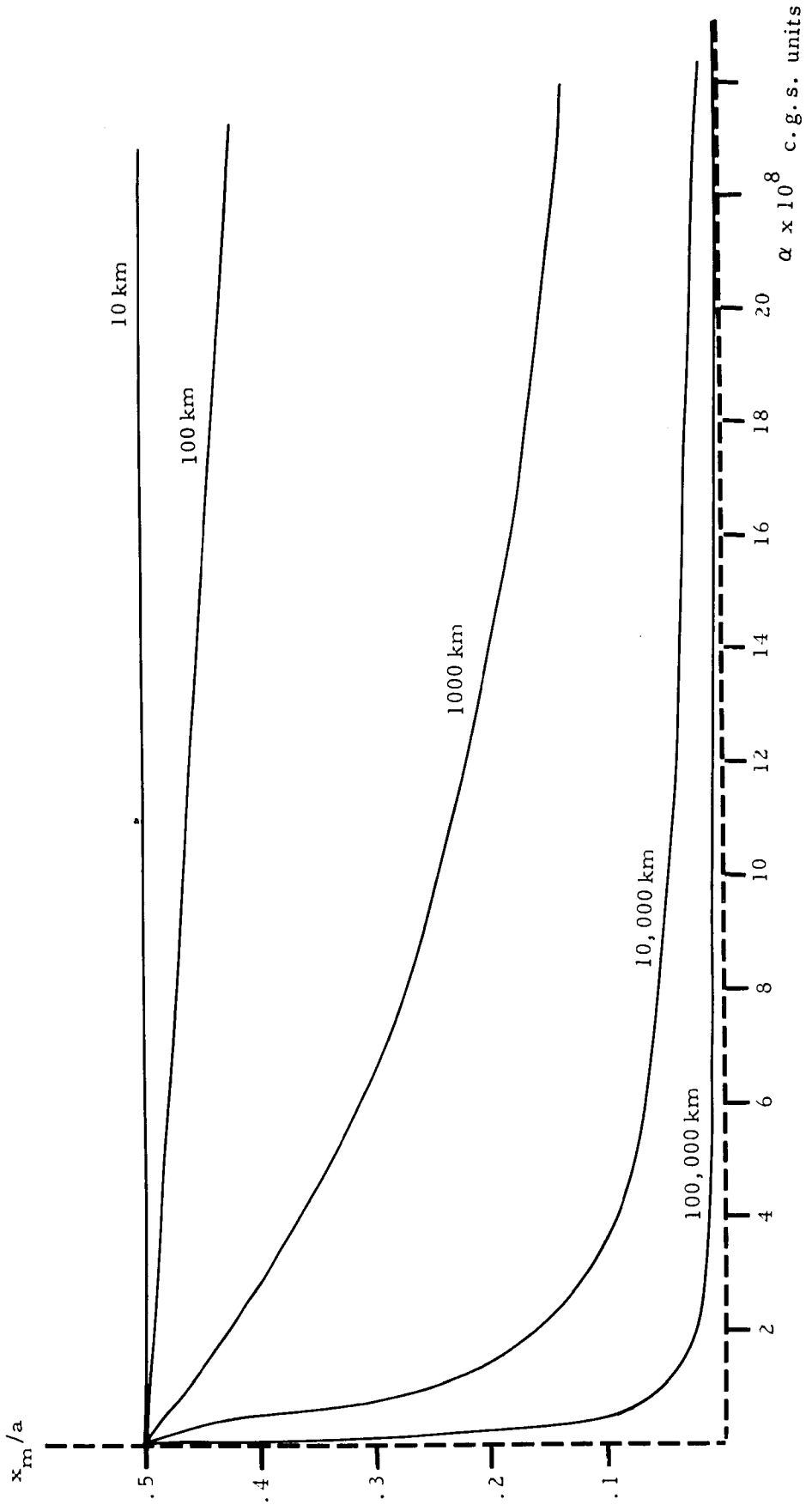

Figure 5.2 Variation of the abscissa, x_{max}, of the maximum stream function corresponding to the situation described in Figure 5.1.

based on the variable depth vorticity equation (4.27) will now be considered, leaving for later consideration objections already mentioned concerning its derivation.

Omission of terms representing convergence of meridians on a spherical earth reduces equation (4.27) to:

$$\nabla^2\Psi + \left(\frac{1}{K}\frac{\partial f}{\partial y} - \frac{f}{KD}\frac{\partial D}{\partial y} - \frac{1}{D}\frac{\partial D}{\partial x}\right)\frac{\partial \Psi}{\partial x} + \left(\frac{f}{KD}\frac{\partial D}{\partial x} - \frac{1}{D}\frac{\partial D}{\partial y}\right)\frac{\partial \Psi}{\partial y}$$

$$= -\frac{1}{K}\,\mathrm{curl}_z\vec{\tau} + \frac{1}{KD}\left(\tau_y\frac{\partial D}{\partial x} - \tau_x\frac{\partial D}{\partial y}\right) \qquad (5.5)$$

The following discussion will arbitrarily model the bathymetry of the lower boundary as a function of y only, and will retain only the surface stress component τ_x,

$$\nabla^2\Psi + \frac{f}{K}\left(\frac{1}{f}\frac{\partial f}{\partial y} - \frac{1}{D}\frac{\partial D}{\partial y}\right)\frac{\partial \Psi}{\partial x} - \frac{1}{D}\frac{\partial D}{\partial y}\frac{\partial \Psi}{\partial y} = -\frac{1}{K}\,\mathrm{curl}_z\vec{\tau} - \frac{\tau_x}{KD}\frac{\partial D}{\partial y} \qquad (5.6)$$

Comparison of the model equations (5.2) and (5.6) shows that if the coefficient of $\partial\Psi/\partial x$ is considered to be reduced in magnitude through the development of a meridionally sloping lower boundary, then the "effective wind stress curl" on the right hand side of equation (5.6) will also necessarily be modified. Inclusion of the topographic vorticity further complicates comparison of equation (5.6) with (5.1) or (5.2) through the appearance of a term in the differential equation specifically containing the zonal velocity, $\partial\Psi/\partial y$. The consequent modification of the properties of the stream function will now be considered.

Assuming, for the moment, that one may independently choose the fields of wind stress $\tau_x(y)$ and of the lower boundary depth $D(y)$,

an expression for D is sought which will make the whole coefficient of $\partial\Psi/\partial x$ constant, in an effort to retain comparison with the work of Stommel as far as possible; i.e.,

$$\frac{f}{KD}\frac{\partial D}{\partial y} = k \tag{5.7}$$

where k is some constant.

Since Stommel considered a "beta-plane" configuration in which

$$\frac{\partial f}{\partial y} = \beta \text{ , a constant,} \tag{5.8}$$

the coefficient becomes

$$\frac{\beta y}{KD}\frac{\partial D}{\partial y} = k \tag{5.9}$$

and the form of D(y) is determined by

$$\frac{1}{D}\frac{\partial D}{\partial y} = \frac{c}{y} \tag{5.10}$$

where $c \equiv kK/\beta$.

Integration gives the required depth variation,

$$D = s|y^c| \tag{5.11}$$

where s is an arbitrary constant. The coefficient of $\partial\Psi/\partial x$ now becomes

$$\gamma = \frac{\beta}{K}(1 - c) \tag{5.12}$$

If attention is confined to values of $\gamma \geq 0$, i.e., over-compensation of the planetary vorticity by the topographic term is excluded, c will lie in the interval $0 \leq c \leq 1$; physically interesting lower boundary configurations will, in general, show D monotonic increasing with y (i.e., polewards). Whether the sequence of functions

represented by (5.11) may possibly be consistently applied to any wind-driven circulation model when both thermodynamic and dynamic requirements are examined, is a question which will conveniently be ignored for the time being, in favor of a formal examination of the properties of the differential equation (5.6).

This equation may now be written:

$$\nabla^2\Psi + \gamma \frac{\partial\Psi}{\partial x} - \frac{c}{y}\frac{\partial\Psi}{\partial y} = -\frac{1}{K}(\nabla \times \tau)_z - \frac{\tau_x}{K}\cdot\frac{c}{y} \tag{5.13}$$

The general form of the complementary function of equation (5.13) may be developed as follows:

The homogeneous equation

$$\nabla^2\Psi + \gamma \frac{\partial\Psi}{\partial x} - \frac{c}{y}\frac{\partial\Psi}{\partial y} = 0 \tag{5.14}$$

is separable. Consider a solution of the form:

$$\Psi(x, y) = \xi(x)\cdot\eta(y) \tag{5.15}$$

where ξ is a function of x only, and η is a function of y only.

Differentiation of (5.15) and substitution in (5.14) yields:

$$\eta\frac{d^2\xi}{dx^2} + \xi\frac{d^2\eta}{dy^2} + \gamma\eta\frac{d\xi}{dx} - \frac{c}{y}\xi\frac{d\eta}{dy} = 0 \tag{5.16}$$

i.e.,

$$\frac{d^2\xi}{dx^2} + \gamma\frac{d\xi}{dx} - \mu^2\xi = 0 \tag{5.17}$$

and

$$\frac{d^2\eta}{dy^2} - \frac{c}{y}\frac{d\eta}{dy} + \mu^2\eta = 0 \tag{5.18}$$

where $\mu^2 > 0$ is the separation constant chosen for the problem. The integral of (5.17) is (5.19).

$$\xi = A e^{mx} + B e^{nx} \tag{5.19}$$

where

$$m = -\frac{\gamma}{2} + \sqrt{\left(\frac{\gamma}{2}\right)^2 + \mu^2} \tag{5.20}$$

and

$$n = -\frac{\gamma}{2} - \sqrt{\left(\frac{\gamma}{2}\right)^2 + \mu^2} \tag{5.21}$$

and A, B are integration constants to be determined.

Equation (5.18) is a form of Bessel's equation, and it may be shown (e.g., Wylie, 1960, p. 422) that it has for general integral:

$$\eta = y^{\nu} [L J_{\nu}(\mu y) + L' Y_{\nu}(\mu y)] \tag{5.22}$$

where $J_{\nu}(t)$, $Y_{\nu}(t)$ are the Bessel and Neumann functions respectively, of order ν where

$$\nu = \frac{1}{2}(1 + c) ; \qquad \gamma = \frac{2\beta}{K}(1 - \nu) \tag{5.23}$$

Values of ν of interest in this discussion will range from 1/2 to 1, inclusive. L, L' are arbitrary integration constants.

From equations (5.15), (5.19), and (5.22), the complementary function of (5.13), or the solution of (5.14), is given by equation (5.24).

$$\Psi = (Ae^{mx} + Be^{nx})(L J_{\nu}(\mu y) + L' Y_{\nu}(\mu y)) y^{\nu} \tag{5.24}$$

The constants A, B, L, L' permit application of boundary conditions to assist a choice of solution, appropriate to a particular problem, from the multiple infinity of functions represented by equation (5.24). First, however, a particular integral of equation (5.13) must be found in order that boundary conditions may be applied to the complete solution. It thus becomes necessary to specify the functional form

of the applied wind stress at this point in the discussion. Following Stommel, a wind stress system will first be considered which varies in the y-direction only in such a way as to model the essential directive features of lower latitudes easterly winds and higher latitude westerlies. A function that shows both these characteristics and the orthogonality relationships with the y-dependent terms in the complementary function, thus leading to a closed solution, is given by equation (5.25).

$$\tau_x = F\left(\frac{y}{b}\right)^{\nu} J_{\nu-1}(\mu_1 y) \; ; \qquad \tau_y = 0 \tag{5.25}$$

where μ_1 is such that $(\mu_1 b)$ is the first-zero of $J_\nu(t)$. F is the maximum magnitude of the wind stress.

With the use of equation (5.25), the vorticity equation (5.13) may now more specifically be defined as:

$$\nabla^2\Psi + \gamma \frac{\partial\Psi}{\partial x} - \frac{c}{y}\frac{\partial\Psi}{\partial y} = -\frac{F}{Kb}\left(\frac{y}{b}\right)^{\nu-1}[\mu_1 y\, J_{\nu-2}(\mu_1 y) + (1 - c)\, J_{\nu-1}(\mu_1 y)] \tag{5.26}$$

A particular integral of equation (5.26) is given by (5.27):

$$\Psi = -\frac{F}{K}\left(\frac{y}{b}\right)^{\nu} J_\nu(\mu_1 y) \tag{5.27}$$

Since equation (5.13) is linear in Ψ, its complete solution is expressed by the sum of the complementary function (5.24) and the particular integral (5.27); the former consisting, in general, of the linear combination of all terms like (5.24) resulting from the (as yet) arbitrary nature of the integration constants; i. e.,

$$\Psi = y^{\nu} \int_0^{\infty} \{(Ae^{mx} + Be^{nx})(LJ_{\nu}(\mu y) + L'Y_{\nu}(\mu y)\} \, d\mu - \frac{F}{K} J_{\nu}(\mu_1 y) \tag{5.28}$$

Side conditions will now be applied to make the rectangular ocean boundary a streamline, viz.:

$$\begin{aligned} \Psi(x, 0) &= 0 = \Psi(x, b) \\ \Psi(0, y) &= 0 = \Psi(a, y) \end{aligned} \tag{5.29}$$

(i) $\underline{\Psi(x, 0) = 0}$

Since $\lim_{\xi \to 0} [\xi^{\nu} Y_{\nu}(\xi)] \neq 0$, all the coefficients L_i' must separately vanish, and the choice of solutions is reduced to:

$$\Psi = y^{\nu} \int_0^{\infty} J_{\nu}(\mu y) \cdot [Ae^{mx} + Be^{nx}] \, d\mu - \frac{F}{Kb^{\nu}} J_{\nu}(\mu_1 y) \tag{5.30}$$

where the constants L have been absorbed in the A and B.

(ii) $\underline{\Psi(x, b) = 0}$

i.e., $$b^{\nu} \int_0^{\infty} J_{\nu}(\mu b) \cdot [Ae^{mx} + Be^{nx}] \, d\mu = 0 \tag{5.31}$$

Since b is non-zero, and if the function of x is not to vanish identically, this last equation requires the selection of a particular infinite set of the separation constants, μ_i, already defined following equation (5.25), from zeros of the Bessel function.

The solution may thus be reduced from an integral representation to an infinite series

$$\Psi = y^{\nu} \sum_{i=1}^{\infty} J_{\nu}(\mu_i y) \left[A_i e^{m_i x} + B_i e^{n_i x} \right] - \frac{F}{Kb^{\nu}} J_{\nu}(\mu_1 y) \tag{5.32}$$

and it remains to determine the coefficients $\{A_i, B_i\}$. In passing, it may be noted from (5.11) that the parameter values $c = 0$; $\nu = \frac{1}{2}$ characterize an ocean of constant depth. Since

$$J_{\frac{1}{2}}(\xi) = \sqrt{\frac{2}{\pi \xi}} \cdot \sin\xi ,$$

the general solution for such an ocean has the form

$$\Psi \sim \sum_i \sin(\mu_i y) \cdot \left(A_i e^{m_i x} + B_i e^{n_i x} \right) + (\text{particular integral})$$

--in essence, the same as equation (3.37) derived by Stommel for such an ocean.

(iii) $\underline{\Psi(0, y) = 0}$

Application of this condition gives:

$$\sum_{i=1}^{\infty} M_i J_\nu(\mu_i y) = \frac{1}{y^\nu} \frac{F}{K} J_\nu(\mu_1 y) \qquad (5.33)$$

where $M_i \equiv A_i + B_i$.

The species M_i is thus identified as the set of coefficients of the Fourier-Bessel expansion of the function on the right hand side of equation (5.33) over the range $y = [0, b]$. These coefficients may be evaluated by a generalized Fourier procedure. In the operations of multiplication of each side of (5.33) by $yJ_\nu(\mu_j y)$, successively, with $j = 1, 2, 3, \cdots$, and integration each time from $y = 0$ to $y = b$, the orthogonality relationships among the Bessel functions provide that all terms of the integral resulting from the summation in (5.32) vanish, except for one where $i = j = 1$. Thus

$$M_1 = A_1 + B_1 = 1 \tag{5.34}$$

(iv) If $\Psi(a, y) = 0$

$$\left(A_1 e^{m_1 a} + B_1 e^{n_1 a}\right) J_\nu(\mu_1 y) = + J_\nu(\mu_1 y)$$

or
$$A_1 e^{m_1 a} + B_1 e^{n_1 a} = + 1 \tag{5.35}$$

but from (5.34)

$$A_1 = 1 - B_1 \tag{5.36}$$

Substitution of (5.36) in (5.35) now defines the constants A_1, B_1 as follows:

$$A_1 = \frac{e^{n_1 a} - 1}{e^{n_1 a} - e^{m_1 a}} \tag{5.37}$$

and

$$B_1 = \frac{1 - e^{m_1 a}}{e^{n_1 a} - e^{m_1 a}} \tag{5.38}$$

while the constants m_1, n_1 may be derived from equations (5.20), (5.21) with $\mu = \mu_1$.

With these values of A, B, p, and q, a simple expression for the stream function solution of equation (5.13) may be derived in the form (5.39) similar to Stommel's expression (3.43).

$$\Psi = \frac{F}{K}\left(\frac{y}{b}\right)^\nu J_\nu(\mu_1 y)\left(A_1 e^{m_1 x} + B_1 e^{n_1 x} - 1\right) \tag{5.39}$$

It will be recalled from equations (5.11) and (5.23), that the parameter ν specifies the configuration of the lower boundary,

and that variation of this parameter was designed to represent varying degrees of compensation of the planetary vorticity by the topographic vorticity, in terms of a simplified version of Neumann's equation (4.27). Since ν appears also in the expression chosen to represent the applied wind stress (equation 5.25), variation of this parameter does not, strictly, illustrate the effect of varying topographic influence, all other influences being constant. This is part of the price paid to maintain as close a parallel in the above analysis to Stommel's treatment (section 3), including the closed form of the solution. Variation in the wind stress pattern over the range of ν considered is not too drastic, however, the general theme of low latitude easterlies and high latitudes westerlies being preserved. Meridional sections of D and τ_x for $\nu = 0.5$, 1.0 (0.1) are shown in figure 5.3, and the streamline patterns for an ocean basin similar in dimensions to that of Stommel, have been calculated from equation (5.39). These patterns are plotted in figures 5.4 to 5.9. For these calculations, $F = 1$*, $K = 10^{-6}$ sec^{-1}, $a = 10^9$ cm, $b = 6 \times 10^8$ cm, $\beta = 10^{-13} sec^{-1}$ cm^{-1}. Bessel functions were obtained from a subroutine of the library of the AEC-NYU computing center, where the calculations were performed. Zeros of these functions (μ_i in the above analysis) were obtained from the relation given, for example, by Jahnke and Emde. (1945, p. 143). For $\nu = 0.5$, Stommel's constant depth analysis is virtually duplicated by the present treatment; this may be seen by comparison of figures 3.1 and 5.4. As ν is increased in value, the "westward intensification" induced by the planetary vorticity becomes less

---

*dyne cm^{-2}.

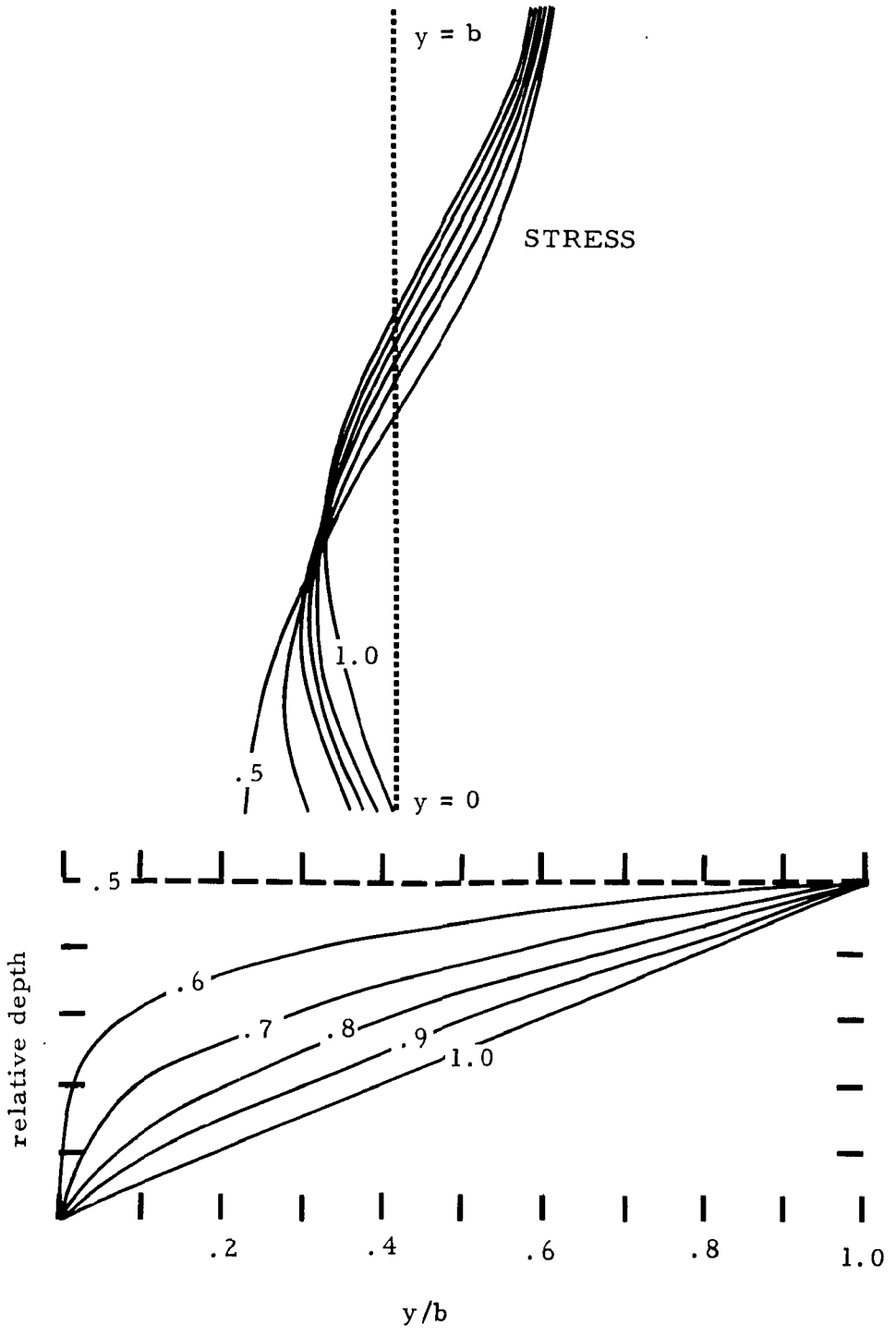

Figure 5.3 Sequences of functions chosen to model the meridional variation of the zonally directed wind stress (upper) and the meridional variation of the lower boundary of the wind-driven circulation (lower) in equations (5.25) and (5.11), for six values of the parameter lying between $\nu = 0.5$ and 1.0.

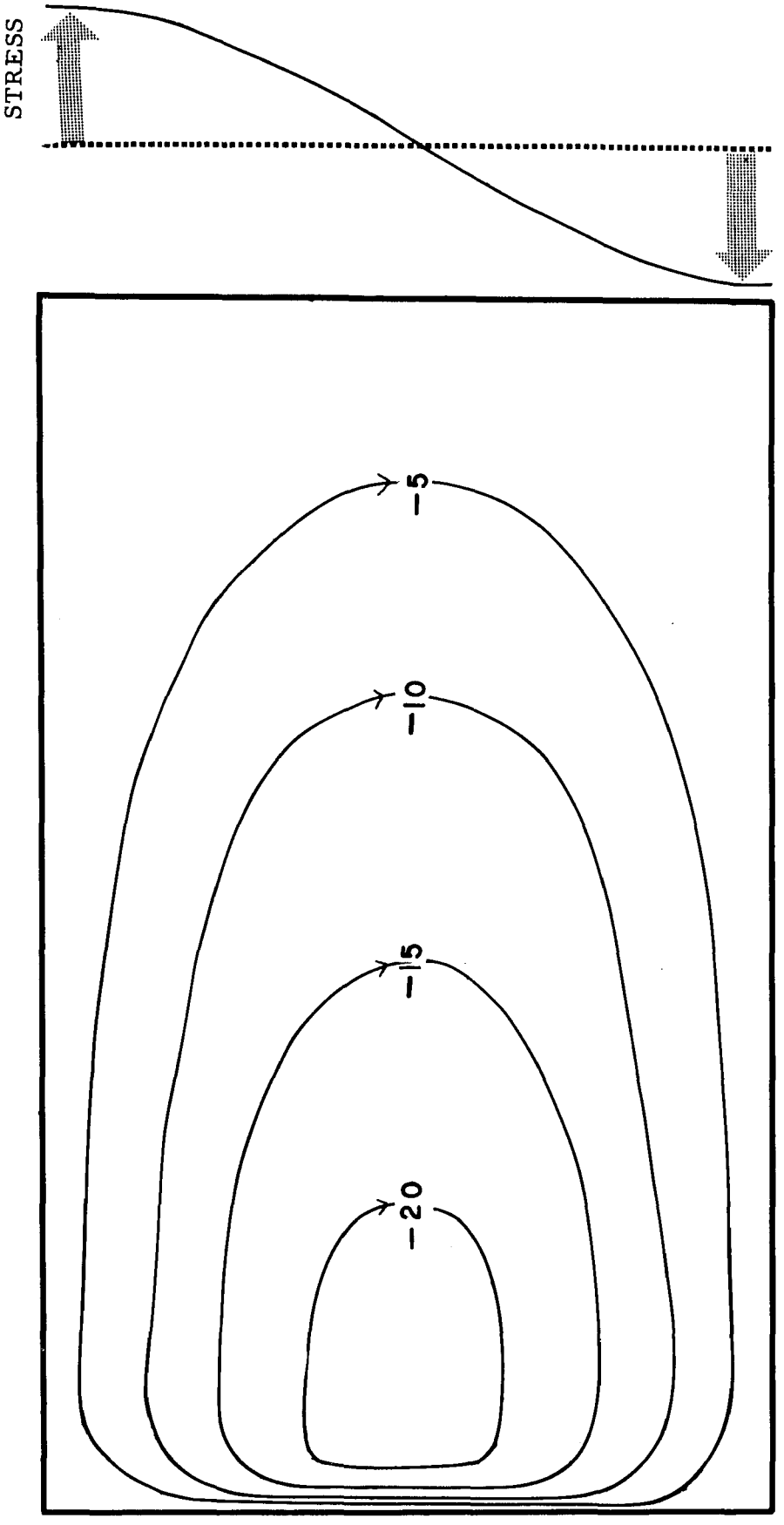

Figure 5.4 Streamlines of the vertically integrated mass transport (c.g.s. units $\times 10^{-8}$) in a simplified Neumann ocean according to equation (5.39) with $\nu = 0.5$.

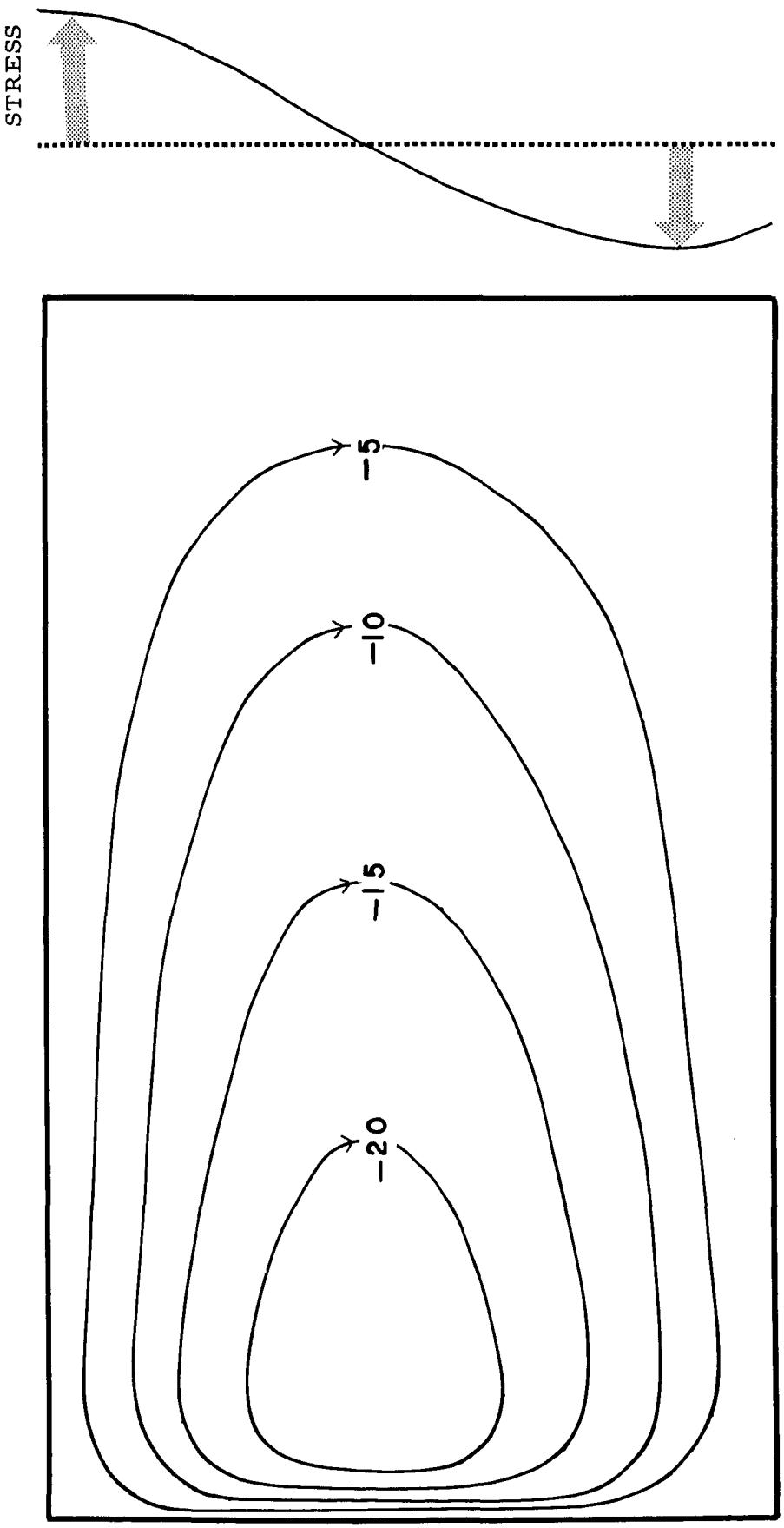

Figure 5.5 Streamlines of the vertically integrated transport (c.g.s. units $\times 10^{-8}$) in a simplified Neumann ocean according to equation (5.39) with $\nu = 0.6$. The form of the wind stress is shown at the right.

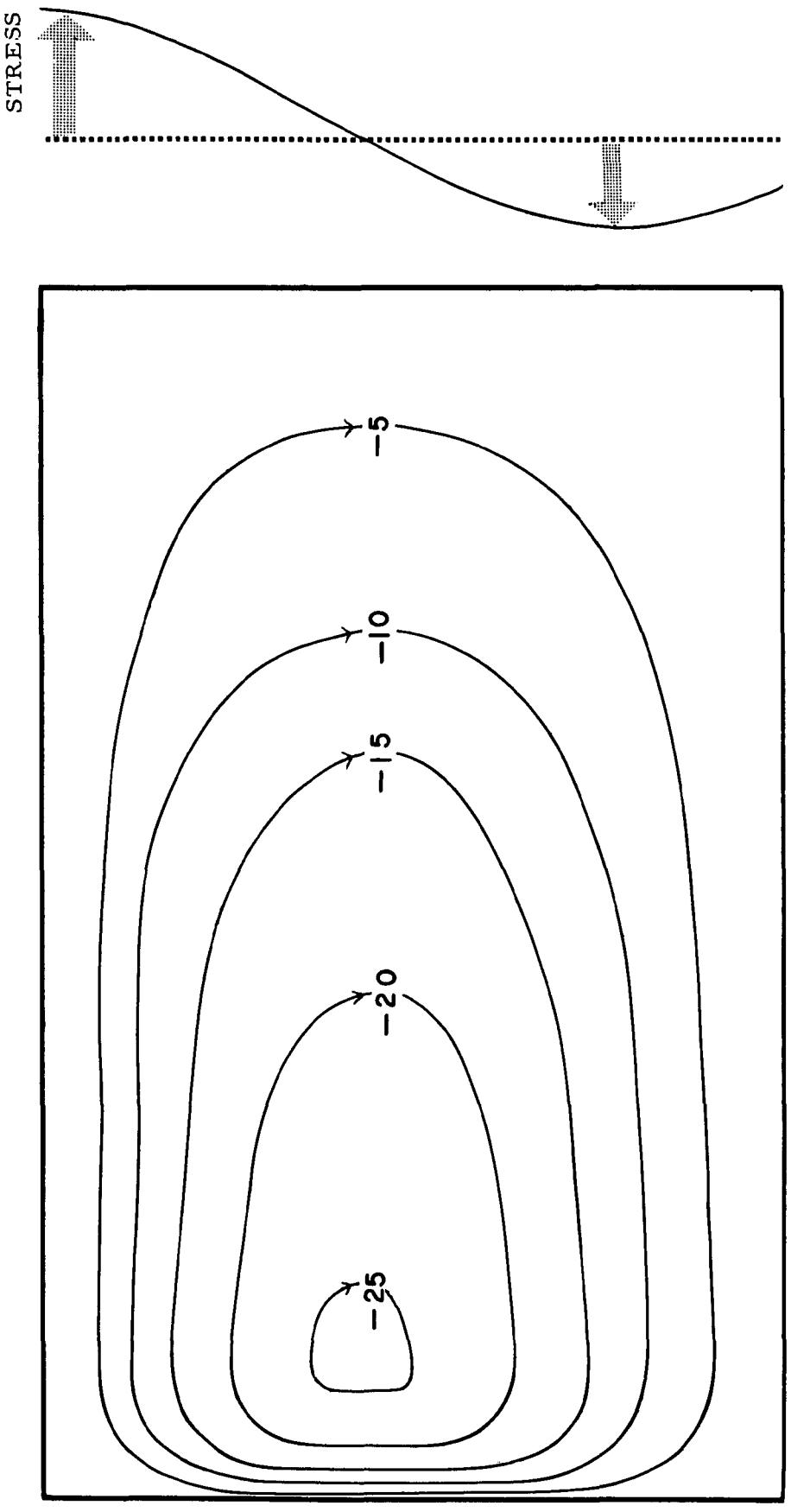

Figure 5.6 Streamlines of the vertically integrated transport (c.g.s. units $\times 10^{-8}$) in a simplified Neumann ocean according to equation (5.39) with $\nu = 0.7$. The form of the wind stress is shown at the right.

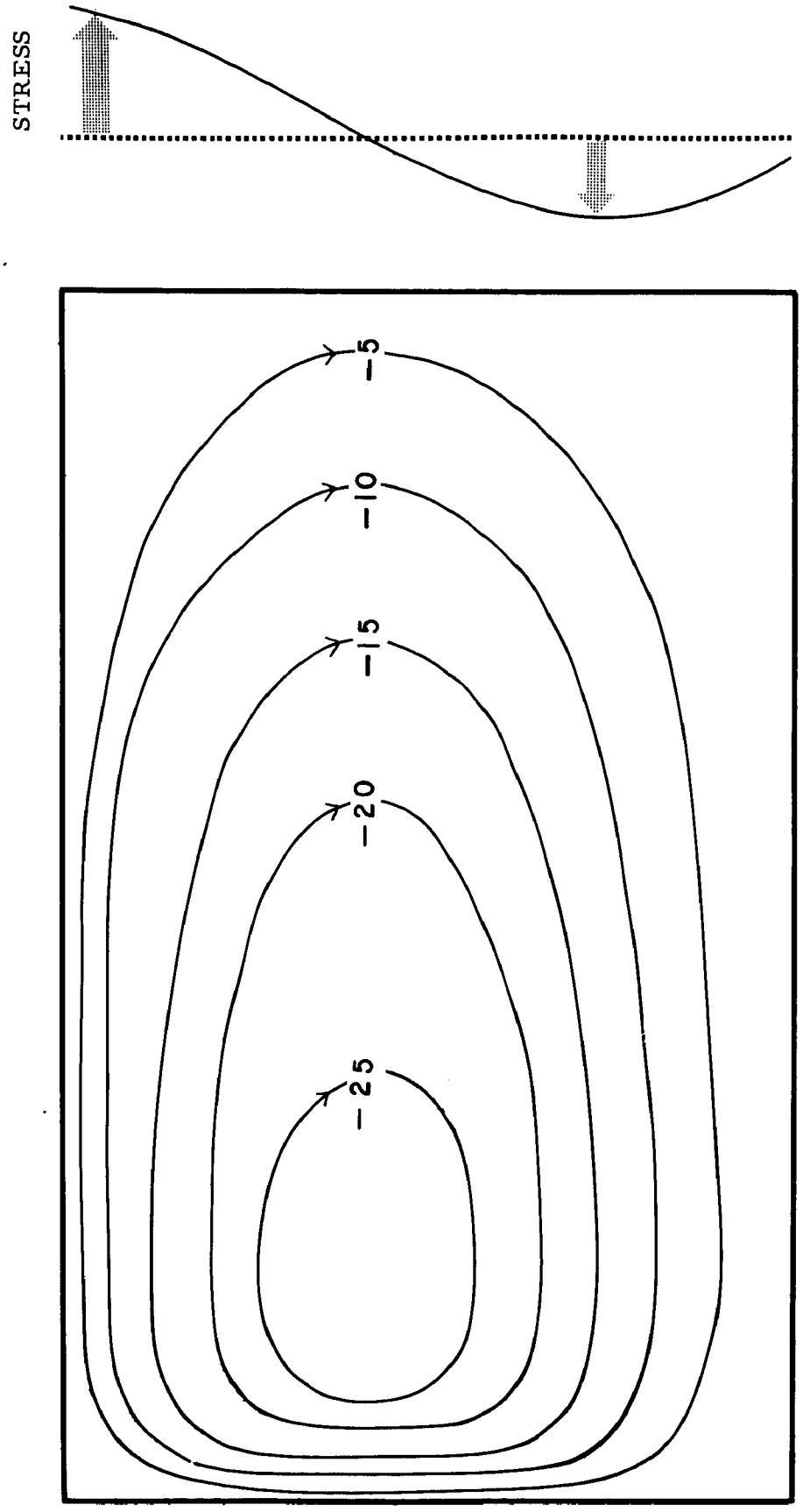

Figure 5.7 Streamlines of the vertically integrated transport (c.g.s. units $\times 10^{-8}$) in a simplified Neumann ocean according to equation (5.39) with $\nu = 0.8$. The form of the wind stress is shown at the right.

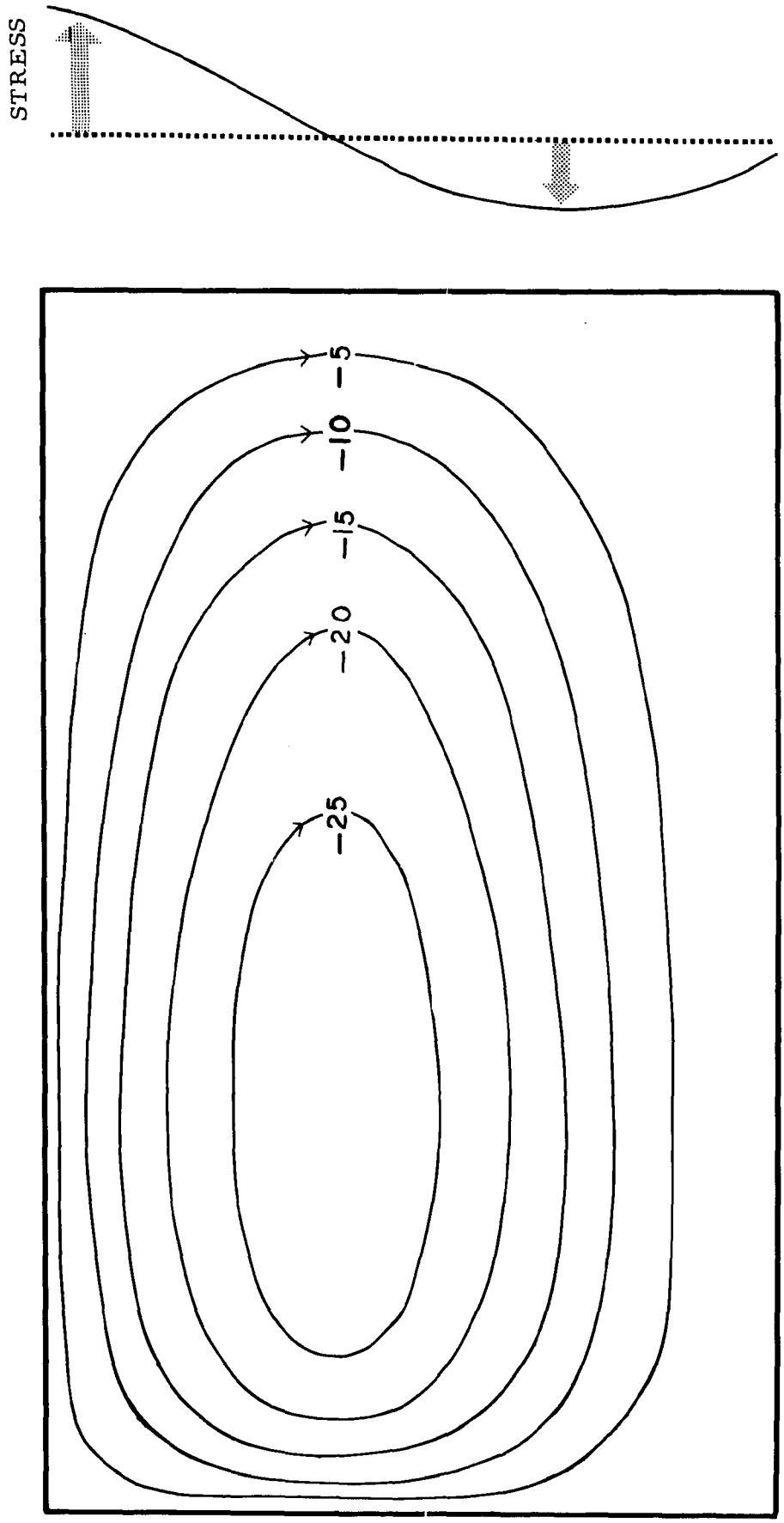

Figure 5.8 Streamlines of the vertically integrated transport (c.g.s. units $\times 10^{-8}$) in a simplified Neumann ocean according to equation (5.39) with $\nu = 0.9$. The form of the wind stress is shown at the right.

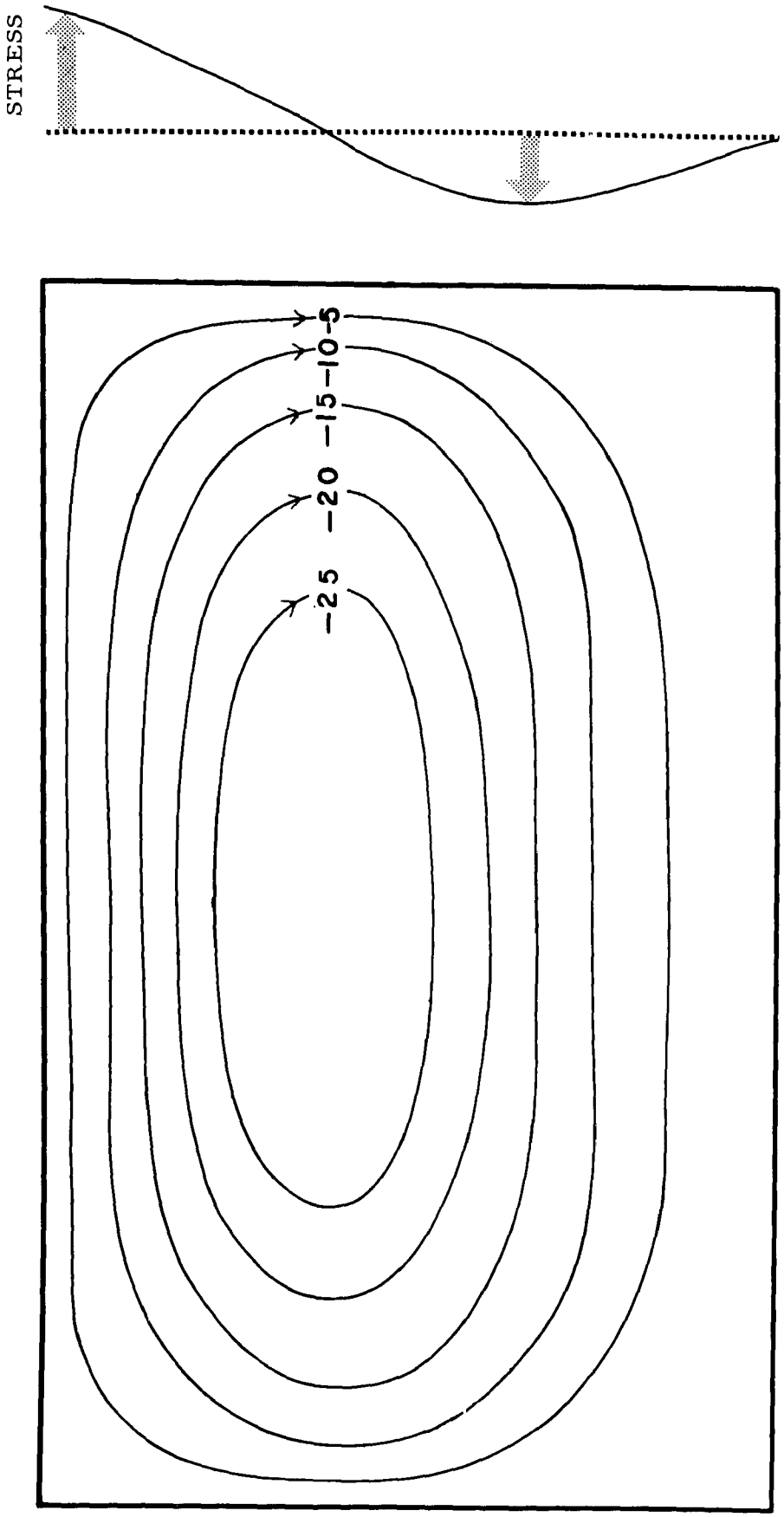

Figure 5.9 Streamlines of the vertically integrated transport (c.g.s. units · 10^{-7}) in a simplified Neumann ocean according to equation (5.39) with ν = 1.0. The form of the wind stress is shown at the right.

pronounced, and with $\nu = 1.0$, complete zonal symmetry in the streamline pattern is achieved. At the same time, the maximum value of the stream function increases, following the trend suggested by figure 5.1. A small part of this variation will be due to variations in the applied wind stress field. The meridional asymmetry which accompanies increase in the value of ν is due to the progressive northwards shift in the maximum wind stress. Any contribution to this meridional asymmetry from variation of the coefficient of $\partial\Psi/\partial y$ will be masked by this effect.

The foregoing analysis serves two purposes. Firstly, it emphasizes the relationship between the functional form of the wind stress and the orthogonality properties of those functions which appear in the y-dependent separated equation derived from the Stommel-type boundary value problem. Secondly, while maintaining a close parallel with Stommel's model, it gives some feeling for the introduction of varying amounts of topographic influence, in the Neumann sense. The introduction of this influence has been made here in a formal and very artificial manner. Retaining the formalism, various degrees of freedom may be assigned to the lower boundary geometry by appropriate choice of the x-y dependence of the coefficients of $\partial\Psi/\partial x$ and $\partial\Psi/\partial y$ in equations (4.27) or (5.5) so that the various differential equations that appear in the separation process become those whose solutions have been studied in detail as the "special functions" of mathematical physics. This approach would probably be more instructive as a mathematical exercise than helpful in gaining an appreciation of ocean transport dynamics, however, and will not be followed further in this study. The method of handling a general wind stress in the Stommel

analysis, by expansion as a series in the appropriate orthogonal functions, has been explained in section 3.5 . The properties of the variable depth model just outlined may be used in a similar Fourier-Bessel series expansion of the applied wind stress to discuss the effects of wind patterns other than the representation (5.25).

6. Neumann transport in the Atlantic Ocean

6.1 Introduction

Means for obtaining analytic solutions of various formal simplifications of Neumann's variable depth vorticity equation in terms of orthogonal functions, have been outlined in the previous section. For those forms of this equation, including the full relation (4.27), which are not amenable to this treatment, the method of numerical integration using a finite difference approximation for the differential equation may be used. Prompted by the earlier work of Neumann and Ostapoff (1957), and of Neumann (1958), who reported the results of such a numerical integration applied to the North Atlantic, the properties of equation (4.27) were related to one interpretation of conditions as they actually obtain over the whole Atlantic Ocean. Details of this work are reported by Garner, Neumann, and Pierson (1962), and a summary of the results will be included here to complete the discussion of the Neumann model.

A field of points was established on a two degree grid of latitude and longitude. Coastal boundaries were approximated by a series of straight lines joining those grid points which were nearest to the edge of the continental shelves of bordering land masses. The

boundary thus constructed may be compared with the actual coastal outline of the Atlantic Ocean in figure 6.1. An idealized "Caribbean Island" was constructed from those grid points which best defined the land masses and relatively shallow water associated with the islands and banks of this region. Flow into the Gulf of Mexico through the Yucatan Channel balanced outflow through the Straits of Florida to satisfy requirements of continuity.

The mean surface wind pattern over the Atlantic Ocean for February, as estimated by the British Meteorological Office (1948), and charts published by Schott (1944, Plate 22) were used to derive the wind stress distribution using the empirical relation of Neumann (1948)

$$\tau = 0.09 \rho' W^{3/2} \qquad (6.1)$$

where the wind stress on the sea surface, τ, is measured in dynes cm^{-2} if the wind velocity, W, at anemometer height is measured in cm sec^{-1}. ρ' is the air density, here given a constant value of 1.25×10^{-3} gms cm^{-3}. At each interior grid point of the system, the depth of no motion was determined from the chart published by Defant (1941), with some extrapolation and modification particularly in the South-West Atlantic and the Southern Ocean. The patterns of wind and depth of no motion finally used in the investigation are sketched in figures 6.1 and 6.2; the actual numerical values and details of the computation are set down by Garner, et al. (1962). A value of 3.3×10^{-6} sec^{-1} was entered for the coefficient of internal friction, K. This figure was obtained by Neumann (1954, p. 31) from observations of the geostrophic deviation of the mass transport vector in the Atlantic Ocean, north of

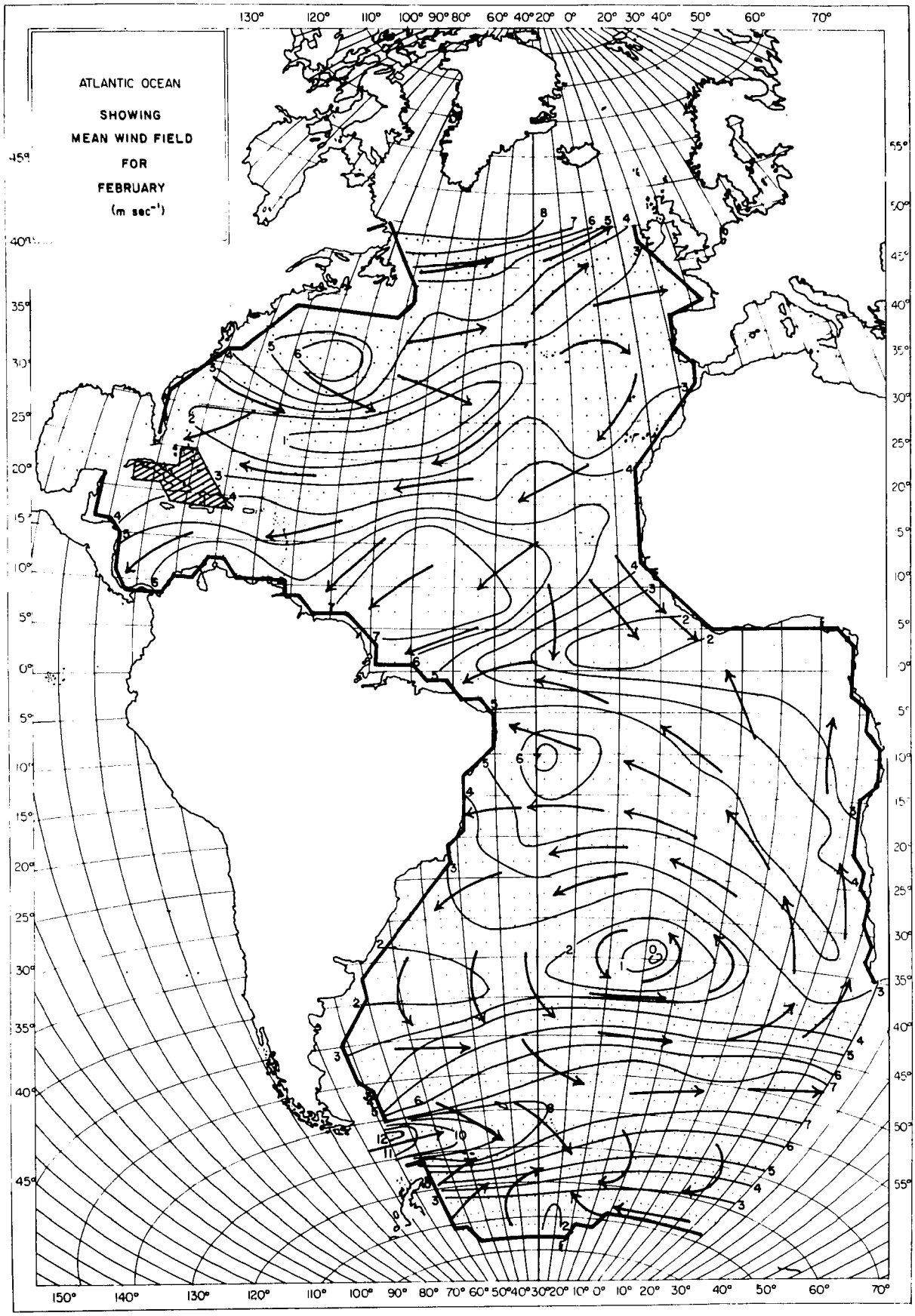

Figure 6.1 Mean surface wind field over the Atlantic Ocean used in the ocean circulation calculations. Isotachs in m sec^{-1} are shown as continuous lines. The arrows show the general wind direction.

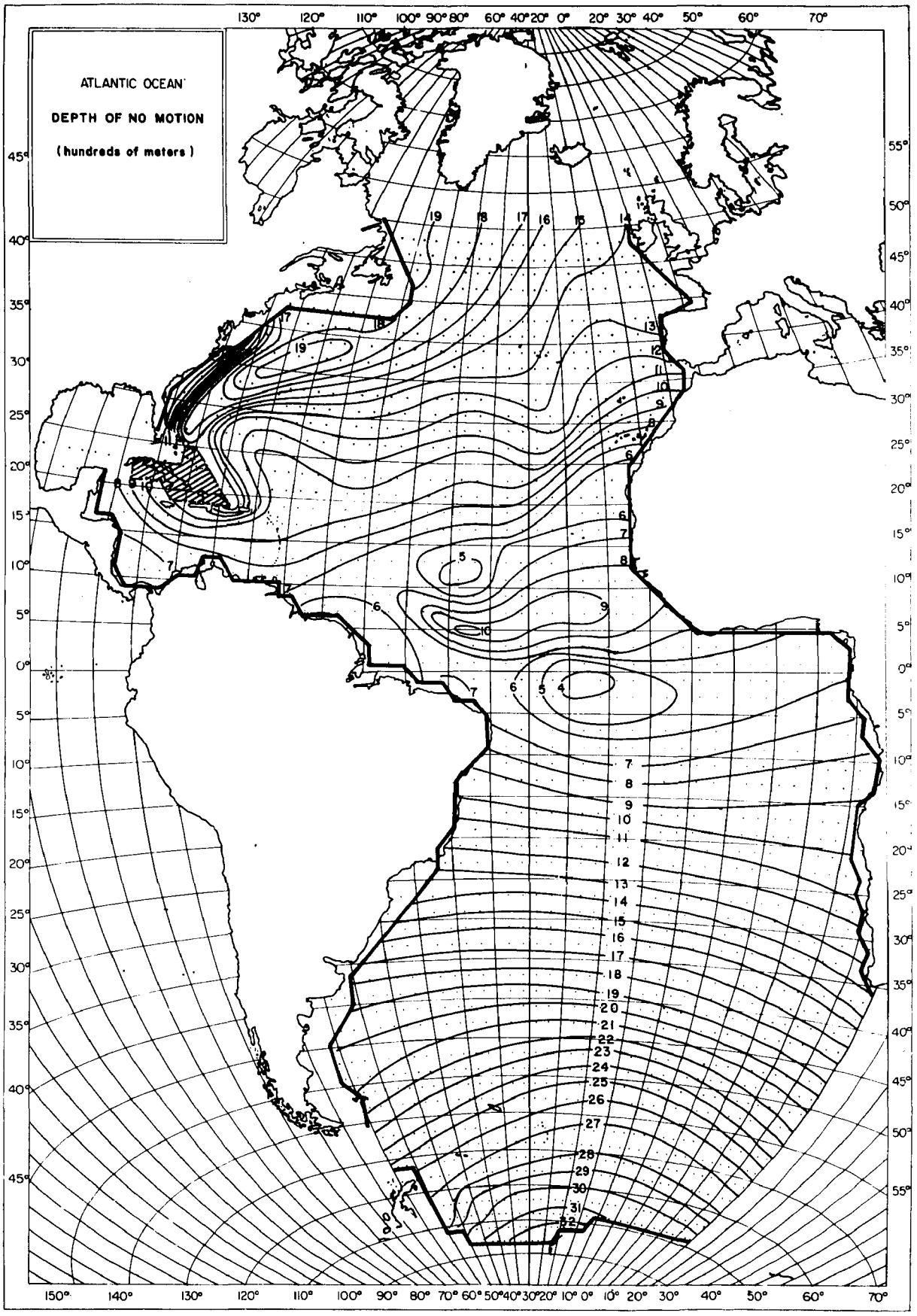

Figure 6.2 Depth of the lower boundary of the wind-driven ocean circulation used in the ocean circulation calculations, based on Defant (1941).

the Azores.

Fixed coastal boundaries were taken to be streamlines. Constant values of the stream function, Ψ, were then assigned to each continuous section of coastal boundary, the values of which were determined by the transport of water assumed to flow into or out from the field of integration, according to equations (2.55, 2.56). Values for the strengths of these sources and sinks were adopted as follows: A small source northeast of Newfoundland represented the Labrador Current which carries 4 million tons sec^{-1} into the North Atlantic Ocean. A larger sink of 10 million tons sec^{-1} was assigned between Iceland and the British Isles where the North Atlantic Current flows into the Norwegian Sea. No flow across the northern boundary was permitted between west longitudes 33° and 45°. These figures were based on discussion by Sverdrup (1942, Chap. 15). In the southwest corner of the field of integration is the Drake Passage between Cape Horn and the Palmer Peninsula, Clowes (1933) estimated that the Antarctic Circumpolar Current carried about 110 million tons sec^{-1} eastwards through this passage above the 3,500 decibar surface, and this value was used here as the source strength in this region. In the southeast is the passage between the Cape of Good Hope and the Antarctic Continent. A sink has been assigned at this boundary of 110 million tons sec^{-1}, assuming that all of the water entering the South Atlantic Ocean through the Drake Passage passes into the Indian Ocean sector of the Southern Ocean. An additional source of 20 million tons sec^{-1} has been placed between the Cape of Good Hope and latitude 39°S, representing a branch of the Agulhas

Current which enters the Atlantic Ocean, according to Dietrich (see Sverdrup, 1942, p. 696) in this area. 14 million tons sec^{-1} of this inflow was then carried eastward back into the South Indian Ocean with the Antarctic Circumpolar Current, leaving the remainder of 6 million tons sec^{-1} as a contribution to the Atlantic circulation. These figures were chosen keeping in mind an estimated northward transport across the equator of 6 million tons sec^{-1} in the Guiana Current along the northeast coast of South America (Sverdrup, 1942, p. 629). The "Caribbean Island" was treated as a "floating" boundary. Provision was made for the stream function to remain constant over all points of this set, but the numerical value of this constant was determined by the geography and dynamics of the situation, except for an assumption that in the immediate vicinity of the southeastern point of the island, one quarter of the total flow joins the Antilles Current, the remaining three quarters entering the Caribbean Sea.

The stream function was held constant along portions of the northern boundary south of Greenland. For other oceanic boundary point, an interpolation for the imposed value of stream function was made between neighboring fixed boundaries.

6.2 Presentation of results

Five different solutions of equation (4.27) were obtained for various combinations of wind stress and topography of the depth of no motion surface. The resulting streamline patterns are shown in figures 6.3 through 6.7.

(a) Variable stress, variable depth solution

For the general fields of wind and depth of no motion

described previously, the streamline pattern is plotted in figure 6.3. This calculation incorporates all the vorticity terms considered in the derivation of equation (4.27).

(b) Variable depth, zero stress solution

Figure 6.4 shows the result of repeating the above calculations with zero wind velocity. All other factors, including the depth distribution were unchanged. Formally, this represents a complementary function of equation (4.27) with its boundary conditions, defining that part of the complete solution (figure 6.3) that may be attributed to the choice of sources and sinks.

(c) Variable stress, constant depth solution

The calculations were then repeated retaining the general wind pattern but setting the depth constant (1000 m) and the resulting streamline pattern is shown in figure 6.5. In a sense, this calculation acts as a control experiment. The difference between figures 6.2 and 6.5 provides some measure of the dynamic significance of the variable depth terms in equation (4.27) (but see the remarks in section 6.4).

(d) Constant depth, zero wind stress solution

Figure 6.6 shows the result of repetition of the constant depth integration just described with a vanishing wind stress. This shows the contribution of boundary sources and sinks to the complete solution of the constant depth equation.

(e) Variable stress, depth proportional to the sine of latitude solution

The final series of calculations used the general wind stress pattern for February but replaced the depth field by the following scheme:

$$D = 2300\ |\sin\phi|\ ;\quad |\phi| > 9°$$

$$D = 2300 \sin 9°;\quad 0 \leq |\phi| \leq 9°$$

With the depth proportional to the sine of the latitude, the relations

$$\frac{1}{D}\frac{\partial D}{\partial y} = \frac{1}{f}\frac{\partial f}{\partial y}\ ;\qquad \frac{\partial D}{\partial x} = 0 \tag{6.2}$$

are fulfilled, and as Neumann has suggested, any effect of the planetary vorticity in producing a zonal asymmetry in the circulation will be exactly balanced. This situation corresponds to that realized in the Bessel function solution of the previous section for $\nu = 1$ (figure 5.9), where the functional form of the meridional variation of D also matched that of the Coriolis parameter.

Due to difficulties in running this problem, calculations had to be stopped well before complete convergence was achieved, and with North Atlantic results only, being significant. The partially converged streamline pattern is presented (figure 6.7) to contribute to the discussion following.

In each of the circulation patterns presented, streamlines represent constant value of the transport stream function, Ψ, with the indicated value $\times 10^{12}$ c. g. s. units. Between adjacent streamlines, then, there is represented a vertically integrated volume transport whose value is given by the difference of the indicated contour values in millions of (metric) tons a second.

6.3 Discussion of the results

(a) General: An attempt has been made in this work to derive the vertically integrated wind-driven circulation of the Atlantic

Ocean choosing boundary conditions, wind patterns, and variations of the thickness of the wind-driven current system as realistically as possible. The extent to which the result of the general integration, as shown in figure 6.3, provides an acceptable description of the situation as it obtains in nature is then, in some sense, an estimate of the practical usefulness of the model used.

One must beware, however, of attaching too much significance to such a "test". The first difficulty in discussing the streamline patterns in these terms is the general lack of comprehensive comparative observations of the vertically integrated transport of the major ocean current systems. In the discussion following, various sections of the transport pattern will be referred to in terms of the familiar nomenclature of the associated surface water movements, but it should be remembered that such transports are not due simply to these surface currents, considerable complexities being expected in the vertical velocity profile in many areas. A further caution to be observed in interpreting the transport patterns concerns the assumed topography of the depth of no motion. It should be noted that Defant's chart represents conditions ranging over the two-year duration of the Meteor observations, and also incorporates data from other expeditions both before and after the Meteor cruises. The effects of seasonal variations in this "depth of no motion" thus remain undefined. The wind stress pattern used, on the other hand, represents long term mean conditions for February, so some inconsistency may result in expecting realistic transport patterns from an application of these fields in a steady state equation such as (4.27).

The propriety of identification of the surface D in equation (4.27) with Defant's surface of no motion may also be open to question, for reasons advanced in section 4.

(b) Variable wind stress-variable depth solution

The circulation in the North Atlantic Ocean as plotted in figure 6.3 and derived from the general integration was dominated by a great anticyclonic gyre which, north of latitude 10°N, is similar in form to its atmospheric counterpart. Due to the merging of the Bermuda and Azores anticyclones, the mean wind pattern (figure 6.1) shows a zone of low speeds, with an abrupt shift in wind direction more or less along the parallel of 30°N from the North American coast to longitude 25°W that separates the trades and westerlies.

The center of the oceanic circulation gyre in figure 6.3 was displaced well to the west of the geographical center of the North Atlantic Ocean resulting in an intensification of the Gulf Stream branch relative to the more diffuse Canary Current branch.

A total mass transport in the Gulf Stream system off the east coast of North America of just over 40 million tons sec^{-1} was derived. This may be compared with the figure of about 48 million tons sec^{-1} derived by Wüst (1936) who used as reference level the oxygen minimum layer which is found on the coastal side of the Gulf Stream at a depth of about 400 m and on the Sargasso Sea side at a depth of about 900 m. The net transport through the section used in Wüst's computations, made geostrophically with respect to a reference level similar to that used in the present

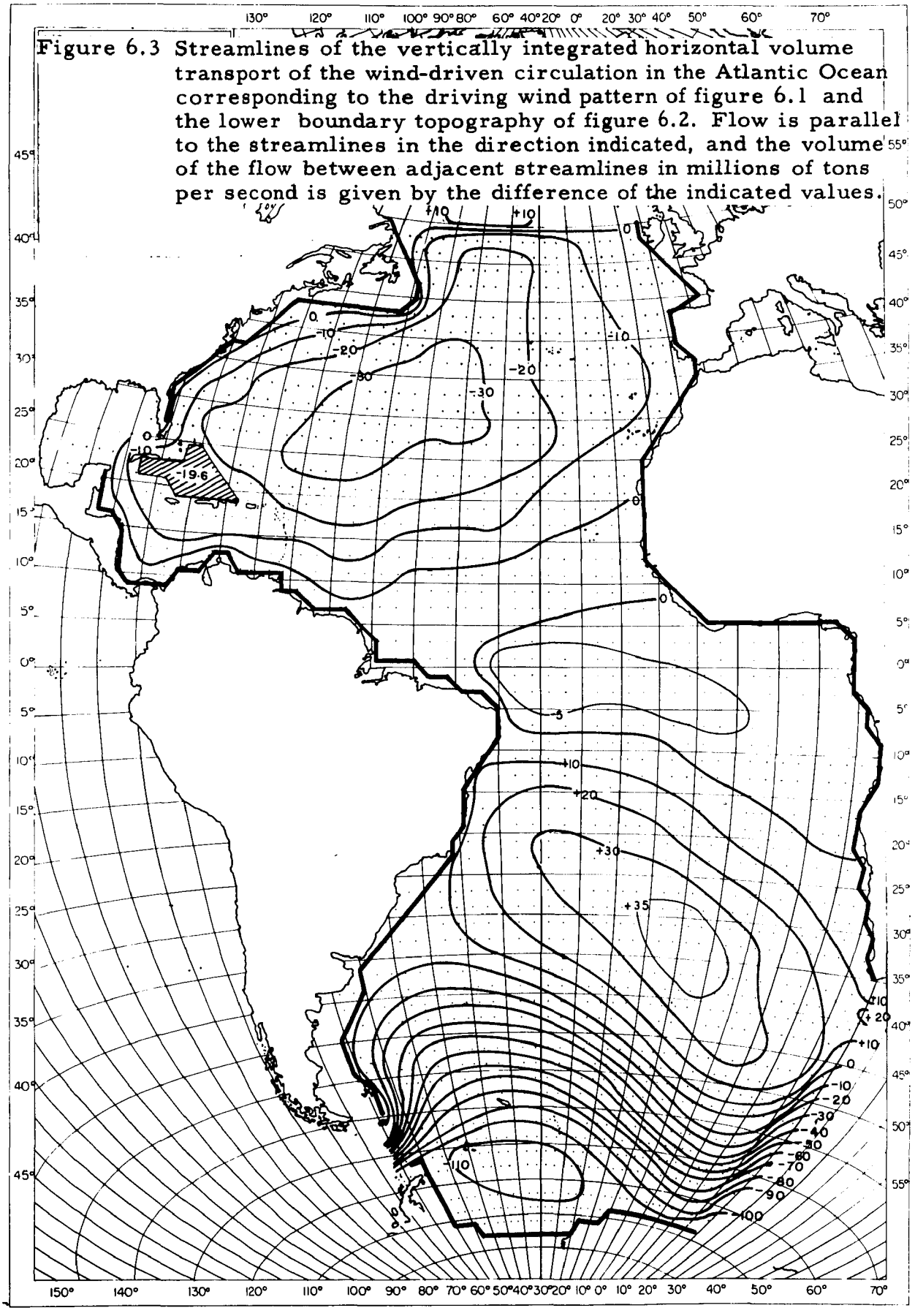

Figure 6.3 Streamlines of the vertically integrated horizontal volume transport of the wind-driven circulation in the Atlantic Ocean corresponding to the driving wind pattern of figure 6.1 and the lower boundary topography of figure 6.2. Flow is parallel to the streamlines in the direction indicated, and the volume of the flow between adjacent streamlines in millions of tons per second is given by the difference of the indicated values.

model, is 53 million tons sec^{-1}. These varying values may be explained by different assumptions about the lower boundary of the circulation and by seasonal or secular variations.

A strong flow of nearly 26 million tons sec^{-1} entered the Caribbean Sea from the North Equatorial Current. Between the equator and north latitude 7° there is weak development of an equatorial countercurrent extending across most of the Atlantic Ocean from about west longitude 35° into the Gulf of Guinea. This eastward flow is closely associated geographically with the doldrum belt in the applied wind field (figure 6.2). A very weak net transport was indicated in the Antilles Current region. Sverdrup (1942, p. 676) summarized the then available information to indicate that about 12 million tons sec^{-1} from the Antilles Current joins the Florida Current which leaves the Straits with a flow of about 26 million tons sec^{-1}.

North of Grand Banks, the solution shows north-going flow in an area that in nature is dominated at the surface by the Labrador Current. All inflow into the field of integration southeast of Greenland, imposed as a boundary condition, was turned abruptly eastward in the model to leave the field again in the North Atlantic Current. There is little in the wind pattern used here to encourage the production of a Labrador Current.

The central South Atlantic was also dominated by a large anticyclonic gyre centered around 33°S, 10°W. Little westward intensification of the Brazil Current branch was evident. Separation of flow of the South Equatorial Current into the Guiana and Brazil Current branches occurred approximately at 10°S, south of Cape San Roque.

Streamlines representing the Benguela Current off the southwest African coast trend northeastward away from the coast between the Cape of Good Hope and Cape Frio, and leave a large area of weak circulation between this point and Cape Palmas.

Unlike its northern hemisphere counterpart, the anticyclonic wind system over the South Atlantic has a simple cellular structure in the mean wind pattern for February (figure 6.1) with a center at about 35°S, 13°W that is close to the center of the corresponding transport pattern in the ocean. The main anticyclonic gyre in the South Atlantic Ocean circulation is elongated, with its main axis extending southeastward far into the Southern Ocean nearly to latitude 50°S near the eastern boundary of the field of integration. This configuration results in a marked southeastward trend to streamlines representing the flow of the Antarctic Circumpolar Current in the far southeastern Atlantic. Had boundary conditions that forced the flow of this current to be concentrated in the center of the passage not been imposed, it seems likely that the greater part of this flow of the Circumpolar Current from the South Atlantic into the South Indian Ocean would have been developed in very high latitudes, say between 60°S and the Antarctic coast, according to the model and the data used. As the calculated circulation does not seem realistic compared with the known properties of water movements in the Southern Ocean, the model's behavior in this area would repay further examination.

On entering the Atlantic sector of the Southern Ocean through the Drake Passage, streamlines in the Circumpolar flow underwent a marked deflection northward, and a well-developed flow corresponding

to the Falkland Current appears in figure 6.3 off the east coast of Argentina. This converges with the south-flowing Brazil Current branch approximately in latitude 32°S, just north of the River Plate. As far as near surface water movements are concerned, this corresponds closely to the observed position of the subtropical convergence in this area during the southern hemisphere summer.

It is interesting that this northward deflection of streamlines east of Cape Horn is so pronounced without the benefit of the South Sandwich Ridge to assist this deflection (Sverdrup, 1942, p. 615). As may be seen in figure 6.2, a highly smoothed topography of the depth of no motion was used in this region. The configuration of the South Sandwich Ridge could not adequately be represented with the gridpoint spacing used, and preliminary calculations indicated that some difficulty with instability of the solution might have arisen with a more complicated topography. The present solution converged rather slowly in this region. However, it seems likely that a closer approximation to Defant's original estimation of the topography of the surface of no motion in this area would be necessary to derive a less vigorous, and hence more realistic, northward deflection of streamlines in the southwest Atlantic.

The whole of the Southern Ocean sector may repay further analysis using a finer grid mesh, a more realistic pattern of wind and depth of no motion, and with closer attention paid to the imposed boundary conditions. From the elliptic form of equation (4.27) it appears that a unique solution would, in general, be obtained using mixed boundary conditions, specifying the full stream function, Ψ,

along all fixed coastal boundaries, but the gradient of this function normal to the boundary, only, along oceanic boundary lines. This would allow the model freedom to choose the streamline configuration at those boundaries most appropriate to its natural dynamical properties.

(c) Zero wind, variable depth solution

On comparing the zero wind, variable depth solution (figure 6.4) with the general integration (figure 6.3) it may be seen that most of the large scale wave structure of the Southern Ocean streamlines, and hence the remarkable southeastward elongation of the axis of the South Atlantic gyral, is due to interaction of the flow between the source and the sink in this region with the assumed topography of the lower boundary. The impressed wind field has little effect.

A comparison of the zero and variable stress results also shows that the transfer of 6 million tons sec^{-1} of sea water northward across the equator required by the boundary condition tends, in the absence of wind, to be derived wholly from the inflow past Cape Horn. The strong anticyclonic vorticity influence east of Cape Horn confines this northward flow in a narrow filament along the southeast coast of South America. To the north of 30°S latitude, where the main flow of the Circumpolar Current has been turned back toward the Africa-Antarctic sink, this western boundary flow spreads out and covers a large area in the western North Atlantic. This boundary flow accounts for 3 million tons sec^{-1}, or about 12 percent of the flow through the Straits of Florida in the general

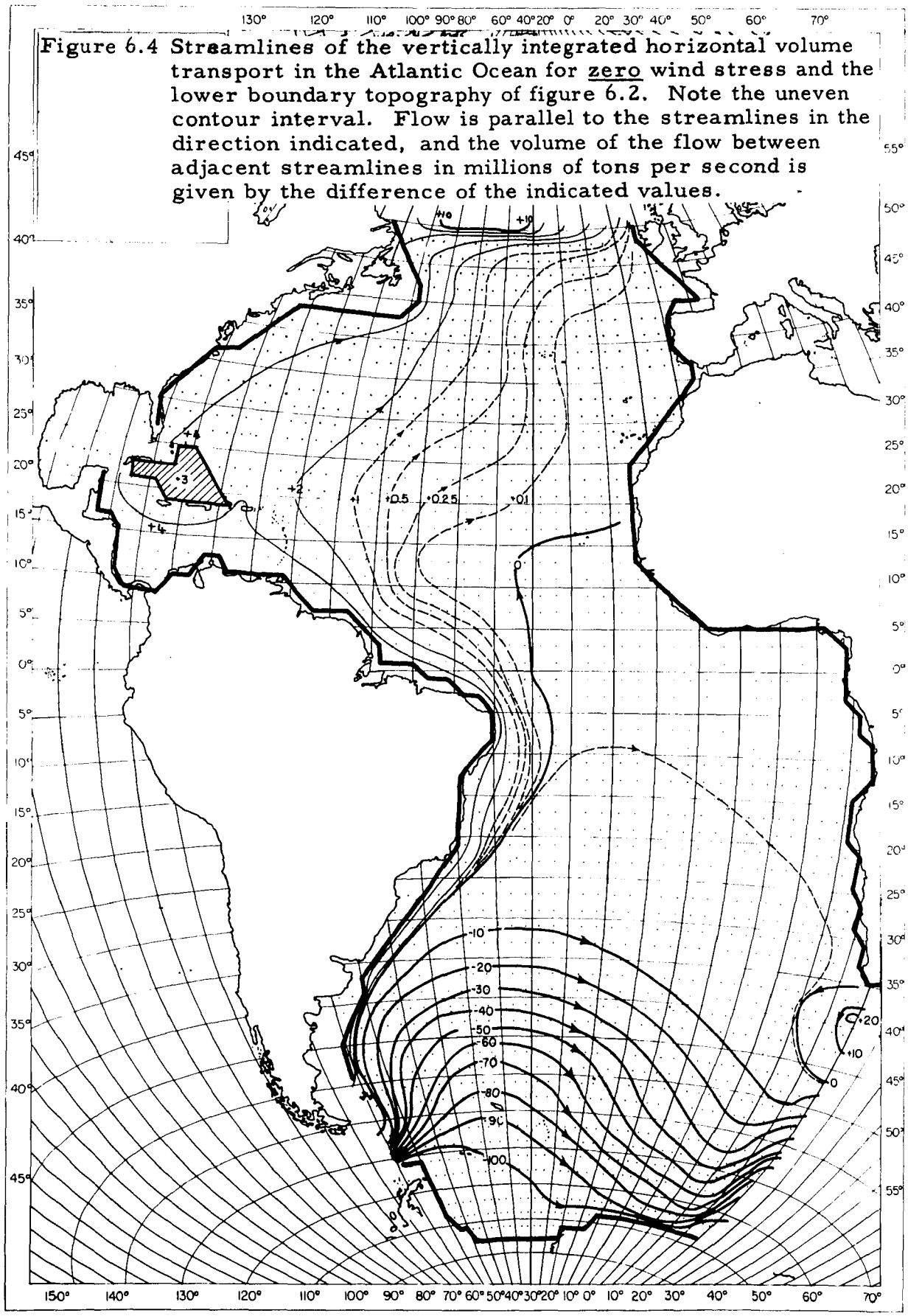

Figure 6.4 Streamlines of the vertically integrated horizontal volume transport in the Atlantic Ocean for <u>zero</u> wind stress and the lower boundary topography of figure 6.2. Note the uneven contour interval. Flow is parallel to the streamlines in the direction indicated, and the volume of the flow between adjacent streamlines in millions of tons per second is given by the difference of the indicated values.

integration. Addition of the wind stress curl alters this situation considerably, however, the northward transfer of water across the equator now having its source south of the Cape of Good Hope and flowing via the Benguela and South Equatorial Current branches of the circulation pattern.

(d) Constant depth solutions

With D constant, Neumann's vorticity equation (4.27) becomes

$$K\nabla^2 + \frac{\partial f}{\partial y}\frac{\partial \Psi}{\partial x} - \frac{K}{R}\tan\phi \cdot \frac{\partial \Psi}{\partial y} = -(\nabla \times \tau)_z - \frac{\tau_x}{R}\tan\phi \qquad (6.3)$$

Since the factor D appears only in equation (4.27) divided into one of its space gradient components, equation (6.3) is independent of the actual value assumed for D.

The result of numerically integrating equation (6.3), with the same computer program, wind stress data, constants and boundary conditions used for the variable depth calculations, is plotted in figure 6.5. Compared with the circulation derived for the variable depth case (figure 6.3), the centers of the major gyres have been displaced westward and that the total volume of water circulating in these gyres has been reduced by about 25 percent in the North Atlantic, and about 39 percent in the South Atlantic. This behavior may be compared with the properties of the curves plotted in figures 5.1, 5.2. The Florida Current has been reduced by some 16 percent only, however, most of the North Atlantic loss being

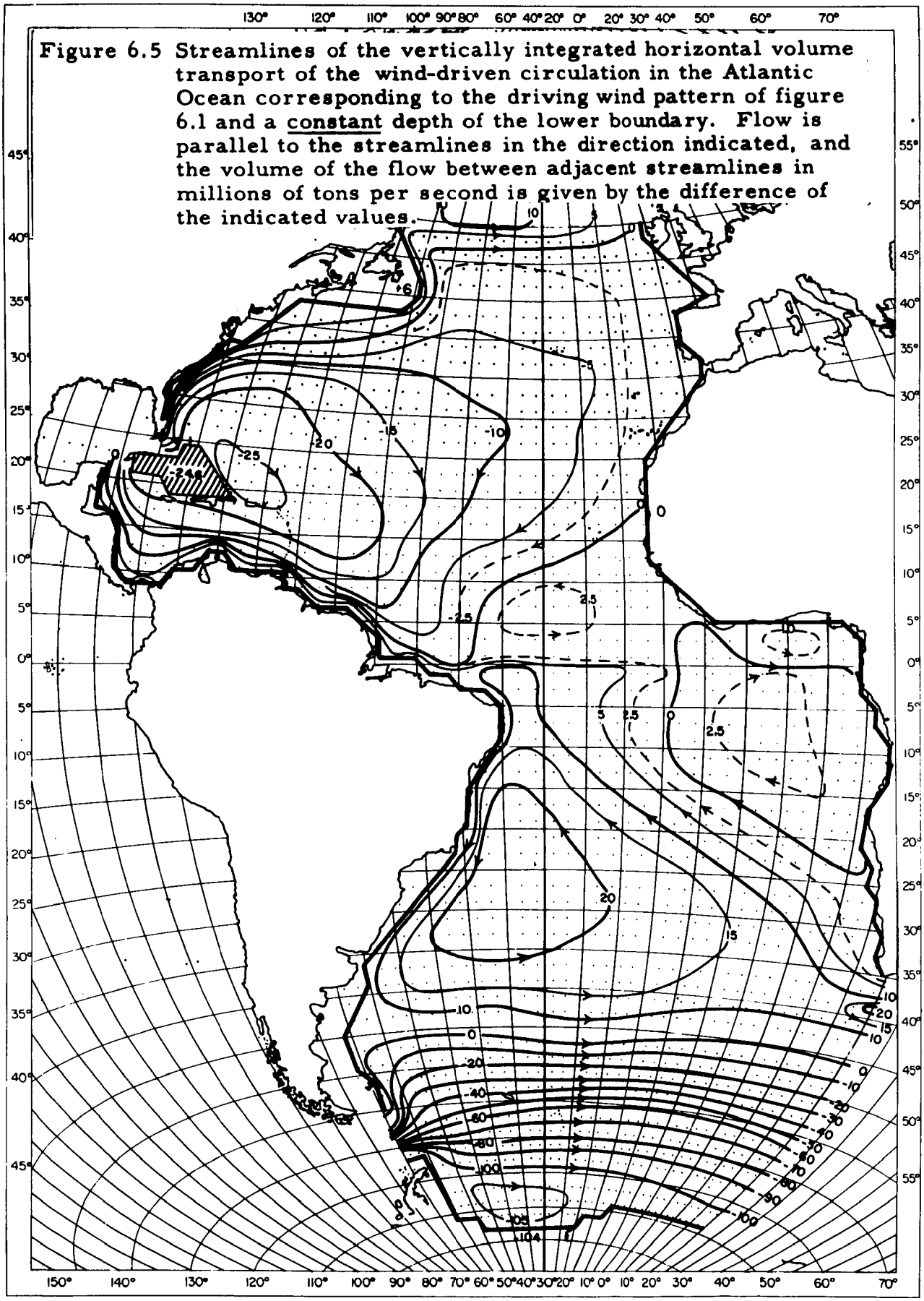

Figure 6.5 Streamlines of the vertically integrated horizontal volume transport of the wind-driven circulation in the Atlantic Ocean corresponding to the driving wind pattern of figure 6.1 and a constant depth of the lower boundary. Flow is parallel to the streamlines in the direction indicated, and the volume of the flow between adjacent streamlines in millions of tons per second is given by the difference of the indicated values.

associated with the virtual extinction of the Antilles Current. It is possible, however, that this may have largely been due to conditions imposed on the gridpoint at the southeast tip of the "Caribbean Island".

Use of a constant depth in the calculations has resulted in other changes in the circulation when compared with the variable depth case. In the equatorial region, the relatively simple countercurrent system developed in the variable depth model has been complicated by a strong northwesterly trend to streamlines of the "south equatorial current" system which, in the constant depth case extended from the Cape of Good Hope as far north as the equator. Any suggestion of an equatorial countercurrent is, in the constant depth analysis, confined to the eastern side of the ocean, say east of longitude 25°W. A large cyclonic eddy fills the Gulf of Guinea.

In the Southern Ocean, the constant depth situation yields a greatly reduced northward deflection of streamlines northeast of the Drake Passage, and these streamlines show a simple zonal trend south of 45°S and east of 50°W. That this behavior is due primarily to the depth pattern and is influenced little by the wind, is demonstrated by comparison between figure 6.5 and the associated zero stress, constant depth model (figure 6.6). The main effect of the wind-induced anticyclonic gyral in the constant depth model is to confine the streamlines of the circumpolar flow into a much narrower meridional compass than was evident in the simple unconstrained flow from source to sink (figure 6.6). The "convergence" between the Brazil Current and the Falkland Current in the variable stress constant depth model is found in south latitude 45°, about 15 degrees

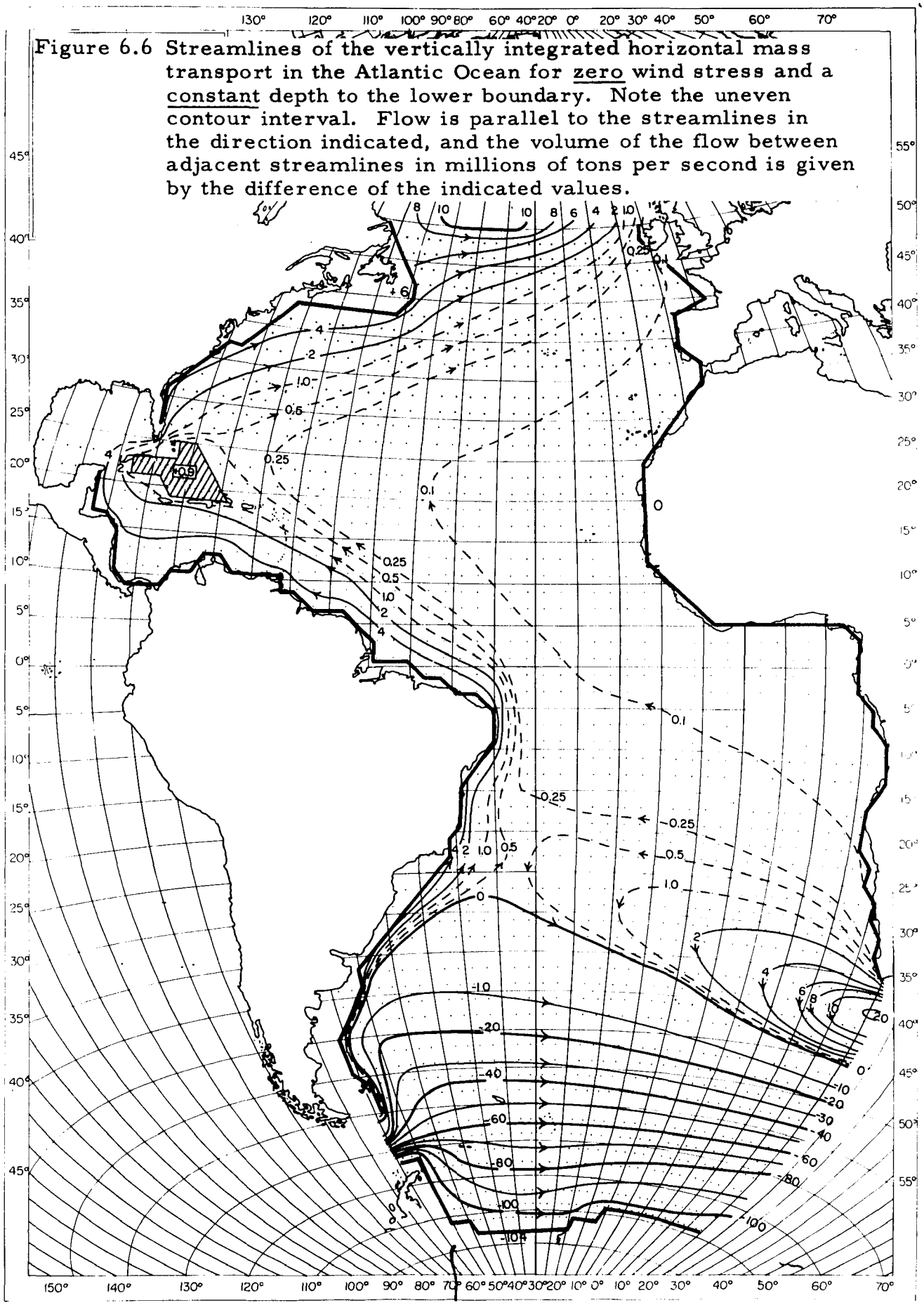

Figure 6.6 Streamlines of the vertically integrated horizontal mass transport in the Atlantic Ocean for zero wind stress and a constant depth to the lower boundary. Note the uneven contour interval. Flow is parallel to the streamlines in the direction indicated, and the volume of the flow between adjacent streamlines in millions of tons per second is given by the difference of the indicated values.

of latitude further south than it appeared on the variable depth model, due to the pronounced westward displacement of the South Atlantic gyre in the former model.

As in the zero stress variable depth model, a narrow filament of current carried most of the required northward flow across the equator from the Drake Passage (figure 6.6). In contrast, however, the constant depth flow remained concentrated on the western side of the North Atlantic, mostly flowing through the Caribbean and the Straits of Florida, to account for nearly 17 percent of the total "Florida Current" appearing in the variable stress, constant depth situation.

The large cyclonic eddy filling the Weddell Sea in both versions of the variable stress models (figures 6.3 and 6.5) is a feature observed on most current maps of this area, and appears to be due primarily to the wind pattern, since no trace of this structure appears in the corresponding zero stress results (figure 6.4 and 6.6).

(e) Solution with depth proportional to $\sin\phi$

It is interesting to confirm that the complete compensation of the planetary vorticity by the assumption of a lower layer topography proportional to the sine of the latitude results in a circulation pattern remarkably symmetrically placed between the eastern and western boundaries (figure 6.7). It must be emphasized that this figure represents only a partially converged solution. Little change in the geometrical streamline configuration is expected by completion of the solution, but considerable changes in the values of the stream function at any point will occur.

The center of the North Atlantic gyral is displaced poleward in the general integration (figure 6.3) compared with the extreme

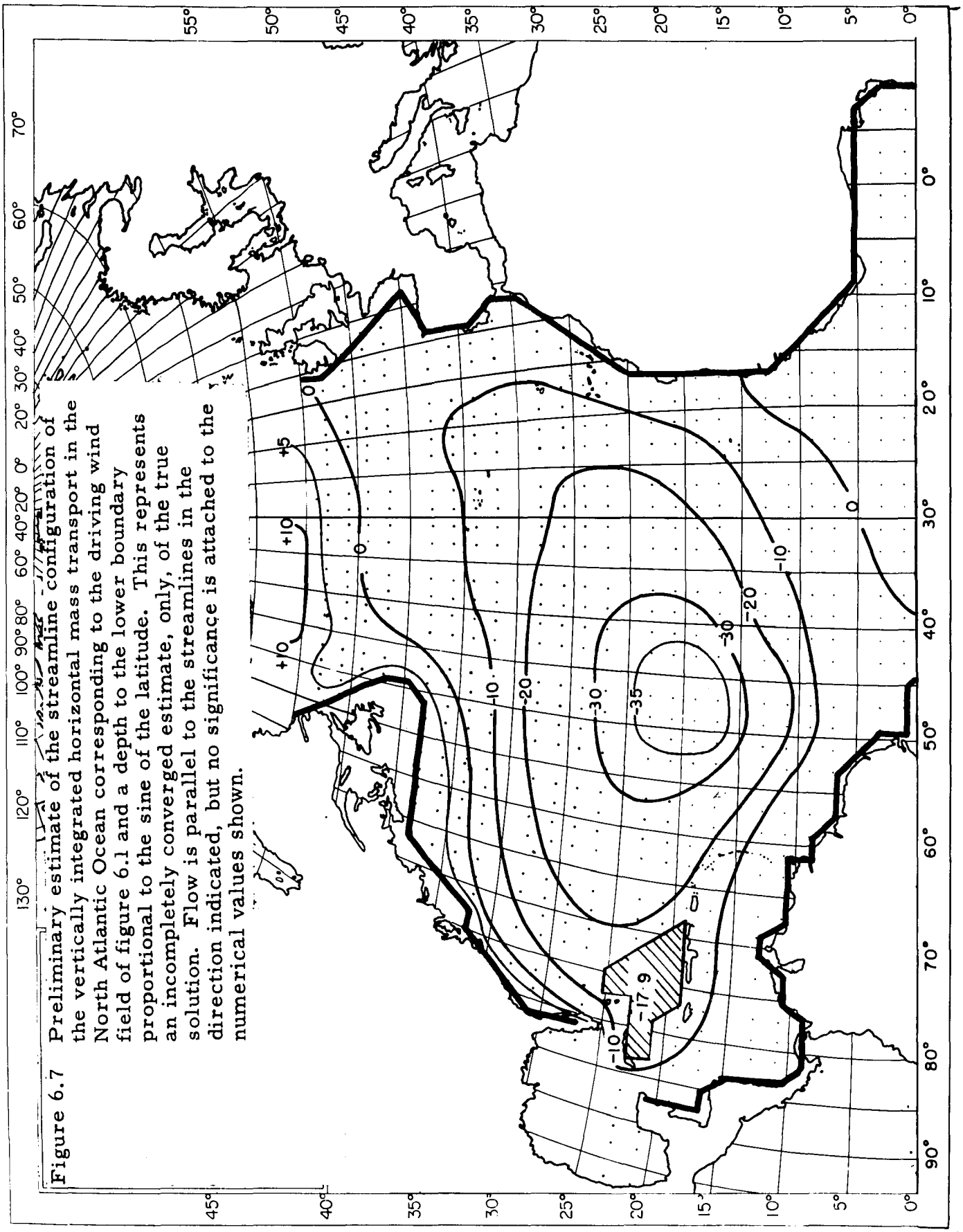

Figure 6.7 Preliminary estimate of the streamline configuration of the vertically integrated horizontal mass transport in the North Atlantic Ocean corresponding to the driving wind field of figure 6.1 and a depth to the lower boundary proportional to the sine of the latitude. This represents an incompletely converged estimate, only, of the true solution. Flow is parallel to the streamlines in the direction indicated, but no significance is attached to the numerical values shown.

situations represented by figures 6.5 and 6.7. In this connection it would be of interest to look into the effect of variations in the magnitude of the coefficient of $\partial\Psi/\partial y$, the zonal transport, on meridional asymmetry in the circulation pattern.

6.4 Conclusions

The results of the foregoing calculations provide an interesting source of speculation concerning the nature of the topographic, or "thickness" influence on ocean circulation. They can, however, claim to provide verification neither of the importance of the topographic vorticity terms in the case of a "natural" depth of no motion, nor of the choice of the Defant surface as an appropriate realization of this depth, until the questions raised in section 4 have been resolved. The suggestion of that section was that the topographic vorticity (4.19) vanishes when the lower boundary of the wind-driven circulation is a frictionless surface. If this is true, then the dissimilarity between the transport patterns of figures 6.3 and 6.5 must be interpreted not as a measure of the dynamic significance of the topographic terms but as a demonstration that the Defant surface lies above the lower boundary of the circulation induced in the model by the particular wind pattern used.

Vertical shrinking or stretching in the vertical extent of circulating water may certainly be expected to introduce vorticity changes of the flow in individual levels, compared with the constant thickness situation. The previous analysis suggests, however, that the vertically integrated transport pattern should be identical for any given ocean system irrespective of whether the integration is carried just to the naturally developed lower limit

of the moving water or beyond this limit to a level surface in a layer of motionless water. To investigate this question it will be necessary to undertake a three-dimensional analysis of the problem leaving calculation of the vertically integrated transports till the final step.

If Defant's surface is not the upper boundary of a layer of no motion, then it must mark either

(a) a layer of water moving in geostrophic equilibrium and without sensible vertical shear, or

(b) a region in which flow is markedly ageostrophic due to friction.

Little can be said at present about friction in the deep ocean. Most theories have been framed in terms of Ekman's concept of frictional flow being most significantly concentrated in the surface layers directly stirred by the wind. In the middle latitude regions of migratory cyclones and anticyclones it is conceivable that a description of the ocean in terms of a steady state model, even with the field accelerations included, is entirely inadequate. "Storm slopes" induced on the surface by the rapid passage of weather systems may well induce transient gradient currents that reach to the bottom, in the first instance, and which never have time to induce complete mutual adjustment between the mass and velocity fields. It would be interesting to continue calculations of the development of the depth of no motion for variously modelled fields of wind stress and of ocean density, along the lines indicated by Neumann (1955, pp. 18-22). If time dependent effects were included, a time average of the stress-distribution in the vicinity

of the "average surface of no motion" may provide a new basis for discussion of the significance of the topographic vorticity. Introduction of a particular field of mass into an ocean model is tantamount to specifying a particular thermodynamic driving force into the system and this should properly be included in the equations of motion. No discussion of the behavior of the depth of no motion can be realistic without the inclusion of thermodynamic argument, for, while the details of the topography of such a surface will reflect the interaction of dynamic processes as represented in the equations of motion, its formation is primarily governed by the oceanic mass field which owes its existence to climatologically induced passage of heat and water across the air-sea interface.

The Defant surface reflects the reaction of the oceanic mass distribution to the total oceanic velocity field. Thus, in regions where a thermohaline driven circulation might possibly be expected to form a significant contribution to the total flow, the Defant reference level cannot be simply identified with a lower boundary of the wind-driven component of the total circulation. Indeed, the wind-driven and thermohaline components will not, in general, be separable because of frictional coupling between the two components and nonlinearities in the thermodynamic equations. This complication may be particularly evident near the western oceanic boundary where the deep thermodynamic circulation may be concentrated, or in surface source regions for the deep water masses.

Stommel (1956) presented some evidence which could claim the occurrence of maximum vertical velocities at the level of no meridional motion. This of course, represents a rather different

model from the one on which equation (4.27) is based, in which the depth D is one of no absolute motion.

The inclusion of thermohaline considerations into a theory of ocean circulation appears to present a very difficult problem, and the literature awaits definitive contributions in this field. Stommel (1960, p. 160) has indicated how some modification of the Sverdrup analysis might be effected to include elementary thermodynamic argument. No attempt will be made in this study either to discuss the analytic treatment of the thermohaline circulation or to provide a representative bibliography of this field. Recent papers of general dynamical interest which also treat certain thermodynamic aspects of the circulation problem are by Wyrtki (1961) and by Stommel and Webster (1962).

7. Variational methods

Neumann (1955) suggested that a baroclinic ocean reacts to the combined constraints of wind stress torque and of non-uniform rotation, by assuming various combinations of westward intensification (section 3) and of adjustment of the topography of the lower boundary of the layer of circulating water driven by the wind (section 4). It was further suggested that specific ocean areas showed a characteristic partition among these reactions, many regions tending completely to balance the planetary vorticity by the lower boundary adjustment.

The question then arises: what determines the degree of partition among the two modes of reaction, westward intensification and topographic adjustment, of an ocean's reaction to an applied wind stress pattern in any given dynamical situation? A sufficiently general answer to this question would also resolve the difficulties mentioned in section 4 concerning the dynamical significance of the "topographic vorticity" in a deep ocean. An answer would further be provided to the question raised in section 5 concerning the admissibility of separately specifying wind stress and free lower boundary topography in an ocean model.

In general terms, the particular reaction of any dynamical system having several degrees of freedom, or various possible modes of reaction to a given set of constraints, may be derived from a variational technique involving the classical Hamiltonian description of the system. These techniques, standard in "particle dynamics" and in generalized field theory, seem to have found little application in oceanographic studies, and at least in the writer's experience,

are not normally included in formal courses on dynamical oceanography. It will thus be of interest to summarize here the principles involved. The principal sources of information tapped here were Goldstein (1958), and Hirschfelder, et al (1954).

Generalized coordinates

In formal dynamical studies it is often convenient to introduce a set of generalized coordinates to describe the system studied. There will be as many of these (independent) coordinates as there are degrees of freedom of the dynamical system. Any quantities appropriate to the particular problem may be used as these generalized coordinates, from the conventional position coordinates to quantities with dimensions such as energy or momentum. The k^{th} generalized coordinate shall here be denoted as $q_k(x, y, z, t)$ and $\dot{q}_k$ shall be the corresponding generalized velocity, which need not necessarily have the dimensions $[LT^{-1}]$.

A conservative system is one in which the net work done in passing around any closed path in the system, is zero., i.e.

$$\oint \vec{F} \cdot d\vec{s} = 0 \tag{7.1}$$

If this relation holds, the force $\vec{F}$, and the system in which it acts, is called conservative. For such a system, the force $\vec{F}$ may be derived from a potential function, Φ, such that

$$F = -\nabla \Phi \tag{7.2}$$

$d\vec{s}$ is an element of the closed path.

The Lagrangean function, or simply, the Lagrangean, characteristic of a dynamical system, is defined as

$$L(q_1, q_2, \cdots; \dot{q}_1, \dot{q}_2, \cdots) = T - \Phi \tag{7.3}$$

where T is the system kinetic energy and Φ is the system potential energy function. The Lagrangean is called by some writers the kinetic potential.

Hamilton's Principle. If a dynamical system may be fully described by a set of n independent generalized coordinates $(q_1, q_2, \cdots, q_n)$ then the dynamical state of the whole system at any instant may be conveniently represented by a point in a Cartesian n-dimensional hyperspace ("configuration space") for which the q_k's represent the n coordinate axes. This system point traces out a curve in configuration space as time goes on. This curve will be referred to as the "dynamical path" or the "motion" of the system, and time represents a parameter of the curve.

For a conservative system, Hamilton's Principle states that the motion of the system from time t_1 to time t_2 is such that the line integral I (i.e., the integral along the dynamical path),

$$I = \int_{t_1}^{t_2} L\,dt \tag{7.4}$$

is an extremum. In other words, out of all the possible paths by which the system point could have moved through configuration space between the initial and final states represented by t_1 and t_2, it will actually move along that path for which the integral I is an extremum (usually a minimum). Since the integral I represents the time interval $(t_2 - t_1)$ multiplied into the average value of the Lagrangean over this interval, Hamilton's Principle implies that the differences between the time averages of the system kinetic and

and potential energies have a stationary value. For the actual motion of the system point, then, the average kinetic energy approaches the average potential energy more closely than for any other motion (between the same initial and final states) or else diverges from it more than any other motion.

Use of the notation of the calculus of variations enables equation (7.4) to be written as a zero variation of the integral I, i.e.,

$$\delta \int_{t_1}^{t_2} L\,dt = 0 \tag{7.5}$$

where

$$\delta I = (\partial I/\partial \alpha)_{\alpha=0}\, d\alpha \tag{7.6}$$

in which α represents a parameter differentiating between all the possible paths of the system point through configuration space.

Lagrange's equations of motion. From Hamilton's Principle (7.5), may be derived the Euler-Lagrange equations of motion (7.7).

$$\frac{d}{dt}\left(\frac{\partial L}{\partial \dot{q}_i}\right) - \frac{\partial L}{\partial q_i} = 0\,; \quad i = 1, 2, \cdots, n \tag{7.7}$$

The equations (7.7) are sometimes referred to simply as Lagrange's Equations, and are not to be confused with the "Lagrangean representation", as opposed to the Eulerian representation of the equations of motion (2.6) as usually employed in hydrodynamics (Lamb,1945, p. 12). The quantity

$$p_i = \frac{\partial L}{\partial \dot{q}_i} \tag{7.8}$$

is called the "generalized momentum" (sometimes "canonical" or "conjugate" momentum) corresponding to the coordinate q_i. p_i will have the dimensions $[MLT^{-1}]$ only if q_i is a Cartesian coordinate.

The Lagrange equations (7.7) represent a general form of Newton's Second Law (1.1) and, for a system having n degrees of freedom, form a set of n second order ordinary differential equations whose solution may be specified by means of a complete set (n) of generalized coordinates (q_i) and velocities $(\dot{q}_i)$ at a given time, (t).

The dynamics of conservative systems may thus be described using the variational principle (7.5) as the basic postulate, rather than Newton's laws of motion. Such a procedure has important advantages. Firstly, it replaces the equations of Newton, which contain vector forces and accelerations, by a formulation that contains only the two scalar functions T and Φ, which are independent of the particular choice of generalized coordinates. More important, however, is the unification that may be achieved within the framework of the formal Hamiltonian formulation of the analytical treatment of many branches of physics, in particular, the general theory of fields.

Extension to non-conservative systems. For certain kinds of dynamical systems in which non-conservative forces are acting it is possible to define a Lagrangean, L, such that the formal structure of the Lagrange equations (7.7) may still be employed.

For the present application to ocean dynamics, the most important non-conservative element in the balance of forces is due to friction. In the foregoing sections, frequent use has been made

of a frictional force per unit mass which is proportional to the velocity

$$\vec{F} = K\vec{V} \tag{7.9}$$

A force of this type may be obtained from a "dissipation function", $\mathcal{F}$, introduced by Rayleigh (Lamb, 1945, p. 580).

$$\mathcal{F} = \frac{1}{2} K(\vec{V} \cdot \vec{V}) \tag{7.10}$$

$2\mathcal{F}$ represents the rate of energy dissipation due to friction. Use of this function enables Lagrange's equation (7.7) to be written in the form (7.11).

$$\frac{d}{dt}\left(\frac{\partial L}{\partial \dot{q}_i}\right) - \frac{\partial L}{\partial q_i} + \frac{\partial \mathcal{F}}{\partial \dot{q}_i} = 0 \tag{7.11}$$

Similar "generalized potentials" may be defined for the derivation of other models of frictional forces. For example, the Airy stress function, used in theories of elasticity, might be modified to generate frictional forces which depend on the gradient of stress within a fluid.

A corresponding generalization of the variational principle (7.5), may be made so that non-conservative forces, obtained from a generalized potential, may be included. The extended Hamilton's Principle turns out to be (Goldstein, 1959, p. 38)

$$\delta I = \delta \int_{t_1}^{t_2} (T + W)\, dt = 0 \tag{7.12}$$

where δW represents the work done by all forces on the system during the virtual (instantaneous) variation of the path of motion of the system through configuration space.

The Hamilton Equations of Motion. The Lagrange equations of motion (7. 7) provide description of a dynamical system with n degrees of freedom in terms of n second order differential equations containing the generalized coordinates and the generalized velocities as independent variables, and time as a parameter. It is often convenient to utilize instead the Hamiltonian formulation in which the independent variables are the generalized coordinates, q_i, and the generalized momenta, p_i, defined in equation (7. 8). Transformation from the $(q_i, \dot{q}_i, t)$ set of equations (7. 7) to a (q_i, p_i, t) set requires introduction of the Hamiltonian Function, H, characteristic of the dynamical system, where

$$H(p, q, t) = \sum_i \dot{q}_i p_i - L(q, \dot{q}, t) \tag{7.13}$$

The generalized velocities, $\dot{q}_i$ appear in the Hamiltonian both explicitly in the first term on the right hand side of (7.13) and implicitly in the Lagrangean, L. The Hamiltonian is numerically equal to the total energy, $T + \Phi$, and is thus a constant of the motion for a conservative system.

The equations of motion may then be reduced to the following set:

$$\dot{q}_i = \frac{\partial H}{\partial p_i} \tag{7.14}$$

$$-\dot{p}_i = \frac{\partial H}{\partial q_i} \tag{7.15}$$

$$-\frac{\partial L}{\partial t} = \frac{\partial H}{\partial t} \tag{7.16}$$

known as the "canonical equations of Hamilton". They replace the n second order Lagrange equations by 2n first order equations. The lower order equations have been obtained at the expense of raising

the range of independent variables from n to 2n by freeing the generalized momenta from any defined relationship to the generalized coordinates, except through the equations of motion themselves.

A more general variational process. In a configuration space formed from the n generalized coordinates, the initial and final configurations of the system at times t_1 and t_2 respectively, are each represented by a point. The term "variation of the integral" refers to the variation in the value of the integral (7.4) as the path traversed by the system point between the two end points is changed. For the δ-variation (7.6), the variation is described as occurring for constant time. The end point times are therefore held fixed so that the "travel time" between the two configurations is the same for all paths. In addition, the varied paths are considered to be built up from a succession of virtual displacements from the points of the actual path traversed. This involves no change in t, in contrast to an actual displacement which occurs in a time interval dt during which the forces and constraints may change.

If each of the possible paths in configuration space is labelled with a parameter α, the coordinates of a point in this space become functions of both t and α, the latter indicating which path of integration is used.

$$\delta \rightarrow d\alpha \frac{\partial}{\partial \alpha} \tag{7.17}$$

(7.17) thus corresponds to virtual displacements in which the time is held fixed and the coordinates are varied subject to the constraints imposed on the system. Such a virtual displacement does not always coincide with a possible actual displacement occurring in the course

of the motion. Consequently the varied path in the δ-process need not correspond to a possible path of motion for the system; in particular the Hamiltonian may not be conserved in the variation. In contrast, a "Δ-variation" process may be defined which deals with displacements which do involve a change, dt, in the time. It may thus be required that the varied paths shall be consistent with the physical motion in such a p rocess. The time of transit along the varied paths need now no longer be the same, for the system point may have to "speed up" or "slow down" to keep the Hamiltonian constant. As a result the Δ-process includes a variation of t even at the end points, while the variation of the q_i still remains zero.

It turns out that

$$\Delta q = \delta q + \dot{q}\Delta t \tag{7.18}$$

This variational principle which perhaps is most appropriate to the ocean dynamical problem leads to the Principle of Least Action

$$\Delta A = 0 \tag{7.19}$$

where A is the Action,

$$A = \int_{t_1}^{t_2} \sum_i p_i \dot{q}_i \, dt \tag{7.20}$$

Some further consequences of the Hamiltonian formulation, which may find application in the present problem, may be outlined as follows.

Consider a property of the system

$$F = F(q_i, p_i, t) \tag{7.21}$$

which depends on the dynamical state of the system and, in general, explicitly on time. F may be any system property; in the present context, for example, it might be the depth of no motion. The change of F with time following a point along a natural trajectory is given by equation (7.22).

$$\frac{dF}{dt} = \frac{\partial F}{\partial t} + \sum_i \left(\frac{\partial F}{\partial q_i} \dot{q}_i + \frac{\partial F}{\partial p_i} \dot{p}_i \right) \tag{7.22}$$

Use of the canonical equations of Hamilton yields equation (7.23).

$$\frac{dF}{dt} = \frac{\partial F}{\partial t} + [F, H] \tag{7.23}$$

where [F, H] is the Poisson bracket of F and H,

$$[F, H] = \sum_i \left(\frac{\partial F}{\partial q_i} \frac{\partial H}{\partial p_i} - \frac{\partial F}{\partial p_i} \frac{\partial H}{\partial q_i} \right) \tag{7.24}$$

Phase space. In analogy to configuration space in Lagrangean formulation, a 2n-dimensional Cartesian space formed of coordinates $(q_1, q_2, \cdots, q_n, p_1, p_2, \cdots, p_n)$, known as phase space, may be defined. The complete dynamical specification of a mechanical system will be given by a point in phase space.

Since the past and future history of a system is determined by its present state, a point in phase space uniquely determines a trajectory that the representative point of a system traces out in phase space as time goes on. This motion is referred to as the natural motion of the phase point and is described by Hamilton's canonical equations (7.14), (7.15), and (7.16).

If a collection of non-interacting systems be considered, each member of which differs from the others only in its initial state, the state of the entire system may be described by a cluster of phase points. For a sufficiently large number of systems this cluster may be represented by a continuous distribution function $\sigma(q_i, p_i, t)$, the "density in phase space". The specification of this density function may be made arbitrarily for some initial instant but will then be determined for all later times by the equations of motion. Since there can be no sources and sinks of phase points, the density function will satisfy a generalized form of the continuity equation (7.25).

$$\frac{\partial \sigma}{\partial t} + \sum_i \left[\frac{\partial}{\partial q_i} (\dot{q}_i \sigma) + \frac{\partial}{\partial p_i} (\dot{p}_i \sigma) \right] = 0 \qquad (7.25)$$

Use of Hamilton's canonical equations in (7.25) derives Liouville's Equation (7.26).

$$\frac{d\sigma}{dt} = \frac{\partial \sigma}{\partial t} + [\rho, H] = 0 \qquad (7.26)$$

i. e., the density of systems in the phase space neighborhood of some given system is constant through time.

Means will be sought to make application of the foregoing principles to the ocean circulation problem outlined at the beginning of this section.

In the absence of a wholly general method of attack, it may be instructive to make direct calculations of the dynamical path followed by a cluster of system points whose initial specification is designed to cover the range of initial conditions of applied wind stress and ocean mass distribution of physical interest. The

time history of this cluster, calculated with the aid of Hamilton's Principle and Liouville's Theorem, will provide information about the relative importance of assumptions of initial conditions in terms of the distribution of the cluster of final state phase points. In addition the behavior of specific realizations of an ocean model will perhaps give a guide to solution of the general problem.

It was noted in the closing paragraphs of section 5 that it would be at lease desirable, and probably necessary, to include thermodynamic constraints in any attempt to define the unique dynamical structure of an ocean system under given conditions.

Brief mention of the use of the principle of minimum entropy production to define uniqueness in an ocean circulation model was noted in an abstract by Veronis (1961); the full paper has not been available to the present author at the time of writing. Veronis suggests that dynamical considerations alone cannot yield unique solutions for the wind-driven ocean circulation without the introduction of thermodynamic constraints.

A continuous medium having stationary boundary conditions will generally evolve toward a non-equilibrium stationary state that corresponds to a constant non-zero entropy production. A formulation of the principle of minimum entropy production was developed by Glansdorf, Prigognine and Hays (1962) to include irreversible process due to friction in a viscous, incompressible fluid with temperature gradients. These authors combine this thermodynamic argument with the mechanical variational principles outlined previously to define a Lagrangean density and hence to derive the Euler-Lagrange equations of motion for their general fluid system.

The use of variational principles for the general specification of a hydrodynamic system does not appear to have been thoroughly explored. In a recent survey of this subject Eckart (1960) underlines its importance by quoting the opinion of J. von Neumann that "the difficulty of solving the hydrodynamic equations arises, not from their non-linear character, but from the lack of a variation principle." Eckart goes on to show that this development has been retarded on the one hand, by a traditional preference for working with the Eulerian representation of the hydrodynamic equations of change, and on the other hand, by a natural derivation of equations of motion in the Lagrangean representation from an application of the variational principle. Some progress toward closing this gap is evident in the literature. For instance, Pierson (1962) has found it profitable to formulate certain problems in dynamical oceanography using the Lagrangean representation. From the other side of the gap, the example may be quoted of Whitlock (1962) who showed how to formulate directly in an Eulerian representation a Lagrangean function characteristic of a homogeneous frictionless compressible fluid flow first set out in terms of Lagrangean representation by Katz (1961). Both of these last-quoted references are oriented primarily toward a study of plasma physics. It appears from a preliminary search of the literature that the requirements of research into the magneto-hydrodynamics and thermodynamics of plasmas is likely to produce significant contributions to the development of variational techniques in hydrodynamics. Perhaps from this product of the space age will come new tools for the dynamical oceanographer to construct his models from a new point of view.

8. Natural radiocarbon and ocean circulation

The further development of ocean circulation theories requires guidance from measurements of the velocity structure at all levels in the real ocean. One source of indirect estimation for deep water movements may possibly be contained in measurements of the concentration of the radio isotope ^{14}C in the ocean, relative to that of the stable isotope ^{12}C. During recent years some such measurements have accumulated from the Atlantic Ocean (Broecker et al., 1960), the eastern Pacific Ocean (Bien, et al., 1960), and the southwest Pacific Ocean (Burling and Garner, 1959). The source of natural radiocarbon lies in the interaction between the neutron component of the cosmic ray flux and atmospheric nitrogen. The carbon isotope ^{14}C formed during this process is unstable, suffering β-decay to a stable form of the same element, ^{13}C, with a half-life of approximately 5600 years. The concentration of radiocarbon in the oceanic upper mixed layer will be governed basically by those processes which exchange carbon dioxide across the air-sea interface. These processes have been the subject of much recent investigation, discussed for example by Bolin (1960). In deeper waters, the $(^{14}C/^{12}C)$ ratio will depend on

(a) the physical processes of advection by the gross oceanic circulation, diffusion across concentration gradients by turbulent exchange and radioactive decay of the unstable isotope; and

(b) chemical and biological processes which may precipitate into, or dissolve from the sediments, consume, or redistribute the two carbon isotopes, perhaps introducing fractionation effects

because of the difference in isotopic weights.

If the processes in (b) above may be neglected--an assumption that needs careful investigation, however--these carbon measurements seem to offer, at least in principle, a means for the estimation of the kinematics of deeper ocean waters, through the radioactive decay process. Derivation of deep current velocities has been attempted in the references cited above, for example, simply by using the apparent "ages" of water samples (i. e., the time elapsed since the sample has been in free exchange with the atmosphere) separated by a known distance. Such a treatment ignores the effects of mixing, however, a process known to be of great importance in governing both the distribution of material dissolved or suspended in ocean water and the dynamics of flow. The gross results of mixing applied to the distribution of natural radiocarbon have been discussed by Craig (1957) and by Broecker (1962) who computed average exchange rates between, and residence times of radiocarbon particles in, three-reservoir "box model" systems consisting of the atmosphere, the oceanic upper mixed layer, and the deep ocean below the permanent thermocline. Each of these reservoirs was regarded as being completely mixed, and first order exchange processes between reservoirs were assumed.

If, now, interest is focussed on details of the oceanic velocity and mass structure rather than on the ocean/atmosphere exchange problem, the whole oceanic carbon reservoir system will need to be modelled in a way that will permit consideration of continuous variation of velocity, concentration, and mixing, especially in the vertical direction. The following discussion attempts a

preliminary evaluation of the extent to which carbon-14 measurements may be useful as an index of movement and mixing in the deep ocean.

To this end, a simple model will be considered which incorporates both vertical and horizontal velocity components in one vertical cross-section, with lateral and vertical mixing expressed in elementary form. There is no component of concentration gradient, and hence no flux of property occurs normal to the cross-section in this model. Let the cross-section to be considered lie in the y-z plane and let A_y, A_z be, respectively, the eddy coefficients of diffusion for material dissolved in sea water, assumed to be constant and independent of the nature of the dissolved material. If $X = X(y, z, t)$ be the concentration of such material, then

$$\frac{dX}{dt} = v \frac{\partial X}{\partial y} + w \frac{\partial X}{\partial z} + \frac{\partial X}{\partial t} \tag{8.1}$$

It is now specified that the distribution of all relevant concentrations X is stationary in this model so that $(\partial X/\partial t = 0)$ and

$$v \frac{\partial X}{\partial y} + w \frac{\partial X}{\partial z} - \frac{A_y}{\rho} \frac{\partial^2 X}{\partial y^2} - \frac{A_z}{\rho} \frac{\partial^2 X}{\partial z^2} + Q = 0 \tag{8.2}$$

where Q is the rate at which the property X is removed from the system by non-conservative processes. In the case of total salt concentration (salinity), such a process might be precipitation or evaporation at the sea surface. For dissolved oxygen, it might be the respiration of marine animals or the oxidation of organic material. For carbon-14 it would ideally be only the radioactive decay process, except for the source region in the

sea surface so that $Q_c = \lambda C$ where λ is the isotope's decay constant and C is the carbon-14 concentration. Below surface influence, the salinity, S, will be a conservative property with its distribution governed by physical movements and mixing only, so that $Q_s = 0$. Equations of the form of (8.2) may thus be constructed which describe stationary distributions of salt and carbon-14 in this highly idealized model situation.

$$\rho v \frac{\partial S}{\partial y} + \rho w \frac{\partial S}{\partial z} - A_y \frac{\partial^2 S}{\partial y^2} - A_z \frac{\partial^2 S}{\partial z^2} = 0 \tag{8.3}$$

$$\rho v \frac{\partial C}{\partial y} + \rho w \frac{\partial C}{\partial z} - A_y \frac{\partial^2 S}{\partial y^2} - A_z \frac{\partial^2 S}{\partial z^2} + \rho \lambda C = 0 \tag{8.4}$$

If all other quantities are known, equations (8.3) and (8.4) will determine v(y, z) and w(y, z), provided the determinant of their coefficients does not vanish, i.e.,

$$\frac{\partial S}{\partial y}\frac{\partial C}{\partial z} - \frac{\partial C}{\partial y}\frac{\partial S}{\partial z} \neq 0 \tag{8.5}$$

An equality in (8.5) would require the concentration gradients of salt and carbon everywhere to lie parallel. In this case, C could be expressed as one function of S over the whole section. Such a correlation between S and C is here denied, in principle, through the radioactive decay of one component. Whether the magnitude of the radioactive decay constant in relation to oceanic rates of movement and mixing is appropriate to maintain the above determinant sufficiently well-conditioned for practical computation, remains to be seen. Solution of equations (8.3) and (8.4) for the velocity components yields

$$\frac{v}{\rho\begin{vmatrix} \frac{\partial S}{\partial z} & (-M_s) \\ \frac{\partial C}{\partial z} & (-M_c) \end{vmatrix}} = \frac{-w}{\rho\begin{vmatrix} \frac{\partial S}{\partial y} & (-M_s) \\ \frac{\partial C}{\partial y} & (-M_c) \end{vmatrix}} = \frac{1}{\rho^2\begin{vmatrix} \frac{\partial S}{\partial y} & \frac{\partial C}{\partial y} \\ \frac{\partial S}{\partial z} & \frac{\partial C}{\partial z} \end{vmatrix}} \qquad (8.6)$$

where $M_s \equiv A_y \frac{\partial^2 S}{\partial y^2} + A_z \frac{\partial^2 S}{\partial z^2}$

and $M_c \equiv A_y \frac{\partial^2 C}{\partial y^2} + A_z \frac{\partial^2 C}{\partial z^2} - \lambda C$.

All oceanic radiocarbon measurements made to date have been published in the form of "activity", proportional to the ratio of the number of atoms of ^{14}C in the sample to the number of atoms of ^{12}C present. Figures published usually represent percent "enrichments", E, of C^{14} activity with respect to a standard sample.

$$E = \frac{a - a^*}{a^*} \times 100\% \qquad (8.7)$$

where $a = {}^{14}C/{}^{12}C$ for the sample and a^* represents the activity of the standard. The quantity C in equations (8.4) to (8.6) should strictly be identified with the quantity ^{14}C above, and its space derivatives would thus have the form

$$\frac{\partial C}{\partial x} = \frac{a^*}{100}\left[{}^{12}C\,\frac{\partial E}{\partial x} + (100 + E)\,\frac{\partial}{\partial x}({}^{12}C)\right] \qquad (8.8)$$

$$\frac{\partial^2 C}{\partial x^2} = \frac{a^*}{100}\left[{}^{12}C\,\frac{\partial^2 E}{\partial x^2} + 2\,\frac{\partial\,{}^{12}C}{\partial x}\,\frac{\partial E}{\partial x} + (100+E)\,\frac{\partial^2}{\partial x^2}\,({}^{12}C)\right] \qquad (8.9)$$

In the discussion following, however, the quantity C of equations (8.4) to (8.6) will be identified with the enrichment, E. This amounts to an assumption of spatial constancy of the concentration of carbon-12. Data on this concentration are generally lacking and will be required for any analysis of the kind attempted here to be properly definitive. From carbon dioxide measurements made in the Atlantic Ocean (e. g., see Defant, 1962, p. 78), it would appear that the constancy of carbon content in the deeper waters, say below 1500 m, may be a fair approximation. In shallower waters, however, relatively large concentration gradients are evident, especially in the vertical, biological effects producing a wide-spread maximum in the CO_2 concentration/depth curve at a depth of some 500 m. In shallow and intermediate depths, therefore, the present discussion may well be unrealistic. Conveniently ignoring all this for the present model, equation (8.4) will now be written as (8.10).

$$\rho v \frac{\partial E}{\partial y} + \rho w \frac{\partial E}{\partial z} - A_y \frac{\partial^2 E}{\partial y^2} - A_z \frac{\partial^2 E}{\partial z^2} + \rho\lambda(100+E) = 0 \qquad (8.10)$$

The carbon-14 data used in the calculations that follow are based on sections in the southwest Pacific Ocean in the vicinity of the 180^{th} meridian, one extending northwards from New Zealand toward the Tokelau Islands, the other extending southwards from New Zealand towards the Ross Sea. The originally published enrichments (Burling and Garner, 1959) showed small positive values at and near the sea surface; for convenience here, these values were normalized by subtracting the greatest positive value from all others so that $E \leq 0$ everywhere. The enrichment values thus

modified which were finally adopted for computation are listed in Table 8.1. It must be stressed that these figures represent only an idealization, the form of which has been suggested by observation. The enrichment figures tabulated here do not pretend necessarily to be representative of conditions in the real ocean. A corresponding idealized salinity section has also been constructed from values in Table 8.1. These values have been suggested by data taken north of New Zealand at Dana stations 3580, 3585, 3626, and 3639, and Galathea station 677 and to the south at stations worked by Burling (1961, fig. 9). The structure of these idealized sections is illustrated by the plotted cross-sections of figures 8.1 and 8.2. As may be seen in Table 8.1, the grid point spacings adopted for the numerical representation of these sections was 5° latitude in the horizontal, and 300 m in the vertical. The adequacy of these spacings to represent gradients and curvatures in finite difference form is illustrated in figure 8.3 for the salinity distribution at the "station" in latitude 30°S. Values of the velocity components v and w were calculated from equation (8.6) at each gridpoint for four different mixing regimes:

(a) $A_y = 10$ gm cm^{-1} sec^{-1} ; $A_z = 10^6$ gm cm^{-1} sec^{-1} to study the combined effects of both horizontal and vertical mixing using representative orders of magnitude of the diffusion coefficients. Velocity distributions derived are plotted in figures 8.4 and 8.5.

(b) $A_y = 0$; $A_z = 10$ c. g. s. ; vertical mixing only (figures 8.6 and 8.7).

(c) $A_y = 10^6$ c. g. s. , $A_z = 0$; horizontal mixing only (figures 8.8 and 8.9).

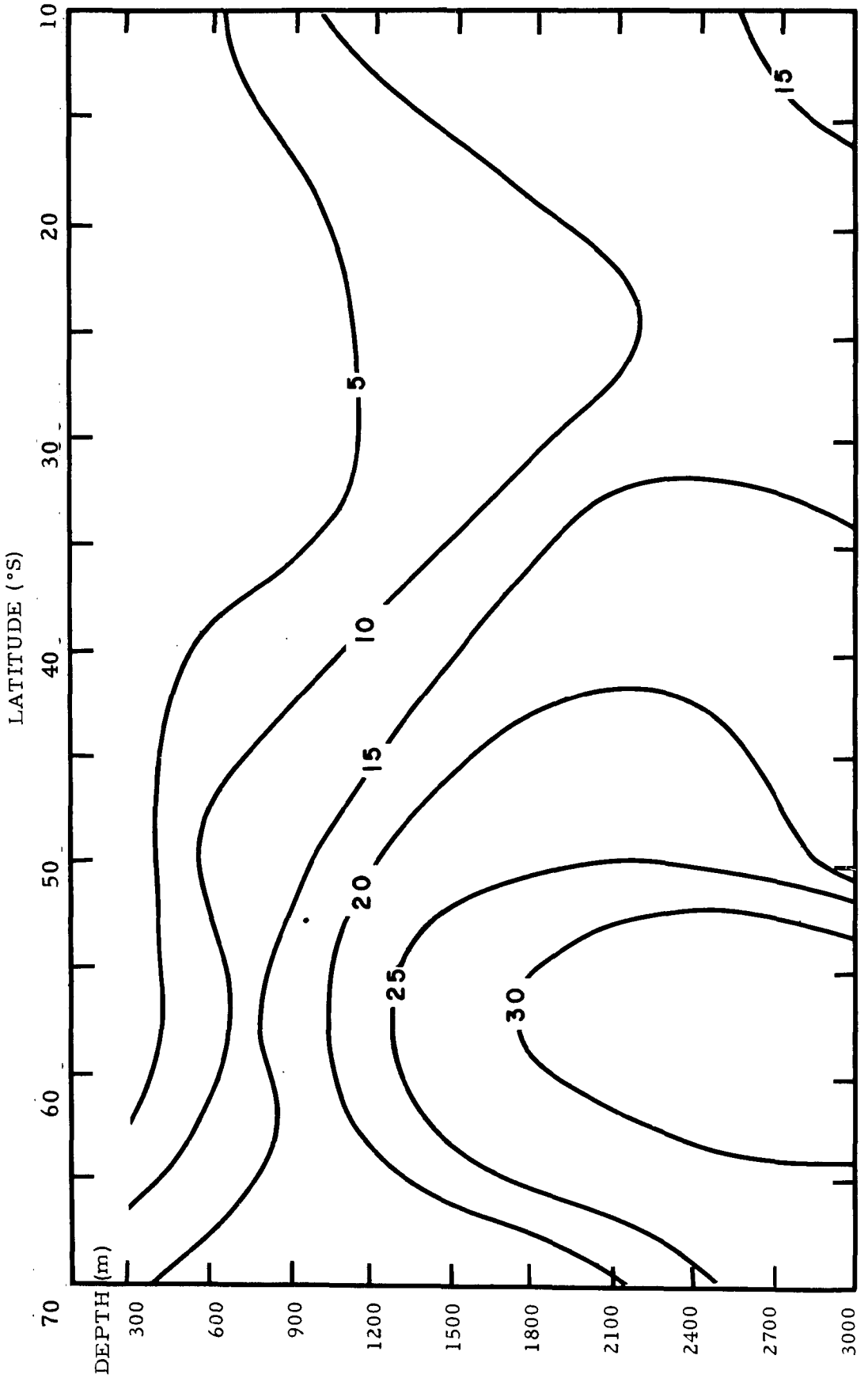

Figure 8.1 A model meridional vertical section of percent depletion of carbon-14 activity with respect to the surface in the southwest Pacific Ocean in the vicinity of longitude 180°, drawn from the figures of Table 8.1.

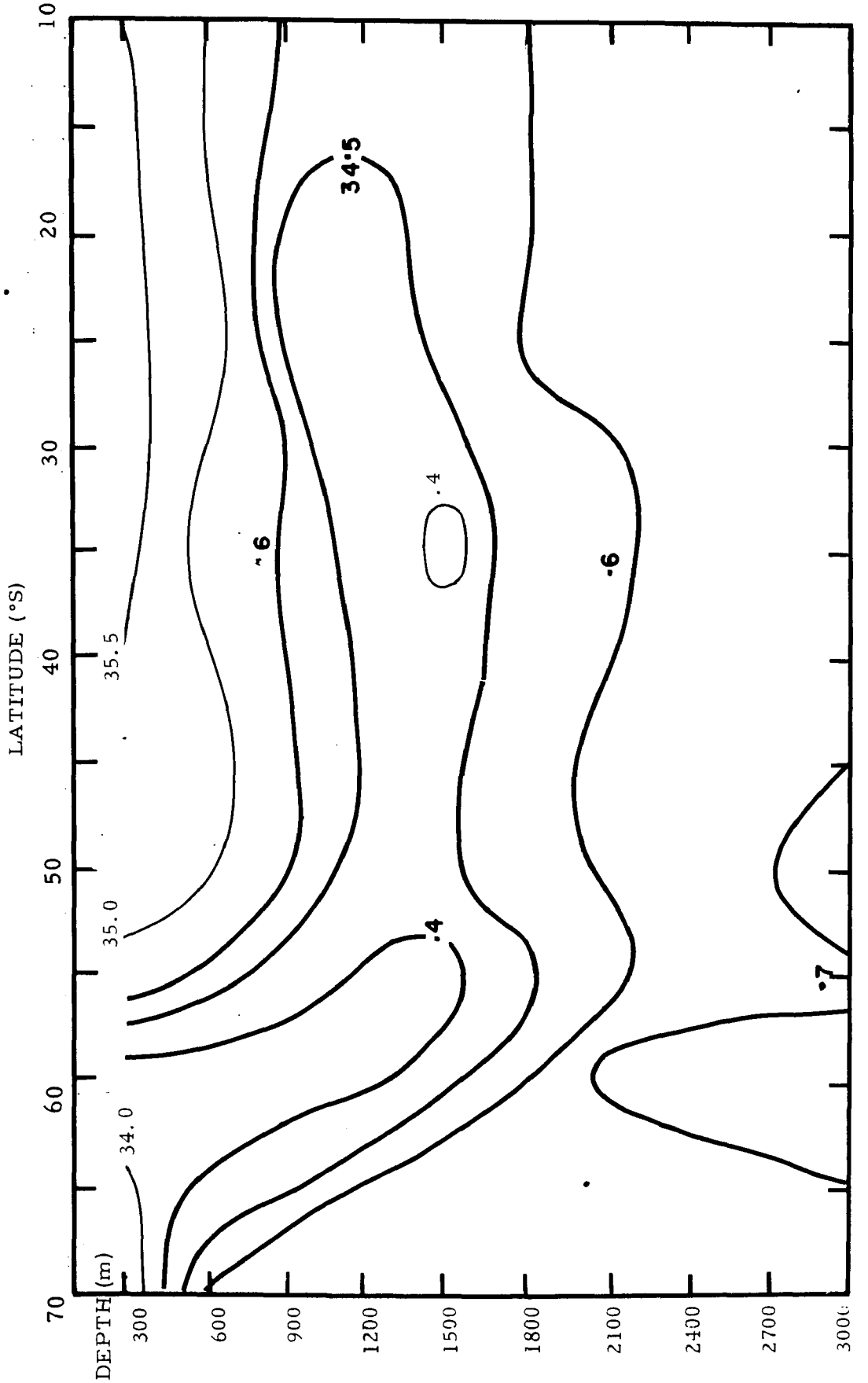

Figure 8.2 A model meridional vertical section of salinity in the southwest Pacific Ocean in the vicinity of longitude 180°, drawn from the figures of Table 8.1.

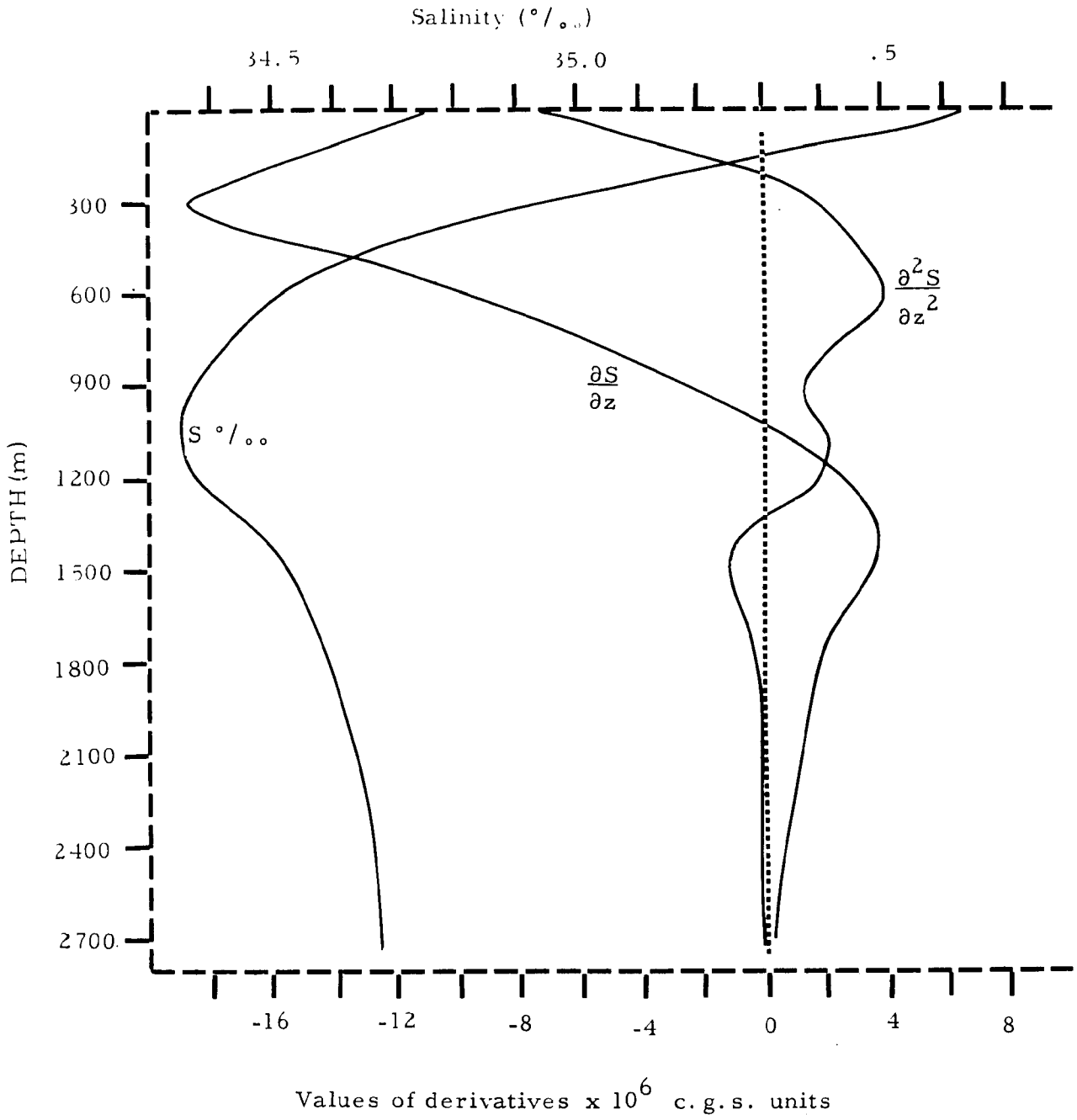

Figure 8.3. Salinity-depth variation at latitude 30°S in the section of figure 8.3 with the values of the first and second depth derivatives derived from the numerical methods adopted in the analysis.

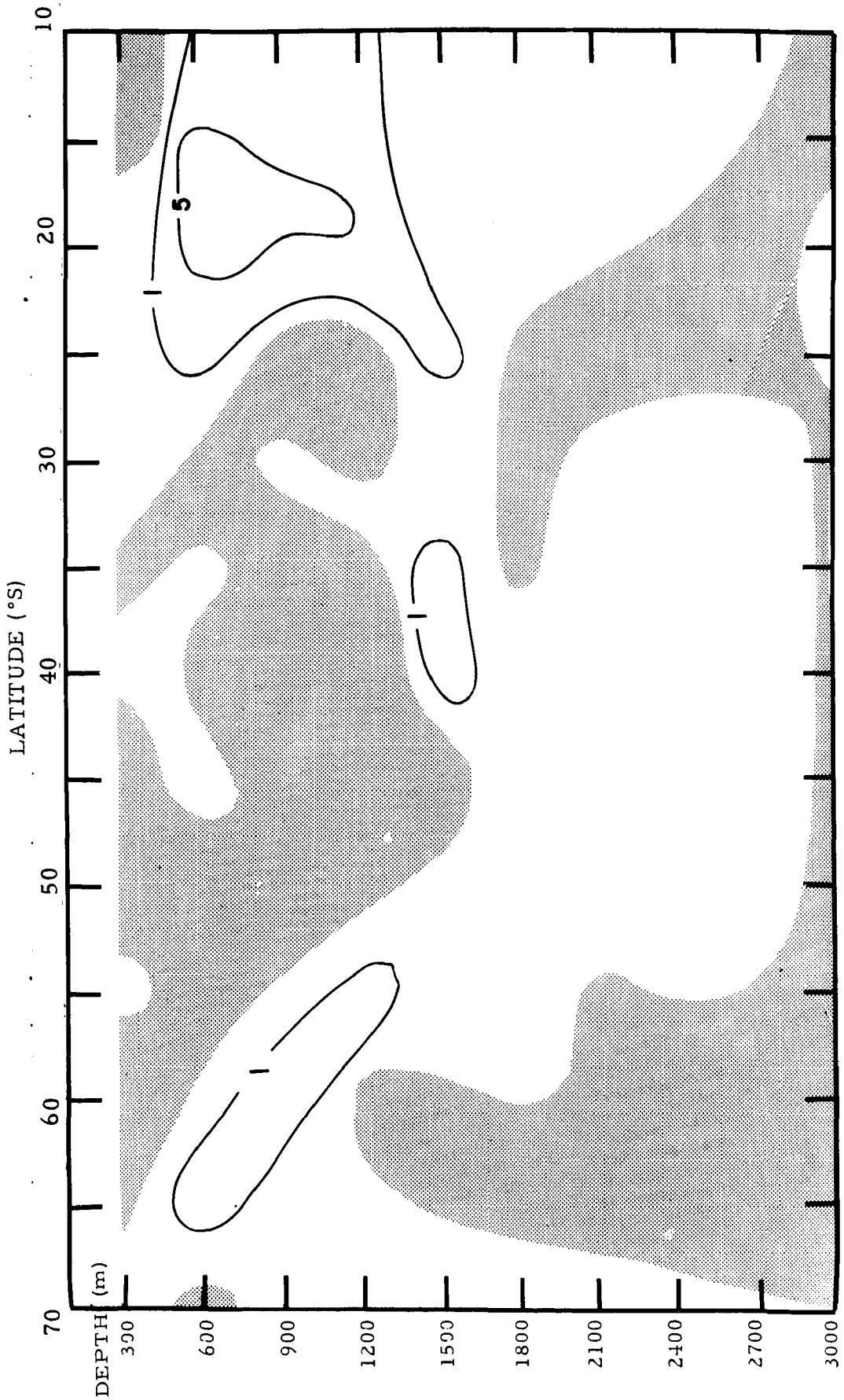

Figure 8.4 Distribution of the meridionally-directed velocity component, v, derived from equation (8.6), the data of Table 8.1, and with both horizontal ($A_y = 10^2$ c.g.s) and vertical ($A_z = 10$ c.g.s.) mixing coefficients acting. Shaded areas mark south-going components; unshaded areas mark north-going components. Isotachs are in cm sec^{-1}.

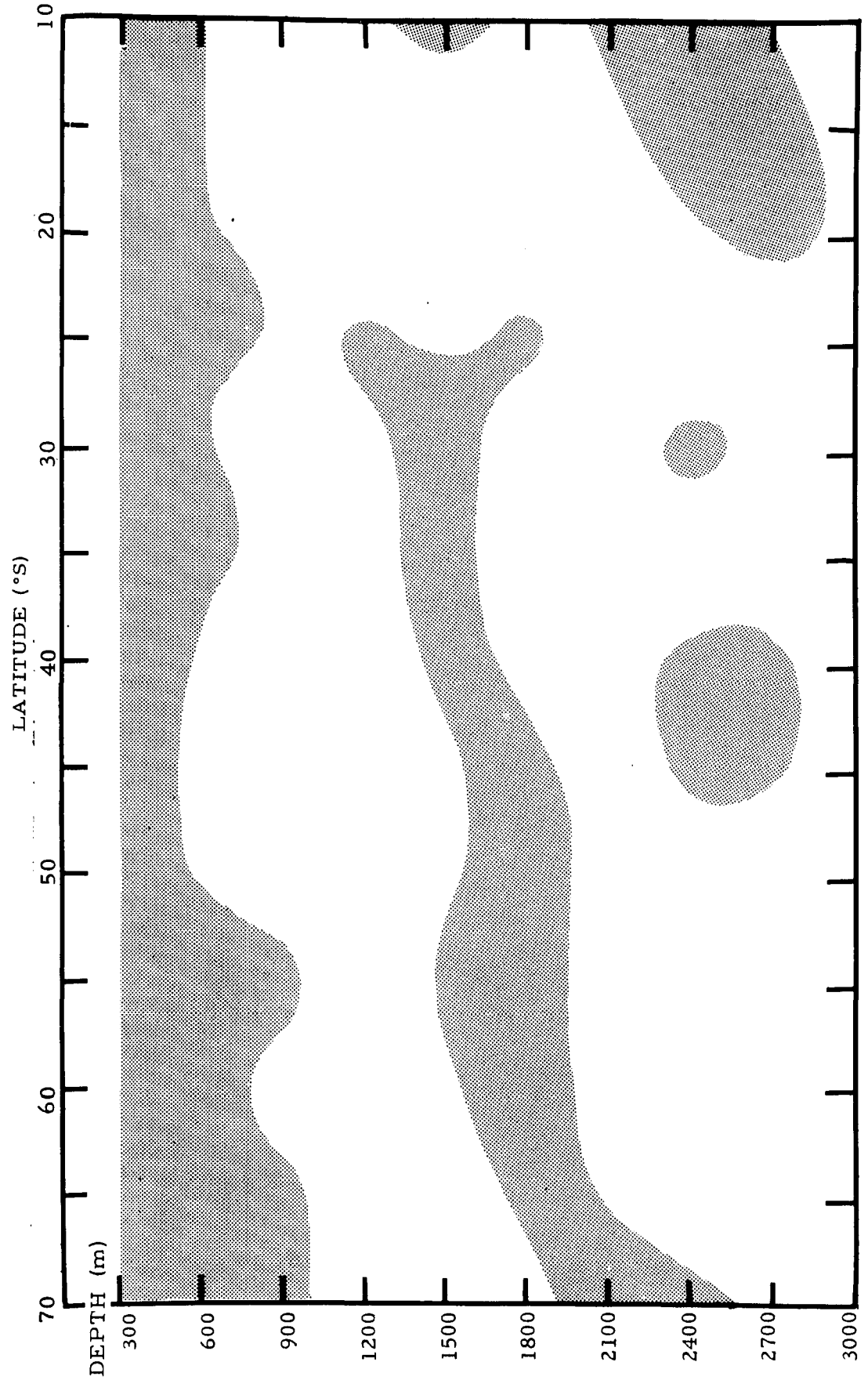

Figure 8.5 Distribution of the vertically directed velocity component, w, associated with the situation described in Figure 8.4. Shaded areas contain components directed downwards, unshaded areas contain components directed upwards.

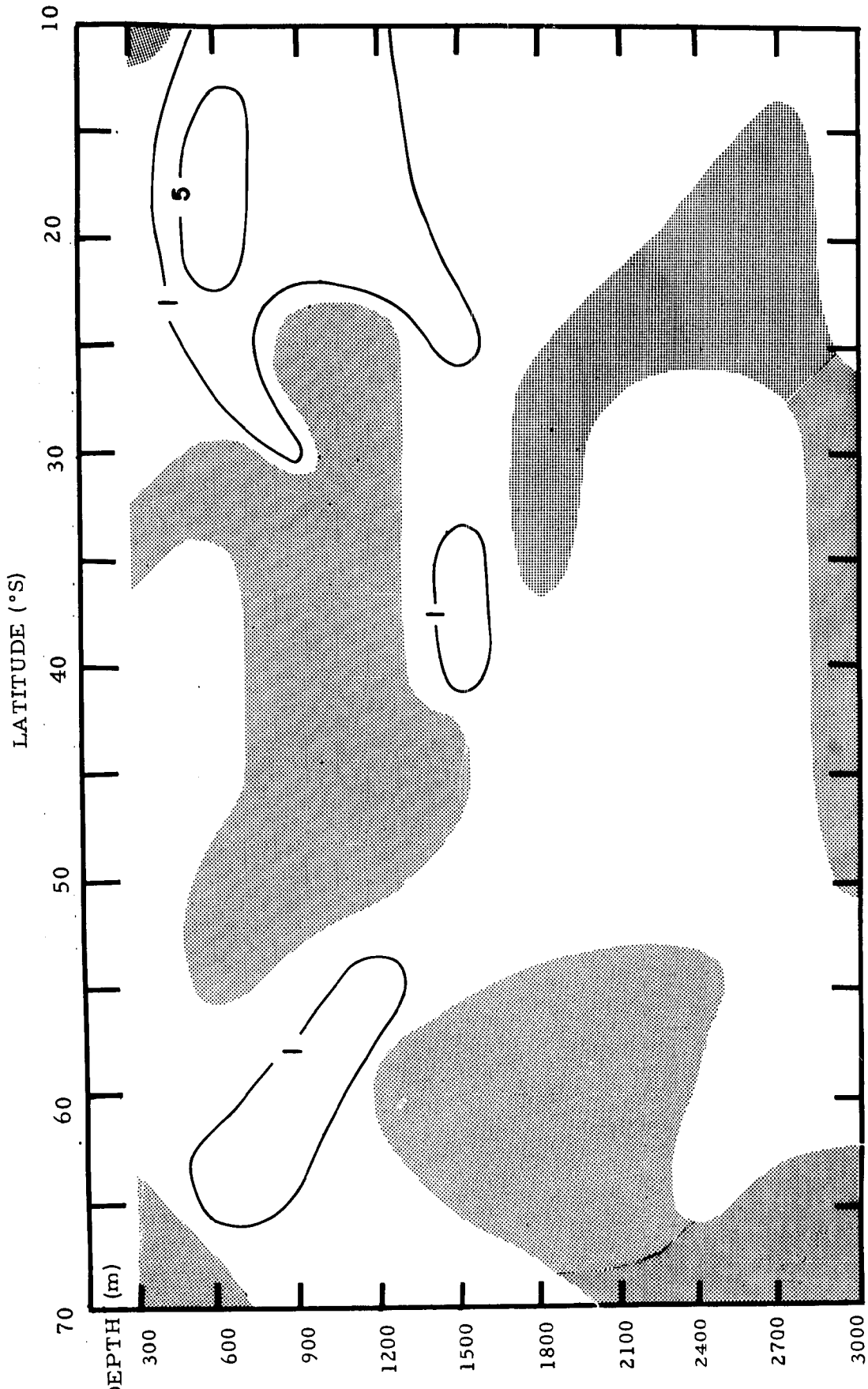

Figure 8.6 Distribution of the meridionally-directed velocity component, v, derived for the same situation as was described in Figure 8.4 but with no horizontal mixing acting ($A_y = 0$, $A_z = 10$ c.g.s.). Shaded areas mark south-going components, unshaded areas mark north-going components.

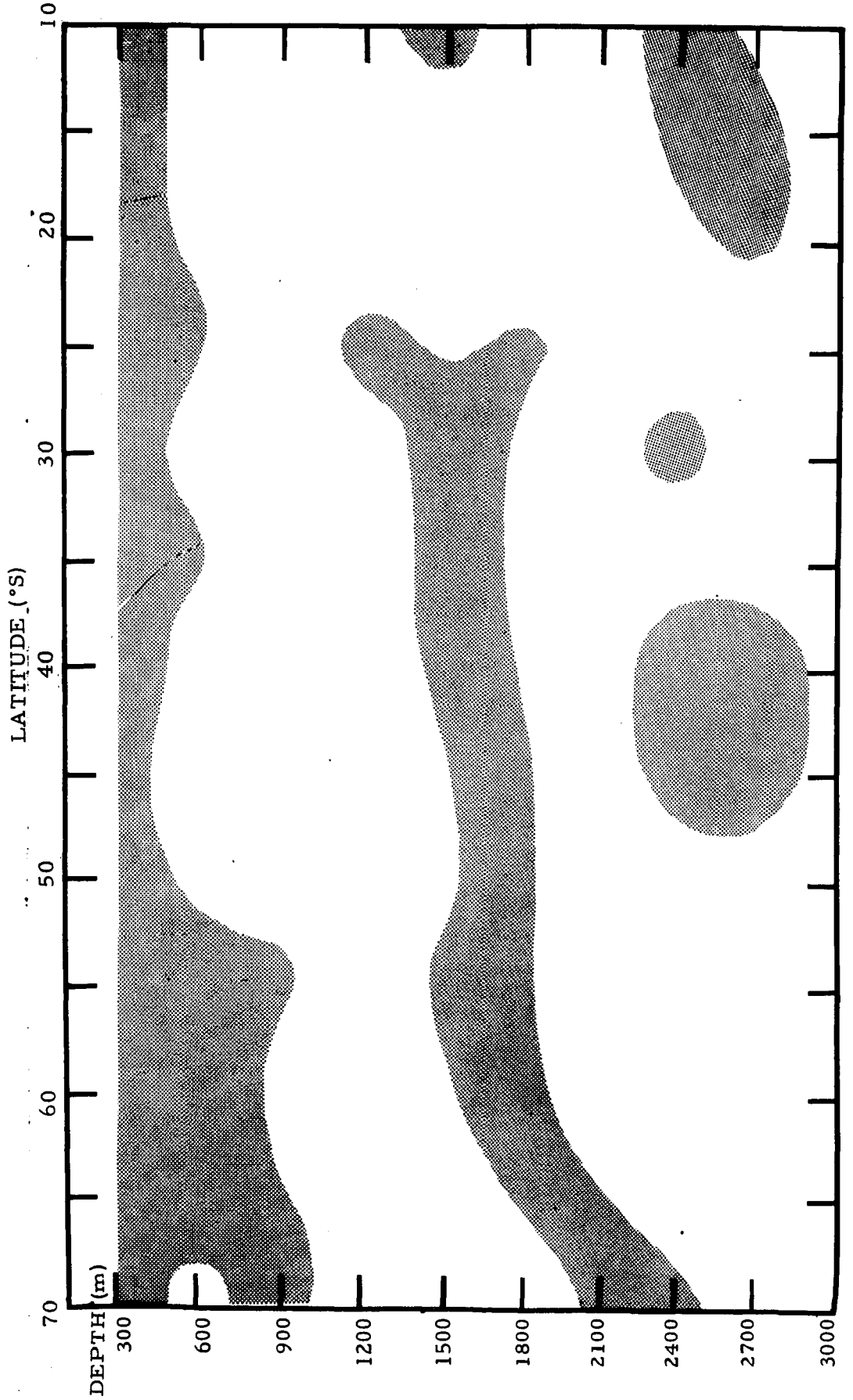

Figure 8.7 Distribution of the vertically-directed velocity component, w, associated with the situation described for Figure 8.6, i.e., with only vertical mixing acting. Shaded areas contain components directed downwards, unshaded areas contain components directed upwards.

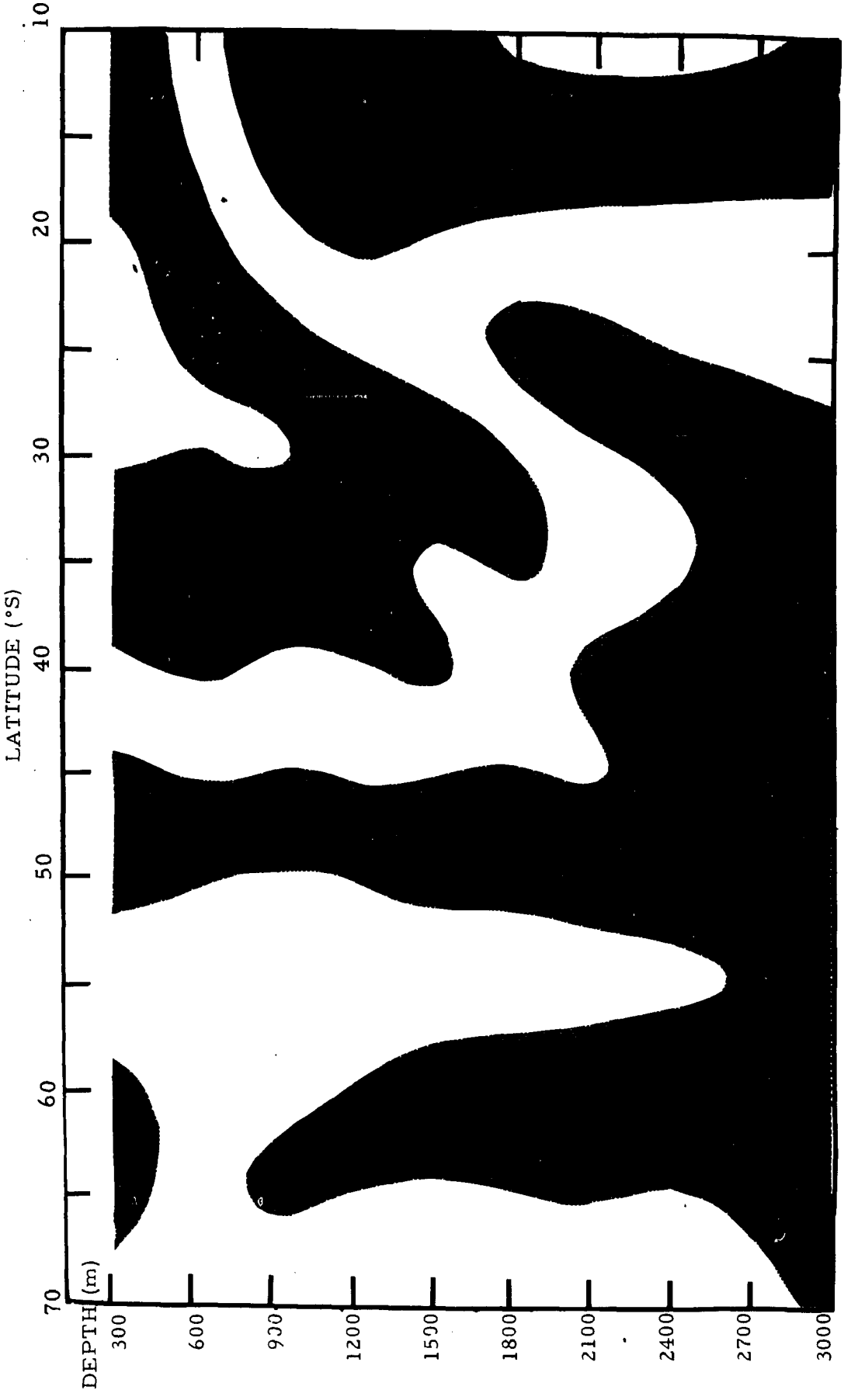

Figure 8.8 Distribution of the meridionally-directed velocity component, v, derived for the same situation as was described in Figure 8.4, but with no vertical mixing acting ($A_y = 10^6$ c.g.s., $A_z = 0$). Shaded areas mark south-going components, unshaded areas mark north-going components.

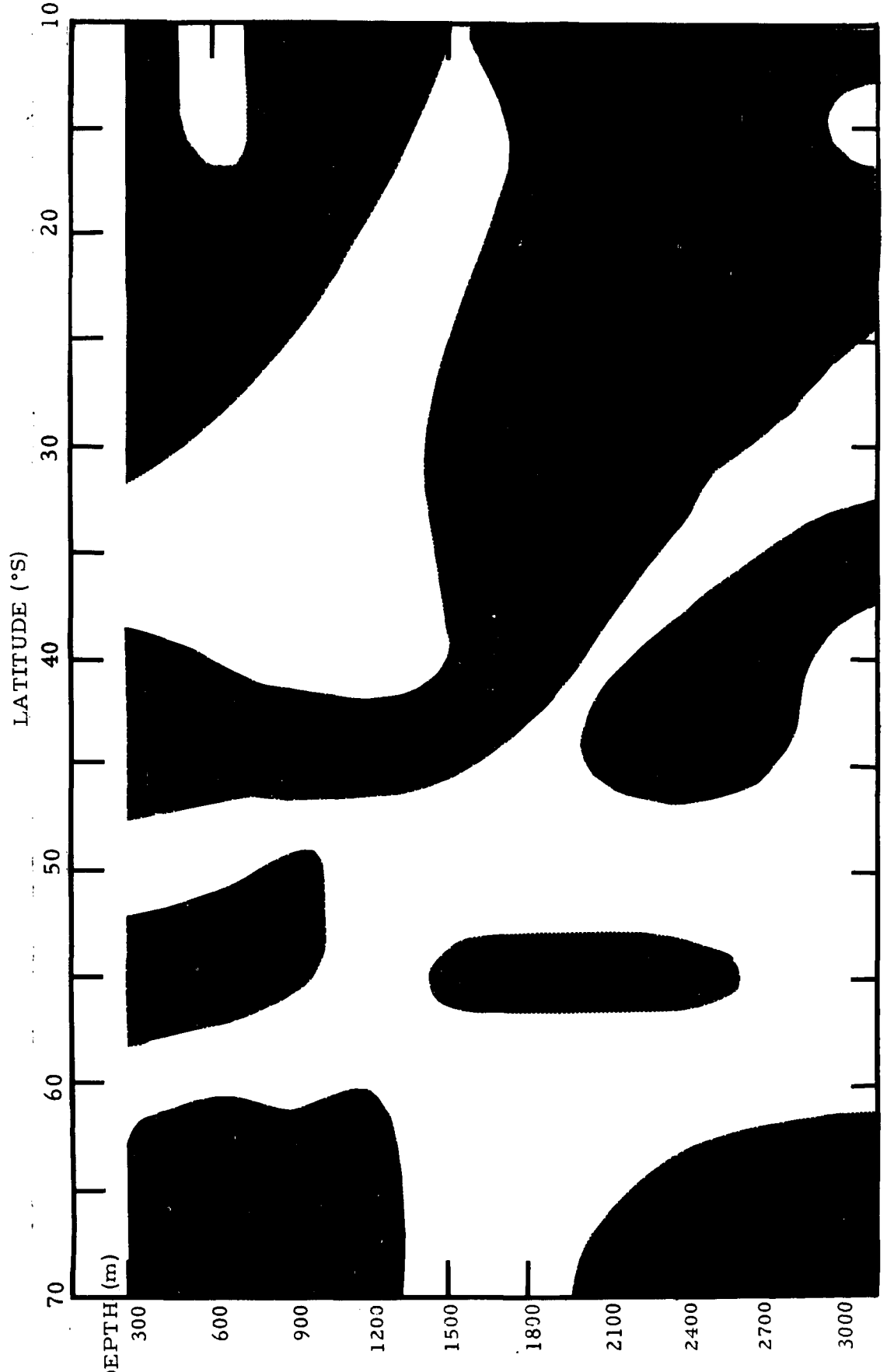

Figure 8.9 Distribution of the vertically directed velocity component, w, associated with the situation described for Figure 8.8, i.e., with only horizontal mixing acting. Shaded areas contain components directed downwards, unshaded areas contain components directed upwards.

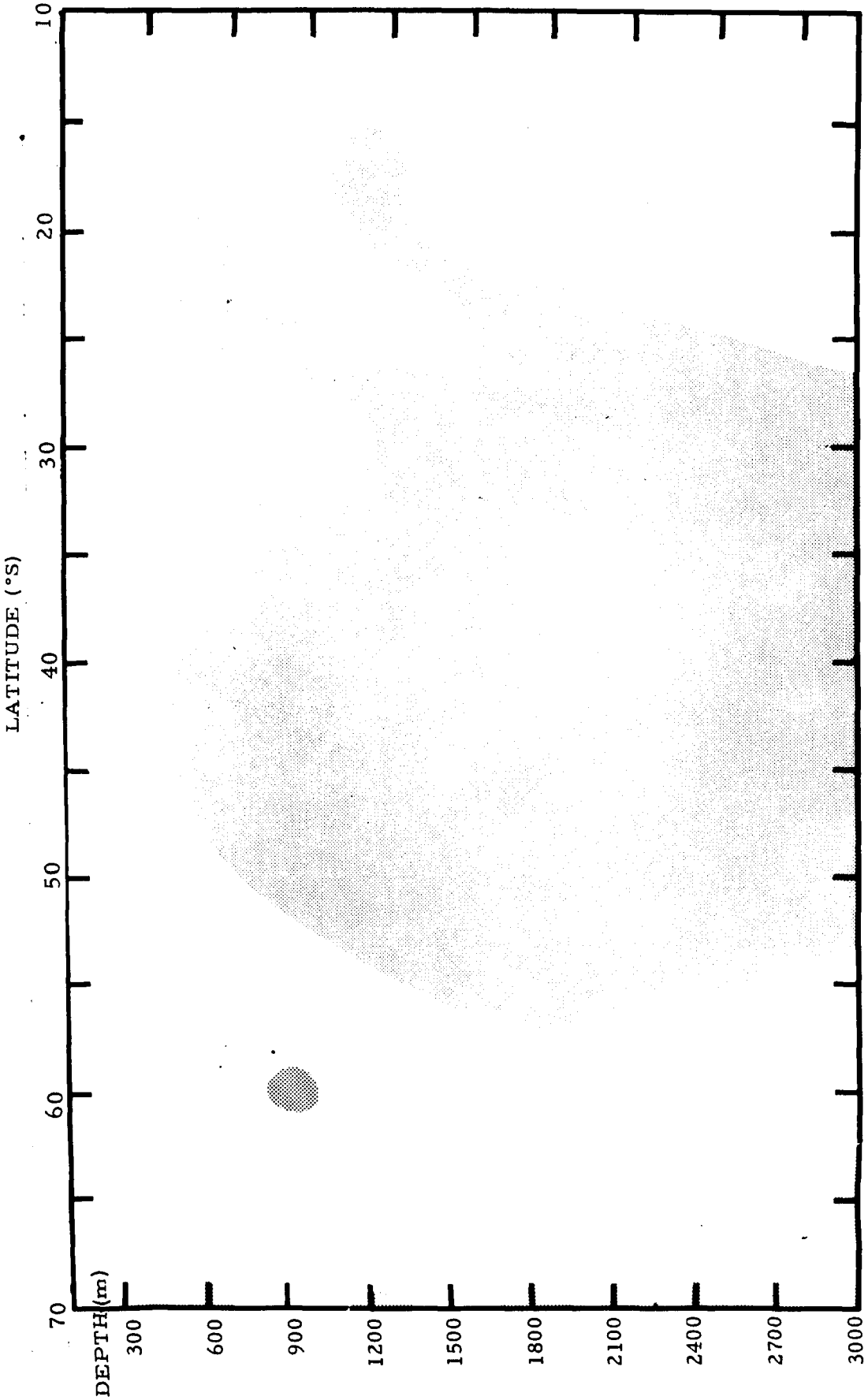

Figure 8.10 Distribution of the meridionally directed component, v, derived for the same situation as was described for Figure 8.4 but with no mixing acting in the section ($A_y = 0 = A_z$). Shaded areas mark south-going components, unshaded areas mark north-going components.

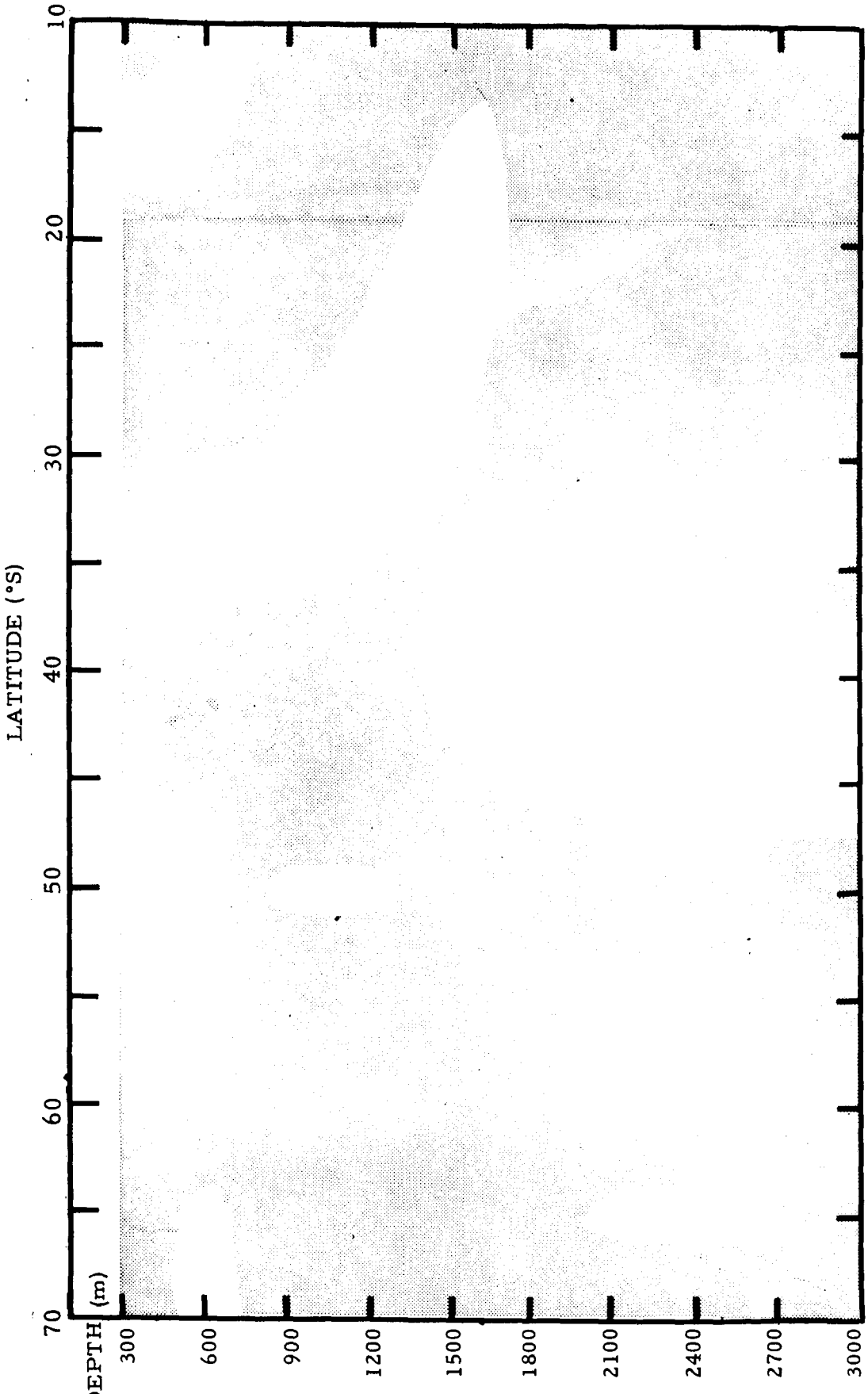

Figure 8.11 Distribution of the vertically directed velocity component, w, associated with the situation described for Figure 8.10, i.e., with advection alone acting in the section. Shaded areas contain components directed downwards, unshaded areas contain components directed upwards.

(d) $A_y = 0 = A_z$; no mixing, advection acting alone (figures 8.10 and 8.11).

Values of $\rho = 1.0$ gm cm^{-3} and $\lambda = 3.9 \times 10^{-12}$ sec^{-1} were used throughout the computations.

The salinity pattern of figure 8.1 permits a general description of the water mass characteristics in the chosen section in terms of conventional hydrological interpretation. Dominating the pattern is the tongue of low salinity originating near the surface in the southern part of the section and extending northwards at a depth of around 1000 m. This represents the Antarctic Intermediate Water. Below the intermediate water lies the Pacific Deep Water of relatively high salinity. This water approaches the surface in higher latitudes. Above the intermediate layer, water properties are influenced by the presence of sub-tropical, sub-antarctic and antarctic surface water. The detailed distribution of salinity due to these influences is not seen in section 8.1, both because of the relatively wide horizontal spacings of "stations", and because the section has deliberately not been extended to the sea surface where water properties are certainly not conservative. The Sub-tropical and Antarctic Convergences are thus not resolved, but there is clearly a rapid meridional change of salinity in upper water layers between latitudes 50° and 60° S. This will reflect mainly the presence of the Antarctic Convergence.

The percentage depletion of carbon-14 activity in the model distribution of figure 8.2 is greatest in the Pacific Deep Water under the region of formation of the Antarctic Intermediate Water. This probably represents the entry into the Pacific Ocean of "old" Deep Water from the Atlantic and Indian Oceans via the circumpolar

current. Spreading northward from this core is suggested by a maximum in the depletion-depth relationship measured at a mid-latitude station.

A fuller discussion of the carbon-14 activity pattern as a water-mass indicator was given by Burling and Garner (1959); the present discussion is concerned rather with an attempt numerically to derive circulation patterns based on the model situation described in previous paragraphs.

A digest of the results of these computations is presented in figures 8.4 through 8.11. Because of the simplicity of the model used it is not desired to discuss the results of this experiment from a quantitative point of view, but rather to make a general qualitative assessment of the usefulness of the principles involved. To this end the figures show the gross velocity structure simply by differentiating between north- and south-going components for the "meridional" sections (figures 8.4, 8.6, 8.8, and 8.10) and between components directed upward and downward for the "vertical" sections (figures 8.5, 8.7, 8.9, and 8.11). Only where unusually high velocity values (> 1 cm sec^{-1}) appeared, were isotachs inserted in the diagrams (e.g., figures 8.4 and 8.6). Meridionally directed velocity components were generally of the order of 10^{0} to 10^{-1} cm sec^{-1}, and vertically directed components were of the order of 10^{-3} to 10^{-5} cm sec^{-1}.

(a) Combination of horizontal and vertical mixing.

Figures 8.4 and 8.5 summarize the results of calculations based on equations (8.6) and the data of Table 8.1, and making use of representative values of the mixing coefficients described previously. The following features may be noted. Vertical

velocity components were generally directed upwards. One band of movement downward was defined in the upper layers extending throughout most of the section to a depth of five to six hundred meters. At the southern end of the section where the sinking of Antarctic Intermediate Water is expected to occur, this band of down-moving water extended to about a thousand meters of depth. A second band of downward motion was defined which extended northward to about latitude 20°S just below the depth of the salinity minimum of the Antarctic Intermediate Water. In upper layers of the southern part of the section, meridional components of flow were north-going, and flow in this direction was traced along the core of the Antarctic Intermediate Water and in the Deep Water of mid-latitudes. Higher salinity water above the Intermediate core supported mainly south-flowing meridional components in mid-latitudes, but quite strong north-going components were found in low latitudes.

(b) Vertical mixing

If the calculations which derived figures 8.4 and 8.5 are repeated with a zero value for the horizontal mixing coefficient, A_y, the patterns of figures 8.6 and 8.7 are obtained. Clearly, the process of horizontal mixing is relatively unimportant in the model used, for the two sets of figures are practically identical.

(c) Horizontal mixing

Retention of the horizontal mixing coefficient, A_y, and setting the vertical coefficient, A_z, to zero, yields the patterns shown in figures 8.8 and 8.9. Compared with the results of the two previous experiments, the circulation patterns derived are relatively incoherent and do not suggest a realistic situation.

(d) No mixing

With both horizontal and vertical mixing coefficients set to zero so that only advection and radioactive decay remain in the model, the calculations yield the patterns of figures 8.10 and 8.11. These patterns also do not suggest a reasonable circulation pattern, at least in terms of conventional ideas on the meridional circulation pattern.

The foregoing calculations illustrate several points.

(i) The importance of including appropriate mixing processes in any discussion of the significance of Carbon-14 "dating" to ocean circulation studies is stressed.

(ii) The relative unimportance of horizontal mixing over vertical exchange over large ocean areas is suggested. If such an assumption were tolerable, considerable economy in observation could be achieved, since only horizontal gradients, and not second derivatives, of water properties would need to be defined in the neighborhood of the point at which the velocity structure were to be determined. The horizontal diffusive flux of property is probably greatest in the neighborhood of the major water mass boundaries.

(iii) Use of this model should be restricted carefully to situations where the zonal velocities and/or zonal gradients of property are sufficiently small. Perhaps suitable regions might best be sought in the Southern Ocean to fulfill this condition. The equation of continuity could be used to derive a field of zonal velocity components implied by those of the meridional and vertical components found by the foregoing calculations. It would be interesting to discover whether reasonable values would be so derived.

(iv) A modification of the above model might be used to estimate the spatial variation of the exchange coefficients in a region where detailed and direct measurements of both velocity and water properties have been made. The work of Knauss (1960) in the Equatorial Undercurrent of the Pacific Ocean appears to provide data for a preliminary evaluation of these ideas.

Table 8.1 Showing salinity (‰) and relative Carbon-14 enrichment (%) figures used in the numerical analysis of circulation in a model meridional section in the southwest Pacific Ocean.

Salinity (‰)

Depth (m) \ Latitude °S	10	15	20	25	30	35	40	45	50	55	60	65	70
300	35.50	35.82	35.77	35.72	35.62	35.64	35.50	35.41	35.20	34.61	34.32	33.88	33.35
600	35.00	35.05	35.27	35.52	35.55	34.99	35.00	35.01	35.00	34.60	34.41	34.21	34.64
900	34.59	34.57	34.50	34.43	34.71	34.51	34.55	34.63	34.62	34.45	34.31	34.42	34.73
1200	34.55	34.52	34.47	34.42	34.41	34.38	34.44	34.50	34.45	34.38	34.36	34.58	34.72
1500	34.57	34.57	34.55	34.53	34.42	34.37	34.43	34.49	34.49	34.39	34.42	34.62	34.68
1800	34.60	34.60	34.60	34.61	34.52	34.53	34.54	34.55	34.55	34.47	34.54	34.64	34.67
2100	34.62	34.62	34.63	34.64	34.58	34.59	34.61	34.62	34.65	34.57	34.71	34.68	34.67
2400	34.63	34.63	34.64	34.66	34.62	34.63	34.63	34.64	34.68	34.63	34.73	34.69	34.67
2700	34.64	34.64	34.65	34.67	34.67	34.66	34.66	34.67	34.70	34.63	34.73	34.69	34.67
3000	34.65	34.67	34.68	34.69	34.69	34.67	34.69	34.70	34.72	34.63	34.73	34.69	34.67

(Continued)

Table 8.1 (Continued)

Carbon-14 (%)

Depth (m) \ Latitude °S	10	15	20	25	30	35	40	45	50	55	60	65	70
300	- 2.80	- 2.30	- 0.40	- 0.40	- 0.40	- 0.50	- 1.10	- 2.30	- 3.30	- 1.80	- 4.10	- 5.50	-14.40
600	- 4.70	- 3.20	- 2.70	- 1.90	- 2.90	- 3.30	- 5.30	- 9.50	-10.20	- 7.80	- 8.90	-12.00	-15.10
900	- 9.40	- 7.30	- 4.40	- 4.90	- 4.30	- 4.70	- 9.00	-10.30	-13.00	-15.40	-16.80	-15.30	-15.30
1200	-11.20	- 9.50	- 6.00	- 5.10	- 5.10	- 6.10	-10.50	-13.30	-18.00	-23.90	-24.20	-19.30	-17.10
1500	-12.60	-11.30	- 7.50	- 5.50	- 5.50	- 9.30	-14.10	-19.20	-22.10	-26.50	-27.00	-23.70	-17.50
1800	-13.30	-12.50	- 8.80	- 7.00	- 8.50	-13.00	-18.30	-21.50	-23.60	-28.40	-28.30	-25.30	-18.30
2100	-14.10	-13.40	-10.80	- 9.00	-11.50	-15.80	-19.40	-22.10	-23.60	-30.80	-33.40	-27.40	-19.30
2400	-14.70	-13.90	-11.90	-10.50	-13.10	-16.70	-19.00	-21.00	-22.50	-34.10	-33.40	-27.40	-21.30
2700	-15.40	-14.80	-12.70	-11.50	-13.50	-16.30	-17.90	-19.10	-20.50	-34.10	-33.40	-27.40	-27.30
3000	-16.30	-15.50	-13.30	-12.10	-13.10	-15.60	-16.30	-17.00	-18.10	-34.10	-33.40	-27.40	-27.30

References

Arthur, R.S., 1960: A review of the calculation of ocean currents at the equator. Deep Sea Research, vol. 6, pp. 287-297.

Bien, G.S., N.W. Rakestraw, and H.E. Suess, 1960: Radiocarbon concentration in Pacific Ocean water. Tellus, vol. 12, no. 4, pp. 436-443.

Bolin, B., 1960: On the exchange of carbon dioxide between the atmosphere and the sea. Tellus, vol. 12, no. 3, pp. 274-281.

British Meteorological Office, 1948: Climatological Atlas of the Atlantic Ocean.

Broecker, W.S., R. Gerard, M. Ewing, and B.C. Heezen, 1960: Natural radiocarbon in the Atlantic Ocean. J. Geophys. Res., vol. 65, no. 9, pp. 2903-2931.

Broecker, W.S., 1961: "Geochemistry and Physics of Ocean Circulation" in Oceanography, American Association for the Advancement of Science, Washington, D.C., ed. Mary Sears.

Burling, R.W., and D.M. Garner, 1959: A section of ^{14}C activities of sea water between 9°S and 66°S in the south-west Pacific Ocean. New Zealand J. of Geol. and Geophys., vol 2, no. 4, pp. 799-824.

Burling, R.W., 1961: Hydrology of circumpolar waters south of New Zealand. New Zealand D.S.I.R. Bulletin 143, 66 pp.

Carrier, G.F., A.R. Robinson, 1962: On the theory of the wind driven ocean circulation. J. Fluid Mech., vol. 12, no. 1, pp. 49-80.

Charney, J.G., 1955: The Gulf Stream as an inertial boundary layer. Proc. Nat. Acad. Sci., Wash., vol. 41, no. 10, pp. 731-740.

Clowes, A.J., 1933: Influence of the Pacific on the circulation in the southwest Atlantic Ocean. Nature, 131:189-191.

Courant, R., 1937: Differential and Integral Calculus, Vol. II. Blackie, London (second edition).

Craig, H., 1957: The natural distribution of radiocarbon and the exchange time of carbon dioxide between the atmosphere and the sea. Tellus, vol. 9, pp. 1-17.

Defant, A., 1941: Die absolute Topographie des physikalischen Meeresniveaus und der Druckflächen, sowie die Wasserbewungen im Atlantischen Ozean. Deutsche Atl. Exp. "Meteor", 1925-1927. Wiss. Erg., Bd. VI, 2 Teil 5, pp. 191-260.

Defant, A., 1961: Physical Oceanography, Vol. 1. Pergamon Press, New York, 729 pp.

Durell, C. V., 1946: Advanced Trigonometry. London, Bell, 335 pp.

Eckart, C., 1960: Variation principles of hydrodynamics. Physics of Fluids, vol. 3, no. 3, pp. 421-424.

Ekman, V. W., 1905: On the influence of the earth's rotation on ocean currents. Ark. för Mat. Astr. och Fysik, vol. 2, no. 11, pp. 1-53.

Ekman, V. W., 1923: Uber Horizontalzirkulation bei winderzeugten Meeresströmungen. Ark. för Mat. Astr. och Fysik, vol. 17, no. 26.

Garner, D. M., G. Neumann, and W. J. Pierson, 1962: The average horizontal wind driven mass transport of the Atlantic for February as obtained by numerical methods. Scientific report under contract Nonr 285(03), New York University, College of Engineering, Research Division. (In preparation.)

Glansdorff, P., I. Prigognine, and D. F. Hays, 1961: Variational properties of a viscous liquid at a non-uniform temperature. Physics of Fluids, vol. 5, no. 2, pp. 144-149.

Goldstein, H., 1959: Classical Mechanics. Addison-Wesley, Reading, Mass., 399 pp.

Haltiner, G. J., and F. L. Martin, 1957: Dynamical and Physical Meteorology. McGraw Hill, New York, 470 pp.

Hassan, E. S. M., 1961: "Models for the numerical computation of the oceanic circulation." In Contribution to the Problem of Oceanic Circulation, New York University, College of Engineering, Research Division, Report on Contract No. N-62036-794, October 1961.

Hassan, E. S. M., 1962: The general oceanic circulation; some computations and hypothesis. Submitted to J. of Marine Research.

Hirschfelder, J. O., C. F. Curtiss, and R. B. Bird, 1954: Molecular Theory of Gases and Liquids. Wiley, New York, 1219 pp.

Jahnke, E., and F. Emde (1945): Tables of Functions with Formulae and Curves. 4th Ed., Dover, New York, 382 pp.

Katz, S., 1961: Lagrangean density for an inviscid, perfect, compressible plasma. Physics of Fluids, vol. 4, no. 3, pp. 345-348.

Knauss, J. A., 1960: Measurements of the Cromwell Current. Deep Sea Res., vol. 6, pp. 265-285.

Lamb, H., 1945: Hydrodynamics. First American Edition, Dover, New York, 738 pp.

McLachlan, N. W., 1947: Theory and Application of Mathieu Functions. Oxford, 401 pp.

Montgomery, R. B., 1959: Henry Stommel, "The Gulf Stream". (Review). Trans. Amer. Geophys. Un., vol. 40, no. 3, p. 225.

Morgan, G. W., 1954: On the integration over depth of the equations for the wind-driven ocean circulation. Woods Hole Oceanographic Institution, Reference No. 54-89. (Unpublished manuscript), 15 pp.

Morgan, G. W., 1956: On the wind-driven ocean circulation. Tellus, vol. 8, no. 3, pp. 301-320.

Munk, W., 1950: On the wind-driven ocean circulation. J. of Met., vol. 7, pp. 79-93.

Munk, W. H., S. W. Groves , and G. F. Carrier, 1950: Note on the dynamics of the Gulf Stream. J. Mar. Res., vol. 9, no. 3, pp. 218-238.

Neumann, G., 1948: Uber den Tangentialdruck des Windes und die Rauhigkeit der Meeresoberfläche. Zeit. f. Meteor., 2, pp. 193-203.

Neumann, G., 1954: Notes on the wind-driven ocean circulation. New York University, College of Engineering, Research Division. Report prepared for Office of Naval Research, Prelim. Distr., May 1954.

Neumann, G., 1955: On the dynamics of wind-driven ocean currents. Meteor. Papers, vol. 2, no. 4, 33 pp. New York University Press.

Neumann, G., 1956: Wind stress on water surfaces. Bull. A. M. S., vol. 37, no. 5, pp. 211-217.

Neumann, G., and F. Ostapoff, 1957: Mean water transport by wind-driven ocean currents in the North Atlantic for the month of February. In Contributions to the study of ocean circulation. Research Division, College of Engineering, Dept. of Meteorology and Oceanography, New York University. Report prepared for the Office of Naval Research under contract Nonr 285(12).

Neumann, G., 1958: On the mass transport of wind-driven currents in a baroclinic ocean with application to the North Atlantic. Zeit. für Meteor., 12, 138-147.

Pierson, W. J., 1962: Perturbation analysis of the Navier-Stokes equations in Lagrangian form, with selected linear solutions. J. Geophys. Res., vol. 67, no. 8, pp. 3151-3160.

Reid, R. O., 1948: The equatorial currents of the eastern Pacific as maintained by the stress of the wind. J. Mar. Res., vol. 7, no. 2, pp. 74-99.

Schott, G., 1944: Geographie des Atlantischen Ozeans. Boysen, Hamburg.

Stommel, H., 1948: The westward intensification of ocean currents. Trans. Amer. Geophys. Un., vol. 29, no. 2, pp. 202-206.

Stommel, H., 1953: Examples of the possible role of inertia and stratification in the dynamics of the Gulf Stream system. J. Mar. Res., vol. 12, pp. 184-195.

Stommel, H., 1956: On the determination of the depth of no meridional motion. Deep Sea Res., vol. 3, pp. 273-278.

Stommel, H., 1957: A survey of ocean current theory. Deep Sea Res., vol. 4, pp. 149-184.

Stommel, H., 1960: The Gulf Stream. University of California Press, Berkeley, 202 pp.

Stommel, H., and J. Webster, 1962: Some properties of thermocline equations in a subtropical gyre. J. Mar. Res., vol. 20, no. 1, pp. 42-56.

Sverdrup, H. U., et al, 1942: The Oceans. Prentice-Hall, New Jersey.

Sverdrup, H. U., 1947: Wind-driven currents in a baroclinic ocean. Proc. Nat. Acad. Sci., Washington, vol. 33, no. 11. pp. 318-326.

Veronis, G., 1961: On the problem of uniqueness of ocean circulation. Preliminary papers, Int. Symp. on Fund. Prob. in Turb. and their Relation to Geophysics, Sept. 1961, Marseilles, France.

Whitlock, R. T., 1962: Comments on "Variational principle for a perfect, compressible plasma." Physics of Fluids, vol. 5, no. 1, pp. 123-124.

Wüst, G., 1936: Kuroshio und Golfstrom. Berlin Univ., Institut f. Meereskunde, Veröff., N. F., A. Geogr. -naturwiss. Reihe, Heft 29, 69 pp.

Wylie, C. R., 1960: Advanced Engineering Mathematics, Second Edition. McGraw Hill, New York, 696 pp.

Wyrtki, K., 1961: The thermohaline circulation in relation to the general circulation in the ocean. Deep Sea Res., vol. 8, no. 1, pp. 39-64.

APPENDIX I

Summary of Notation

A eddy exchange coefficient (2.29); constant (3.24).

a zonal width of rectangular ocean (3.29); a parameter (3.69).

B constant (3.24)

b meridional width of rectangular ocean (3.29)

C carbon-14 concentration (8.4).

c constant (3.25); velocity (4.24); an index (5.10).

D depth-of-no-motion (3.2).

$\mathcal{D}$ diffusive flux (1.3)

d differential operator; a particular depth (2.8).

E Ekman mass transport (2.23); carbon-14 enrichment (8.7).

e base of the natural logarithm (3.24).

$\mathcal{F}$ Rayleigh dissipation function (7.10).

F force (1.1), (7.1); friction (1.2); constant (2.39), (2.48); a function (4.1).

f Coriolis parameter (2.6); a function (4.1).

G geostrophic mass transport (2.24); a constant (2.63).

g acceleration due to gravity (2.4).

H Hamiltonian function.

h constant (3.25).

I an integral (7.4).

i index of summation (1.1); unit vector in x-direction (2.3).

J Bessel function

j unit vector in y-direction (2.3); an index (3.36).

K constant (2.36); coefficient of friction (3.7).

k unit vector in z-direction (2.3); constant (5.9).

L a constant (5.22); Lagrangean function (7.3).

ℓ an index (3.41); a function (4.1).

M a constant (5.33); mixing function (8.6).

m mass (1.1); a parameter (5.20).

N a parameter (3.73).

n an index (1.1), (2.41); a parameter (5.21).

P integrated pressure function (2.8).

p pressure (2.6); constant (3.24); generalized momentum (7.8).

Q non-conservative removal rate of property (8.2).

q constant (3.24); a parameter (3.69); generalized coordinate (7.3).

R radius of earth (1.2).

r an index (2.61).

S a surface (4.5); salinity (8.3).

s order of Legendre's equation (3.61); a parameter (3.65).

T integrated mass transport (2.10); kinetic energy (7.3).

t time (1.1).

U x-component of integrated mass transport (2.9).

u x-component of velocity (2.3).

V total velocity (1.1); y-component of integrated mass transport (2.8).

v x-component of velocity (2.3).

W work (7.12); wind speed (6.1).

w z-component of velocity (2.3).

X a function of x (3.21).

x horizontal (zonal) coordinate.

Y a function of y (3.21).

y horizontal (meridional) coordinate.

Z a function of latitude (3.68).

z vertical coordinate; a function of latitude (3.61).

α a parameter (3.20), (7.6); carbon-14 activity (8.7).

β $\partial f/\partial y$ (3.49).

γ a parameter (5.12).

Δ variational operator (7.18) .

δ variational operator (7.5).

ζ z-coordinate of the sea surface (2.8).

η an index (2.38); a coordinate (4.1); a function of y (5.15).

θ a function of latitude (3.67).

λ longitude (2.45); carbon-14 decay constant (8.4).

μ a constant (5.17).

ν a parameter (5.23).

ξ generalized horizontal coordinate (2.11); a function of x (5.15).

Π continued product.

π 3.1416...

ρ density (1.2).

Σ summation

σ density in phase space (7.25).

τ stress (2.5).

Φ potential function (1.2), (7.2).

ϕ geographical latitude.

Ψ stream function for the integrated mass transport (2.30).

ω angular velocity of rotation of earth (1.2).

APPENDIX II

Properties of the Sverdrup Model Driven by a Zonally Oriented Wind Stress Which Varies Sinusoidally in the Meridional Direction, as Described in Section 2.

Column I	The value of n in equations (2.41, 2.42, 2.59, 2.60)
Column II	The value of $\phi°$ in equations (2.41, 2.42, 2.59, 2.60)
Column III	The value of x/R in equations (2.41, 2.42)
or	the value of $\lambda° \times 0.01$ in equations (2.59, 2.60)
Column IV	The value of $2\Omega\psi/FR$ in equation (2.41)
Column V	The value of P/FR in equation (2.42)
Column VI	The value of $2\Omega\psi/FR$ in equation (2.59)
Column VII	The value of P/FR in equation (6.60)

[This Table (22 pages) is available upon request from New York University.]

APPENDIX II

Properties of the Sverdrup Model Driven by a Zonally Oriented Wind Stress Which Varies Sinusoidally in the Meridional Direction, as Described in Section 2.

Column I	The value of n in equations (2.41, 2.42, 2.59, 2.60)
Column II	The value of $\phi°$ in equations (2.41, 2.42, 2.59, 2.60)
Column III	The value of x/R in equations (2.41, 2.42)
or	the value of $\lambda° \times 0.01$ in equations (2.59, 2.60)
Column IV	The value of $2\Omega\psi/FR$ in equation (2.41)
Column V	The value of P/FR in equation (2.42)
Column VI	The value of $2\Omega\psi/FR$ in equation (2.59)
Column VII	The value of P/FR in equation (6.60)

I	II	III	IV	V	VI	VII
2	0	0.	0.	-0.	0.	0.
		0.05	0.050	-0.	0.175	0.
		0.10	0.100	-0.	0.349	0.
		0.15	0.150	-0.	0.524	0.
		0.20	0.200	-0.	0.698	0.
		0.25	0.250	-0.	0.873	0.
		0.30	0.300	-0.	1.047	0.
		0.35	0.350	-0.	1.222	0.
		0.40	0.400	-0.	1.396	0.
		0.45	0.450	-0.	1.571	0.
		0.50	0.500	-0.	1.745	0.
		0.55	0.550	-0.	1.920	0.
		0.60	0.600	-0.	2.094	0.
		0.65	0.650	-0.	2.269	0.
		0.70	0.700	-0.	2.443	0.
		0.75	0.750	-0.	2.618	0.
		0.80	0.800	-0.	2.793	0.
		0.85	0.850	-0.	2.967	0.
		0.90	0.900	-0.	3.142	0.
		0.95	0.950	-0.	3.316	0.
		1.00	1.000	-0.	3.491	0.
2	5	0.	0.	0.	0.	0.
		0.05	0.049	0.000	0.171	0.000
		0.10	0.099	0.000	0.341	0.000
		0.15	0.148	0.000	0.512	0.001
		0.20	0.198	0.000	0.682	0.001
		0.25	0.247	0.000	0.853	0.001
		0.30	0.297	0.000	1.023	0.001
		0.35	0.346	0.000	1.194	0.002
		0.40	0.395	0.001	1.364	0.002
		0.45	0.445	0.001	1.535	0.002
		0.50	0.494	0.001	1.706	0.002
		0.55	0.544	0.001	1.876	0.003
		0.60	0.593	0.001	2.047	0.003
		0.65	0.643	0.001	2.217	0.003
		0.70	0.692	0.001	2.388	0.003
		0.75	0.741	0.001	2.558	0.003
		0.80	0.791	0.001	2.729	0.004
		0.85	0.840	0.001	2.899	0.004
		0.90	0.890	0.001	3.070	0.004
		0.95	0.939	0.001	3.241	0.004
		1.00	0.989	0.001	3.411	0.005

I	II	III	IV	V	VI	VII
2	10	0.	0.	0.	0.	0.
		0.05	0.048	0.001	0.159	0.002
		0.10	0.095	0.001	0.317	0.004
		0.15	0.143	0.002	0.476	0.005
		0.20	0.191	0.002	0.635	0.007
		0.25	0.239	0.003	0.794	0.009
		0.30	0.286	0.003	0.952	0.011
		0.35	0.334	0.004	1.111	0.013
		0.40	0.382	0.004	1.270	0.015
		0.45	0.429	0.005	1.429	0.016
		0.50	0.477	0.005	1.587	0.018
		0.55	0.525	0.006	1.746	0.020
		0.60	0.573	0.006	1.905	0.022
		0.65	0.620	0.007	2.064	0.024
		0.70	0.668	0.007	2.222	0.026
		0.75	0.716	0.008	2.381	0.027
		0.80	0.763	0.009	2.540	0.029
		0.85	0.811	0.009	2.699	0.031
		0.90	0.859	0.010	2.857	0.033
		0.95	0.906	0.010	3.016	0.035
		1.00	0.954	0.011	3.175	0.037
2	15	0.	0.	0.	0.	0.
		0.05	0.045	0.002	0.139	0.006
		0.10	0.090	0.004	0.279	0.012
		0.15	0.134	0.005	0.418	0.018
		0.20	0.179	0.007	0.558	0.024
		0.25	0.224	0.009	0.697	0.030
		0.30	0.269	0.011	0.837	0.036
		0.35	0.314	0.013	0.976	0.042
		0.40	0.359	0.014	1.116	0.048
		0.45	0.403	0.016	1.255	0.054
		0.50	0.448	0.018	1.395	0.061
		0.55	0.493	0.020	1.534	0.067
		0.60	0.538	0.022	1.674	0.073
		0.65	0.583	0.023	1.813	0.079
		0.70	0.628	0.025	1.952	0.085
		0.75	0.672	0.027	2.092	0.091
		0.80	0.717	0.029	2.231	0.097
		0.85	0.762	0.031	2.371	0.103
		0.90	0.807	0.032	2.510	0.109
		0.95	0.852	0.034	2.650	0.115
		1.00	0.897	0.036	2.789	0.121

2	20	0.	0.	C.	0.	C.
		0.05	0.041	0.004	0.113	0.C14
		0.10	0.082	0.009	0.227	C.C28
		0.15	0.122	0.013	0.340	0.042
		0.20	0.163	0.017	0.453	C.C56
		0.25	0.204	0.021	0.566	C.C70
		0.30	0.245	0.026	0.680	C.C84
		0.35	0.285	0.030	0.793	0.098
		0.40	0.326	0.034	0.906	C.112
		0.45	0.367	0.038	1.020	C.126
		0.50	0.408	0.043	1.133	0.140
		0.55	0.448	0.047	1.246	0.154
		0.60	0.489	0.051	1.359	0.168
		0.65	0.530	0.055	1.473	0.182
		0.70	0.571	0.060	1.586	0.196
		0.75	0.611	0.064	1.699	0.209
		0.80	0.652	0.068	1.813	0.223
		0.85	0.693	C.072	1.926	0.237
		0.90	0.734	0.077	2.039	C.251
		0.95	0.774	0.081	2.152	0.265
		1.00	0.815	0.085	2.266	C.279
2	25	0.	0.	C.	0.	C.
		0.05	0.035	C.008	0.C81	0.026
		0.10	0.071	0.017	0.162	0.053
		0.15	0.106	0.025	0.243	C.C79
		0.20	0.142	0.033	0.324	C.105
		0.25	0.177	0.042	0.405	C.132
		0.30	0.213	0.050	0.486	0.158
		0.35	0.248	0.058	0.567	C.184
		0.40	0.284	0.067	0.648	C.211
		0.45	0.319	C.075	0.729	C.237
		0.50	0.355	0.083	0.810	0.263
		0.55	0.390	C.092	0.891	C.290
		0.60	0.426	C.100	0.972	0.316
		0.65	0.461	C.108	1.053	C.343
		0.70	0.496	0.117	1.134	0.369
		0.75	0.532	0.125	1.215	0.395
		0.80	0.567	0.133	1.296	0.422
		0.85	0.603	0.142	1.377	0.448
		0.90	0.638	0.150	1.458	0.474
		0.95	0.674	0.158	1.539	0.501
		1.00	0.709	0.167	1.620	0.527

2	30	0.	0.	0.	0.	C.
		0.05	0.029	0.014	0.044	0.044
		0.10	0.058	0.029	0.087	0.087
		0.15	0.087	0.043	0.131	0.131
		0.20	0.115	0.058	0.175	0.175
		0.25	0.144	0.072	0.218	0.218
		0.30	0.173	0.087	0.262	0.262
		0.35	0.202	0.101	0.305	0.305
		0.40	0.231	0.115	0.349	0.349
		0.45	0.260	0.130	0.393	0.393
		0.50	0.289	0.144	0.436	C.436
		0.55	0.318	0.159	0.480	0.480
		0.60	0.346	0.173	0.524	C.524
		0.65	0.375	0.188	0.567	0.567
		0.70	0.404	0.202	0.611	0.611
		0.75	0.433	0.217	0.654	C.655
		0.80	0.462	0.231	0.698	0.698
		0.85	0.491	0.245	0.742	0.742
		0.90	0.520	0.260	0.785	0.785
		0.95	0.548	0.274	0.829	0.829
		1.00	0.577	0.289	0.873	0.873
2	35	0.	0.	C.	0.	0.
		0.05	0.021	C.023	0.002	C.066
		0.10	0.042	C.046	0.005	0.132
		0.15	0.063	C.069	0.007	C.198
		0.20	0.C84	0.092	0.009	0.263
		0.25	0.104	0.115	0.011	C.329
		0.30	0.125	C.138	0.014	C.395
		0.35	0.146	0.161	0.016	C.461
		0.40	0.167	C.184	0.018	0.527
		0.45	0.188	0.207	0.020	C.593
		0.50	0.209	C.230	0.023	0.659
		0.55	0.230	C.253	0.025	C.725
		0.60	0.251	C.276	0.027	0.790
		0.65	0.271	C.299	0.030	C.856
		0.70	0.292	C.323	0.032	0.922
		0.75	0.313	0.346	0.034	0.988
		0.80	0.334	0.369	0.036	1.054
		0.85	0.355	0.392	0.039	1.120
		0.90	0.376	0.415	0.041	1.186
		0.95	0.397	0.438	0.043	1.252

2	40	0.	0.	0.	-0.	0.
		0.05	0.011	0.035	-0.042	0.093
		0.10	0.023	0.069	-0.084	0.185
		0.15	0.034	0.104	-0.125	0.278
		0.20	0.045	0.139	-0.167	0.371
		0.25	0.057	0.173	-0.209	0.464
		0.30	0.068	0.208	-0.251	0.556
		0.35	0.079	0.243	-0.293	0.649
		0.40	0.091	0.277	-0.334	0.742
		0.45	0.102	0.312	-0.376	0.834
		0.50	0.113	0.347	-0.418	0.927
		0.55	0.125	0.381	-0.460	1.020
		0.60	0.136	0.416	-0.502	1.112
		0.65	0.147	0.451	-0.543	1.205
		0.70	0.159	0.485	-0.585	1.298
		0.75	0.170	0.520	-0.627	1.391
		0.80	0.181	0.555	-0.669	1.483
		0.85	0.193	0.589	-0.711	1.576
		0.90	0.204	0.624	-0.753	1.669
		0.95	0.215	0.659	-0.794	1.761
		1.00	0.227	0.693	-0.836	1.854
2	45	0.	-0.	0.	-0.	0.
		0.05	-0.000	0.050	-0.087	0.123
		0.10	-0.000	0.100	-0.175	0.247
		0.15	-0.000	0.150	-0.262	0.370
		0.20	-0.000	0.200	-0.349	0.494
		0.25	-0.000	0.250	-0.436	0.617
		0.30	-0.000	0.300	-0.524	0.740
		0.35	-0.000	0.350	-0.611	0.864
		0.40	-0.000	0.400	-0.698	0.987
		0.45	-0.000	0.450	-0.785	1.111
		0.50	-0.000	0.500	-0.873	1.234
		0.55	-0.000	0.550	-0.960	1.358
		0.60	-0.000	0.600	-1.047	1.481
		0.65	-0.000	0.650	-1.134	1.604
		0.70	-0.000	0.700	-1.222	1.728
		0.75	-0.000	0.750	-1.309	1.851
		0.80	-0.000	0.800	-1.396	1.975
		0.85	-0.000	0.850	-1.484	2.098
		0.90	-0.000	0.900	-1.571	2.221
		0.95	-0.000	0.950	-1.658	2.345
		1.00	-0.000	1.000	-1.745	2.468

2	50	0.	-0.	0.	-0.	0.
		0.05	-0.014	0.070	-0.133	0.157
		0.10	-0.027	0.140	-0.265	0.314
		0.15	-0.041	0.210	-0.398	0.471
		0.20	-0.054	0.280	-0.531	0.628
		0.25	-0.068	0.350	-0.664	0.785
		0.30	-0.081	0.420	-0.796	0.942
		0.35	-0.095	0.490	-0.929	1.098
		0.40	-0.108	0.559	-1.062	1.255
		0.45	-0.122	0.629	-1.195	1.412
		0.50	-0.135	0.699	-1.327	1.569
		0.55	-0.149	0.769	-1.460	1.726
		0.60	-0.162	0.839	-1.593	1.883
		0.65	-0.176	0.909	-1.725	2.040
		0.70	-0.189	0.979	-1.858	2.197
		0.75	-0.203	1.049	-1.991	2.354
		0.80	-0.216	1.119	-2.124	2.511
		0.85	-0.230	1.189	-2.256	2.668
		0.90	-0.243	1.259	-2.389	2.825
		0.95	-0.257	1.329	-2.522	2.981
		1.00	-0.270	1.399	-2.655	3.138
2	55	0.	-0.	0.	-0.	0.
		0.05	-0.030	0.096	-0.177	0.192
		0.10	-0.060	0.192	-0.354	0.384
		0.15	-0.089	0.287	-0.530	0.576
		0.20	-0.119	0.383	-0.707	0.767
		0.25	-0.149	0.479	-0.884	0.959
		0.30	-0.179	0.575	-1.061	1.151
		0.35	-0.209	0.671	-1.238	1.343
		0.40	-0.239	0.767	-1.414	1.535
		0.45	-0.268	0.862	-1.591	1.727
		0.50	-0.298	0.958	-1.768	1.919
		0.55	-0.328	1.054	-1.945	2.111
		0.60	-0.358	1.150	-2.122	2.302
		0.65	-0.388	1.246	-2.299	2.494
		0.70	-0.417	1.342	-2.475	2.686
		0.75	-0.447	1.437	-2.652	2.878
		0.80	-0.477	1.533	-2.829	3.070
		0.85	-0.507	1.629	-3.006	3.262
		0.90	-0.537	1.725	-3.183	3.454
		0.95	-0.566	1.821	-3.359	3.646
		1.00	-0.596	1.917	-3.536	3.837

2	60	0.	-0.	0.	-0.	0.
		0.05	-0.050	0.130	-0.218	0.227
		0.10	-0.100	0.260	-0.436	0.453
		0.15	-0.150	0.390	-0.655	0.680
		0.20	-0.200	0.520	-0.873	0.907
		0.25	-0.250	0.650	-1.091	1.134
		0.30	-0.300	0.779	-1.309	1.360
		0.35	-0.350	0.909	-1.527	1.587
		0.40	-0.400	1.039	-1.745	1.814
		0.45	-0.450	1.169	-1.964	2.041
		0.50	-0.500	1.299	-2.182	2.267
		0.55	-0.550	1.429	-2.400	2.494
		0.60	-0.600	1.559	-2.618	2.721
		0.65	-0.650	1.689	-2.836	2.947
		0.70	-0.700	1.819	-3.054	3.174
		0.75	-0.750	1.949	-3.273	3.401
		0.80	-0.800	2.078	-3.491	3.628
		0.85	-0.850	2.208	-3.709	3.854
		0.90	-0.900	2.338	-3.927	4.081
		0.95	-0.950	2.468	-4.145	4.308
		1.00	-1.000	2.598	-4.363	4.535
2	65	0.	-0.	0.	-0.	0.
		0.05	-0.076	0.176	-0.256	0.260
		0.10	-0.152	0.352	-0.511	0.520
		0.15	-0.228	0.528	-0.767	0.780
		0.20	-0.304	0.705	-1.022	1.039
		0.25	-0.380	0.881	-1.278	1.299
		0.30	-0.456	1.057	-1.533	1.559
		0.35	-0.532	1.233	-1.789	1.819
		0.40	-0.608	1.409	-2.044	2.079
		0.45	-0.684	1.585	-2.300	2.339
		0.50	-0.760	1.762	-2.555	2.599
		0.55	-0.837	1.938	-2.811	2.858
		0.60	-0.913	2.114	-3.067	3.118
		0.65	-0.989	2.290	-3.322	3.378
		0.70	-1.065	2.466	-3.578	3.638
		0.75	-1.141	2.642	-3.833	3.898
		0.80	-1.217	2.818	-4.089	4.158
		0.85	-1.293	2.995	-4.344	4.418
		0.90	-1.369	3.171	-4.600	4.677
		0.95	-1.445	3.347	-4.855	4.937
		1.00	-1.521	3.523	-5.111	5.197

2	70	0.	-0.	0.	-0.	0.
		0.05	-0.112	0.243	-0.288	0.290
		0.10	-0.224	0.485	-0.576	0.579
		0.15	-0.336	0.728	-0.863	0.869
		0.20	-0.448	0.970	-1.151	1.159
		0.25	-0.560	1.213	-1.439	1.448
		0.30	-0.672	1.456	-1.727	1.738
		0.35	-0.784	1.698	-2.015	2.028
		0.40	-0.896	1.941	-2.303	2.317
		0.45	-1.008	2.183	-2.590	2.607
		0.50	-1.120	2.426	-2.878	2.896
		0.55	-1.232	2.669	-3.166	3.186
		0.60	-1.344	2.911	-3.454	3.476
		0.65	-1.456	3.154	-3.742	3.765
		0.70	-1.568	3.397	-4.029	4.055
		0.75	-1.680	3.639	-4.317	4.345
		0.80	-1.792	3.882	-4.605	4.634
		0.85	-1.904	4.124	-4.893	4.924
		0.90	-2.016	4.367	-5.181	5.214
		0.95	-2.128	4.610	-5.469	5.503
		1.00	-2.240	4.852	-5.756	5.793
2	75	0.	-0.	0.	-0.	0.
		0.05	-0.167	0.348	-0.314	0.315
		0.10	-0.335	0.696	-0.628	0.629
		0.15	-0.502	1.045	-0.942	0.944
		0.20	-0.669	1.393	-1.256	1.258
		0.25	-0.837	1.741	-1.570	1.573
		0.30	-1.004	2.089	-1.884	1.888
		0.35	-1.171	2.437	-2.198	2.202
		0.40	-1.338	2.786	-2.512	2.517
		0.45	-1.506	3.134	-2.826	2.831
		0.50	-1.673	3.482	-3.140	3.146
		0.55	-1.840	3.830	-3.454	3.460
		0.60	-2.008	4.179	-3.768	3.775
		0.65	-2.175	4.527	-4.082	4.090
		0.70	-2.342	4.875	-4.396	4.404
		0.75	-2.510	5.223	-4.710	4.719
		0.80	-2.677	5.571	-5.024	5.033
		0.85	-2.844	5.920	-5.338	5.348
		0.90	-3.012	6.268	-5.652	5.663
		0.95	-3.179	6.616	-5.966	5.977
		1.00	-3.346	6.964	-6.280	6.292

2	80	0.	-0.	0.	-0.	0.
		0.05	-0.271	0.550	-0.333	0.333
		0.10	-0.541	1.100	-0.667	0.667
		0.15	-0.812	1.650	-1.000	1.000
		0.20	-1.082	2.200	-1.333	1.334
		0.25	-1.353	2.750	-1.666	1.667
		0.30	-1.623	3.300	-2.000	2.000
		0.35	-1.894	3.850	-2.333	2.334
		0.40	-2.165	4.400	-2.666	2.667
		0.45	-2.435	4.950	-3.000	3.001
		0.50	-2.706	5.500	-3.333	3.334
		0.55	-2.976	6.050	-3.666	3.667
		0.60	-3.247	6.600	-3.999	4.001
		0.65	-3.518	7.150	-4.333	4.334
		0.70	-3.788	7.701	-4.666	4.668
		0.75	-4.059	8.251	-4.999	5.001
		0.80	-4.329	8.801	-5.332	5.334
		0.85	-4.600	9.351	-5.666	5.668
		0.90	-4.870	9.901	-5.999	6.001
		0.95	-5.141	10.451	-6.332	6.335
		1.00	-5.412	11.001	-6.666	6.668
4	0	0.	0.	-0.	0.	0.
		0.05	0.050	-0.	0.349	0.
		0.10	0.100	-0.	0.698	0.
		0.15	0.150	-0.	1.047	0.
		0.20	0.200	-0.	1.396	0.
		0.25	0.250	-0.	1.745	0.
		0.30	0.300	-0.	2.094	0.
		0.35	0.350	-0.	2.443	0.
		0.40	0.400	-0.	2.793	0.
		0.45	0.450	-0.	3.142	0.
		0.50	0.500	-0.	3.491	0.
		0.55	0.550	-0.	3.840	0.
		0.60	0.600	-0.	4.189	0.
		0.65	0.650	-0.	4.538	0.
		0.70	0.700	-0.	4.887	0.
		0.75	0.750	-0.	5.236	0.
		0.80	0.800	-0.	5.585	0.
		0.85	0.850	-0.	5.934	0.
		0.90	0.900	-0.	6.283	0.
		0.95	0.950	-0.	6.632	0.

4	5	0.	0.	0.	0.	0.
		0.05	0.047	0.001	0.325	0.001
		0.10	0.094	0.001	0.651	0.003
		0.15	0.141	0.002	0.976	0.004
		0.20	0.189	0.003	1.302	0.005
		0.25	0.236	0.003	1.627	0.007
		0.30	0.283	0.004	1.952	0.008
		0.35	0.330	0.005	2.278	0.010
		0.40	0.377	0.005	2.603	0.011
		0.45	0.424	0.006	2.929	0.012
		0.50	0.472	0.007	3.254	0.014
		0.55	0.519	0.007	3.579	0.015
		0.60	0.566	0.008	3.905	0.016
		0.65	0.613	0.009	4.230	0.018
		0.70	0.660	0.009	4.556	0.019
		0.75	0.707	0.010	4.881	0.021
		0.80	0.755	0.011	5.206	0.022
		0.85	0.802	0.011	5.532	0.023
		0.90	0.849	0.012	5.857	0.025
		0.95	0.896	0.013	6.183	0.026
		1.00	0.943	0.013	6.508	0.027
4	10	0.	0.	0.	0.	0.
		0.05	0.039	0.005	0.258	0.011
		0.10	0.078	0.010	0.515	0.021
		0.15	0.117	0.015	0.773	0.032
		0.20	0.156	0.020	1.030	0.042
		0.25	0.194	0.026	1.288	0.053
		0.30	0.233	0.031	1.545	0.063
		0.35	0.272	0.036	1.803	0.074
		0.40	0.311	0.041	2.060	0.084
		0.45	0.350	0.046	2.318	0.095
		0.50	0.389	0.051	2.575	0.105
		0.55	0.428	0.056	2.833	0.116
		0.60	0.467	0.061	3.090	0.126
		0.65	0.506	0.067	3.348	0.137
		0.70	0.545	0.072	3.605	0.147
		0.75	0.583	0.077	3.863	0.158
		0.80	0.622	0.082	4.120	0.168
		0.85	0.661	0.087	4.378	0.179
		0.90	0.700	0.092	4.635	0.189
		0.95	0.739	0.097	4.893	0.200
		1.00	0.778	0.102	5.150	0.211

4	15	0.	0.	C.	0.	C.
		0.05	0.026	0.017	0.154	C.033
		0.10	0.052	0.033	0.309	C.066
		0.15	C.078	0.050	0.463	C.099
		0.20	0.104	0.066	0.617	C.132
		0.25	0.129	0.083	0.771	0.165
		0.30	0.155	0.099	0.926	C.198
		0.35	0.181	0.116	1.080	C.231
		0.40	0.207	0.132	1.234	C.265
		0.45	0.233	0.149	1.389	C.298
		0.50	C.259	0.165	1.543	C.331
		0.55	0.285	C.182	1.697	C.364
		0.60	0.311	C.198	1.851	C.397
		0.65	0.336	0.215	2.006	C.430
		0.70	0.362	0.231	2.160	C.463
		0.75	0.388	C.248	2.314	C.496
		0.80	0.414	C.264	2.469	C.529
		0.85	0.440	C.281	2.623	0.562
		0.90	0.466	C.297	2.777	C.595
		0.95	0.492	C.314	2.931	C.628
		1.00	0.518	C.330	3.086	C.661
4	20	0.	0.	C.	0.	C.
		0.05	C.009	C.037	0.029	C.071
		0.10	0.018	C.073	0.059	C.141
		0.15	0.028	C.110	0.088	C.212
		0.20	0.037	C.146	0.117	C.283
		0.25	0.046	C.183	0.147	C.354
		0.30	0.055	C.220	0.176	C.424
		0.35	0.065	C.256	0.205	C.495
		0.40	0.074	C.293	0.235	0.566
		0.45	0.083	C.329	0.264	C.637
		0.50	0.092	C.366	0.293	C.707
		0.55	0.102	C.403	0.323	C.778
		0.60	0.111	0.439	0.352	C.849
		0.65	0.120	0.476	0.381	C.919
		0.70	0.129	0.512	0.411	C.990
		0.75	0.139	0.549	0.440	1.061
		0.80	0.148	0.586	0.469	1.132
		0.85	0.157	0.622	0.499	1.202
		0.90	0.166	0.659	0.528	1.273
		0.95	0.176	0.695	0.557	1.344
		1.00	0.185	0.732	0.587	1.415

4	25	0.	-0.	C.	-0.	C.
		0.05	-0.010	C.065	-0.101	C.120
		0.10	-0.019	C.131	-0.201	C.241
		0.15	-0.029	0.196	-0.302	C.361
		0.20	-0.038	C.262	-0.403	C.482
		0.25	-0.048	C.327	-0.503	C.602
		0.30	-0.057	C.393	-0.604	C.723
		0.35	-0.067	0.458	-0.705	0.843
		0.40	-0.077	C.523	-0.806	C.964
		0.45	-0.086	C.589	-0.906	1.084
		0.50	-0.096	C.654	-1.007	1.204
		0.55	-0.105	C.720	-1.108	1.325
		0.60	-0.115	0.785	-1.208	1.445
		0.65	-0.125	C.851	-1.309	1.566
		0.70	-0.134	C.916	-1.410	1.686
		0.75	-0.144	0.982	-1.510	1.807
		0.80	-0.153	1.047	-1.611	1.927
		0.85	-0.163	1.112	-1.712	2.048
		0.90	-0.172	1.178	-1.812	2.168
		0.95	-0.182	1.243	-1.913	2.288
		1.00	-0.192	1.309	-2.014	2.409
4	30	0.	-0.	C.	-0.	C.
		0.05	-0.029	C.101	-0.218	C.175
		0.10	-0.058	C.202	-0.436	0.349
		0.15	-0.087	C.303	-0.655	C.524
		0.20	-0.115	C.404	-0.873	C.698
		0.25	-0.144	C.505	-1.091	C.873
		0.30	-0.173	C.606	-1.309	1.047
		0.35	-0.202	C.707	-1.527	1.222
		0.40	-0.231	C.808	-1.745	1.396
		0.45	-0.260	0.909	-1.964	1.571
		0.50	-0.289	1.010	-2.182	1.745
		0.55	-0.318	1.111	-2.400	1.920
		0.60	-0.346	1.212	-2.618	2.094
		0.65	-0.375	1.313	-2.836	2.269
		0.70	-0.404	1.415	-3.054	2.443
		0.75	-0.433	1.516	-3.273	2.618
		0.80	-0.462	1.617	-3.491	2.793
		0.85	-0.491	1.718	-3.709	2.967
		0.90	-0.520	1.819	-3.927	3.142
		0.95	-0.548	1.920	-4.145	3.316
		1.00	-0.577	2.021	-4.363	3.491

4	35	0.	-0.	0.	-0.	0.
		0.05	-0.047	0.139	-0.307	0.222
		0.10	-0.094	0.279	-0.613	0.444
		0.15	-0.140	0.418	-0.920	0.666
		0.20	-0.187	0.558	-1.227	0.887
		0.25	-0.234	0.697	-1.533	1.109
		0.30	-0.281	0.837	-1.840	1.331
		0.35	-0.327	0.976	-2.147	1.553
		0.40	-0.374	1.115	-2.453	1.775
		0.45	-0.421	1.255	-2.760	1.997
		0.50	-0.468	1.394	-3.067	2.219
		0.55	-0.514	1.534	-3.373	2.440
		0.60	-0.561	1.673	-3.680	2.662
		0.65	-0.608	1.812	-3.987	2.884
		0.70	-0.655	1.952	-4.294	3.106
		0.75	-0.701	2.091	-4.600	3.328
		0.80	-0.748	2.231	-4.907	3.550
		0.85	-0.795	2.370	-5.214	3.772
		0.90	-0.842	2.510	-5.520	3.993
		0.95	-0.888	2.649	-5.827	4.215
		1.00	-0.935	2.788	-6.134	4.437
4	40	0.	-0.	0.	-0.	0.
		0.05	-0.061	0.175	-0.353	0.250
		0.10	-0.123	0.350	-0.706	0.500
		0.15	-0.184	0.524	-1.059	0.749
		0.20	-0.245	0.699	-1.412	0.999
		0.25	-0.307	0.874	-1.765	1.249
		0.30	-0.368	1.049	-2.118	1.499
		0.35	-0.429	1.224	-2.471	1.749
		0.40	-0.491	1.398	-2.824	1.998
		0.45	-0.552	1.573	-3.178	2.248
		0.50	-0.613	1.748	-3.531	2.498
		0.55	-0.675	1.923	-3.884	2.748
		0.60	-0.736	2.098	-4.237	2.998
		0.65	-0.797	2.272	-4.590	3.247
		0.70	-0.859	2.447	-4.943	3.497
		0.75	-0.920	2.622	-5.296	3.747
		0.80	-0.981	2.797	-5.649	3.997
		0.85	-1.043	2.972	-6.002	4.247
		0.90	-1.104	3.146	-6.355	4.497
		0.95	-1.165	3.321	-6.708	4.746
		1.00	-1.227	3.496	-7.061	4.996

4	45	0.	-0.	0.	-0.	0.
		0.05	-0.071	0.200	-0.349	0.247
		0.10	-0.141	0.400	-0.698	0.494
		0.15	-0.212	0.600	-1.047	0.740
		0.20	-0.283	0.800	-1.396	0.987
		0.25	-0.354	1.000	-1.745	1.234
		0.30	-0.424	1.200	-2.094	1.481
		0.35	-0.495	1.400	-2.443	1.728
		0.40	-0.566	1.600	-2.793	1.975
		0.45	-0.636	1.800	-3.142	2.221
		0.50	-0.707	2.000	-3.491	2.468
		0.55	-0.778	2.200	-3.840	2.715
		0.60	-0.849	2.400	-4.189	2.962
		0.65	-0.919	2.600	-4.538	3.209
		0.70	-0.990	2.800	-4.887	3.456
		0.75	-1.061	3.000	-5.236	3.702
		0.80	-1.131	3.200	-5.585	3.949
		0.85	-1.202	3.400	-5.934	4.196
		0.90	-1.273	3.600	-6.283	4.443
		0.95	-1.344	3.800	-6.632	4.690
		1.00	-1.414	4.000	-6.981	4.937
4	50	0.	-0.	0.	-0.	0.
		0.05	-0.073	0.207	-0.292	0.205
		0.10	-0.146	0.414	-0.585	0.410
		0.15	-0.219	0.621	-0.877	0.615
		0.20	-0.292	0.828	-1.170	0.819
		0.25	-0.365	1.034	-1.462	1.024
		0.30	-0.439	1.241	-1.755	1.229
		0.35	-0.512	1.448	-2.047	1.434
		0.40	-0.585	1.655	-2.340	1.639
		0.45	-0.658	1.862	-2.632	1.844
		0.50	-0.731	2.069	-2.924	2.048
		0.55	-0.804	2.276	-3.217	2.253
		0.60	-0.877	2.483	-3.509	2.458
		0.65	-0.950	2.689	-3.802	2.663
		0.70	-1.023	2.896	-4.094	2.868
		0.75	-1.096	3.103	-4.387	3.073
		0.80	-1.170	3.310	-4.679	3.277
		0.85	-1.243	3.517	-4.972	3.482
		0.90	-1.316	3.724	-5.264	3.687
		0.95	-1.389	3.931	-5.556	3.892
		1.00	-1.462	4.138	-5.849	4.097

4	55	0.	-0.	0.	-0.	C.
		0.05	-0.067	0.187	-0.187	C.121
		0.10	-0.134	C.373	-0.375	C.242
		0.15	-0.200	C.560	-0.562	C.364
		0.20	-0.267	C.747	-0.749	C.485
		0.25	-0.334	0.933	-0.936	0.606
		0.30	-0.401	1.120	-1.124	C.727
		0.35	-0.467	1.307	-1.311	C.849
		0.40	-0.534	1.493	-1.498	C.970
		0.45	-0.601	1.680	-1.686	1.091
		0.50	-0.668	1.867	-1.873	1.212
		0.55	-0.735	2.053	-2.060	1.334
		0.60	-0.801	2.240	-2.247	1.455
		0.65	-0.868	2.427	-2.435	1.576
		0.70	-0.935	2.613	-2.622	1.697
		0.75	-1.002	2.800	-2.809	1.819
		0.80	-1.068	2.987	-2.997	1.940
		0.85	-1.135	3.173	-3.184	2.061
		0.90	-1.202	3.360	-3.371	2.182
		0.95	-1.269	3.547	-3.558	2.304
		1.00	-1.336	3.733	-3.746	2.425
4	60	0.	-0.	C.	-0.	-C.
		0.05	-0.050	C.130	-0.044	-C.CCC
		0.10	-C.100	C.260	-0.087	-C.CCC
		0.15	-0.150	C.390	-0.131	-C.CCC
		0.20	-0.200	C.520	-0.175	-C.CCC
		0.25	-0.250	C.650	-0.218	-C.CCC
		0.30	-0.300	C.779	-0.262	-C.CCC
		0.35	-0.350	C.909	-0.305	-C.CCC
		0.40	-0.400	1.039	-0.349	-C.CCC
		0.45	-0.450	1.169	-0.393	-C.CCC
		0.50	-0.500	1.299	-0.436	-C.CCC
		0.55	-0.550	1.429	-0.480	-C.CCC
		0.60	-0.600	1.559	-0.524	-C.CCC
		0.65	-0.650	1.689	-0.567	-C.CCC
		0.70	-0.700	1.819	-0.611	-C.CCC
		0.75	-0.750	1.949	-0.654	-0.CCC
		0.80	-0.800	2.078	-0.698	-C.CCC
		0.85	-0.850	2.208	-0.742	-0.CCC
		0.90	-0.900	2.338	-0.785	-0.CCC
		0.95	-0.950	2.468	-0.829	-0.CCC
		1.00	-1.000	2.598	-0.873	-0.CCC

4	65	0.	-C.	C.	0.	-C.
		0.05	-0.021	C.025	0.124	-C.148
		0.10	-0.041	C.050	0.247	-0.297
		0.15	-0.062	0.076	0.371	-0.445
		0.20	-0.082	C.101	0.495	-0.594
		0.25	-0.103	C.126	0.618	-C.742
		0.30	-0.123	0.151	0.742	-0.891
		0.35	-0.144	0.177	0.866	-1.039
		0.40	-0.164	C.202	0.990	-1.187
		0.45	-0.185	C.227	1.113	-1.336
		0.50	-0.205	0.252	1.237	-1.484
		0.55	-0.226	C.278	1.361	-1.633
		0.60	-0.247	C.303	1.484	-1.781
		0.65	-0.267	C.328	1.608	-1.929
		0.70	-0.288	0.353	1.732	-2.078
		0.75	-0.308	0.379	1.855	-2.226
		0.80	-0.329	C.404	1.979	-2.375
		0.85	-0.349	C.429	2.103	-2.523
		0.90	-0.370	0.454	2.226	-2.672
		0.95	-0.390	C.479	2.350	-2.820
		1.00	-0.411	C.505	2.474	-2.968
4	70	0.	0.	-C.	0.	-C.
		0.05	0.025	-0.145	0.297	-C.308
		0.10	C.051	-0.289	0.593	-C.616
		0.15	0.076	-C.434	0.890	-C.925
		0.20	0.102	-C.579	1.187	-1.233
		0.25	0.127	-0.723	1.484	-1.541
		0.30	0.152	-C.868	1.780	-1.849
		0.35	0.178	-1.013	2.077	-2.158
		0.40	0.203	-1.157	2.374	-2.466
		0.45	0.228	-1.302	2.671	-2.774
		0.50	0.254	-1.447	2.967	-3.082
		0.55	0.279	-1.591	3.264	-3.391
		0.60	0.305	-1.736	3.561	-3.699
		0.65	0.330	-1.881	3.858	-4.007
		0.70	0.355	-2.025	4.154	-4.315
		0.75	0.381	-2.170	4.451	-4.624
		0.80	0.406	-2.315	4.748	-4.932
		0.85	0.432	-2.459	5.045	-5.240
		0.90	0.457	-2.604	5.341	-5.548
		0.95	0.482	-2.749	5.638	-5.857
		1.00	0.508	-2.893	5.935	-6.165

4	75	0.	0.	-0.	0.	-C.
		0.05	0.097	-C.417	0.457	-C.461
		0.10	0.193	-C.833	0.913	-C.921
		0.15	0.290	-1.25C	1.370	-1.382
		0.20	0.386	-1.666	1.826	-1.842
		0.25	0.483	-2.083	2.283	-2.303
		0.30	0.58C	-2.499	2.74C	-2.764
		0.35	0.676	-2.916	3.196	-3.224
		0.40	0.773	-3.332	3.653	-3.685
		0.45	0.869	-3.749	4.109	-4.145
		0.50	0.966	-4.165	4.566	-4.606
		0.55	1.063	-4.582	5.022	-5.C67
		0.60	1.159	-4.998	5.479	-5.527
		0.65	1.256	-5.415	5.936	-5.988
		0.70	1.352	-5.831	6.392	-6.448
		0.75	1.449	-6.248	6.849	-6.909
		0.80	1.546	-6.664	7.305	-7.369
		0.85	1.642	-7.081	7.762	-7.83C
		0.90	1.739	-7.497	8.219	-8.291
		0.95	1.835	-7.914	8.675	-8.751
		1.00	1.932	-8.330	9.132	-9.212
4	80	0.	0.	-C.	0.	-C.
		0.05	0.221	-C.901	0.586	-C.586
		0.10	0.441	-1.802	1.171	-1.173
		0.15	0.662	-2.703	1.757	-1.759
		0.20	0.882	-3.604	2.342	-2.345
		0.25	1.103	-4.505	2.928	-2.932
		0.30	1.323	-5.406	3.513	-3.518
		0.35	1.544	-6.307	4.099	-4.105
		0.40	1.765	-7.208	4.684	-4.691
		0.45	1.985	-8.109	5.270	-5.277
		0.50	2.206	-9.011	5.855	-5.864
		0.55	2.426	-9.912	6.441	-6.450
		0.60	2.647	-10.813	7.026	-7.C36
		0.65	2.868	-11.714	7.612	-7.623
		0.70	3.088	-12.615	8.197	-8.209
		0.75	3.309	-13.516	8.783	-8.796
		0.80	3.529	-14.417	9.368	-9.382
		0.85	3.750	-15.318	9.954	-9.968
		0.90	3.970	-16.219	10.540	-10.555
		0.95	4.191	-17.120	11.125	-11.141
		1.00	4.412	-18.021	11.711	-11.727

6	0	0.	0.	-C.	0.	C.
		0.05	0.050	-0.	0.524	C.
		0.10	0.100	-C.	1.047	C.
		0.15	0.150	-0.	1.571	C.
		0.20	0.200	-C.	2.094	C.
		0.25	0.250	-C.	2.618	C.
		0.30	0.300	-C.	3.142	C.
		0.35	0.350	-0.	3.665	C.
		0.40	0.400	-C.	4.189	C.
		0.45	0.450	-0.	4.712	C.
		0.50	0.500	-0.	5.236	C.
		0.55	0.550	-0.	5.760	C.
		0.60	0.600	-C.	6.283	C.
		0.65	0.650	-C.	6.807	C.
		0.70	0.700	-0.	7.330	C.
		0.75	0.750	-0.	7.854	C.
		0.80	0.800	-0.	8.378	C.
		0.85	0.850	-C.	8.901	C.
		0.90	0.900	-C.	9.425	C.
		0.95	0.950	-C.	9.948	C.
		1.00	1.000	-C.	10.472	C.
5	5	0.	0.	C.	0.	C.
		0.05	0.043	C.002	0.450	C.C04
		0.10	0.087	C.005	0.899	C.CC9
		0.15	0.130	C.007	1.349	C.C13
		0.20	0.174	0.009	1.799	C.C17
		0.25	0.217	C.011	2.248	C.C21
		0.30	0.261	C.014	2.698	C.C26
		0.35	0.304	C.016	3.147	C.C3C
		0.40	0.348	0.018	3.597	C.C34
		0.45	0.391	0.020	4.047	C.C39
		0.50	0.435	C.023	4.496	C.C43
		0.55	0.478	C.025	4.946	C.C47
		0.60	0.522	0.027	5.396	C.C51
		0.65	0.565	0.030	5.845	C.C56
		0.70	0.609	0.032	6.295	0.C60
		0.75	0.652	0.034	6.744	C.C64
		0.80	0.695	0.036	7.194	C.C68
		0.85	0.739	0.039	7.644	C.C73
		0.90	0.782	0.041	8.093	0.C77
		0.95	0.826	0.043	8.543	0.C81
		1.00	0.869	0.045		

6	10	0.	0.	C.	0.	C.
		0.05	0.025	0.017	0.248	C.C31
		0.10	0.051	0.034	0.497	C.C63
		0.15	0.076	0.051	0.745	0.C94
		0.20	0.102	0.067	0.994	C.125
		0.25	0.127	0.084	1.242	C.156
		0.30	0.152	C.1C1	1.491	C.188
		0.35	0.178	0.118	1.739	C.219
		0.40	0.203	0.135	1.988	C.25C
		0.45	0.228	0.152	2.236	C.282
		0.50	0.254	C.169	2.485	C.313
		0.55	0.279	0.185	2.733	0.344
		0.60	0.305	0.202	2.982	0.375
		0.65	0.330	0.219	3.23C	C.4C7
		0.70	0.355	0.236	3.479	C.438
		0.75	0.381	0.253	3.727	C.469
		0.80	0.406	C.270	3.976	C.5CC
		0.85	C.432	C.286	4.224	C.532
		0.90	0.457	C.3C3	4.473	C.563
		0.95	0.482	C.320	4.721	C.594
		1.00	C.508	C.337	4.969	C.626
6	15	0.	-0.	C.	-0.	C.
		0.05	-0.000	C.050	-0.023	C.C9C
		0.10	-0.000	C.100	-0.047	C.181
		0.15	-0.000	C.150	-0.07C	C.271
		0.20	-0.000	C.2CC	-0.094	C.361
		0.25	-0.000	C.25C	-0.117	C.452
		0.30	-0.000	0.300	-0.14C	C.542
		0.35	-0.000	C.350	-0.164	C.632
		0.40	-0.000	C.4CC	-0.187	C.723
		0.45	-0.000	C.45C	-0.2[illegible]	C.813
		0.50	-0.000	C.500	-0.234	0.903
		0.55	-0.000	0.550	-0.257	C.994
		0.60	-0.000	0.600	-0.281	1.084
		0.65	-0.000	C.650	-0.304	1.174
		0.70	-0.000	0.700	-0.327	1.265
		0.75	-0.000	0.750	-0.351	1.355
		0.80	-0.000	0.800	-0.374	1.446
		0.85	-0.000	0.850	-0.398	1.536
		0.90	-0.000	0.900	-0.421	1.626
		0.95	-0.000	0.950	-0.444	1.717
		1.00	-0.000	1.000	-0.468	1.807

6	20	0.	-0.	0.	-0.	C.
		0.05	-0.027	0.098	-0.289	C.17C
		0.10	-0.053	0.196	-0.579	C.34C
		0.15	-0.08C	C.294	-0.868	C.51C
		0.20	-0.106	C.392	-1.157	C.68C
		0.25	-0.133	0.489	-1.447	0.85C
		0.30	-0.160	C.587	-1.736	1.C2C
		0.35	-C.186	C.685	-2.025	1.19C
		0.40	-C.213	C.783	-2.314	1.36C
		0.45	-0.239	0.881	-2.604	1.53C
		0.50	-C.266	C.979	-2.893	1.70C
		0.55	-C.293	1.077	-3.182	1.87C
		0.60	-C.319	1.175	-3.472	2.04C
		0.65	-C.346	1.273	-3.761	2.21C
		0.70	-0.372	1.371	-4.050	2.38C
		0.75	-C.399	1.468	-4.340	2.55C
		0.80	-C.426	1.566	-4.629	2.719
		0.85	-C.452	1.664	-4.918	2.889
		0.90	-0.479	1.762	-5.208	3.C59
		0.95	-C.505	1.860	-5.497	3.229
		1.00	-0.532	1.958	-5.786	3.399
6	25	0.	-0.	C.	-0.	C.
		0.05	-C.048	C.146	-0.474	C.24C
		0.10	-C.096	C.292	-0.948	C.48C
		0.15	-C.143	C.438	-1.421	C.719
		0.20	-0.191	C.585	-1.895	0.959
		0.25	-0.239	C.731	-2.369	1.199
		0.30	-C.287	C.877	-2.843	1.439
		0.35	-C.334	1.023	-3.317	1.678
		0.40	-0.382	1.169	-3.790	1.918
		0.45	-0.430	1.315	-4.264	2.158
		0.50	-C.478	1.462	-4.738	2.398
		0.55	-0.526	1.608	-5.212	2.638
		0.60	-0.573	1.754	-5.686	2.877
		0.65	-0.621	1.900	-6.159	3.117
		0.70	-0.669	2.046	-6.633	3.357
		0.75	-0.717	2.192	-7.107	3.597
		0.80	-0.764	2.338	-7.581	3.837
		0.85	-0.812	2.485	-8.055	4.C76
		0.90	-0.860	2.631	-8.528	4.316
		0.95	-0.908	2.777	-9.002	4.556
		1.00	-0.956	2.923	-9.476	4.796

6	30	0.	-0.	C.	-0.	C.
		0.05	-0.058	C.173	-0.524	C.262
		0.10	-0.115	C.346	-1.047	C.524
		0.15	-0.173	C.520	-1.571	C.785
		0.20	-0.231	0.693	-2.094	1.C47
		0.25	-0.289	0.866	-2.618	1.309
		0.30	-0.346	1.039	-3.142	1.571
		0.35	-0.404	1.212	-3.665	1.833
		0.40	-0.462	1.386	-4.189	2.C94
		0.45	-0.520	1.559	-4.712	2.356
		0.50	-0.577	1.732	-5.236	2.618
		0.55	-0.635	1.905	-5.760	2.88C
		0.60	-0.693	2.078	-6.283	3.142
		0.65	-0.751	2.252	-6.807	3.403
		0.70	-0.808	2.425	-7.330	3.665
		0.75	-0.866	2.598	-7.854	3.927
		0.80	-0.924	2.771	-8.378	4.189
		0.85	-0.981	2.944	-8.901	4.451
		0.90	-1.039	3.118	-9.425	4.712
		0.95	-1.097	3.291	-9.948	4.974
		1.00	-1.155	3.464	-10.472	5.236
6	35	0.	-0.	C.	-0.	C.
		0.05	-0.053	C.157	-0.423	0.207
		0.10	-0.106	C.314	-0.846	C.414
		0.15	-0.159	C.471	-1.269	C.62C
		0.20	-0.211	C.628	-1.692	C.827
		0.25	-C.264	C.785	-2.114	1.C34
		0.30	-0.317	C.942	-2.537	1.241
		0.35	-0.370	1.098	-2.960	1.448
		0.40	-0.423	1.255	-3.383	1.655
		0.45	-0.476	1.412	-3.806	1.861
		0.50	-0.529	1.569	-4.229	2.C68
		0.55	-0.581	1.726	-4.652	2.275
		0.60	-0.634	1.883	-5.075	2.482
		0.65	-0.687	2.040	-5.498	2.689
		0.70	-0.740	2.197	-5.921	2.895
		0.75	-0.793	2.354	-6.343	3.102
		0.80	-0.846	2.511	-6.766	3.309
		0.85	-0.899	2.668	-7.189	3.516
		0.90	-0.951	2.825	-7.612	3.723
		0.95	-1.004	2.981	-8.035	3.930
		1.00	-1.057	3.138	-8.458	4.136

6	40	0.	-0.	C.	-0.	C.
		0.05	-0.033	C.083	-0.198	C.C70
		0.10	-0.065	C.165	-0.397	C.139
		0.15	-0.098	C.248	-0.595	C.209
		0.20	-0.131	C.330	-0.794	0.278
		0.25	-0.163	0.413	-0.992	C.348
		0.30	-C.196	C.495	-1.19C	C.418
		0.35	-0.228	C.578	-1.389	C.487
		0.40	-C.261	0.660	-1.587	0.557
		0.45	-0.294	C.743	-1.785	0.627
		0.50	-0.326	C.826	-1.984	C.696
		0.55	-C.359	C.908	-2.182	C.766
		0.60	-0.392	C.991	-2.381	C.835
		0.65	-0.424	1.073	-2.579	0.905
		0.70	-0.457	1.156	-2.777	C.975
		0.75	-0.490	1.238	-2.976	1.C44
		0.80	-0.522	1.321	-3.174	1.114
		0.85	-0.555	1.404	-3.372	1.184
		0.90	-0.587	1.486	-3.571	1.253
		0.95	-0.620	1.569	-3.769	1.323
		1.00	-0.653	1.651	-3.968	1.392
6	45	0.	0.	-0.	0.	-0.
		0.05	0.000	-0.050	0.087	-0.123
		0.10	0.000	-0.100	0.175	-0.247
		0.15	0.000	-0.150	0.262	-0.370
		0.20	0.000	-0.200	0.349	-0.494
		0.25	0.000	-0.250	0.436	-0.617
		0.30	0.000	-0.300	0.524	-0.741
		0.35	0.000	-0.350	0.611	-0.864
		0.40	0.000	-0.400	0.698	-0.987
		0.45	0.000	-0.450	0.785	-1.111
		0.50	0.000	-0.500	0.873	-1.234
		0.55	0.000	-0.550	0.960	-1.358
		0.60	0.000	-0.600	1.047	-1.481
		0.65	0.000	-0.650	1.135	-1.604
		0.70	0.000	-0.700	1.222	-1.728
		0.75	0.000	-0.750	1.309	-1.851
		0.80	0.000	-0.800	1.396	-1.975
		0.85	0.000	-0.850	1.484	-2.098
		0.90	0.000	-0.900	1.571	-2.222
		0.95	0.000	-0.950	1.658	-2.345
		1.00	0.000	-1.000	1.745	-2.468

6	50	0.	0.	-0.	0.	-0.
		0.05	0.039	-0.222	0.352	-0.318
		0.10	0.078	-0.444	0.704	-0.636
		0.15	0.117	-0.666	1.056	-0.954
		0.20	0.156	-0.888	1.407	-1.273
		0.25	0.194	-1.110	1.759	-1.591
		0.30	0.233	-1.332	2.111	-1.909
		0.35	0.272	-1.554	2.463	-2.227
		0.40	0.311	-1.777	2.815	-2.545
		0.45	0.350	-1.999	3.167	-2.863
		0.50	0.389	-2.221	3.519	-3.181
		0.55	0.428	-2.443	3.871	-3.499
		0.60	0.467	-2.665	4.222	-3.818
		0.65	0.506	-2.887	4.574	-4.136
		0.70	0.545	-3.109	4.926	-4.454
		0.75	0.583	-3.331	5.278	-4.772
		0.80	0.622	-3.553	5.630	-5.090
		0.85	0.661	-3.775	5.982	-5.408
		0.90	0.700	-3.997	6.334	-5.726
		0.95	0.739	-4.219	6.686	-6.044
		1.00	0.778	-4.441	7.037	-6.363
6	55	0.	0.	-0.	0.	-0.
		0.05	0.075	-0.396	0.516	-0.448
		0.10	0.151	-0.792	1.032	-0.895
		0.15	0.226	-1.188	1.547	-1.343
		0.20	0.302	-1.584	2.063	-1.790
		0.25	0.377	-1.980	2.579	-2.238
		0.30	0.453	-2.376	3.095	-2.685
		0.35	0.528	-2.772	3.610	-3.133
		0.40	0.604	-3.168	4.126	-3.580
		0.45	0.679	-3.564	4.642	-4.028
		0.50	0.755	-3.960	5.158	-4.475
		0.55	0.830	-4.357	5.673	-4.923
		0.60	0.906	-4.753	6.189	-5.370
		0.65	0.981	-5.149	6.705	-5.818
		0.70	1.057	-5.545	7.221	-6.265
		0.75	1.132	-5.941	7.737	-6.713
		0.80	1.208	-6.337	8.252	-7.160
		0.85	1.283	-6.733	8.768	-7.608
		0.90	1.359	-7.129	9.284	-8.055
		0.95	1.434	-7.525	9.800	-8.503
		1.00	1.510	-7.921	10.315	-8.950

6	60	0.	0.	-0.	0.	-0.
		0.05	0.100	-0.520	0.524	-0.453
		0.10	0.200	-1.039	1.047	-0.907
		0.15	0.300	-1.559	1.571	-1.360
		0.20	0.400	-2.078	2.094	-1.814
		0.25	0.500	-2.598	2.618	-2.267
		0.30	0.600	-3.118	3.142	-2.721
		0.35	0.700	-3.637	3.665	-3.174
		0.40	0.800	-4.157	4.189	-3.628
		0.45	0.900	-4.677	4.712	-4.081
		0.50	1.000	-5.196	5.236	-4.534
		0.55	1.100	-5.716	5.760	-4.988
		0.60	1.200	-6.235	6.283	-5.441
		0.65	1.300	-6.755	6.807	-5.895
		0.70	1.400	-7.275	7.330	-6.348
		0.75	1.500	-7.794	7.854	-6.802
		0.80	1.600	-8.314	8.378	-7.255
		0.85	1.700	-8.833	8.901	-7.709
		0.90	1.800	-9.353	9.425	-8.162
		0.95	1.900	-9.873	9.948	-8.616
		1.00	2.000	-10.392	10.472	-9.069
6	65	0.	0.	-0.	0.	-0.
		0.05	0.102	-0.532	0.360	-0.308
		0.10	0.205	-1.064	0.720	-0.615
		0.15	0.307	-1.596	1.080	-0.923
		0.20	0.410	-2.129	1.439	-1.231
		0.25	0.512	-2.661	1.799	-1.539
		0.30	0.615	-3.193	2.159	-1.846
		0.35	0.717	-3.725	2.519	-2.154
		0.40	0.820	-4.257	2.879	-2.462
		0.45	0.922	-4.789	3.239	-2.769
		0.50	1.025	-5.322	3.599	-3.077
		0.55	1.127	-5.854	3.959	-3.385
		0.60	1.230	-6.386	4.318	-3.693
		0.65	1.332	-6.918	4.678	-4.000
		0.70	1.434	-7.450	5.038	-4.308
		0.75	1.537	-7.982	5.398	-4.616
		0.80	1.639	-8.515	5.758	-4.923
		0.85	1.742	-9.047	6.118	-5.231
		0.90	1.844	-9.579	6.478	-5.539
		0.95	1.947	-10.111	6.838	-5.847
		1.00	2.049	-10.643	7.197	-6.154

8	5	0.	C.	C.	0.	C.
		0.05	0.038	C.005	0.530	C.C1C
		0.10	0.077	C.011	1.060	C.C19
		0.15	0.115	C.016	1.590	C.C29
		0.20	0.154	C.021	2.120	C.C39
		0.25	0.192	0.027	2.649	C.C48
		0.30	0.231	C.032	3.179	C.058
		0.35	0.269	C.037	3.709	C.C68
		0.40	0.308	C.043	4.239	C.C78
		0.45	0.346	C.048	4.769	C.C87
		0.50	0.384	C.053	5.299	C.C97
		0.55	0.423	C.059	5.829	C.107
		0.60	0.461	C.064	6.359	C.116
		0.65	0.500	C.069	6.889	C.126
		0.70	0.538	0.075	7.418	C.136
		0.75	C.577	C.08C	7.948	C.145
		0.80	0.615	C.085	8.478	C.155
		0.85	0.654	C.091	9.008	C.165
		0.90	0.692	0.096	9.538	C.175
		0.95	0.731	C.101	10.C68	C.184
		1.00	0.769	C.107	10.598	C.194
8	10	0.	0.	C.	0.	C.
		0.05	C.009	C.037	0.106	C.C66
		0.10	C.C18	C.074	0.212	C.132
		0.15	0.C26	C.111	0.318	C.199
		0.20	0.035	C.148	0.424	C.265
		0.25	0.044	C.185	0.53C	C.331
		0.30	C.053	C.222	0.636	C.397
		0.35	C.062	C.259	0.743	C.464
		0.40	0.071	C.296	0.849	C.53C
		0.45	0.079	C.333	0.955	C.596
		0.50	0.088	C.37C	1.C61	C.662
		0.55	0.097	C.407	1.167	C.728
		0.60	0.106	C.444	1.273	C.795
		0.65	0.115	C.481	1.379	0.861
		0.70	0.123	C.518	1.485	C.927
		0.75	0.132	0.555	1.591	C.993
		0.80	0.141	0.592	1.697	1.C59
		0.85	0.150	0.629	1.803	1.126
		0.90	0.159	0.666	1.909	1.192
		0.95	0.168	0.703	2.015	1.258
		1.00	0.176	0.740	2.121	1.324

8	15	0.	-0.	C.	-0.	0.
		0.05	-C.026	C.097	-0.369	C.169
		0.10	-0.052	0.194	-0.739	C.337
		0.15	-0.078	C.291	-1.108	C.506
		0.20	-0.104	0.388	-1.477	C.674
		0.25	-0.129	C.484	-1.847	C.843
		0.30	-0.155	0.581	-2.216	1.C12
		0.35	-0.181	0.678	-2.585	1.180
		0.40	-0.207	0.775	-2.955	1.349
		0.45	-0.233	C.872	-3.324	1.517
		0.50	-0.259	C.969	-3.693	1.686
		0.55	-0.285	1.066	-4.063	1.854
		0.60	-0.311	1.163	-4.432	2.C23
		0.65	-0.336	1.260	-4.801	2.192
		0.70	-0.362	1.356	-5.17C	2.360
		0.75	-0.388	1.453	-5.540	2.529
		0.80	-0.414	1.550	-5.909	2.697
		0.85	-0.440	1.647	-6.278	2.866
		0.90	-C.466	1.744	-6.648	3.C35
		0.95	-0.492	1.841	-7.017	3.203
		1.00	-0.518	1.938	-7.386	3.372
8	20	0.	-0.	C.	-0.	C.
		0.05	-0.050	C.154	-0.667	C.256
		0.10	-0.100	C.308	-1.334	C.512
		0.15	-0.15C	C.462	-2.001	C.768
		0.20	-0.20C	C.616	-2.668	1.C25
		0.25	-0.25C	C.77C	-3.334	1.281
		0.30	-0.300	C.923	-4.001	1.537
		0.35	-0.35C	1.077	-4.668	1.793
		0.40	-0.400	1.231	-5.335	2.C49
		0.45	-0.45C	1.385	-6.002	2.305
		0.50	-0.500	1.539	-6.669	2.561
		0.55	-0.550	1.693	-7.336	2.818
		0.60	-0.600	1.847	-8.003	3.C74
		0.65	-0.650	2.001	-8.67C	3.33C
		0.70	-0.700	2.155	-9.337	3.586
		0.75	-0.750	2.309	-10.003	3.842
		0.80	-0.800	2.463	-10.67C	4.C98
		0.85	-0.850	2.616	-11.337	4.354
		0.90	-0.900	2.770	-12.004	4.610
		0.95	-0.950	2.924	-12.671	4.867
		1.00	-1.000	3.078	-13.338	5.123

8 25	0.	-0.	C.	-0.	C.
	0.05	-0.052	0.158	-0.642	0.244
	0.10	-0.104	0.316	-1.284	0.489
	0.15	-0.156	0.475	-1.926	0.733
	0.20	-0.207	0.633	-2.568	0.977
	0.25	-0.259	0.791	-3.211	1.222
	0.30	-0.311	0.949	-3.853	1.466
	0.35	-0.363	1.107	-4.495	1.710
	0.40	-0.415	1.265	-5.137	1.955
	0.45	-0.467	1.424	-5.779	2.199
	0.50	-0.518	1.582	-6.421	2.443
	0.55	-0.570	1.740	-7.063	2.687
	0.60	-0.622	1.898	-7.705	2.932
	0.65	-0.674	2.056	-8.347	3.176
	0.70	-0.726	2.214	-8.990	3.420
	0.75	-0.778	2.373	-9.632	3.665
	0.80	-0.829	2.531	-10.274	3.909
	0.85	-0.881	2.689	-10.916	4.153
	0.90	-0.933	2.847	-11.558	4.398
	0.95	-0.985	3.005	-12.200	4.642
	1.00	-1.037	3.163	-12.842	4.886
8 30	0.	-0.	C.	-0.	C.
	0.05	-0.029	0.072	-0.305	0.087
	0.10	-0.058	0.144	-0.611	0.175
	0.15	-0.087	0.217	-0.916	0.262
	0.20	-0.115	0.289	-1.222	0.349
	0.25	-0.144	0.361	-1.527	0.436
	0.30	-0.173	0.433	-1.833	0.524
	0.35	-0.202	0.505	-2.138	0.611
	0.40	-0.231	0.577	-2.443	0.698
	0.45	-0.260	0.650	-2.749	0.785
	0.50	-0.289	0.722	-3.054	0.873
	0.55	-0.318	0.794	-3.360	0.960
	0.60	-0.346	0.866	-3.665	1.047
	0.65	-0.375	0.938	-3.971	1.134
	0.70	-0.404	1.010	-4.276	1.222
	0.75	-0.433	1.083	-4.581	1.309
	0.80	-0.462	1.155	-4.887	1.396
	0.85	-0.491	1.227	-5.192	1.483
	0.90	-0.520	1.299	-5.498	1.571
	0.95	-0.548	1.371	-5.803	1.658
	1.00	-0.577	1.443	-6.109	1.745

8 35	0.	0.	-C.	0.	-C.
	0.05	C.011	-C.098	0.181	-C.174
	0.10	0.021	-C.196	0.363	-C.349
	0.15	0.032	-0.294	0.544	-C.523
	0.20	0.042	-C.392	0.726	-C.698
	0.25	0.053	-C.489	0.907	-C.872
	0.30	0.064	-0.587	1.088	-1.047
	0.35	0.074	-0.685	1.270	-1.221
	0.40	0.085	-C.783	1.451	-1.396
	0.45	0.095	-C.881	1.633	-1.570
	0.50	0.106	-0.979	1.814	-1.745
	0.55	0.117	-1.077	1.996	-1.919
	0.60	C.127	-1.175	2.177	-2.093
	0.65	0.138	-1.272	2.358	-2.268
	0.70	0.148	-1.370	2.540	-2.442
	0.75	0.159	-1.468	2.721	-2.617
	0.80	0.170	-1.566	2.903	-2.791
	0.85	C.180	-1.664	3.084	-2.966
	0.90	0.191	-1.762	3.265	-3.140
	0.95	0.201	-1.860	3.447	-3.315
	1.00	0.212	-1.958	3.628	-3.489
8 40	0.	C.	-C.	0.	-C.
	0.05	0.050	-0.289	0.582	-C.417
	0.10	C.100	-0.579	1.164	-C.834
	0.15	0.150	-C.868	1.746	-1.251
	0.20	C.200	-1.157	2.327	-1.668
	0.25	C.250	-1.446	2.909	-2.085
	0.30	0.300	-1.736	3.491	-2.502
	0.35	0.350	-2.025	4.073	-2.919
	0.40	0.400	-2.314	4.655	-3.336
	0.45	0.450	-2.603	5.237	-3.753
	0.50	0.500	-2.893	5.819	-4.170
	0.55	C.550	-3.182	6.401	-4.587
	0.60	C.600	-3.471	6.982	-5.004
	0.65	0.650	-3.760	7.564	-5.421
	0.70	0.700	-4.050	8.146	-5.838
	0.75	0.750	-4.339	8.728	-6.255
	0.80	C.800	-4.628	9.310	-6.672
	0.85	0.850	-4.917	9.892	-7.089
	0.90	0.900	-5.207	10.474	-7.506
	0.95	0.950	-5.496	11.056	-7.923
	1.00	1.000	-5.785	11.637	-8.340

8 45	0.	0.	-0.	0.	-0.
	0.05	0.071	-0.400	0.698	-0.494
	0.10	0.141	-0.800	1.396	-0.987
	0.15	0.212	-1.200	2.094	-1.481
	0.20	0.283	-1.600	2.793	-1.975
	0.25	0.354	-2.000	3.491	-2.468
	0.30	0.424	-2.400	4.189	-2.962
	0.35	0.495	-2.800	4.887	-3.456
	0.40	0.566	-3.200	5.585	-3.949
	0.45	0.636	-3.600	6.283	-4.443
	0.50	0.707	-4.000	6.981	-4.937
	0.55	0.778	-4.400	7.679	-5.430
	0.60	0.849	-4.800	8.378	-5.924
	0.65	0.919	-5.200	9.076	-6.418
	0.70	0.990	-5.600	9.774	-6.911
	0.75	1.061	-6.000	10.472	-7.405
	0.80	1.131	-6.400	11.170	-7.898
	0.85	1.202	-6.800	11.868	-8.392
	0.90	1.273	-7.200	12.566	-8.886
	0.95	1.344	-7.600	13.265	-9.379
	1.00	1.414	-8.000	13.963	-9.873
8 50	0.	0.	-0.	0.	-0.
	0.05	0.060	-0.333	0.468	-0.322
	0.10	0.119	-0.666	0.936	-0.645
	0.15	0.179	-0.999	1.404	-0.967
	0.20	0.238	-1.332	1.872	-1.290
	0.25	0.298	-1.665	2.340	-1.612
	0.30	0.358	-1.998	2.808	-1.934
	0.35	0.417	-2.331	3.276	-2.257
	0.40	0.477	-2.664	3.744	-2.579
	0.45	0.536	-2.997	4.211	-2.902
	0.50	0.596	-3.330	4.679	-3.224
	0.55	0.655	-3.663	5.147	-3.546
	0.60	0.715	-3.996	5.615	-3.869
	0.65	0.775	-4.329	6.083	-4.191
	0.70	0.834	-4.662	6.551	-4.514
	0.75	0.894	-4.995	7.019	-4.836
	0.80	0.953	-5.328	7.487	-5.159
	0.85	1.013	-5.662	7.955	-5.481
	0.90	1.073	-5.995	8.423	-5.803
	0.95	1.132	-6.328	8.891	-6.126
	1.00	1.192	-6.661	9.359	-6.448

8 55	0.	0.	-0.	-0.	0.
	0.05	0.015	-0.050	-0.002	0.051
	0.10	0.030	-0.100	-0.003	0.101
	0.15	0.045	-0.150	-0.005	0.152
	0.20	0.061	-0.200	-0.006	0.202
	0.25	0.076	-0.250	-0.008	0.253
	0.30	0.091	-0.300	-0.009	0.303
	0.35	0.106	-0.350	-0.011	0.354
	0.40	0.121	-0.400	-0.012	0.404
	0.45	0.136	-0.450	-0.014	0.455
	0.50	0.151	-0.499	-0.015	0.505
	0.55	0.166	-0.549	-0.017	0.556
	0.60	0.182	-0.599	-0.018	0.606
	0.65	0.197	-0.649	-0.020	0.657
	0.70	0.212	-0.699	-0.021	0.708
	0.75	0.227	-0.749	-0.023	0.758
	0.80	0.242	-0.799	-0.024	0.809
	0.85	0.257	-0.849	-0.026	0.859
	0.90	0.272	-0.899	-0.027	0.910
	0.95	0.288	-0.949	-0.029	0.960
	1.00	0.303	-0.999	-0.030	1.011
8 60	0.	-0.	0.	-0.	0.
	0.05	-0.050	0.390	-0.480	0.453
	0.10	-0.100	0.779	-0.960	0.907
	0.15	-0.150	1.169	-1.440	1.360
	0.20	-0.200	1.559	-1.920	1.814
	0.25	-0.250	1.949	-2.400	2.267
	0.30	-0.300	2.338	-2.880	2.721
	0.35	-0.350	2.728	-3.360	3.174
	0.40	-0.400	3.118	-3.840	3.628
	0.45	-0.450	3.508	-4.320	4.081
	0.50	-0.500	3.897	-4.800	4.535
	0.55	-0.550	4.287	-5.280	4.988
	0.60	-0.600	4.677	-5.760	5.442
	0.65	-0.650	5.066	-6.240	5.895
	0.70	-0.700	5.456	-6.720	6.348
	0.75	-0.750	5.846	-7.200	6.802
	0.80	-0.800	6.236	-7.680	7.255
	0.85	-0.850	6.625	-8.160	7.709
	0.90	-0.900	7.015	-8.640	8.162
	0.95	-0.950	7.405	-9.120	8.616
	1.00	-1.000	7.794	-9.600	9.069

8	65	0.	-0.	0.	-0.	0.
		0.05	-0.111	0.823	-0.720	0.665
		0.10	-0.222	1.646	-1.440	1.330
		0.15	-0.334	2.470	-2.160	1.996
		0.20	-0.445	3.293	-2.880	2.661
		0.25	-0.556	4.116	-3.600	3.326
		0.30	-0.667	4.939	-4.320	3.991
		0.35	-0.778	5.762	-5.040	4.656
		0.40	-0.889	6.585	-5.760	5.322
		0.45	-1.001	7.409	-6.480	5.987
		0.50	-1.112	8.232	-7.200	6.652
		0.55	-1.223	9.055	-7.920	7.317
		0.60	-1.334	9.878	-8.640	7.982
		0.65	-1.445	10.701	-9.361	8.647
		0.70	-1.556	11.525	-10.081	9.313
		0.75	-1.668	12.348	-10.801	9.978
		0.80	-1.779	13.171	-11.521	10.643
		0.85	-1.890	13.994	-12.241	11.308
		0.90	-2.001	14.817	-12.961	11.973
		0.95	-2.112	15.640	-13.681	12.639
		1.00	-2.224	16.464	-14.401	13.304
8	70	0.	-0.	0.	-0.	0.
		0.05	-0.137	1.016	-0.574	0.529
		0.10	-0.275	2.031	-1.148	1.058
		0.15	-0.412	3.047	-1.722	1.588
		0.20	-0.549	4.062	-2.296	2.117
		0.25	-0.687	5.078	-2.870	2.646
		0.30	-0.824	6.094	-3.444	3.175
		0.35	-0.962	7.109	-4.018	3.704
		0.40	-1.099	8.125	-4.592	4.234
		0.45	-1.236	9.141	-5.166	4.763
		0.50	-1.374	10.156	-5.740	5.292
		0.55	-1.511	11.172	-6.314	5.821
		0.60	-1.648	12.187	-6.888	6.350
		0.65	-1.786	13.203	-7.462	6.879
		0.70	-1.923	14.219	-8.036	7.409
		0.75	-2.061	15.234	-8.610	7.938
		0.80	-2.198	16.250	-9.184	8.467
		0.85	-2.335	17.265	-9.758	8.996
		0.90	-2.473	18.281	-10.332	9.525
		0.95	-2.610	19.297	-10.906	10.055
		1.00	-2.747	20.312	-11.480	10.584

8	75	0.	-0.	0.	-0.	0.
		0.05	-0.097	0.703	-0.067	0.045
		0.10	-0.193	1.406	-0.134	0.090
		0.15	-0.290	2.109	-0.201	0.135
		0.20	-0.386	2.812	-0.268	0.181
		0.25	-0.483	3.515	-0.335	0.226
		0.30	-0.580	4.219	-0.402	0.271
		0.35	-0.676	4.922	-0.469	0.316
		0.40	-0.773	5.625	-0.536	0.361
		0.45	-0.869	6.328	-0.603	0.406
		0.50	-0.966	7.031	-0.670	0.452
		0.55	-1.062	7.734	-0.737	0.497
		0.60	-1.159	8.437	-0.804	0.542
		0.65	-1.256	9.140	-0.871	0.587
		0.70	-1.352	9.843	-0.938	0.632
		0.75	-1.449	10.546	-1.005	0.677
		0.80	-1.545	11.249	-1.072	0.722
		0.85	-1.642	11.952	-1.139	0.768
		0.90	-1.739	12.656	-1.206	0.813
		0.95	-1.835	13.359	-1.273	0.858
		1.00	-1.932	14.062	-1.340	0.903
8	80	0.	0.	-0.	0.	-0.
		0.05	0.050	-0.443	0.609	-0.614
		0.10	0.100	-0.886	1.217	-1.229
		0.15	0.150	-1.330	1.826	-1.843
		0.20	0.200	-1.773	2.435	-2.457
		0.25	0.250	-2.216	3.043	-3.072
		0.30	0.300	-2.659	3.652	-3.686
		0.35	0.350	-3.103	4.261	-4.300
		0.40	0.400	-3.546	4.869	-4.915
		0.45	0.450	-3.989	5.478	-5.529
		0.50	0.500	-4.432	6.086	-6.143
		0.55	0.550	-4.876	6.695	-6.758
		0.60	0.600	-5.319	7.304	-7.372
		0.65	0.650	-5.762	7.912	-7.986
		0.70	0.700	-6.205	8.521	-8.601
		0.75	0.750	-6.648	9.130	-9.215
		0.80	0.800	-7.092	9.738	-9.829
		0.85	0.850	-7.535	10.347	-10.444
		0.90	0.900	-7.978	10.956	-11.058
		0.95	0.950	-8.421	11.564	-11.672
		1.00	1.000	-8.865	12.173	-12.287

10	0	0.	0.	-C.	0.	C.
		0.05	0.050	-C.	0.873	C.
		0.10	0.100	-C.	1.745	C.
		0.15	0.150	-C.	2.618	C.
		0.20	0.200	-C.	3.491	C.
		0.25	0.250	-C.	4.363	C.
		0.30	0.300	-C.	5.236	C.
		0.35	0.350	-C.	6.109	C.
		0.40	0.400	-0.	6.981	C.
		0.45	0.450	-C.	7.854	C.
		0.50	0.500	-C.	8.727	C.
		0.55	0.550	-C.	9.599	C.
		0.60	0.600	-C.	10.472	C.
		0.65	0.650	-C.	11.345	C.
		0.70	0.700	-C.	12.217	C.
		0.75	0.750	-C.	13.090	C.
		0.80	0.800	-C.	13.963	C.
		0.85	0.850	-C.	14.835	C.
		0.90	0.900	-C.	15.708	C.
		0.95	0.950	-C.	16.581	C.
		1.00	1.000	-C.	17.453	C.
10	5	0.	0.	C.	0.	C.
		0.05	0.032	C.010	0.555	C.018
		0.10	0.065	C.020	1.110	C. [illegible]
		0.15	0.097	C.031	1.665	[illegible]
		0.20	0.129	C.041	2.220	[illegible]
		0.25	0.161	C.051	2.775	[illegible]
		0.30	0.194	C.061	3.330	[illegible]
		0.35	0.226	C.071	3.885	[illegible]
		0.40	0.258	C.081	4.441	[illegible]
		0.45	0.290	C.092	4.996	[illegible]
		0.50	0.323	C.102	5.551	C.182
		0.55	0.355	C.112	6.106	C.200
		0.60	0.387	C.122	6.661	C.219
		0.65	0.419	C.132	7.216	C.237
		0.70	0.452	C.143	7.771	C.255
		0.75	0.484	C.153	8.326	C.273
		0.80	0.516	C.163	8.881	C.291
		0.85	0.548	C.173	9.437	C.310
		0.90	0.581	C.183	9.992	C.328
		0.95	0.613	C.193	10.547	C.346
		1.00	0.645	C.204	11.102	C.364

10	10	0.	-C.	C.	-0.	C.
		0.05	-0.009	0.065	-0.167	C.114
		0.10	-C.018	0.129	-0.333	C.227
		0.15	-0.026	C.194	-0.500	C.341
		0.20	-0.035	C.258	-0.667	C.454
		0.25	-0.044	C.323	-0.833	C.568
		0.30	-0.053	C.387	-1.000	C.681
		0.35	-C.062	C.452	-1.167	C.795
		0.40	-C.071	C.516	-1.334	C.909
		0.45	-0.079	C.581	-1.500	1.022
		0.50	-C.088	C.646	-1.667	1.136
		0.55	-C.097	C.710	-1.834	1.249
		0.60	-C.106	C.775	-2.000	1.363
		0.65	-C.115	0.839	-2.167	1.477
		0.70	-C.123	C.904	-2.334	1.590
		0.75	C.132	C.968	-2.500	1.704
		0.80	C.141	1.033	-2.667	1.817
		0.85	C.150	1.097	-2.834	1.931
		0.90	C.159	1.162	-3.000	2.044
		0.95	C.168	1.226	-3.167	2.158
		1.00	-C.176	1.291	-3.334	2.272
10	15	0.	-C.	C.	-0.	C.
		0.05	-C.045	C.141	-0.767	C.241
		0.10	-C.090	C.282	-1.535	C.482
		0.15	-C.134	C.423	-2.302	C.722
		0.20	-C.179	C.564	-3.070	C.963
		0.25	-C.224	C.705	-3.837	1.204
		0.30	-C.269	C.846	-4.605	1.445
		0.35	-C.314	C.987	-5.372	1.685
		0.40	-C.359	1.128	-6.140	1.926
		0.45	-C.403	1.269	-6.907	2.167
		0.50	-C.448	1.410	-7.674	2.408
		0.55	-C.493	1.551	-8.442	2.649
		0.60	-C.538	1.692	-9.209	2.889
		0.65	-C.583	1.833	-9.977	3.130
		0.70	-0.628	1.974	-10.744	3.371
		0.75	-0.672	2.115	-11.512	3.612
		0.80	-0.717	2.256	-12.279	3.852
		0.85	-0.762	2.397	-13.047	4.093
		0.90	-0.807	2.538	-13.814	4.334
		0.95	-0.852	2.679	-14.581	4.575
		1.00	-0.897	2.821	-15.349	4.816

10	20	0.	-0.	C.	-0.	C.
		0.05	-0.050	C.154	-0.809	C.249
		0.10	-0.100	C.308	-1.618	C.497
		0.15	-0.150	C.462	-2.428	C.746
		0.20	-0.200	C.616	-3.237	C.995
		0.25	-0.250	C.770	-4.046	1.244
		0.30	-0.300	C.923	-4.855	1.492
		0.35	-0.350	1.077	-5.664	1.741
		0.40	-0.400	1.231	-6.473	1.990
		0.45	-0.450	1.385	-7.283	2.238
		0.50	-0.500	1.539	-8.092	2.487
		0.55	-0.550	1.693	-8.901	2.736
		0.60	-0.600	1.847	-9.710	2.984
		0.65	-0.650	2.001	-10.519	3.233
		0.70	-0.700	2.155	-11.328	3.482
		0.75	-0.750	2.309	-12.138	3.731
		0.80	-0.800	2.463	-12.947	3.979
		0.85	-0.850	2.616	-13.756	4.228
		0.90	-0.900	2.770	-14.565	4.477
		0.95	-0.950	2.924	-15.374	4.725
		1.00	-1.000	3.078	-16.183	4.974
10	25	0.	-0.	C.	-0.	C.
		0.05	-0.019	C.033	-0.260	C.C36
		0.10	-0.038	C.066	-0.520	C.C71
		0.15	-0.057	C.098	-0.781	C.107
		0.20	-0.075	C.131	-1.041	C.143
		0.25	-0.094	C.164	-1.301	C.178
		0.30	-0.113	C.197	-1.561	C.214
		0.35	-0.132	C.229	-1.822	C.250
		0.40	-0.151	C.262	-2.082	C.285
		0.45	-0.170	C.295	-2.342	C.321
		0.50	-0.189	C.328	-2.602	C.357
		0.55	-0.208	C.360	-2.862	C.392
		0.60	-0.226	C.393	-3.123	C.428
		0.65	-0.245	C.426	-3.383	C.464
		0.70	-0.264	C.459	-3.643	C.499
		0.75	-0.283	C.491	-3.903	C.535
		0.80	-0.302	C.524	-4.164	C.570
		0.85	-0.321	C.557	-4.424	C.606
		0.90	-0.340	C.590	-4.684	C.642
		0.95	-0.358	C.622	-4.944	C.677
		[illegible]	[illegible]	[illegible]	[illegible]	C.713

10	30	0.	0.	-C.	0.	-C.
		0.05	0.029	-C.188	0.480	-C.305
		0.10	C.058	-C.375	0.960	-C.611
		0.15	0.087	-C.563	1.440	-C.916
		0.20	C.115	-C.751	1.920	-1.222
		0.25	0.144	-C.938	2.400	-1.527
		0.30	0.173	-1.126	2.880	-1.833
		0.35	0.202	-1.313	3.360	-2.138
		0.40	C.231	-1.501	3.840	-2.444
		0.45	C.260	-1.689	4.320	-2.749
		0.50	C.289	-1.876	4.800	-3.054
		0.55	C.318	-2.064	5.280	-3.360
		0.60	C.346	-2.252	5.760	-3.665
		0.65	C.375	-2.439	6.240	-3.971
		0.70	C.404	-2.627	6.720	-4.276
		0.75	C.433	-2.815	7.200	-4.582
		0.80	C.462	-3.002	7.680	-4.887
		0.85	C.491	-3.190	8.160	-5.192
		0.90	C.520	-3.378	8.640	-5.498
		0.95	C.548	-3.565	9.120	-5.803
		1.00	C.577	-3.753	9.600	-6.109
10	35	0.	0.	-C.	0.	-C.
		0.05	0.060	-C.353	0.870	-C.511
		0.10	0.120	-0.707	1.740	-1.023
		0.15	0.180	-1.060	2.610	-1.534
		0.20	0.240	-1.414	3.480	-2.046
		0.25	0.301	-1.767	4.350	-2.557
		0.30	0.361	-2.121	5.220	-3.069
		0.35	0.421	-2.474	6.090	-3.580
		0.40	0.481	-2.828	6.960	-4.091
		0.45	0.541	-3.181	7.830	-4.603
		0.50	0.601	-3.535	8.700	-5.114
		0.55	0.661	-3.888	9.570	-5.626
		0.60	0.721	-4.242	10.440	-6.137
		0.65	0.781	-4.595	11.310	-6.649
		0.70	0.842	-4.949	12.180	-7.160
		0.75	0.902	-5.302	13.050	-7.672
		0.80	0.962	-5.655	13.920	-8.183
		0.85	1.022	-6.009	14.790	-8.694
		0.90	1.082	-6.362	15.660	-9.206
		0.95	1.142	-6.716	16.530	-9.717
		1.00	1.202	-7.069	17.400	-10.229

10	40	0.	0.	-0.	0.	-0.
		0.05	0.050	-0.289	0.621	-0.356
		0.10	0.100	-0.579	1.243	-0.713
		0.15	0.150	-0.868	1.864	-1.069
		0.20	0.200	-1.157	2.486	-1.426
		0.25	0.250	-1.446	3.107	-1.782
		0.30	0.300	-1.736	3.729	-2.139
		0.35	0.350	-2.025	4.350	-2.495
		0.40	0.400	-2.314	4.971	-2.852
		0.45	0.450	-2.603	5.593	-3.208
		0.50	0.500	-2.893	6.214	-3.565
		0.55	0.550	-3.182	6.836	-3.921
		0.60	0.600	-3.471	7.457	-4.278
		0.65	0.650	-3.760	8.078	-4.634
		0.70	0.700	-4.050	8.700	-4.991
		0.75	0.750	-4.339	9.321	-5.347
		0.80	0.800	-4.628	9.943	-5.704
		0.85	0.850	-4.917	10.564	-6.060
		0.90	0.900	-5.207	11.186	-6.417
		0.95	0.950	-5.496	11.807	-6.773
		1.00	1.000	-5.785	12.428	-7.130
10	45	0.	-0.	0.	-0.	0.
		0.05	-0.000	0.050	-0.087	0.127
		0.10	-0.000	0.100	-0.175	0.247
		0.15	-0.000	0.150	-0.262	0.377
		0.20	-0.000	0.200	-0.349	0.499
		0.25	-0.000	0.250	-0.437	0.617
		0.30	-0.000	0.300	-0.524	0.737
		0.35	-0.000	0.350	-0.611	0.858
		0.40	-0.000	0.400	-0.699	0.977
		0.45	-0.000	0.450	-0.786	1.098
		0.50	-0.000	0.500	-0.873	1.218
		0.55	-0.000	0.550	-0.960	1.338
		0.60	-0.000	0.600	-1.047	1.461
		0.65	-0.000	0.650	-1.135	1.585
		0.70	-0.000	0.700	-1.222	1.728
		0.75	-0.000	0.750	-1.309	1.851
		0.80	-0.000	0.800	-1.397	1.975
		0.85	-0.000	0.850	-1.484	2.098
		0.90	-0.000	0.900	-1.571	2.222
		0.95	-0.000	0.950	-1.658	2.345
		1.00	-0.000	1.000	-1.746	2.469

10	50	0.	-0.	0.	-0.	0.
		0.05	-0.060	0.489	-0.735	0.599
		0.10	-0.119	0.977	-1.471	1.199
		0.15	-0.179	1.466	-2.206	1.798
		0.20	-0.238	1.954	-2.941	2.398
		0.25	-0.298	2.443	-3.677	2.997
		0.30	-0.358	2.932	-4.412	3.596
		0.35	-0.417	3.420	-5.148	4.196
		0.40	-0.477	3.909	-5.883	4.795
		0.45	-0.536	4.398	-6.618	5.394
		0.50	-0.596	4.886	-7.354	5.994
		0.55	-0.655	5.375	-8.089	6.593
		0.60	-0.715	5.863	-8.824	7.193
		0.65	-0.775	6.352	-9.560	7.792
		0.70	-0.834	6.841	-10.295	8.391
		0.75	-0.894	7.329	-11.030	8.991
		0.80	-0.953	7.818	-11.766	9.590
		0.85	-1.013	8.306	-12.501	10.189
		0.90	-1.073	8.795	-13.237	10.789
		0.95	-1.132	9.284	-13.972	11.388
		1.00	-1.192	9.772	-14.707	11.988
10	55	0.	-0.	0.	-0.	0.
		0.05	-0.086	0.695	-0.838	0.678
		0.10	-0.172	1.389	-1.676	1.355
		0.15	-0.258	2.084	-2.513	2.033
		0.20	-0.343	2.778	-3.351	2.710
		0.25	-0.429	3.473	-4.189	3.388
		0.30	-0.515	4.167	-5.027	4.065
		0.35	-0.601	4.862	-5.864	4.743
		0.40	-0.687	5.556	-6.702	5.420
		0.45	-0.773	6.251	-7.540	6.098
		0.50	-0.858	6.945	-8.378	6.776
		0.55	-0.944	7.640	-9.215	7.453
		0.60	-1.030	8.335	-10.053	8.131
		0.65	-1.116	9.029	-10.891	8.808
		0.70	-1.202	9.724	-11.729	9.486
		0.75	-1.288	10.418	-12.566	10.163
		0.80	-1.374	11.113	-13.404	10.841
		0.85	-1.459	11.807	-14.242	11.519
		0.90	-1.545	12.502	-15.080	12.196
		0.95	-1.631	13.196	-15.917	12.874
		1.00	-1.717	13.891	-16.755	13.551

10	60	0.	-0.	C.	-0.	C.
		0.05	-0.050	C.390	-0.305	C.227
		0.10	-0.100	0.779	-0.611	C.453
		0.15	-0.150	1.169	-0.916	C.68C
		0.20	-0.200	1.559	-1.222	C.907
		0.25	-0.250	1.948	-1.527	1.134
		0.30	-0.300	2.338	-1.832	1.360
		0.35	-0.350	2.728	-2.138	1.587
		0.40	-0.400	3.118	-2.443	1.814
		0.45	-0.450	3.507	-2.749	2.04C
		0.50	-0.500	3.897	-3.054	2.267
		0.55	-0.550	4.287	-3.360	2.494
		0.60	-0.600	4.676	-3.665	2.720
		0.65	-0.650	5.066	-3.97C	2.947
		0.70	-0.700	5.456	-4.276	3.174
		0.75	-0.750	5.845	-4.581	3.401
		0.80	-0.800	6.235	-4.887	3.627
		0.85	-0.850	6.625	-5.192	3.854
		0.90	-0.900	7.015	-5.497	4.081
		0.95	-0.950	7.404	-5.803	4.307
		1.00	-1.000	7.794	-6.108	4.534
10	65	0.	0.	-C.	0.	-C.
		0.05	0.040	-0.414	0.474	-0.465
		0.10	0.081	-0.827	0.949	-0.929
		0.15	0.121	-1.241	1.423	-1.394
		0.20	0.162	-1.655	1.897	-1.858
		0.25	0.202	-2.069	2.372	-2.323
		0.30	0.243	-2.482	2.846	-2.787
		0.35	0.283	-2.896	3.320	-3.252
		0.40	0.324	-3.31C	3.795	-3.716
		0.45	0.364	-3.724	4.269	-4.181
		0.50	0.405	-4.137	4.743	-4.646
		0.55	0.445	-4.551	5.218	-5.11C
		0.60	0.486	-4.965	5.692	-5.575
		0.65	0.526	-5.379	6.167	-6.039
		0.70	0.567	-5.792	6.641	-6.504
		0.75	0.607	-6.206	7.115	-6.968
		0.80	0.647	-6.620	7.590	-7.433
		0.85	0.688	-7.034	8.064	-7.898
		0.90	0.728	-7.447	8.538	-8.362
		0.95	0.768	-7.861	9.013	-8.827
		1.00	[illegible]	[illegible]	[illegible]	[illegible]

10	70	0.	0.	-C.	0.	-C.
		0.05	0.137	-1.308	0.902	-0.858
		0.10	0.275	-2.616	1.804	-1.716
		0.15	C.412	-3.924	2.706	-2.574
		0.20	0.550	-5.232	3.608	-3.431
		0.25	0.687	-6.540	4.51C	-4.289
		0.30	0.824	-7.848	5.412	-5.147
		0.35	0.962	-9.156	6.314	-6.CC5
		0.40	1.099	-1C.464	7.216	-6.863
		0.45	1.236	-11.772	8.118	-7.721
		0.50	1.374	-13.08C	9.020	-8.579
		0.55	1.511	-14.388	9.922	-9.436
		0.60	1.649	-15.696	10.825	-1C.294
		0.65	1.786	-17.CC4	11.727	-11.152
		0.70	1.923	-18.312	12.629	-12.C1C
		0.75	2.061	-19.620	13.531	-12.868
		0.80	2.198	-2C.928	14.433	-13.726
		0.85	2.335	-22.236	15.335	-14.584
		0.90	2.473	-23.544	16.237	-15.441
		0.95	2.61C	-24.852	17.139	-16.299
		1.CC	2.748	-26.160	18.041	-17.157
10	75	0.	0.	-C.	0.	-C.
		0.05	0.167	-1.591	0.593	-C.561
		0.10	C.335	-3.182	1.186	-1.123
		0.15	C.502	-4.773	1.779	-1.684
		0.20	0.669	-6.364	2.372	-2.246
		0.25	0.837	-7.955	2.964	-2.807
		0.30	1.004	-9.546	3.557	-3.368
		0.35	1.171	-11.137	4.150	-3.930
		0.40	1.338	-12.728	4.743	-4.491
		0.45	1.506	-14.319	5.336	-5.C53
		0.50	1.673	-15.91C	5.929	-5.614
		0.55	1.840	-17.501	6.522	-6.175
		0.60	2.008	-19.092	7.115	-6.737
		0.65	2.175	-20.683	7.708	-7.298
		0.70	2.342	-22.274	8.300	-7.859
		0.75	2.510	-23.865	8.893	-8.421
		0.80	2.677	-25.456	9.486	-8.982
		0.85	2.844	-27.047	10.079	-9.544
		0.90	3.011	-28.638	10.672	-10.105
		0.95	3.179	-30.229	11.265	-10.666
		1.00	[illegible]	[illegible]	[illegible]	[illegible]

6	70	0.	0.	-C.	0.	-C.
		0.05	0.073	-C.369	0.054	-C.C25
		0.10	0.146	-C.738	0.108	-C.C50
		0.15	0.219	-1.106	0.162	-0.075
		0.20	0.292	-1.475	0.217	-C.100
		0.25	0.365	-1.844	0.271	-C.125
		0.30	0.439	-2.213	0.325	-C.150
		0.35	0.512	-2.582	0.379	-C.175
		0.40	0.585	-2.950	0.433	-C.200
		0.45	0.658	-3.319	0.487	-C.225
		0.50	0.731	-3.688	0.541	-0.250
		0.55	0.804	-4.057	0.596	-C.275
		0.60	0.877	-4.426	0.650	-C.300
		0.65	0.950	-4.795	0.704	-C.325
		0.70	1.023	-5.163	0.758	-C.350
		0.75	1.096	-5.532	0.812	-C.376
		0.80	1.169	-5.901	0.866	-C.401
		0.85	1.243	-6.270	0.921	-C.426
		0.90	1.316	-6.639	0.975	-C.451
		0.95	1.389	-7.007	1.029	-C.476
		1.00	1.462	-7.376	1.083	-C.501
6	75	0.	-C.	C.	-0.	C.
		0.05	-C.000	C.050	-0.326	C.337
		0.10	-C.000	C.100	-0.651	C.674
		0.15	-C.000	C.150	-0.977	1.012
		0.20	-0.000	C.200	-1.303	1.349
		0.25	-0.000	C.250	-1.628	1.686
		0.30	-0.000	C.300	-1.954	2.023
		0.35	-0.000	C.350	-2.280	2.360
		0.40	-0.000	C.400	-2.606	2.697
		0.45	-0.000	C.450	-2.931	3.035
		0.50	-0.000	C.500	-3.257	3.372
		0.55	-0.000	C.550	-3.583	3.709
		0.60	-0.000	0.600	-3.908	4.046
		0.65	-0.000	0.650	-4.234	4.383
		0.70	-0.000	0.700	-4.560	4.721
		0.75	-0.000	0.750	-4.885	5.058
		0.80	-0.000	0.800	-5.211	5.395
		0.85	-0.000	0.850	-5.537	5.732
		0.90	-0.000	0.900	-5.863	6.069
		0.95	-0.000	0.950	-6.188	6.407
		1.00	-0.000	1.000	-6.514	6.744

6	80	0.	-0.	C.	-0.	C.
		0.05	-C.144	C.894	-0.690	C.693
		0.10	-0.288	1.788	-1.381	1.386
		0.15	-0.432	2.682	-2.071	2.079
		0.20	-0.576	3.576	-2.762	2.772
		0.25	-0.720	4.470	-3.452	3.465
		0.30	-0.864	5.364	-4.143	4.158
		0.35	-1.008	6.258	-4.833	4.851
		0.40	-1.152	7.152	-5.523	5.544
		0.45	-1.296	8.046	-6.214	6.237
		0.50	-1.440	8.940	-6.904	6.931
		0.55	-1.584	9.834	-7.595	7.624
		0.60	-1.728	10.728	-8.285	8.317
		0.65	-1.872	11.622	-8.975	9.010
		0.70	-2.016	12.517	-9.666	9.703
		0.75	-2.160	13.411	-10.356	10.396
		0.80	-2.304	14.305	-11.047	11.089
		0.85	-2.448	15.199	-11.737	11.782
		0.90	-2.592	16.093	-12.428	12.475
		0.95	-2.736	16.987	-13.118	13.168
		1.00	-2.880	17.881	-13.808	13.861
8	0	0.	0.	-C.	0.	C.
		0.05	0.050	-C.	0.698	C.
		0.10	0.100	-C.	1.396	C.
		0.15	0.150	-0.	2.094	0.
		0.20	0.200	-C.	2.793	C.
		0.25	0.250	-C.	3.491	C.
		0.30	0.300	-C.	4.189	C.
		0.35	0.350	-0.	4.887	0.
		0.40	0.400	-C.	5.585	C.
		0.45	0.450	-C.	6.283	C.
		0.50	0.500	-0.	6.981	0.
		0.55	0.550	-0.	7.679	0.
		0.60	0.600	-C.	8.378	C.
		0.65	0.650	-C.	9.076	C.
		0.70	0.700	-0.	9.774	0.
		0.75	0.750	-0.	10.472	0.
		0.80	0.800	-0.	11.170	0.
		0.85	0.850	-C.	11.868	C.
		0.90	0.900	-0.	12.566	0.
		0.95	0.950	-0.	13.265	0.
		1.00	1.000	-0.	13.963	0.

10	80	0.	0.	-0.	-0.	0.
		0.05	0.050	-0.443	-0.336	0.346
		0.10	0.100	-0.886	-0.672	0.691
		0.15	0.150	-1.329	-1.008	1.037
		0.20	0.200	-1.772	-1.344	1.383
		0.25	0.250	-2.215	-1.679	1.729
		0.30	0.300	-2.658	-2.015	2.074
		0.35	0.350	-3.102	-2.351	2.420
		0.40	0.400	-3.545	-2.687	2.766
		0.45	0.450	-3.988	-3.023	3.111
		0.50	0.500	-4.431	-3.359	3.457
		0.55	0.550	-4.874	-3.695	3.803
		0.60	0.600	-5.317	-4.031	4.149
		0.65	0.650	-5.760	-4.367	4.494
		0.70	0.700	-6.203	-4.703	4.840
		0.75	0.750	-6.646	-5.038	5.186
		0.80	0.800	-7.089	-5.374	5.531
		0.85	0.850	-7.532	-5.710	5.877
		0.90	0.900	-7.975	-6.046	6.223
		0.95	0.950	-8.419	-6.382	6.569
		1.00	1.000	-8.862	-6.718	6.914